Non-equilibrium Dynamics of Disordered Quantum Many-Body Systems

Dissertation submitted
for the award of the title

"Doctor of Natural Sciences"

to the Faculty of Physics, Mathematics, and Computer Science
of Johannes Gutenberg University Mainz
in Mainz

Hossein Hosseinabadi

Born in Tehran, Iran

Mainz, 14 August 2025

Supervisor: Prof. Dr. Jamir Marino
Date of examination: 15 January 2026

To Reyhaneh,
for her love and support.

Abstract

Recent advances in theoretical physics have increasingly focused on the dynamics of quantum systems with many interacting degrees of freedom, while ultracold atom platforms now enable the realization of diverse theoretical models with precise control over system parameters and advanced monitoring techniques. A prominent example is cavity quantum electrodynamics (CQED), where large atomic or molecular ensembles are coupled to high-finesse optical cavities, enabling strong interaction with confined electromagnetic modes and leading to phenomena such as the superradiant phase transition, in which atoms and photons form a coherent state. Most theoretical studies of CQED have concentrated on regimes of spatially uniform atom–cavity coupling, where collective behavior allows a description in terms of the classical dynamics of a few macroscopic variables. However, experimental capabilities now permit exploration beyond this limit, though theoretical progress is hindered by the exponential computational complexity of simulating large quantum systems, particularly when environmental coupling is included. This thesis addresses such challenges by developing efficient approaches, within the Keldysh formalism of non-equilibrium quantum field theory, to study systems with strongly disordered interactions coupled to external reservoirs. Two representative models are considered: a disordered spin–boson model describing light–matter interactions with quenched disorder, relevant to recent CQED experiments in confocal cavities, and a fermion–phonon system governed by the Yukawa–Sachdev–Ye–Kitaev (Yukawa-SYK) model. Both systems are quantum critical, exhibiting a continuum of low-energy modes above their stationary states, yet disorder produces qualitatively distinct dynamical behaviors: in the spin–boson system it induces slow, glassy relaxation, whereas in the Yukawa-SYK model it leads to rapid thermalization. These contrasting outcomes reveal the non-trivial role of disorder in quantum many-body systems and motivate further investigation into its effects on non-equilibrium quantum dynamics.

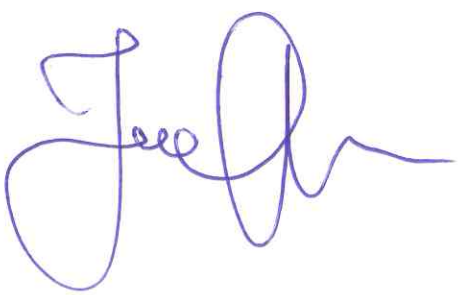

Contents

Acknowledgements

First, I want to thank my advisor, Prof. Jamir Marino, for his support, encouragement, and guidance throughout these years. His trust in giving me the freedom to explore different areas, and involving me in various collaborations made this PhD a fruitful and memorable journey. The countless hours we spent talking about physics, and many other things, are some of my favorite moments from this time.

I am also grateful to my collaborators, especially Prof. Jörg Schmalian, Prof. Eugene Demler, and Prof. Yaroslav Tserkovnyak, for their insights and help. A special thanks goes to Prof. Darrick Chang, not only for being a great collaborator, but also for generously supporting my visits to ICFO.

Thanks as well to my thesis committee members, Prof. Stefan Weinzierl, Prof. Jure Demsar, and Prof. Windpassinger, for their time and thoughtful feedback.

I am thankful as well to my colleagues for the friendly and stimulating environment they created over these years. In particular, I owe much to Riccardo Valencia-Tortora for helping me learn exact diagonalization, and to Oksana Chelpanova for guiding me through semiclassical methods. I would also like to thank our group secretary, Damaris Blümer, for her tremendous help with administrative matters.

Finally, I'm deeply thankful to my family and friends for always being there for me. Most of all, I owe everything to my wife for her patience, care, and for quietly sharing the weight of this journey every step of the way.

Publications

The current thesis is based on the following publications in a cumulative format:

[1] **Hossein Hosseinabadi**, Darrick E. Chang and Jamir Marino. *Far from equilibrium field theory for strongly coupled light and matter: dynamics of frustrated multimode cavity QED*, Phys. Rev. Res. 6, 043314 (2024).

[2] **Hossein Hosseinabadi**, Darrick E. Chang and Jamir Marino. *Quantum-to-classical crossover in the spin glass dynamics of cavity QED simulators*, Phys. Rev. Res. 6, 043313 (2024).

[3] **Hossein Hosseinabadi**, Shane P. Kelly, Jörg Schmalian and Jamir Marino, *Thermalization of non-Fermi-liquid electron-phonon systems: Hydrodynamic relaxation of the Yukawa-Sachdev-Ye-Kitaev model*, Phys. Rev. B 108, 104319 (2023).

Beyond the primary scope of this thesis, my PhD research encompasses several additional topics, which have culminated in the following publications as the leading author:

[4] **Hossein Hosseinabadi***, Oksana Chelpanova* and Jamir Marino. *User-friendly truncated Wigner approximation for dissipative spin dynamics.* arXiv:2503.17443. Accepted to PRX Quantum (2025). (*co-first author).

[5] **Hossein Hosseinabadi**, Yaroslav Tserkovnyak, Eugene Demler, and Jamir Marino. *Magnon Nesting in Driven Two-Dimensional Quantum Magnets.* arXiv:2505.10531 (2025). Submitted to Nature Communications.

[6] **Hossein Hosseinabadi**, Pavel E. Dolgirev, Sarang Gopalakrishnan, Amir Yacoby, Eugene Demler, and Jamir Marino. *Theory of correlation spectroscopy with two qubits.* Under preparation.

[7] **Hossein Hosseinabadi**, Riccardo J. Valencia-Tortora, Aleksandr N. Mikheev, Darrick E. Chang, Johannes Zeiher, Roderich Mössner and Jamir Marino. *Scarred dynamics of Rydberg arrays in optical cavities.* Under preparation.

In works [1–5] and [7], I contributed to the development of the ideas, carried out all analytical and numerical calculations, and wrote the manuscripts in their entirety. In work

[6], I was involved in the development of the idea, performed most of the analytical and numerical calculations, and wrote the majority of the manuscript.

I have also contributed to the following projects as the secondary author:

[8] Viktor A.S.V. Bittencourt, **Hossein Hosseinabadi**, Jairo Sinova, Libor Smejkal and Jamir Marino. *Quantum-impurity sensing of altermagnetic order.* arXiv:2508.04788 (2025). Submitted to PRL.

[9] Aleksandr N. Mikheev, **Hossein Hosseinabadi** and Jamir Marino. *Prethermalization of light and matter in cavity-coupled Rydberg arrays.* arXiv:2504.06267 (2025). Submitted to PRL.

In both works, I contributed to the development of the ideas, assisted in interpreting the results, and participated in writing parts of the manuscripts.

Introduction

In recent years, an active research direction has emerged in the study of non-equilibrium dynamics in quantum many-body systems [1, 2]. While this surge of interest is relatively recent, the intellectual roots of the field date back to the mid-20th century. In the 1950s and 1960s, seminal works by Schwinger, Keldysh, Kadanoff, and Baym [3, 4, 5] laid the theoretical foundations through the formulation of quantum mechanics on a closed time contour, knwon as the Schwinger–Keldysh formalism. Building on these developments, Barouch and McCoy [6] investigated the dynamics of a one-dimensional spin chain subjected to a sudden change in system parameters, a study that predated the modern terminology of the quantum quench by decades. Despite these early contributions, sustained research activity in this area remained sporadic until the 1990s, when the pioneering works of Deutsch and Srednicki introduced the eigenstate thermalization hypothesis (ETH) [7, 8], providing a statistical framework to explain the emergence of thermal behavior in isolated quantum systems.

Several factors have contributed to the resurgence of interest in non-equilibrium quantum dynamics over the past few decades. On the theoretical side, the dramatic increase in computational power, driven by advances in computer hardware and high-performance computing, has made it possible to simulate the dynamics of quantum systems of appreciable, though still finite, size. In parallel, the development of methods based on tensor network representations of quantum states [9, 10, 11, 12], particularly for one-dimensional and quasi-one-dimensional systems, has opened powerful new avenues for tracking and analyzing the time evolution of many-body states, with prospects for scaling to effectively infinite systems. These methodological breakthroughs have enabled detailed studies of a wide variety of model systems composed of bosons [13], fermions [14, 15], and spins [10, 16], leading to significant insights into phenomena such as thermalization in isolated systems, entanglement dynamics, and transport properties, among others.

On the experimental front, remarkable progress in controlling and probing quantum systems has transformed the study of non-equilibrium dynamics from a largely theoretical pursuit into a vibrant interplay between theory and experiment. Ultracold atomic gases [17, 18, 19, 20], trapped ions [21, 22], superconducting qubits [23, 24], and cavity quantum electrodynamics (CQED) [25, 26] platforms now offer highly tunable, nearly isolated settings where quantum many-body dynamics can be engineered and monitored

with unprecedented precision. In ultracold atom experiments, for instance, optical lattices enable the realization of clean lattice models with controllable dimensionality, interaction strength, and disorder [27, 28]. CQED systems introduce the ability to study strong long-range interactions in a many-body context, enabling the exploration of phenomena such as superradiance, driven-dissipative phase transitions, and collective quantum dynamics [29, 30, 31]. Together, these advances have made it possible to experimentally probe quantum quenches, thermalization, and localization, phenomena that were once accessible only through theoretical models and numerical simulations.

Within this growing interest in non-equilibrium physics, disorder has emerged as a key ingredient for exploring new dynamical regimes in quantum many-body systems. While its exact definition depends on the specific system, it can generally be described as spatial variations in a system's parameters that lack periodic structure. Examples include impurity atoms randomly distributed in a material or dislocations that disrupt an otherwise regular crystal lattice. For many years, the effect of disorder on quantum transport was thought to mirror that in classical systems, primarily changing the transport profile from ballistic to diffusive. This view shifted significantly in the mid-20th century with two important theoretical developments that revealed a more profound role for disorder in physical systems.

The first of these developments was the discovery of Anderson localization [32, 33]. In 1958, Anderson demonstrated that in a sufficiently disordered quantum system, interference between multiple scattering paths can completely suppress wave propagation, leading to the absence of diffusion even at finite energies. In contrast to the classical picture, where disorder merely slows transport, Anderson's result showed that quantum interference can localize particles, turning them into effectively immobile states. This phenomenon has since been observed in a variety of physical settings, including electronic transport in solids [34, 35], light propagation in disordered media [36], and cold-atom experiments [37]. While Anderson's original work focused on non-interacting particles, it provided the conceptual basis for later studies that asked how localization might persist or break down in the presence of interactions, a question that eventually led to the modern framework of many-body localization (MBL). In such systems, disorder and interactions combine to prevent thermalization, so that the system retains memory of its initial state for arbitrarily long times [38, 39]. Unlike conventional thermalizing systems, MBL phases exhibit atypical dynamical features such as slow entanglement growth and the absence of conventional transport [40, 41].

The second major development was the emergence of spin glass physics, which placed disorder at the core of a new class of phenomena in condensed matter and statistical physics [42, 43]. In the 1970s, Edwards and Anderson introduced a model of magnetic systems in which the interactions between spins are both random in sign and magnitude [44]. This quenched disorder leads to frustration, preventing the system from settling

into a single ordered ground state. Instead, spin glasses are characterized by frozen spin configurations with no global magnetization. Each configuration belongs to a highly complex energy landscape with a multitude of nearly degenerate minima, giving rise to slow, history-dependent dynamics. A proper characterization of spin glass phases and their transitions was achieved only after a series of seminal works by Parisi [45, 46, 47, 48], which established what is now known as replica symmetry breaking (RSB). In this framework, the spin glass order parameter is not a single number but a distribution function describing the overlaps between all possible low-energy states of the system, i.e. replicas, each separated by large energy barriers.

Recent experimental advances have enabled the realization of frustrated spin systems with long-range interactions. In such setups, disordered spin–spin couplings can be engineered by coupling an ensemble of atoms or ions to a large number of cavity modes, with photon-mediated interactions providing both tunability and the means to introduce controlled disorder [49, 50, 51]. These CQED realizations offer a unique opportunity to study some of the most intriguing phenomena in complex disordered systems. Among these are associative memories [52, 53, 54] and spin glasses. CQED platforms allow direct imaging of the emergence of these phases with exceptional precision. In particular, the ability to take snapshots of the spin configuration has recently made it possible to directly observe replica symmetry breaking (RSB), which had previously been detected only indirectly through its influence on macroscopic properties of the system, such as magnetic susceptibility.

While spin glasses were first identified in classical systems, later studies explored the existence of spin glass phases as ground states of disordered quantum systems, with particular attention to the role of quantum fluctuations in modifying or destabilizing spin glass order. Notably, Sachdev and Ye (SY) [55] showed that the ground state of certain disordered spin systems[1] lacks spin glass order and remains paramagnetic due to strong quantum fluctuations. Such a quantum paramagnetic state, also known as a quantum spin liquid, is characterized by a continuum of low-energy excitations, called spinons, which emerge from the fractionalization of the original spins into spinon pairs [56]. Nearly two decades later, interest in the SY model was revived by Kitaev [57], who introduced a variant now known as the Sachdev–Ye–Kitaev (SYK) model, revealing deep connections both to holography and to the theory of quantum chaos. In the latter context, the SYK model was shown to be maximally chaotic [58], with a Lyapunov exponent saturating the upper bound derived by Maldacena, Shenker, and Stanford [59]. Since then, extensive research on the SYK model and its generalizations has spanned a remarkably diverse range of fields, including holography [60], quantum information theory [61], and, in particular, the theory of non–Fermi liquids [62, 63, 64]. More recent studies have demonstrated that

[1] We note that the spins in the SY model belong to representations of the $su(M)$ Lie algebra with $M > 2$.

SYK-like models can capture key aspects of the strange metal phase observed in high-temperature superconductors and heavy fermion compounds [65, 66], where conducting electrons display universal properties, such as a linear-in-temperature resistivity, that starkly contrast with conventional Fermi liquid behavior [67, 68].

Remarkably, recent proposals also demonstrate the possibility of simulating SYK model in CQED platforms. The natural ability of optical cavities to mediate long-range interactions between atoms, combined with controlled spatial disorder, allow to simulate the fully connected random couplings of the SYK Hamiltonian. Both multimode cavity architectures with static disorder [69] and single-mode cavities with rapidly cycled disorder configurations [70] have been proposed, and numerical studies indicate that key SYK signatures remain robust under experimentally realistic conditions.

The experimental realizations of spin glasses and the SYK model discussed above highlight multimode optical cavities as powerful platforms for simulating disordered quantum systems. The distinct spatial mode structures produce position-dependent coupling strengths, giving rise to geometric frustration. This versatility makes multimode CQED architectures well suited for engineering a broad range of frustrated many-body Hamiltonians, potentially including quantum spin liquids. In parallel, recent experiments have demonstrated programmable spin–exchange interactions in single-mode cavity setups [71], providing a complementary route to realize and control frustration in many-body systems.

The developments discussed above illustrate how disorder, interactions, and quantum fluctuations can combine to produce a wide variety of novel phases. In certain respects, these effects can lead to strikingly opposite behaviors: while in spin glasses they suppress relaxation and prevent thermalization, in SYK models they give rise to maximal chaos and highly efficient thermalization. The present thesis aims to investigate the non-equilibrium dynamics of both classes of systems within a unified technical framework, while maintaining close contact with relevant experimental advances wherever possible.

This thesis investigates the non-equilibrium open-system dynamics of two classes of disordered systems, spin glasses and SYK models, within a unified technical framework: the Schwinger–Keldysh formulation of quantum field theory [4, 72, 73]. This approach offers several key advantages: it treats these systems directly in the thermodynamic limit while preserving their essential physical characteristics, and it incorporates disorder in a straightforward way without resorting to methods such as the replica trick. It naturally captures the markedly different dynamical behaviors of the two cases, describing both the fast thermalization characteristic of SYK models and the slow, frustrated dynamics of spin glasses. In addition, the Schwinger–Keldysh formalism seamlessly includes the effects of coupling to an external environment without the exponential growth in computational cost that hampers many treatments of open quantum systems [74, 75]. In the simplest approaches to system–environment interactions, the Hilbert space must be doubled, quickly rendering exact methods intractable for large systems [76, 77]. the

Schwinger–Keldysh framework avoids this limitation while remaining analytically and computationally tractable.

The contents of this thesis are organized as follows.

In **Chapter 1**, we briefly discuss how the notion of disorder is incorporated into the theoretical modeling of physical systems. By distinguishing between annealed and quenched disorder, we provide a concise overview of the challenges associated with treating quenched disorder and lay the groundwork for the chapters that follow.

In **Chapter 2**, we discuss the dynamics of a system of fermions and bosons that are coupled to each other via random interactions. This model, also known as the Yukawa–SYK model due to the similarity of the interaction between bosons and fermions to the Yukawa model of nuclear interactions, belongs to the class of SYK models with a critical zero-temperature phase and fast thermalization behavior upon quenches in the system's parameters.

In **Chapter 3**, we address far-from-equilibrium dynamics in a spin–boson problem with random interactions. This model captures the essential aspects of spin glasses realized in CQED experiments, where the cavity mode induces an effective interaction among spins, leading to a spin-glass phase. Particular attention is given to the role of quantum fluctuations, which are controlled by the spin size, as well as to the influence of photons as active dynamical degrees of freedom, beyond their role in mediating effective spin–spin interactions.

In **Chapter 4**, we conclude by discussing various possible future directions.

Chapter 1

A primer on disorder

From a physical perspective, disorder refers to elements of a system that remain fixed, or vary only very slowly in time, while perturbing an otherwise clean system. Examples include impurities embedded in a host material, or dislocations and defects in the underlying lattice, whose locations are typically random. There are also cases where nothing in the system is inherently random, yet it is a good approximation to treat certain quasi-random parameters as random variables. This perspective will become particularly relevant in our discussion of the CQED setup in Chapter 3.

Mathematically, disorder is typically represented by a set of random parameters in the model, sampled from a given probability distribution. Consequently, no two points in the system are identical, and the microscopic details depend on the specific realization of the disorder. Nevertheless, certain quantities, particularly macroscopic ones that depend only on spatial averages of microscopic variables over sufficiently large regions, can often be obtained by averaging over many disorder realizations. Systems, or more precisely quantities, that satisfy this property are termed self-averaging. While many disordered systems are self-averaging, there are also cases where this property fails, at least for some observables. A prominent example is provided by spin glasses. Even in such cases, however, averaging over disorder, equivalent to repeating experiments with different disorder realizations, can yield valuable information about the macroscopic properties of the system [42, 43].

Disorder: quenched versus annealed

In statistical mechanics, the most direct route to calculating thermodynamic properties is through the partition function

$$Z = \mathrm{Tr}\, e^{-\beta H(\eta)}, \tag{1.1}$$

where η denotes a particular realization of the disorder variables. In a clean system, Z is uniquely defined. In a disordered system, however, it depends explicitly on η. Since thermodynamic potentials are derived from the free energy

$$F = -T \log Z, \tag{1.2}$$

a fundamental question arises: should we average the partition function over disorder realizations before or after taking the logarithm? The answer is not just a matter of computational complexity, and is related the physical interpretation of disorder.

If one averages Z first and then takes the logarithm,

$$F_{\text{ann}} = -T \log \overline{Z}, \tag{1.3}$$

one obtains what is known as the annealed free energy. In contrast, if one takes the logarithm first and then averages,

$$F_{\text{que}} = -T\overline{\log Z}, \tag{1.4}$$

one obtains the quenched free energy. The distinction is mathematically subtle but physically important. Because logarithm is a concave function one has

$$F_{\text{ann}} \leq F_{\text{que}}, \tag{1.5}$$

which reflects the fact that averaging before the logarithm overestimates the system's ability to explore different disorder realizations.

The physical meaning becomes clear when we consider the dynamics of the disorder variables relative to the degrees of freedom described by the partition function. In quenched disorder, the disorder configuration is effectively frozen over the timescale relevant for the thermal fluctuations of the system's microscopic variables. Each disorder realization constitutes a static background, and the system must adapt to it. Examples include magnetic impurities in a metal, random defects in a crystal, or the random couplings in a spin glass: in all these cases, the positions and strengths of the disorder sources are fixed during the experiment. The appropriate approach is thus to compute the free energy for each fixed realization, and then average, yielding Eq. (1.4).

In annealed disorder, by contrast, the disorder degrees of freedom fluctuate rapidly compared to the system's equilibration time, allowing them to explore their own configuration space during the course of the system's thermal dynamics. Here, the system's microscopic variables and the disorder variables effectively thermalize together, and the correct statistical treatment involves including the disorder variables in the partition sum before taking the logarithm, leading to Eq. (1.3). A classic example is an alloy at sufficiently

high temperature, where the atomic species can diffuse and redistribute on experimental timescales.

The difference between these two cases can be substantial. In quenched disorder, the system is constrained by a single realization, and rare but energetically costly disorder configurations can dominate physical properties. In annealed disorder, such rare configurations are suppressed by the disorder's self-adjustment. For the problems discussed in this thesis, we always assume to work with quenched disorder.

Quenched disorder poses a theoretical challenge due to the need to average the logarithm in Eq. (1.4). Two approaches are widely used to address this problem. The first is the replica method [44, 43], in which multiple copies of the system are introduced to facilitate disorder averaging. The second is the Schwinger-Keldysh formalism [73], used in this thesis, which treats the problem directly in real time and is particularly well suited for non-equilibrium dynamics. A third technique, known as supersymmetry [78], can also be employed, but is applicable only to disordered systems of free bosons and fermions. Below, we briefly discuss the first two approaches, while omitting supersymmetry due to its limited application and lack of relevance to the content of the thesis.

The replica trick

To handle averaging in the presence of quenched disorder, Anderson introduced the replica trick, which relies on the following identity

$$\ln Z = \lim_{R\to 0} \frac{Z^R - 1}{R}. \tag{1.6}$$

In this approach, the disorder-averaged free energy is obtained by first considering R replicas of the original system, computing the averaged quantity $\overline{Z^R}$, and then analytically continuing the result from integer R to real values before taking the limit $R \to 0$. A crucial consequence of disorder averaging is that it couples degrees of freedom belonging to different replicas, thereby generating an effective interaction between them.

A natural outcome of the replica approach is the emergence of correlations between observables belonging to different replicas, arising from their shared disorder realizations. These correlations are quantified by functions of the form

$$C_{\alpha\beta}(i,j) = \overline{\langle O_{\alpha,i}\, O_{\beta,j}\rangle}, \tag{1.7}$$

where (α, β) denote replica indices and (i, j) represent other physical labels, such as the position. In general, whether such correlations vanish for $\alpha \neq \beta$ (replica-diagonal property) or remain finite (replica off-diagonal property) is not known a priori, and must be checked for each specific model and for different parameter regimes within the same

model.

A representative example of a system with a replica-diagonal structure is the SYK model (see Chapter 2), in which annealed and quenched disorder yield identical physical results [79, 80]. By contrast, glassy systems exhibit a replica off-diagonal structure. Remarkably, such systems often display replica symmetry breaking (RSB), where $C_{\alpha\beta}$ is not only finite for $\alpha \neq \beta$, but also depends on the specific pair of replicas [42]. A subtle aspect of the replica trick is the $R \to 0$ limit, which must be taken carefully, following a prescription first introduced by Parisi [45, 46, 47, 48], in order to obtain physically meaningful results.

The Schwinger-Keldysh formalism

The starting point of the Schwinger–Keldysh formalism is the identity [73]

$$1 = \mathrm{Tr}\,\rho(t) = \mathrm{Tr}\Big(e^{-iHt}\,\rho_0\,e^{+iHt}\Big), \tag{1.8}$$

where ρ_0 is the initial density matrix of the system. Dividing each exponential into small time increments allows one to proceed in a manner analogous to the derivation of the Feynman path integral. The resulting expression involves two path integrals, corresponding to the forward and backward branches of the time contour:

$$1 = \int D[\phi_+,\phi_-]\ \langle\phi_+(0)|\,\rho_0\,|\phi_-(0)\rangle\ e^{iS[\phi_+]-iS[\phi_-]}, \tag{1.9}$$

where $\phi_\pm$ denote the fields on the two branches, and $S[\phi_\pm]$ has the same form as the standard action but with opposite overall signs. The expectation value of $\phi(t)$ is then given by

$$\langle\phi(t)\rangle = \int D[\phi_+,\phi_-]\,\phi_+(t)\ \langle\phi_+(0)|\,\rho_0\,|\phi_-(0)\rangle\ e^{iS[\phi_+]-iS[\phi_-]}. \tag{1.10}$$

If the Hamiltonian H, and hence the action S, contains random variables, the disorder average can be performed directly:

$$\overline{\langle\phi(t)\rangle} = \int D[\phi_+,\phi_-]\,\phi_+(t)\ \langle\phi_+(0)|\,\rho_0\,|\phi_-(0)\rangle\ \overline{e^{iS[\phi_+]-iS[\phi_-]}}. \tag{1.11}$$

This step has no direct analogue in the equilibrium formalism, where the partition function appears in the denominator of thermal averages, complicating the disorder average. In writing Eq. (1.11) we have assumed that the initial state is uncorrelated with the disorder. This assumption fails, for example, when the initial state is the thermal or ground state of H for the same disorder realization. Such cases can often be handled by starting from an uncorrelated initial state and adiabatically introducing the disorder or cooling the system to the desired correlated state, in analogy with adiabatic state preparation.

How does quenched disorder manifest itself in the real-time approach? According to Eq. (1.11), it does so by generating effective interactions between fields on opposite branches of the time contour. As we will see in Chapters 2 and 3, this coupling between forward and backward contours is sufficient to capture all of the nontrivial dynamics in the SYK model and in spin glasses, respectively.

Chapter 2

Thermalization dynamics of a critical electron-phonon system

In this chapter, we present our results on the dynamics of the Yukawa–SYK model, as reported in one of our previous works (Ref. [81]). Since the Yukawa–SYK model extends the SYK model, we begin with a brief overview of the latter to provide the necessary background for our discussion of thermalization dynamics in the Yukawa–SYK framework.

A synopsis of the SYK model

The SYK model describes a system of N Majorana fermions governed by the Hamiltonian [57, 64]

$$H_{\text{SYK}} \equiv -\frac{1}{4!}\sum_{i,j,k,l=1}^{N} J_{ijkl}\,\chi_i\chi_j\chi_k\chi_l, \tag{2.1}$$

where the operators χ_i satisfy the Majorana algebra

$$\{\chi_i, \chi_j\} = \delta_{ij}, \tag{2.2}$$

and J_{ijkl} are fully antisymmetric random couplings drawn from a Gaussian distribution with

$$\overline{J_{ijkl}} = 0, \quad \overline{J_{ijkl}^2} = \frac{3!\,J^2}{N^3}. \tag{2.3}$$

The model becomes exactly solvable in the large-N limit after averaging over the disorder, and assuming a replica diagonal solution (cf. Chapter 1). In this limit, the imaginary-time Green's function,

$$G_{ij}(\tau_1, \tau_2) = G(\tau_1, \tau_2)\delta_{ij} \equiv -\langle T\chi_i(\tau_1)\chi_j(\tau_2)\rangle, \tag{2.4}$$

satisfies a closed set of equations. Specifically, the Dyson equation reads

$$G(i\omega) = \frac{1}{i\omega - \Sigma(i\omega)}, \tag{2.5}$$

where the self-energy Σ is determined self-consistently from

$$\Sigma(\tau_1, \tau_2) = J^2 \Big[G(\tau_1, \tau_2)\Big]^3. \tag{2.6}$$

The large-N limit ensures that all other contributions to Σ vanish.

Although these equations generally require numerical solution, the low-energy (long-time) behavior of G can be extracted analytically. Assuming time-translation symmetry and using the ansatz $G(\tau) \propto 1/|\tau|^\alpha$, one finds

$$G(\tau) \approx -\left(\frac{1}{4\pi J^2}\right)^{1/4} \frac{\mathrm{sgn}(\tau)}{\sqrt{|\tau|}}, \tag{2.7}$$

demonstrating that interactions strongly renormalize the Green's function at low energies.

This straightforward calculation might give the impression that the SYK model is of limited physical interest while in fact, its physics is remarkably rich, which explains its popularity in recent years. In the following, we briefly highlight some of these notable features.

Conformal symmetry– In the infrared (IR) limit, corresponding to $\omega \to 0$, we may omit the $i\omega$ term in the denominator of Eq. (2.5). In this limit, using Eq. (2.6) we get in the time domain

$$\int [G(\tau_1, \tau_3)]^3 G(\tau_3, \tau_2)\, d\tau_3 = -\delta(\tau_1, \tau_2). \tag{2.8}$$

This equation admits a family solutions connected to each other by the following reparametrization

$$\sigma \equiv f(\tau), \quad G(\tau_1, \tau_2) = |\partial_1 f(\tau_1) \partial_2 f(\tau_2)|^{1/4} G(\sigma_1, \sigma_2). \tag{2.9}$$

For instance, we can choose $f(\tau) = e^{2\pi i T \tau}$, where T is the temperature, and subsequently perform analytical continuation to real time via $\tau = -it$, to find the finite-temperature Green's function

$$G_\beta(t) = -\frac{\pi^{1/4}}{\sqrt{2J \sinh(\pi T t)/T}} \overset{Tt \gg 1}{\sim} e^{-\pi T t/2}, \tag{2.10}$$

showing that correlations decay exponentially at long times. A notable property of Eq. (2.10) is the sole dependence of the decay rate on T. Such behavior is a characteristic of quantum critical systems, such as those close to quantum phase transitions. This is not surprising as the fermions of the SYK model are also critical, as can be seen from the zero temperature limit of Eq. (2.10). We also notice that this solution breaks the symmetry in Eq. (2.9). Since the symmetry is continuous, we expect a continuum of

Goldstone modes to appear in the spectrum. However, this result follows from neglecting the ultraviolet (UV)–relevant term $i\omega$ in Eq. (2.5). The UV corrections, which explicitly break conformal symmetry, generate a finite energy gap for these Goldstone modes. An effective theory for them can be constructed by deriving the so-called $G\Sigma$ action—an effective action expressed in terms of the Green's function G and self-energy Σ [58]. The saddle-point equations of this action reproduce Eqs. (2.5) and (2.6), while the leading-order fluctuations about the saddle point capture the dynamics of the gapped Goldstone modes. Although we will not derive this action here, we will discuss the relevance of these fluctuations in the context of quantum chaos below, which connects to the thermalization of the system.

Quantum chaos– While chaos in quantum systems can be characterized in various ways, such as through energy-level statistics, in the SYK model it is most commonly diagnosed via the out-of-time-ordered correlator (OTOC) [58]

$$C_{ij}(t_1, t_2) \equiv \left\langle \{\chi_i(t_1), \chi_j(t_2)\}^2 \right\rangle, \tag{2.11}$$

which generalizes $\langle [A_i(t_1), B_j(t_2)]^2 \rangle$, which holds for bosonic operators, to fermionic operators. Intuitively, $C(t_1, t_2)$ measures the sensitivity of a measurement at time t_2 to a prior measurement at time t_1. By analogy with classical chaos, we expect that in a chaotic system

$$C(t_1, t_2) \sim e^{\lambda_L |t_1 - t_2|}, \tag{2.12}$$

where λ_L is the quantum Lyapunov exponent. From Eq. (2.11), evaluating the OTOC in the SYK model requires computing fermionic four-point functions. This can be done in two equivalent ways [82]. The first is the standard method: solving the self-consistent Bethe–Salpeter equation for the four-point function. The second exploits the fact that the fermionic four-point function can be recast as a two-point function of Green's functions, with its excitations corresponding to the gapped Goldstone modes discussed earlier. In both approaches, a lengthy calculation in the strong-coupling limit $J/T \gg 1$ yields [58, 82]

$$\lambda_L = 2\pi T. \tag{2.13}$$

This value saturates the universal upper bound on quantum chaos derived in Ref. [59], making the SYK model a prototypical example of a maximally chaotic system. However, Eq. (2.13) is valid only up to the scrambling time t_{scr}, beyond which the growth of the OTOC saturates. The scrambling time characterizes the timescale over which the local entropy approaches its maximum value following a perturbation to the system.

The SYK model admits various extensions. Examples include introducing higher-order interaction vertices in Eq. (2.1) [58], adding a quadratic random hopping term, or formu-

lating the model with complex fermions [63], all of which involve purely fermionic degrees of freedom. Extensions to bosonic variables are more subtle: the appearance of negative-energy modes renders the system unstable unless additional non-random stabilizing terms are included to bound the spectrum from below. Even when stabilized, purely bosonic random models typically exhibit glassy phases, as we discuss later in Chapter 3.

Possible realizations of SYK in CQED systems

While extensions of the SYK model to finite dimensions have found relevance across strongly correlated electron systems [83, 66], there are also proposals to directly simulate the SYK Hamiltonian in CQED platforms. Below we summarize two complementary approaches.

In the first approach [69], one makes use of a multimode optical cavity loaded with ultracold fermions. A spatially disordered AC-Stark shift introduces random position-dependent detunings for the atoms. By adiabatically eliminating the excited atomic states and cavity photons, the effective low-energy theory contains all-to-all random four-fermion interactions among the fermionic motional modes. The degree of randomness and connectivity can be tuned by varying the number of participating cavity modes and the spatial overlap between the atomic cloud and cavity field. Numerical simulations of this scheme indicate characteristic SYK signatures such as the profile of OTOCs.

A complementary proposal [70] achieves similar physics using a single-mode cavity, but with time-dependent disorder. In this scheme, independent realizations of a disordered optical potential are applied in rapid succession, so that each short time segment realizes a different sparse random coupling pattern. Over many cycles, the effective couplings become dense, mimicking the fully connected random interactions of the SYK model. This approach avoids the technical complexity of multimode cavities while still allowing access to the same dynamical signatures.

In both architectures, the randomness is generated by controlled spatial inhomogeneities in the atom–light coupling, and the cavity photons mediate the long-range interactions. As we will discuss in Chapter 3, a similar approach can be used to realize spin glass phases in CQED systems.

The Yukawa-SYK model

One of the prominent theoretical frameworks in condensed matter physics to study critical systems are fermion–boson models, in which gapless fermions interact with a bosonic field that may be tuned close to its critical point [84]. Such proximity enhances fluctuations in both the fermionic and bosonic sectors and has been proposed as a mechanism underlying phenomena such as high-temperature superconductivity and strange metal behavior. In

most cases, fermion–boson problems are treated using uncontrolled approximations, so it is desirable to identify versions of these models that allow for a controlled expansion or, ideally, can be solved exactly. Remarkably, the SYK model can be extended to an exact solvable model of strongly interacting fermions and bosons. This extension, known as the Yukawa–SYK model [85], is define as

$$H_{\mathrm{YSYK}} = \frac{1}{2}\sum_{k=1}^{M}\left(\pi_k^2 + \omega_0^2\phi_k^2\right) + \frac{1}{N}\sum_{i,j=1}^{N}\sum_{k=1}^{M}\sum_{\sigma=\uparrow,\downarrow} g_{ij,k}\,\phi_k\,\psi_{i\sigma}^{\dagger}\psi_{j\sigma}, \tag{2.14}$$

for $2N$ fermionic and M bosonic species satisfying the (anti-)commutation relations $\{\psi_{i\sigma}^{\dagger}, \psi_{j\sigma'}\} = \delta_{ij}\delta_{\sigma\sigma'}$ and $[\phi_k, \pi_l] = i\,\delta_{kl}$. The bosons can be interpreted as phonon-like modes, and the random couplings $g_{ij,k}$ are drawn from a Gaussian distribution. Ref. [85] demonstrated that this model hosts a critical state at low temperatures, with critical exponents depending on the ratio N/M [86]. Remarkably, the ground state exhibits superconducting order when the random couplings are purely real, with Cooper pairs formed from incoherent fermions displaying strong non–Fermi-liquid behavior. Subsequent works have extended the Yukawa–SYK model to finite spatial dimensions and explored its potential relevance to the strange-metal phase observed in strongly correlated electron systems [66, 65], as well as holography [87].

In the work presented below [81], we investigate the non-equilibrium dynamics of the Yukawa–SYK model coupled to an external environment. The non-equilibrium dynamics of the SYK model, in both regimes of closed and open system dynamics, has been discussed in other works [88, 89, 90]. Our goal is to examine how the interaction between the system and environment influences the relaxation of the system toward equilibrium, and to characterize the distinct temporal evolution of its two components, fermions and phonons, prior to equilibration.

Thermalization of non-Fermi-liquid electron-phonon systems: Hydrodynamic relaxation of the Yukawa-Sachdev-Ye-Kitaev model

Hossein Hosseinabadi,[1,*] Shane P. Kelly,[1] Jörg Schmalian,[2,3] and Jamir Marino[1]
[1]*Institut für Physik, Johannes Gutenberg-Universität Mainz, 55099 Mainz, Germany*
[2]*Institut für Theorie der Kondensierten Materie, Karlsruher Institut für Technologie, 76131 Karlsruhe, Germany*
[3]*Institut für Quantenmaterialien und Technologien, Karlsruher Institut für Technologie, 76131 Karlsruhe, Germany*

(Received 7 June 2023; accepted 20 September 2023; published 28 September 2023)

We study thermalization dynamics in a fermion-phonon variant of the Sachdev-Ye-Kitaev model coupled to an external cold thermal bath of harmonic oscillators. We find that quantum critical fermions thermalize more efficiently than phonons, in sharp contrast to the behavior in the Fermi liquid regime. In addition, after a short prethermal stage, the system acquires a quasithermal distribution given by a time-dependent effective temperature, reminiscent of "hydrodynamic" relaxation. All physical observables relax at the same rate which scales with the final temperature through an exponent that depends universally on the low-energy spectrum of the system and the bath. Such relaxation rate is derived using a hydrodynamic approximation in full agreement with the numerical solution of a set quantum kinetic equations derived from the Keldysh formalism for nonequilibrium Green's functions. Our results hint toward further research on the applicability of the hydrodynamic picture in the description of the late time dynamics of open quantum systems despite the absence of conserved quantities in regimes dominated by conserving collisions.

DOI: 10.1103/PhysRevB.108.104319

I. INTRODUCTION

Thermalization of isolated and open quantum many-body systems has been a subject of intense research since the early 2010s [1–4]. The combination of the large number of degrees of freedom and extended correlations in these systems restricts the applicability of numerical and perturbative methods. Not suffering from these limitations, exactly solvable models can be valuable platforms for the study of relaxation in quantum many-body systems. Instances of these systems. include integrable models [5–8] and the large-N limit of quantum $O(N)$ field theories [9–11] featuring ergodicity breaking and the phenomenon of prethermalization [12,13].

A pivotal case of exact solvability is the celebrated Sachdev-Ye-Kitaev model (SYK) [14–17] consisting of a system of randomly interacting Majorana fermions which admits an exact solution in the limit of a very large number of fermions. The SYK model features a low-temperature non-Fermi liquid (NFL) critical state, Planckian dissipation together with the saturation of the upper bound on quantum chaos [18,19]. Last, it is shown that the SYK model has a holographic dual as a theory of gravity in AdS background [15,20,21]. Another class of SYK models, called Yukawa-SYK models, comprises systems of complex fermions interacting randomly with phonons [22–26] or similar bosonic excitations [27] with a plethora of interesting properties in addition to those of purely fermionic SYK systems. These include an NFL to unconventional superconducting phase transition [22,23,25,28,29] beyond the BCS theory [30] and self-tuned quantum criticality for phonons where the phonon gap vanishes at $T \to 0$ regardless [22–25,31] of the strength of the interaction and the phonon gap. Extensions of these models to lattice systems [32–36] and to the Kondo problem [37] have also been studied in the past.

In this paper, we study the dynamics of a Yukawa-SYK system coupled to an external bath of thermal phonons by using the Keldysh formalism of nonequilibrium quantum field theory [38–40]. Previous works have addressed various out-of-equilibrium aspects of isolated [41–44], open [45–47], and periodically driven [48] fermionic SYK models. Our motivation for considering the dynamics of Yukawa-SYK model is threefold: (i) Phonons and other bosonic excitations are always present in real electronic systems and therefore the Yukawa-SYK model is a convenient framework to study their effects on the NFL behavior. As we will see, the model is an example for the complex nonequilibrium dynamics of a multicomponent systems with strongly interacting parts. (ii) Most of the studies of the dynamics of open SYK systems consider critical NFL fermionic baths which usually are modeled by another SYK system, while in realistic settings, there are no such restrictions on the nature of the external bath. Instead, in this work we consider a generic Caldeira-Leggett [49] bath of harmonic oscillators coupled to the phonons of the system. Below we demonstrate that this is indeed the most relevant bath coupling of our system. (iii) The fermion sector of the Yukawa-SYK model has a $U(1)$ symmetry and has a finite local Hilbert space while these features are absent in the phonon sector. The $U(1)$ symmetry of the Yukawa-SYK model can break, yielding a superconducting state. Thus, our study of the symmetric limit is a necessary first step to nonequilibrium superconductivity [50–56] in these systems.

*hhossein@uni-mainz.de

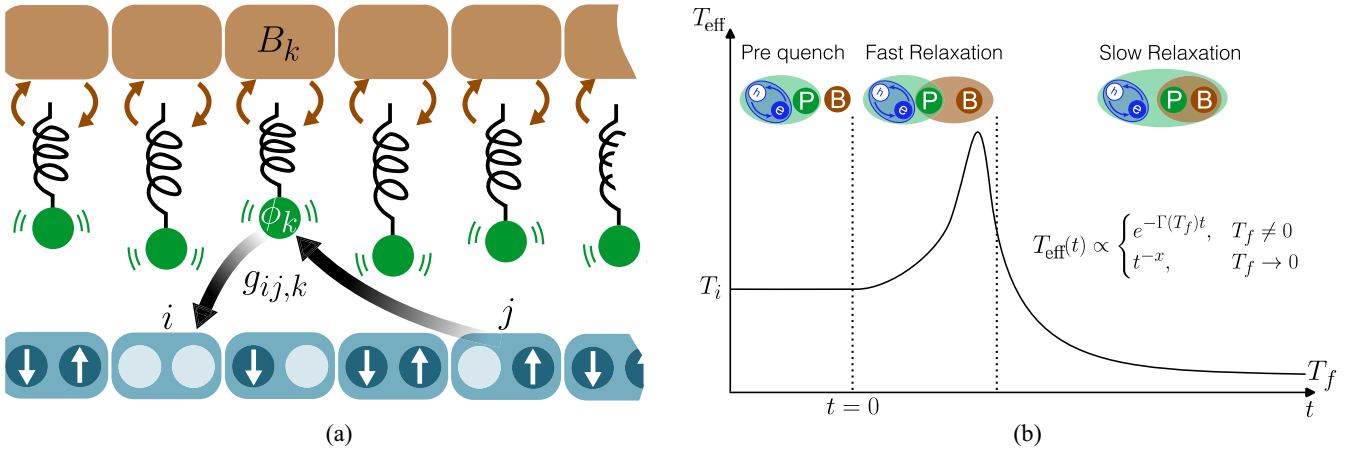

FIG. 1. (a) Schematics of the Yukawa-SYK model where fermions (blue dots with white arrows indicating spin) are scattered by phonons (green dots) from one site to another with a random amplitude $g_{ij,k}$. Each phonon mode ϕ_k is coupled to a separate thermal bath B_k. (b) Qualitative evolution of the effective temperature in a bath-coupled Yukawa-SYK system. Prior to the quench, phonons and fermion density fluctuations are in a hybrid critical state. Immediately after the quench, the system undergoes a fast process which is followed by a long-lasting process of thermalization where a hydrodynamical description of the system is possible.

While environments are usually perceived as sources of decoherence that adversely affect interesting quantum effects, open quantum systems can host novel phases of matter which are inaccessible in isolated systems [57–60]. Therefore, it is natural to study the dynamics of the SYK model as a prototype for NFL systems in presence of coupling to an environment. The importance of the nature of the bath and the type of system-bath coupling on both the intermediate and long-time behavior of purely fermionic SYK models has been highlighted by Refs. [45–47]. As a controlled theory for the dynamics of a strongly interacting electron-phonon system coupled to an external bath, the Yukawa-SYK model can provide valuable insights into the nonequilibrium dynamics of similar but more complex systems.

We first show that the critical phase survives for couplings to Ohmic, super-Ohmic, and a range of sub-Ohmic baths. The distributions of fermionic and phononic excitations display clear qualitative differences over the course of the evolution. Shortly after the quench, the system shows local (in time) equilibrium, where the distribution of excitations is given by a thermal function at an effective, time-dependent temperature. This is similar to the late-time regime of "hydrodynamic" relaxation [61–65] although with important differences which are addressed in Sec. V D. We show that the NFL and Fermi liquid (FL) regimes have different signatures in the thermalization profiles of fermions and phonons. In the NFL regime, fermions thermalize more efficiently than phonons despite the latter's direct coupling to the cold bath. Interestingly, the effective temperature of fermionic excitations is lower than that of phonons at later times. On the other hand, in the FL regime, phonons thermalize faster than fermions and are colder during the intermediate and late stages of thermalization.

The paper has the following structure: In Sec. II we demonstrate the theoretical setup and give a summary of our results. In Sec. III we introduce the Yukawa-SYK model and characterize different types of baths that we can couple to the system. In Sec. IV we briefly review the Keldysh formalism and derive the quantum kinetic equations (QKE) for the Yukawa-SYK model. The results of the numerical solution of QKE and their interpretation are presented in Sec. V. Finally, we conclude the paper and propose some future directions in Sec. VI.

II. OVERVIEW OF RESULTS

The Yukawa-SYK model describes a system of Einstein phonons randomly interacting with the density fluctuations of a system of complex fermions [Fig. 1(a)]. The random fermion-phonon coupling is chosen from a Gaussian ensemble with zero mean and second moment proportional to g^2. This system is always in a quantum critical state at low temperatures characterized by the strong hybridization of phonons and fermion density fluctuations [22,23,25]. At $t = 0$, we couple each phonon species to a separate non-Markovian thermal system of phonons. By assuming a large number of degrees of freedom in each local bath, we neglect the effect of system-bath coupling on the environment. At low energies, the bath density of states (DOS) has a power-law behavior $J(\omega) \sim \omega|\omega|^{a-1}$ where the exponent a characterizes the low-energy behavior of the environment.

The effect of the bath on the system crucially depends on the scaling behavior of $J(\omega)$ at small frequencies. We call the bath infrared (IR) *irrelevant* when the exponent a given above satisfies $a > a_c$, for a universal value a_c determined only by the Yukawa-SYK model. In this case, the bath DOS goes to zero fast enough at low energies such that the tunneling of phonons between the system and the bath cannot affect the low-energy spectrum of the system. The bath is called *marginal* for $a = a_c$, where at low energies, the system-bath coupling and fermion-phonon interactions scale with energy in the same way and similar to the irrelevant bath. Therefore, we do not expect any qualitative change in the spectrum of the system when coupled to a marginal bath. Finally, the bath is termed relevant when $a < a_c$ where we expect the system-bath coupling to affect the low-energy spectrum of the system. We will not focus on a relevant bath in the following, since it tends to destroy the critical phase as shown for purely

fermionic SYK systems [46]. The limitation to an irrelevant bath coupling is not substantial. We will see that it always includes the regime of an Ohmic and super-Ohmic bath and excludes only certain sub-Ohmic environments.

After turning on the system-bath coupling at $t = 0$, the evolution of the system follows a two-stage process. An initial and quick stage of dynamics characterized by large energy transfer between the system and the bath as a result of the lack of complete overlap between the eigenstates of pre- and postquench Hamiltonians followed by a slow and long-lasting period of quasiequilibrium behavior [Fig. 1(b)]. During the first stage of dynamics, the population of phonons in the system is found to deviate significantly from equilibrium, while the population of fermions appears to be closer to a thermal distribution. As explained below, the relative robustness of the distribution of fermions is a result of Pauli's exclusion principle and the $U(1)$ symmetry of fermions which restrict the available phase space for fermion scattering. The insensitivity of the fermion population allows us to assign fermions an effective temperature using the fluctuation-dissipation ratio (FDR) from the earliest instants of dynamics.

During the second stage of the evolution, both fermions and phonons satisfy fluctuation-dissipation theorem (FDT) at low to moderate energies (with respect to the bare gap of the phonons). The effective temperature can be deduced from FDT ([45,46]), showing a monotonic decrease toward its final value. Interestingly, fermions appear to be slightly colder than phonons during the second stage of the dynamics, despite the direct coupling of phonons to the bath. We show that the same phenomenon does not occur in an FL variant of the Yukawa-SYK model with the same strength of interactions and conclude that it is a result of the strong correlations between fermions and phonons in the NFL system. We note that such comparison between fermions and phonons is not possible in the quench dynamics of purely fermionic SYK models studied in the past [41,45–47,66].

Looking at the evolution of effective temperature quantitatively, we observe an exponential relaxation of temperature and other observables such as energy with the same rate. We call this rate Γ which is defined via $T - T_f \sim e^{-\Gamma t}$. We see that Γ follows a power-law behavior in terms of the final temperature $\Gamma \sim T_f^x$ where the exponent x is universally determined by the low-energy behavior of the system and the bath, and it increases linearly with a. This observation suggests that the evolution of every physical quantity is uniquely determined through its dependence on the effective temperature. Thus, the knowledge of the time evolution of the effective temperature is sufficient to describe the behavior of all of the observables. We solve for the complete nonequilibrium dynamics by numerically integrating the QKE. However, to check the mentioned hypothesis and to physically illustrate our numerical results, we also perform a "hydrodynamic" approximation (see Sec. V D for remarks on the usage of this term) by finding a closed set of equations for the total energy and the rate of energy transfer between the system and the bath as functions of effective temperature. By solving them, we find the dependence of the temperature relaxation rate on final temperature in complete agreement with the results obtained from the numerical integration of QKE. Furthermore, we show that the evolution during the slow phase of the dynamics can itself be separated into two additional stages with different scaling behavior if the bath is at very low temperatures. During the time window where $T \gg T_f$ and for an irrelevant bath, temperature displays power-law behavior in time given by

$$T_{\text{eff}}(t) \propto t^{-\frac{1}{a-a_c}}, \tag{1}$$

while for a marginal bath $T_{\text{eff}}(t) \propto e^{-\Gamma t}$. For $T - T_f \ll T_f$ there is a crossover where the power-law decay for the irrelevant bath becomes exponential in time. We find the scaling form of the decay rate during this stage to be

$$\Gamma \propto T_f^{a-a_c}, \tag{2}$$

for the NFL phase and $\Gamma \propto T^{1+a}$ for FL phase (see Appendix D). The faster relaxation at low temperatures can be considered as a fingerprint of the NFL phase.

III. THE MODEL

A. The Yukawa-SYK model

The Yukawa-SYK model is a system of N phonon and $2N$ fermion species in the exactly solvable limit $N \to \infty$. The Hamiltonian of the system is

$$H = \frac{1}{2}\sum_{k=1}^{N}\left(\pi_k^2 + \omega_0^2\phi_k^2\right) + \frac{1}{N}\sum_{\substack{ijk\\ \sigma=\pm}}^{N} g_{ij,k}\phi_k\psi_{i\sigma}^{\dagger}\psi_{j\sigma}. \tag{3}$$

The phonon fields ϕ_k and their conjugate momenta π_k satisfy the commutation relation $[\phi_k, \pi_l] = i\delta_{kl}$ and have the bare gap ω_0, while fermion operators are defined by the anticommutation relation $\{\psi_{i\sigma}, \psi_{j\sigma'}^{\dagger}\} = \delta_{ij}\delta_{\sigma\sigma'}$. The random couplings $g_{ij,k} \equiv g'_{ij,k} + ig''_{ij,k}$ are chosen from Gaussian ensembles with zero means and equal second moments given by

$$\overline{g'_{ij,k}g'_{nm,l}} = \frac{g^2}{2}(\delta_{in}\delta_{jm} + \delta_{im}\delta_{jn})\delta_{kl}, \tag{4}$$

$$\overline{g''_{ij,k}g''_{nm,l}} = \frac{g^2}{2}(\delta_{in}\delta_{jm} - \delta_{im}\delta_{jn})\delta_{kl}. \tag{5}$$

We note that one can define the Yukawa-SYK model for N fermion and M phonon species. The resulting theory is still critical at low temperatures in the limit $N, M \to \infty$ as long as $\frac{N}{M}$ is finite [22,25]. The strength of g' and g'' can also be different. This will give an effective interaction between fermions in the Cooper channel. Since we are only interested in the dynamics of the model in the normal phase, we increase the pair-breaking and thus tune the superconducting pairing to zero by taking the same variance for g' and g'' [28].

The Hamiltonian in Eq. (3) becomes exactly solvable in the limit $N \to \infty$ as the vertex corrections vanish in this limit and a closed system of self-consistent equations for fermion and phonon Green's functions can be obtained [22]. A key feature of the system is that particle-hole fluctuations always renormalize the effective phonon gap down to zero as $T \to 0$. This is a consequence of the large DOS of fermions at low frequencies in the large-N limit. Unlike the usual scenario where the quantum critical point is reached by tuning a parameter in the Hamiltonian, this model has self-tuned criticality at sufficiently low temperatures for all values of g and ω_0 [22,23,25,27,28,31]. Due to the disappearance of the phonon

gap, both fermions and phonons become critical at low temperatures where the system is in the NFL phase. In this regime, the diagonal element of imaginary time Green's functions have the following behavior at large time separations:

$$G(\tau) \equiv -\frac{1}{2N}\sum_{i\sigma}\langle\psi_{i\sigma}(\tau)\psi^{\dagger}_{i\sigma}(0)\rangle \propto \frac{\mathrm{sgn}(\tau)}{|\tau|^{2\Delta}}, \tag{6}$$

$$D(\tau) \equiv -\frac{1}{N}\sum_{k}\langle\phi_k(\tau)\phi_k(0)\rangle \propto \frac{1}{|\tau|^{2-4\Delta}}. \tag{7}$$

The parameter Δ is independent of the microscopic details and reads

$$\Delta \approx 0.42. \tag{8}$$

Therefore the scaling dimensions of the fields at the NFL fixed point are given by $[\psi] = \Delta$ and $[\phi] = 1 - 2\Delta$. One can show that the effective phonon gap scales with temperature as $\omega^2_{\mathrm{eff}} \sim T^{4\Delta-1}$ at low temperatures. At high temperatures, phonons act as static impurities for fermions and the system is in the universality class of the SYK_2 model given by Eq. (19) with constant fermionic DOS at low energies. For more detail about the Yukawa-SYK model, we refer the reader to Refs. [22,25].

B. The bath

1. General considerations

Thermalization is a by-product of coupling the degrees of freedom in the bath to the degrees of freedom in the system. In general, the Hamiltonian of system-bath coupling is given by

$$H_{\mathrm{SB}}(t) = \sum_{ij}\left[a_{ij}\mathcal{O}^S_i(t)\mathcal{O}^B_j(t) + \mathrm{H.c.}\right], \tag{9}$$

where the operators $\mathcal{O}^S_i$ and $\mathcal{O}^B_i$ only contain the degrees of freedom in the system and the bath, respectively. In order to proceed, we assume that the effect of the system-bath coupling on the bath degrees of freedom is negligible. This means that the evolution of $\mathcal{O}^B_i$ is approximately given by $\frac{d}{dt}\mathcal{O}^B_i \approx i[H_B, \mathcal{O}^B_i]$, which is justified as long as the number of degrees of freedom in the bath is much larger than the number of degrees of freedom in the system.

We assume that the temperature of the bath is low enough that the system eventually will end up in the critical phase. As a result, we expect the scaling dimension of $\mathcal{O}^S_i$ to be determined by the scaling dimensions of ϕ_k and $\psi_{i\sigma}$ at the NFL fixed point. For $\mathcal{O}^S_i \sim \psi^{\dagger n}\psi^{n'}\phi^m$ by using Eqs. (6) and (7) we find the scaling dimension of the coupling a_{ij} at the NFL fixed point

$$[a_{ij}] = 1 - (n+n')\Delta - m(1-2\Delta) - \left[\mathcal{O}^B_j\right]. \tag{10}$$

Couplings can be organized according to the sign of their scaling dimension as relevant ($[a_{ij}] > 0$), marginal ($[a_{ij}] = 0$), and irrelevant ($[a_{ij}] < 0$). In the language of renormalization group, the effect of relevant couplings is pronounced at low energies. Marginal and irrelevant couplings are supposed to only alter the nonuniversal properties of the system, since their effect is suppressed at low energies. This does not mean, though, that irrelevant couplings are unimportant as they still can thermalize the system via coupling to high-energy modes.

Based on Eq. (10), we see that couplings with higher powers of fermion and phonon operators are generally less efficient. Therefore, it is permissible to neglect higher-order operators and to only keep those with the lowest-order consistent with the symmetries.

Below, we consider two general classes of phonon and fermion baths relevant to the Yukawa-SYK model. Using aforementioned scaling arguments, we will explain that the setup in Fig. 1(a) is the physically most relevant one that preserves the NFL phase at low temperatures.

2. Phonon bath

A phonon bath consists of a set of phonon displacement operators $\{X_l\}$ together with their conjugate momenta $\{P_l\}$. We assume that instead of having H_B, we know all of the connected correlation functions of the bath. For our purposes, though, only the two-point functions are required,

$$\mathfrak{D}_{ij}(t,t') = -i\langle X_i(t)X_j(t')\rangle. \tag{11}$$

We have assumed that the bath is Z_2 symmetric, so correlation functions with an odd number of phonon operators vanish. We want to find the net effect of system-bath coupling on the dynamics of the system. In order to do so, we need to integrate out the bath degrees of freedom. Due to the potentially nonlocal behavior of the correlation functions in Eq. (11), integrating out the bath degrees of freedom can induce correlations in the system that are nonlocal in time. Also, coupling to the bath can make the off-diagonal Green's functions of the system like $\langle\phi_k\phi_l\rangle$ nonvanishing. While the former effect is actually a desirable feature that can lead to interesting physics, the latter can ruin the exact solvability of the model. Two ways to work around this issue is to use an SYK-like random system-bath coupling where the induced off-diagonal elements vanish in the large-N limit [45–47] or to couple each degree of freedom in the system to a separate bath. While we explicitly take the latter route, one can show that the former approach gives similar results.

The lowest-order terms in Eq. (9) for a phonon bath have the form $X\phi$. Note that the coupling of the bath phonons to density fluctuations of fermions $X\psi^{\dagger}\psi$ is less relevant than the phonon coupling and can be ignored. We assume that for every phonon mode in the system ϕ_k, there is effectively one independent but similar mode in the bath X_k coupled to the phonon mode. As a result, we can write

$$H_{\mathrm{SB}} = \sum_k \phi_k X_k. \tag{12}$$

Therefore, we are taking each X_k to be a separate Caldeira-Leggett bath [40,49]. The bath correlation functions are diagonal and time-translation invariant:

$$\langle X_i(t)X_j(t')\rangle = i\delta_{ij}\mathfrak{D}(t-t'). \tag{13}$$

The response and Keldysh correlation functions of the bath are defined as

$$\mathfrak{D}^R(t) = \Theta(t)[\mathfrak{D}(t) - \mathfrak{D}(-t)], \tag{14}$$

$$\mathfrak{D}^K(t) = \mathfrak{D}(t) + \mathfrak{D}(-t). \tag{15}$$

The spectral density of phonons in the bath $J(\omega)$ can be found from $J(\omega) = -\mathrm{Im}\,\mathfrak{D}^R(\omega)$. We assume that $J(\omega)$ is given by the generic expression

$$J(\omega) = \gamma \sin\left(\frac{\pi a}{2}\right) \mathrm{sgn}\,(\omega)|\omega|^a e^{-|\omega|/\omega_c}. \tag{16}$$

The parameter γ determines the strength of system-bath coupling and ω_c is a cut-off energy scale assumed to be larger than relevant energy scales in the system. Depending on the value of a, the bath is usually called Ohmic ($a = 1$), super-Ohmic ($a > 1$), or sub-Ohmic ($a < 1$). The real part of $\mathfrak{D}^R$ can be found from $J(\omega)$ using Kramers-Kronig relations. The Keldysh function $\mathfrak{D}^K$ is found from the condition of thermal equilibrium for the bath and using FDT (28). The low-frequency limit of Eq. (16) gives us the scaling dimension of X

$$[X] = \frac{1+a}{2}. \tag{17}$$

Putting this in Eq. (10) we see that H_{SB} is irrelevant for

$$a > a_c \equiv 4\Delta - 1. \tag{18}$$

The value for the threshold exponent a_c coincides with the power of the frequency or temperature divergence of critical phonons [22]. Hence, the NFL phase of the Yukawa-SYK model survives after coupling the system to a wide range of generic cold phonon baths, unlike coupling to a fermion bath were the simplest system-bath coupling consisting of direct charge transfer between the system and the reservoir destroys the NFL phase as was shown before [45,46,67]. This point becomes relevant by noting that in the real-world electron-phonon systems, thermalization dominantly occurs through the interaction of phonons with the environment.

Notice, with the above given value for Δ follows $a_c \approx 0.68$. Hence, our analysis applies to super-Ohmic, Ohmic, and $a > a_c$ sub-Ohmic baths. By varying the ratio M/N of the phonon and fermion modes the exponent Δ varies between $\frac{1}{4}$ and $\frac{1}{2}$ [22], such that $0 < a_c < 1$. Hence, our analysis is always applicable to the Ohmic and super-Ohmic regime.

3. Fermion bath

We consider a particle-hole symmetric fermion bath described by the set of fermion operators $(\chi^\dagger_{i\sigma}, \chi_{i\sigma})$. We assume the bath respects $SU(2)$ and $U(1)$ symmetries and therefore conserves total spin and charge. Again, we use Eq. (10) and only consider the lowest-order terms in ψ and ϕ that conserve spin and charge in the system-bath mixture to see that the most relevant terms in H_{SB} are direct fermion tunneling $\chi^\dagger_\sigma \psi_\sigma + \psi^\dagger_\sigma \chi_\sigma$ and fermion-phonon scattering $\chi^\dagger_\sigma \chi_\sigma \phi$. A generic fermion bath has a nearly uniform density of states at low energies and is conveniently modeled by a SYK_2 system defined as

$$H_{\mathrm{SYK2}} = -\frac{1}{\sqrt{N_B}} \sum_{\substack{ij \\ \sigma=\pm}}^{N_B} t_{ij} \chi^\dagger_{i\sigma} \chi_{j\sigma}. \tag{19}$$

The random hopping term $t_{ij} = -t^\star_{ij}$ is chosen from a Gaussian ensemble with zero mean and second moment $\overline{|t_{ij}|^2} = t^2$. The Hamiltonian in Eq. (19) can be solved after taking the average over the random hopping, resulting in the well-known semicircular DOS. A convenient way to define the tunneling Hamiltonian such that it preserves the exact solvability of the model is to take

$$H_{\mathrm{SB}} = -\frac{1}{\sqrt{N_B}} \sum_{i}^{N} \sum_{j}^{N_B} \sum_{\sigma=\pm} (\alpha_{ij} \psi^\dagger_{i\sigma} \chi_{j\sigma} + \mathrm{H.c.}), \tag{20}$$

where $\overline{|\alpha_{ij}|^2} = \alpha^2$ and $\overline{\alpha_{ij}} = 0$. The prefactor in Eq. (20) ensures that the effect of system-bath coupling on the bath is $\mathcal{O}(N/N_B)$ and therefore the bath is not affected by H_{SB} when $N_B \gg N$. According to Eq. (19), the scaling dimension of χ is $\frac{1}{2}$. By putting this in Eq. (10), we see that (20) is a relevant coupling destroying the NFL phase and as a result, the low-energy limit of the system is a FL with linearly Landau-damped phonons.

In case of coupling phonons to a bath of fermions described by Eq. (19), we can use a Yukawa vertex similar to the original model in Eq. (3)

$$H_{\mathrm{SB}} = \frac{1}{\sqrt{NN_B}} \sum_{k}^{N} \sum_{\substack{ij \\ \sigma=\pm}}^{N_B} \lambda_{ij,k} \chi^\dagger_{i\sigma} \chi_{j\sigma} \phi_k. \tag{21}$$

It is easy to check that this coupling is irrelevant and due to the uniform DOS of the bath, contributes to linear Landau damping of phonons similar to second term in Eq. (D9). At low energies, this regime is similar to coupling phonons to an Ohmic phonon bath corresponding to $a = 1$ in Eq. (16) and hence does not require a separate treatment.

IV. KELDYSH FORMALISM

A. General definitions

We only mention briefly the essential concepts used in our work and refer readers to Ref. [40] for a detailed treatment of Keldysh formalism. In Keldysh approach, we work with greater $G^>$ and lesser $G^<$ correlation functions

$$G^>(t,t') \equiv -i\langle \hat{a}(t)\hat{a}^\dagger(t')\rangle, \tag{22}$$

$$G^<(t,t') \equiv -i\xi\langle \hat{a}^\dagger(t')\hat{a}(t)\rangle, \tag{23}$$

where $\xi = \pm$ corresponds to bosonic (+) and fermionic (−) statistics for $\hat{a}$. In the equilibrium formalism, the central objects of study are time-ordered correlation functions and the *physically measurable* correlation functions are only found at the end of calculation using analytical continuation, whereas in Keldysh field theory the response and Keldysh (symmetric) correlation functions can be found directly from Eq. (22),

$$G^R(t,t') \equiv \Theta(t-t')[G^>(t,t') - G^<(t,t')], \tag{24}$$

$$G^A(t,t') = [G^R(t,t')]^\dagger, \tag{25}$$

$$G^K(t,t') \equiv G^>(t,t') + G^<(t,t'). \tag{26}$$

In Keldysh field theory we are not limited to thermal states and, in general, the evolution of Green's functions in (22) is given by QKE which are a set of self-consistent integrodifferential equations between correlation functions of different order. For a generic interacting system there are an infinite

number of these equations, a quantum counterpart of the BBGKY hierarchy [68]. Accordingly, a truncation of QKE is often required which inevitably results in approximate solutions. For SYK models, however, and, as we show below, QKE become closed at the level of two-point functions in the limit $N \to \infty$, allowing us to monitor the dynamics exactly.

For steady states, Green's functions depend on $t - t'$, allowing us to take their Fourier transform. The spectral density of single-particle states $\mathcal{A}(\omega)$ is determined by

$$\mathcal{A}(\omega) = -2\,\mathrm{Im}\,G^R(\omega). \tag{27}$$

Particularly in thermal equilibrium and at temperature T, the FDT relates $G^K(\omega)$ to $\mathcal{A}(\omega)$ via

$$\left[\frac{iG^K(\omega)}{\mathcal{A}(\omega)}\right]^{\xi} = \tanh\frac{\omega}{2T}. \tag{28}$$

One usually can regard Eq. (28) as a relation that gives G^K in terms $\mathcal{A}$ when the temperature is known. Out of equilibrium, time-translation symmetry is usually broken and Green's functions are not only functions of $t - t'$. As a result, there is no a unique way to extend Eqs. (27) and (28) to out-of-equilibrium situations. Two commonly used extensions are the Wigner transformation defined by [40]

$$G(t,\omega) \equiv \int_{-\infty}^{+\infty} G\left(t + \frac{\tau}{2}, t - \frac{\tau}{2}\right) e^{i\omega\tau}\, d\tau, \tag{29}$$

and Fourier transformation along the "corner slice" given by [66]

$$G(t,\omega) \equiv \int_{-\infty}^{+\infty} [\Theta(\tau)G(t, t-\tau) + \Theta(-\tau)G(t+\tau, t)]e^{i\omega\tau}\, d\tau. \tag{30}$$

Both definitions are expected be equivalent for steady states and also non-steady states if the change in $G(t,t')$ along the center-of-mass coordinate $\frac{t+t'}{2}$ is slower than the change along $t - t'$. As a result, the two definitions in Eqs. (29) and (30) can give quite different results out of equilibrium. Although the Wigner transformation is the most commonly used definition, it violates the causal structure of kinetic equations given in Eq. (52) below. The same does not happen for integration over the corner slice which is actually the natural choice considering how Green's functions are evolved in time by QKE (Appendix A). For instance, in a quench at $t = t_0$, the function $G(t,\omega)$ defined according to Eq. (29) displays nontrivial dynamics at $t < t_0$ before the quench happens. This issue becomes more pronounced in critical systems where memory effects are strong due to the slow decay of correlations in time. Henceforth, we employ the corner slice to define time-dependent Green's functions in the frequency domain. The spectral density at time t is defined analogously to Eq. (27). We define the FDR as

$$F(t,\omega) = \left[\frac{iG^K(t,\omega)}{\mathcal{A}(t,\omega)}\right]^{\xi}, \tag{31}$$

which can be used to find the nonequilibrium one-particle distribution function $n(t,\omega)$ according to [40]

$$F(t,\omega) = [1 + 2\xi\, n(t,\omega)]^{-\xi}. \tag{32}$$

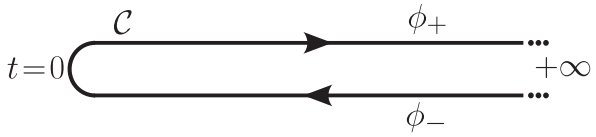

FIG. 2. The closed time contour in the Schwinger-Keldysh formalism starts at the initial moment of the evolution ($t = 0$) and goes to infinite future and back. Every field is defined on $\mathcal{C}$. Equivalently, each field is decomposed to its forward and backward components.

An effective temperature $T_{\mathrm{eff}}(t)$ can be defined if for small frequencies $n(t,\omega)$ is approximated by the Bose-Einstein (Fermi-Dirac) distribution for bosons (fermions)

$$\tanh\frac{\omega}{2T_{\mathrm{eff}}(t)} \approx F(t,\omega). \tag{33}$$

Note that, in out-of-equilibrium situations the temperature is found by the best fitting of a hyperbolic function to $F(t,\omega)$. In equilibrium, FDT is used to obtain G^K in terms of spectral density and temperature.

Keldysh field theory can also be expressed in the path integral language. This can be easily seen by looking at the evolution of density matrix

$$\rho(t) = U(t,0)\rho_0 U^{\dagger}(t,0), \tag{34}$$

where ρ_0 is the initial density matrix and U is the unitary time-evolution operator. By decomposing time-evolution operators on each side into the multiplication of time-evolution operators over small time steps, inserting resolutions of identity between them and applying a Trotter expansion, we get a path integral for each side corresponding to forward (left side) and backward (right side) directions of integration. The quantum fields of opposite directions are not independent. They are coupled through the matrix element of ρ_0 between the fields of opposite contours at $t = 0$. Moreover, since the trace of $\rho(t)$ is to be calculated eventually, the value of the fields on opposite branches should coincide at the final time. As a result, one can define quantum fields on a closed time contour $\mathcal{C}$ shown in Fig. 2. Naively, the usual temporal integration in the action is replaced by integration over the contour

$$\int_{-\infty}^{+\infty} L(t)\, dt \to \oint_{\mathcal{C}} L(t_c)\, dt_c, \tag{35}$$

while keeping in mind to take care of the boundary conditions mentioned above. Instead of time ordering in the equilibrium formalism, the correlation functions are contour ordered

$$iG(t_c, t_c') \equiv \langle T_{\mathcal{C}} a(t_c)\bar{a}(t_c')\rangle = \xi\langle T_{\mathcal{C}}\bar{a}(t_c')a(t_c)\rangle, \tag{36}$$

where $T_{\mathcal{C}}$ is the contour ordering operator. Equivalently, we can assign each field an extra index corresponding to whether it is on the forward or backward branches of the contour. Then, we have an alternative expression for the greater and lesser correlation functions given in Eq. (22) as

$$G^{>}(t,t') \equiv G(t-,t'+), \tag{37}$$

$$G^{<}(t,t') \equiv G(t+,t'-). \tag{38}$$

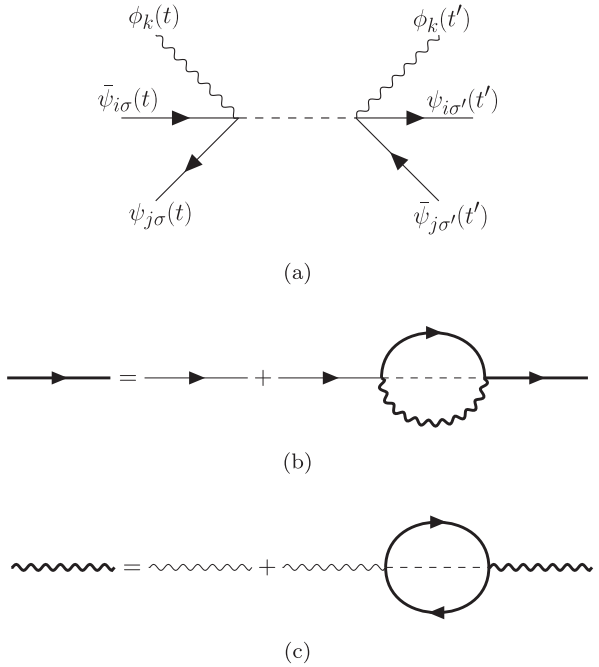

FIG. 3. (a) The interaction vertex for the Yukawa-SYK model after averaging over random interactions. [(b) and (c)] Diagrammatic representation of Dyson equations for (b) fermions and (c) phonons. Narrow lines are bare Green's functions.

B. Keldysh action for the Yukawa-SYK model

When the system is isolated, its evolution follows Eq. (3). Therefore, we can use the Keldysh action of Eq. (3) to describes the dynamics. This action is given by

$$S = S_f + S_{\rm ph} + S_{\rm int}, \tag{39}$$

$$S_f = \sum_{\substack{i \\ \sigma=\pm}}^{N} \oint_{\mathcal{C}} dt_c \, i\bar{\psi}_{i\sigma}(t_c)\partial_{t_c}\psi_{i\sigma}(t_c), \tag{40}$$

$$S_{\rm ph} = -\frac{1}{2}\sum_{k}^{N} \oint_{\mathcal{C}} dt_c \left(\dot{\phi}_k^2 + \omega_0^2\phi_k^2\right), \tag{41}$$

$$S_{\rm int} = -\frac{1}{N}\sum_{\substack{ijk \\ \sigma=\pm}}^{N} g_{ij,k} \oint_{\mathcal{C}} dt_c \, \phi_k(t_c)\bar{\psi}_{i\sigma}(t_c)\psi_{j\sigma}(t_c). \tag{42}$$

In Keldysh formalism, disorder averaging is implemented directly, without the need to use methods like replica trick [69] or supersymmetry [70]. By evaluating the Gaussian integrals over disorder realizations, we get the effective interaction vertex in Fig. 3(a) given by the nonlocal action

$$S_{\rm eff} = \frac{ig^2}{2N^2}\sum_{ij,k}^{N}\sum_{\sigma,\sigma'=\pm} \oint\oint dt_c dt_c' \, \phi_k(t_c)\phi_k(t_c') \times \bar{\psi}_{i\sigma}(t_c)\psi_{j\sigma}(t_c)\bar{\psi}_{j\sigma'}(t_c')\psi_{i\sigma'}(t_c'). \tag{43}$$

The fermion and phonon Green's functions are defined by

$$G(t_c, t_c') = -i\langle T_{\mathcal{C}}\psi_{i\sigma}(t_c)\bar{\psi}_{i\sigma}(t_c')\rangle, \tag{44}$$

$$D(t_c, t_c') = -i\langle T_{\mathcal{C}}\phi_k(t_c)\phi_k(t_c')\rangle, \tag{45}$$

and are assumed to be independent of field indices. The Green's functions satisfy Dyson equations

$$G = G_0 + G_0 \otimes \Sigma \otimes G, \tag{46}$$

$$D = D_0 + D_0 \otimes \Pi \otimes D. \tag{47}$$

G_0 and D_0 are fermion and phonon Green's functions in the absence of interactions and Σ and Π are fermion and phonon self-energies, respectively. For $N \to \infty$, vertex corrections can safely be ignored and self-energies are given by loop diagrams in Figs. 3(b) and 3(c) which read as

$$\Sigma(t_c, t_c') = ig^2 G(t_c, t_c')D(t_c, t_c'), \tag{48}$$

$$\Pi(t_c, t_c') = -2ig^2 G(t_c, t_c')G(t_c', t_c). \tag{49}$$

It may appear that the Dyson equations should be solved self-consistently. Nevertheless, by applying the inverse of free Green's functions on both sides of Eqs. (46) and (47) we get

$$i\partial_{t_c}G(t_c, t_c') = \delta(t_c, t_c') + \oint \Sigma(t_c, \tau_c)G(\tau_c, t_c')\, d\tau_c, \tag{50}$$

$$-\left(\partial_{t_c}^2 + \omega_0^2\right)D(t_c, t_c') = \delta(t_c, t_c') + \oint \Pi(t_c, \tau_c)D(\tau_c, t_c')\, d\tau_c. \tag{51}$$

One can show that (see Appendix A) these equations have a causal structure such that the value of a function at (t, t') only depends on the value of other functions at times (t_1, t_2), satisfying

$$\max\{t_1, t_2\} < \max\{t, t'\}, \tag{52}$$

and therefore we do not need to solve Dyson equations self-consistently. In order to find the dynamics, we have to write Eqs. (50) and (51) in terms of greater and lesser functions and then solve them numerically. While these equations together with FDT are sufficient to find the Green's functions at equilibrium, an accurate numerical solution of integrodifferential equations for time evolution requires us to work with first-order time derivatives. Therefore, we rewrite the equations for phonons (51) in terms of a larger set of first-order equations. This is achieved by introducing two extra correlation functions,

$$B(t_c, t_c') = -i\langle T_{\mathcal{C}}\pi_k(t_c)\phi_k(t_c')\rangle, \tag{53}$$

$$C(t_c, t_c') = -i\langle T_{\mathcal{C}}\pi_k(t_c)\pi_k(t_c')\rangle, \tag{54}$$

where $\pi_k = \dot{\phi}_k$ is the momentum conjugate field of ϕ_k. A detailed discussion of the first-order quantum kinetic equations and their numerical solution can be found in Appendix A.

C. Formulating system-bath coupling

Here we only consider the coupling of phonons to a phonon bath as represented by Eq. (12). For a discussion of fermion bath with the coupling in Eq. (20) in Keldysh language, see Ref. [47].

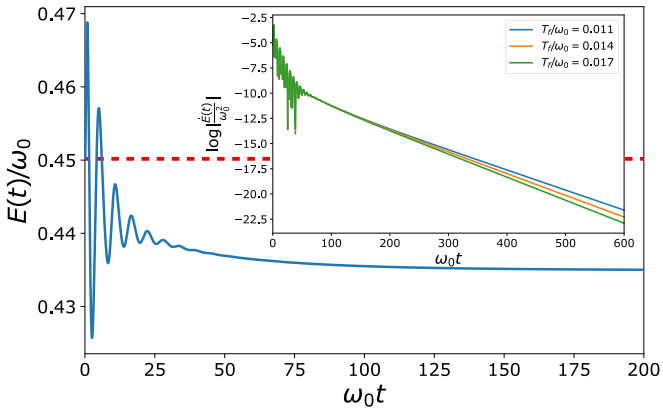

FIG. 4. Total energy as a function of time for $g^2/\omega_0^3 = 0.7$, $a = 1.0$, $T_f/\omega_0 = 0.012$, and $\gamma/\omega_0 = 0.12$. The red dashed line indicates the total energy before the quench. Inset shows the exponential decay of energy at later times with a relaxation rate (given by the slope of the logarithm) that increases with T_f.

Following the arguments of Sec. III B 2, we assume a quadratic Keldysh action for the phonon bath,

$$S_B = \frac{1}{2}\sum_k^N \oint\oint X_k(t_c)\mathfrak{D}^{-1}(t_c, t_c')X_k(t_c')\,dt_c\,dt_c'. \tag{55}$$

The bath Green's function $\mathfrak{D}$ is determined by Eq. (16) and using FDT. Integrating out the bath degrees of freedom and using Eq. (12) gives the action responsible for the thermalization of phonons,

$$S_{\rm SB} = -\frac{1}{2}\sum_k^N \oint\oint \phi_k(t_c)\mathfrak{D}(t_c, t_c')\phi_k(t_c')\,dt_c\,dt_c', \tag{56}$$

which contributes to phonon self-energy in Eq. (49)

$$\Pi(t_c, t_c') = -2ig^2 G(t_c, t_c')G(t_c', t_c) + \mathfrak{D}(t_c, t_c'). \tag{57}$$

V. RESULTS

In Sec. V A we present the results of the numerical solution of QKE [Eqs. (50) and (51)] and by looking at the behavior of effective temperature and the deviation of the system from equilibrium at low energies, we motivate a two-stage picture for dynamics after the quench. In Sec. V B we analyze the first stage of dynamics detail and address the role of phonons and symmetries in the dynamics at early times. The evolution of the system during the second stage of dynamics together with an analytical evaluation of the behavior of relaxation rate are given in Secs. V C and V D, respectively.

A. The two-stage picture of postquench evolution

In this part, we demonstrate the qualitative difference between the behavior of various physical quantities at the early and later periods of the postquench evolution. Accordingly, we separate the dynamics into two stages as was mentioned in Sec. II. By inspecting the total energy (see Appendix B) as a function of time shown in Fig. 4, we observe an oscillatory behavior during the early times after the quench which shortly afterwards turns into a monotonic decrease until the system

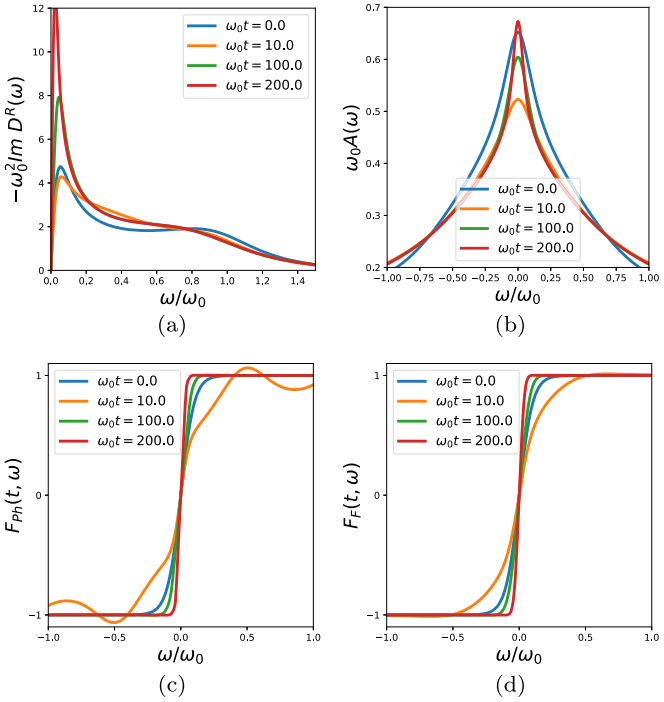

FIG. 5. Top panel: Phonon (a) and fermion (b) spectral densities at different times. We can see a quick deformation in both spectral densities at early times. Bottom panel: FDR for phonons (c) and fermions (d) as a function of frequency at different times. The large early deviation of $F(t, \omega)$ from quasiequilibrium for phonons is clear. After a while, both fermions and phonons display quasiequilibrium behavior. The quench parameters are chosen as $g^2/\omega_0^3 = 0.7$, $a = 1.0$, $\gamma/\omega_0 = 0.12$, $T_i/\omega_0 = 0.05$, and $T_f/\omega_0 = 0.012$.

reaches its final thermal state at $t \to \infty$. This change in the behavior of the energy is the first sign of the two-stage time evolution of the system.

The one particle spectra of fermions and phonons are depicted in Figs. 5(a) and 5(b) at different times. A quick deformation of both fermionic and phononic spectra immediately after the quench is observed throughout the frequency space. On the other hand, the variation in the spectra is slow and gradual at later stages and mostly occurs at low energies. This crossover in the behavior of the evolution of one particle spectrum from early to later stages of the evolution is another manifestation of the fact that the early and later periods require separate physical descriptions.

Another quantity of interest is the distribution of single particle excitations related to the FDR defined in Eq. (31). As it can be seen in Figs. 5(c) and 5(d), the distributions of both phonons and fermions deviate from quasiequilibrium at early times while at later times they appear to be quite close to a thermal state with a time-dependent temperature. A quantitative measure of the deviations from quasiequilibrium can be defined if we assign each species an effective temperature which is read from the slope of the FDR at the origin of the frequency space according to

$$T_{\rm eff}(t) \approx \left.\frac{1}{2\partial_\omega F(t,\omega)}\right|_{\omega\to 0}. \tag{58}$$

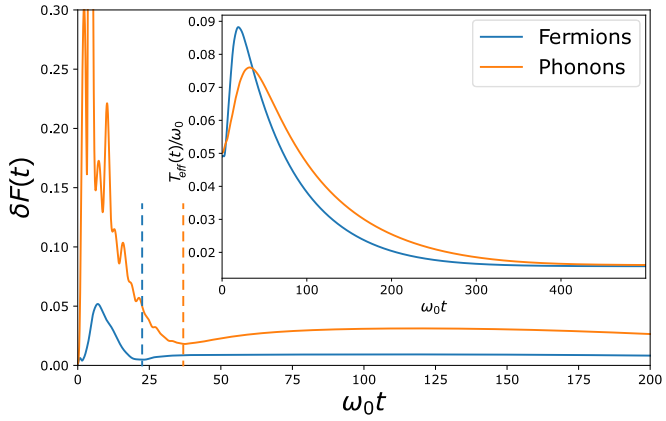

FIG. 6. The deviation of FDR for fermions and phonons from quasiequilibrium defined in Eq. (60) as a function of time. The minima show the transition to the second stage of the dynamics. Furthermore, phonons exhibit considerably larger deviations compared to fermions at all times. Dashed lines indicate the the minima of δF. Inset: The extrapolated effective temperature for fermions and phonons as a function of time. The peaks approximately mark the onset of the second stage of the evolution. The parameters are $g^2/\omega_0^3 = 0.7$, $a = 1.0$, $T_i/\omega_0 = 0.05$, and $\gamma/\omega_0 = 0.12$.

The effective temperatures obtained from Eq. (58) for fermions and phonons is shown in Fig. 6. With the exception of the early times, phonons appear to be at a higher temperature than fermions. This may look counterintuitive from a classical point of view, as phonons are directly coupled to the cold bath while fermions exchange heat with the bath only indirectly via phonons. Nonetheless, quantum effects can explain this behavior as the correlations between fermions and phonons due to their strong interactions render the aforementioned distinction meaningless. This behavior of the strongly interacting NFL phase can be contrasted to the behavior of a similar system with an additional moderate to strong random hopping term for fermions which makes the system a Fermi liquid. In the latter case (see Appendix D), the effective temperature of phonons is smaller than the effective temperature of fermions during the intermediate and later stages of the evolution as the correlations between fermions and phonons are weak compared to the NFL phase.

We use the effective temperatures to define the quasiequilibrium FDRs for phonons and fermions according to

$$F_{\rm eq}(t,\omega) \equiv \tanh \frac{\omega}{2T_{\rm eff}(t)}. \tag{59}$$

The deviation from quasiequilibrium can be defined [46] in terms of the functional norm of the difference between $F(t,\omega)$ found from Eq. (31) and $F_{\rm eq}$ given by Eq. (59),

$$\delta F(t) \equiv \left[\frac{\int_{-\Lambda}^{+\Lambda}[F(t,\omega)-F_{\rm eq}(t,\omega)]^2\,d\omega}{\int_{-\Lambda}^{+\Lambda}F_{\rm eq}^2(t,\omega)\,d\omega}\right]^{\frac{1}{2}}. \tag{60}$$

We have divided the difference by the norm of $F_{\rm eq}$ to obtain the relative deviation. The relative deviation $\delta F(t)$ is shown in Fig. 6 for phonons and fermions. We observe that for both phonons and fermions, there is a temporary increase in $\delta F(t)$ followed by a minimum and then a gradual approach towards the true equilibrium at later times. The oscillations in $E(t)$ stop approximately around the same time (Fig. 4) when $\delta F(t)$ for fermions and phonons reach their minimum. Accordingly, the minima in the deviations of fermions and phonons from quasiequilibrium set a natural boundary between the first and second stages of the evolution.

The separation of the evolution into two stages can also be observed by looking at the behavior of the effective temperature for fermions. We read the effective temperature from the FDR for fermions as their deviation from quasiequilibrium is significantly less than phonons throughout the entire evolution. As it can be seen in Fig. 6, there is a temporary increase in the effective temperature after the quench and as expected from the two-stage picture given above, the location of the peak in the effective temperature is close to the location of the minimum in $\delta F(t)$ for fermions.

Having explained the qualitative differences between early stage and late stage dynamics, we will separately discuss their properties in more details in the following sections.

B. First stage of dynamics

The first distinct feature of the first stage of dynamics is the fast relaxation of both fermion and phonon densities of states [Fig. 5(a) and 5(b)]. Similar behavior has been found in the far from equilibrium dynamics of purely fermionic SYK models [44]. This behavior is pronounced at higher frequencies where the high-frequency components of spectral functions at early times coincide with their value at $t \to \infty$ [see the curves for $\omega_0 t = 10.0$ in Figs. 5(a) and 5(b)].

The second feature is the early oscillatory evolution of total energy. This behavior has not been observed in the thermalization of purely fermionic SYK models [45,46] coupled to IR irrelevant external baths. The appearance of these oscillations may seem inconsistent with the Yukawa-SYK model being in a scale invariant critical state with no characteristic energy scales besides the temperature itself. However, the coupling of the system to the bath introduces new energy scales including the system-bath coupling and the UV cut-off ω_c defined in Eq. (16) which puts a soft upper bound on the energy spectrum of the environment. Furthermore, due to the temporary heating of the system as a result of the sudden coupling of the system to the bath, the system is pushed away from the critical state. This can render the dynamics sensitive to the bare phonon gap ω_0 and the coupling g^2. Phonons as harmonic oscillators exhibit oscillatory behavior and as it can be seen in Figs. 5(a) and 5(c), high-frequency phonons with finite spectral weight are generated in the range of frequencies $\omega \lesssim \omega_0$ after the quench, resulting in the emergence temporary oscillations in the profile of phonon correlation functions over timescales $t \gtrsim 1/\omega_0$ in agreement with the approximate period of initial energy oscillations $\tau \approx 2\pi/\omega_0$ in Fig. 4. For the Yukawa-SYK model, the total energy is given by

$$\frac{E(t)}{N} = \langle \pi^2 \rangle, \tag{61}$$

where the contribution of the potential term ($\sim \frac{1}{2}\omega_0^2\phi^2$) is canceled by the fermion-phonon interaction while the kinetic term is amplified by a factor of 2. We refer the reader to Appendix B for a derivation of this result. The above expression

holds in and out of equilibrium and it directly connects the energy oscillations to the oscillations of phonon correlator as explained before.

The third distinct feature of the first stage of dynamics is the deviation of the populations of both fermions and phonons from a thermal distribution [Figs. 5(c) and 5(d)]. While a temporary distortion in the distribution of particles is naturally expected as a result of the sudden coupling of the system to the bath, the relative robustness of the distribution of fermions compared to phonons as it can be seen in Fig. 6 requires extra physical explanation. At first, one may argue that the substantial difference between the distribution of phonons and fermions comes from coupling the bath directly to phonons while fermions are affected less as they only indirectly interact with the bath through their mutual coupling to phonons. However, this statement cannot fully explain the physics of the problem for two reasons: First, we are dealing with a moderately strong interacting system of fermions and phonons and therefore we expect any perturbations in the phononic sector to be transmitted efficiently to the fermionic sector. Second, the rigidity of the distribution of fermions persists even in case of directly coupling fermions to the bath as long as one crucial condition (see below) is satisfied. The robustness of fermionic distribution can be attributed to two elements: the Pauli's exclusion principle due to fermionic statistics and the global $U(1)$ symmetry of the problem under the transformation $\psi_{i\sigma} \to e^{i\varphi}\psi_{i\sigma}$ which guarantees fermion number conservation. To the extent of our knowledge, the role of $U(1)$ symmetry in the quench dynamics of SYK models has not been investigated before. We will explain below, using Fermi's golden rule arguments, how $U(1)$ symmetry and Fermi statistics restrict the distortion of the fermionic distribution function after a quench.

When we turn on the system-bath coupling by a quench function $f(t)$ [for this work $f(t) \propto \Theta(t)$], excitations are created in the system (the bath is large and assumed to be unaffected by the quench). The energy of these excitations depends crucially on the power spectrum of $f(t)$ defined as $|\tilde{f}(\omega)|^2$, where $\tilde{f}(\omega)$ is the Fourier transform of $f(t)$. The perturbative rate of change in the phonon distribution at energy ω, consistent with the symmetries of the problem to the lowest order in the system-bath coupling, satisfies

$$\partial_t n_{\rm ph}(\omega) \propto \int |\tilde{f}(\epsilon)|^2 J(\omega-\epsilon)\,\rho_{\rm ph}(\omega) \times [n_B(\omega-\epsilon) - n_{\rm ph}(\omega)]\,d\epsilon, \tag{62}$$

where $\rho_{\rm ph}$ is the phonon spectral density, n_B is the distribution of phonons in the bath and $J(\omega)$ is the bath spectral density given in Eq. (16). For a direct coupling between fermions and a phononic bath respecting the $U(1)$ symmetry we have

$$\begin{aligned}\partial_t n_f(\omega) \propto \int d\epsilon \int d\nu\, |\tilde{f}(\epsilon)|^2 \mathcal{A}(\omega) J(\nu)(n_B(\nu)-1) \\ \times \{[1-n_f(\omega)]n_f(\omega-\epsilon-\nu)\mathcal{A}(\omega-\epsilon-\nu) \\ - n_f(\omega)[1-n_f(\omega+\epsilon+\nu)]\mathcal{A}(\omega+\epsilon+\nu)\} \\ + \text{higher-order terms with even powers of } \mathcal{A}(\omega),\end{aligned} \tag{63}$$

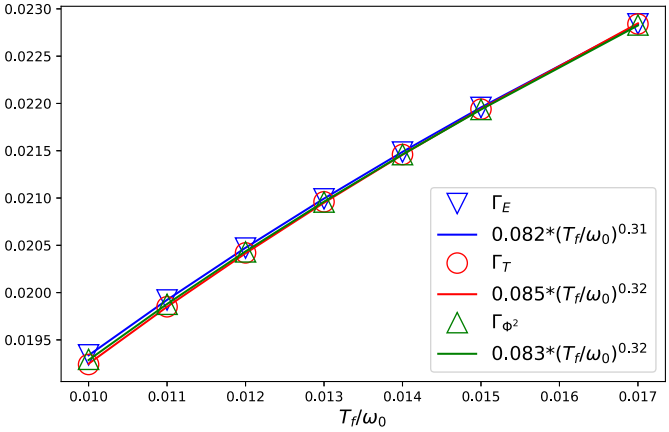

FIG. 7. The relaxation rates of temperature, energy, and $\langle\phi^2\rangle$ together with their power-law fits versus final temperature for $a = 1.0$ (see Table I), $g^2/\omega_0^3 = 0.7$, and $\gamma/\omega_0 = 0.12$.

where $\mathcal{A}(\omega)$ is the fermion spectral density. The fact that we always have even powers of $\mathcal{A}$ is a consequence of the $U(1)$ symmetry in the system. Together with fermionic statistics, this severely restricts the contributing domain of integration in Eq. (63) to excitations close to the Fermi energy. This is in contrast to Eq. (62) for phonons where such restrictions do not hold.

C. Second stage of dynamics

During the second stage of dynamics, we observe a gradual enhancement of the NFL behavior for fermions as the systems cools down which has already been observed in purely fermionic SYK models in the past [46,47]. In addition, phonons are softened over time toward their low-temperature gapless state, an exclusive property of the Yukawa-SYK model.

Shortly after the oscillatory behavior of the energy is over, the energy starts to relax exponentially to its final value (inset of Fig. 4)

$$E(t) \approx E_f + A_E e^{-\Gamma_E t}. \tag{64}$$

The energy relaxation rate Γ_E depends on the final temperature and has a power-law scaling with T_f (Fig. 7).

The effective temperature also follows a monotonic decrease during the second stage. We see that the late stage relaxation follows an exponential trend,

$$T_{\rm eff}(t) \approx T_f + A_T e^{-\Gamma_T t}. \tag{65}$$

TABLE I. Comparison of the exponent of temperature relaxation rate x defined as $\Gamma_T \propto T_f^x$ found from the numerical solution of quantum kinetic equations and the analytical hydrodynamical approximation. The parameters a and Δ are respectively defined in Eqs. (16) and (8).

Bath exponent	Numerics	Analytics $(a+1-4\Delta)$
$a = 1$	0.32	0.32
$a = 1.2$	0.53	0.52
$a = 0.9$	0.21	0.22

The temperature relaxation rate Γ_T (Fig. 7) turns out to be close to the energy relaxation rate Γ_E for different values of a (Table I) and has the same scaling with T_f as Γ_E given by Eq. (66).

The exponential relaxation is not exclusive to total energy and temperature. The fluctuations of phonon displacement $\langle\phi^2\rangle$ also relax exponentially to their final value, with the same rate given above (Fig. 7). Moreover, total energy is proportional to $\langle\pi^2\rangle$ according to Eq. (61) and therefore this quantity has the same relaxation profile. The fact that all of these quantities relax in the same way as temperature suggests that the dynamics of the system is completely captured by the effective temperature. This is consistent with the general picture of quantum critical systems, where temperature is the only relevant energy scale [71]. We will confirm this hypothesis in the next section and find the dependence of Γ on T_f as

$$\Gamma_E \sim T_f^{a-4\Delta+1}, \tag{66}$$

where a is the exponent of the phonon bath defined in Eq. (16) and Δ is given by Eq. (8). We see that the exponent is always positive for an irrelevant bath according to Eq. (18).

We can evaluate the efficiency of the bath to thermalize the critical system by looking at Eq. (66). As the bath becomes less relevant in the IR limit, the relaxation rate gets suppressed at small temperatures. The limit $a = 4\Delta - 1$ when the exponent of T_f in Eq. (66) becomes zero corresponds to a marginal system-bath coupling.

D. Hydrodynamical approximation

As shown before, all physical observables relax with the same rate in the slow stage of thermalization. This can happen, for instance, if all of these quantities could be uniquely determined by only one of them such as the temperature. The SYK model and its variants are all-to-all connected interacting models which can efficiently redistribute energy [18,41,44,48]. When we couple these systems to thermal baths, we expect the energy transfer between the system and the bath to be the slowest relevant process and, thus, determining the rate of relaxation. At every instant of time, the system is in local equilibrium and all of the observables are given by their value in equilibrium at temperature $T_{\rm eff}(t)$. This situation is similar to the "hydrodynamic" relaxation of translationally invariant initial states. Despite the similarity, there is an important difference between our setup and those studied by Refs. [61–63] in which the energy is locally conserved and, hence, is described by a stochastic diffusion equation after local equilibrium has been established. The scale invariance of the diffusion equation results in the power-law decay of observables at long times, whereas in our system, the energy is not conserved due to coupling to the bath and the long time decay is exponential, except for when the bath is at zero temperature (see the end of this section). Possibly, our case is closer to the hydrodynamic regimes discussed in Refs. [64,65] where collisions are faster than losses, although these systems are integrable in the absence of losses in contrast to the Yukawa-SYK model.

To check the validity of such a "hydrodynamic" hypothesis, we assume the system to be in thermal equilibrium at temperature $T_{\rm eff}(t)$ and find energy transfer rate and total energy in terms of $T_{\rm eff}(t)$. We solve this closed set of equations to find the relaxation profile of the temperature and compare the results to the numerics of Sec. V C. The energy transfer rate between the system and the bath can be found in terms of the Green's functions of phonons in the system and the bath (see Appendix C),

$$\begin{aligned}\partial_t E(t) = &-\frac{iN}{2}\int_0^t [\mathfrak{D}^K(t',t)\partial_t D^A(t',t)\\ &+ \mathfrak{D}^R(t,t')\partial_t D^K(t',t)]dt'.\end{aligned} \tag{67}$$

When the system is in a quasithermal state with the slowly varying temperature $T_{\rm eff}(t)$, we can assume time translation symmetry and use the expressions for functions appearing in Eq. (67) at thermal equilibrium to get

$$\begin{aligned}\partial_t E =& N\int \frac{d\omega}{2\pi}\omega J(\omega)\,\mathrm{Im}\,D^R(\omega)\\ &\times\left\{\coth\left[\frac{\omega}{2T_{\rm eff}(t)}\right]-\coth\left(\frac{\omega}{2T_f}\right)\right\},\end{aligned} \tag{68}$$

where $J(\omega)$ was given by Eq. (16). At low temperatures, we can employ the scaling form of the phonon Green's function [22] to find

$$\partial_t E = -N\gamma g^{2(4\Delta-1)}\omega_0^{-8\Delta}T_{\rm eff}^{3+a-4\Delta}f\left(\frac{T_{\rm eff}}{T_f}\right), \tag{69}$$

where $f(x)$ is given by

$$\begin{aligned}f(x) =& -\frac{2^{1+a}\pi\cos(2\pi\Delta)}{\cos(\pi\Delta)\sin^3(\pi\Delta)\Gamma(2\Delta)\Gamma(1-4\Delta)}\\ &\times\left(\frac{2\Delta-1}{8\Delta^2\sin\frac{\pi}{2\Delta}}\right)^{4\Delta}\int_0^\infty y^{a+2-4\Delta}(\coth y-\coth yx)\,dy,\end{aligned} \tag{70}$$

and it has the following limiting behaviors:

$$\lim_{x\to 1} f(x) = 0, \qquad \lim_{x\to\infty} f(x) = \text{const}. \tag{71}$$

For finite T_f and $T_{\rm eff}(t) \gtrsim T_f$, Eq. (69) gives

$$\partial_t E \propto T_f^{2+a-4\Delta}(T_{\rm eff} - T_f). \tag{72}$$

For a zero temperature bath or when $T_f \ll T_{\rm eff} \lesssim g^2/\omega_0^2$, which corresponds to the intermediate stage of the evolution of the system coupled to a finite temperature but sufficiently cold bath, we find

$$\partial_t E \propto T_{\rm eff}^{3+a-4\Delta}. \tag{73}$$

To identify a closed differential equation for the time evolution of the temperature, we note that, similarly to the SYK model [18], the Yukawa-SYK model has a linear specific heat at small temperatures,

$$E(T) - E(0) \approx \tfrac{1}{2}NcT^2, \tag{74}$$

where c is a nonuniversal parameter which can be evaluated numerically. The linear specific heat is a consequence of the reparameterization symmetry of the Yukawa-SYK model in the infrared limit [72] which is spontaneously broken by the saddle-point solution in Eqs. (6) and (7). The degeneracy of

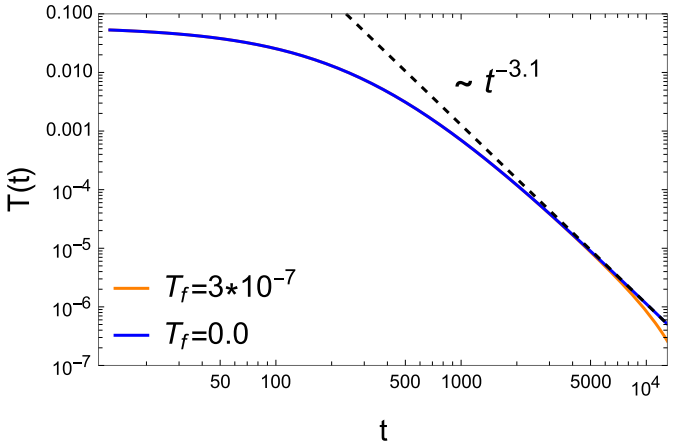

FIG. 8. Numerical solution of Eq. (75) for the two cases of zero and finite-temperature Ohmic baths ($a = 1$). The late time power-law decay of temperature is evident for $T_f = 0$. For a finite-temperature bath, the power-law regime can exists only transiently and it eventually turns into an exponential relaxation at longer times.

the resulting gapless Goldstone modes is lifted by the contributions from UV modes, resulting in a Schwarzian term in the effective action of the fluctuations around the saddle point. Since the irrelevant bath does not affect the low-energy physics of the system, we expect a Schwarzian term to be present in the low-energy action of a system coupled to bath. The Schwarzian results in a linear specific heat [18] at small temperatures.

By combining (69) and (74) we get a kinetic equation that governs the time variation of the temperature:

$$\frac{dT_{\rm eff}}{dt} = -\frac{\gamma}{c} g^{2(4\Delta-1)} \omega_0^{-8\Delta} T_{\rm eff}^{2+a-4\Delta} f\left(\frac{T_{\rm eff}}{T_f}\right). \tag{75}$$

As a result, for the regime $T_{\rm eff}(t) \gtrsim T_f$ the evolution of temperature is given by

$$\frac{dT_{\rm eff}}{dt} \propto -\gamma T_f^{1+a-4\Delta}(T_{\rm eff} - T_f). \tag{76}$$

Therefore T relaxes exponentially to T_f with a rate satisfying (66). The similarity between Γ_E and Γ_T is now clear from (72).

In the limit of a zero or extremely low-temperature bath in Eq. (73), we get a power-law decay for temperature,

$$\frac{dT_{\rm eff}}{dt} \propto -T_{\rm eff}^{2+a-4\Delta} \to \lim_{t\to\infty} T_{\rm eff}(t) \propto t^{-\frac{1}{1+a-4\Delta}}. \tag{77}$$

The result of the numerical evaluation of Eq. (75) is given in Fig. 8 for baths at zero and finite but small temperatures. As it can be seen, the regime of power-law relaxation of temperature can be difficult to access for a finite-temperature bath, as the system may enter the exponential relaxation regime before the power-law behavior can emerge. This is the case for the numerical data presented in this paper as the limited numerical resources prevented us to resolve temperatures which are small enough to observe the power-law decay in Eq. (77).

VI. CONCLUSIONS

In this work, we studied the quench dynamics of a variant of the SYK model with electron-phonon interactions coupled to an external bath. Based on scaling analysis and numerical evaluation of quantum kinetic equations, we showed that for couplings to a generic phonon bath described by the Caldeira-Leggett model, the critical behavior of the system is unaffected. Furthermore, we observed that the system relaxes quickly at short-time/high-frequency scales while global thermalization, corresponding to the equilibration of small-frequency modes, takes longer. The system exhibits quasiequilibrium behavior at a time-dependent effective temperature obtained from the fluctuation-dissipation theorem. Using the quasiequilibrium state of the system, we provided an analytical description of the relaxation profile of total energy and temperature in agreement with our numerics. We found that while phonons are directly coupled to the bath, fermions have a lower temperature due to strong correlations between the two species in the NFL phase, while the opposite is true in the FL state.

There are multiple directions to pursue in the context of the dynamics of what we generally call fermion-boson SYK (FB-SYK) systems. One clear extension of our work is to study quenches in the presence pairing interactions, i.e., when the real and imaginary parts of $g_{ij,k}$ in Eq. (3) have different second moments. This is the direction that we are currently following. One could also study the evolution of FB-SYK systems under the influence of an external periodic drive. The driving field can be coupled to fermions (similarly to Ref. [48] for the SYK model) or phonons. Furthermore, phonons can be driven linearly or parametrically with the possibility of different qualitative and quantitative behaviors. In the superconducting phase, one may investigate the destruction or possibly the transient amplification [50,51] of superconducting correlations in a system with pairing of incoherent fermions.

Note added. During the submission process of this paper, we became aware of a recent work [73] where the quench dynamics of an isolated superconducting Yukawa-SYK model is studied using Keldysh field theory.

ACKNOWLEDGMENTS

This work was supported by the Deutsche Forschungsgemeinschaft (DFG, German Research Foundation) through TRR 288-422213477 (Projects No. B09 and No. A07) and by the Dynamics and Topology Centre funded by the State of Rhineland Palatinate and Topology Centre funded by the State of Rhineland Palatinate. The authors gratefully acknowledge the computing time granted on the supercomputer MOGON 2 at Johannes Gutenberg-University Mainz [74].

APPENDIX A: QUANTUM KINETIC EQUATIONS

We start from an alternative expression for the free phonon action using Legendre transformation

$$\begin{aligned} S_{\rm ph} &= \sum_k^N \oint_{\mathcal{C}} dt_c \left[\pi_k \partial_{t_c} \phi_k - H(\pi_k, \phi_k)\right] \\ &= \frac{1}{2} \sum_k^N \oint_{\mathcal{C}} dt_c \, \Phi_k^T \cdot \mathbf{D_0}^{-1} \cdot \Phi_k, \end{aligned} \tag{A1}$$

where $\Phi_k = (\phi_k, \pi_k)^T$ and

$$\mathbf{D_0}^{-1} = \begin{pmatrix} -\omega_0^2 & -\partial_{t_c} \\ \partial_{t_c} & -1 \end{pmatrix}, \tag{A2}$$

The Green's function matrix is defined as

$$\mathbf{D}(t_c, t_c') \equiv \begin{bmatrix} D(t_c, t_c') & \tilde{B}(t_c, t_c') \\ B(t_c, t_c') & C(t_c, t_c') \end{bmatrix}, \tag{A3}$$

where D, B, and C were defined in Eqs. (45), (53), and (54). We also have $\tilde{B}(t_c, t_c') \equiv B(t_c', t_c)$ where we have avoided using the transpose sign B^T as superscripts are reserved for Keldysh indices. Then, the matrix form of Dyson equation in (51) is given by

$$\mathbf{D_0}^{-1} \cdot \mathbf{D}(t_c, t_c') = \mathbb{1}\delta(t_c, t_c') + \oint \mathbf{\Pi}(t_c, \tau_c) \cdot \mathbf{D}(\tau_c, t_c')\, d\tau_c. \tag{A4}$$

The self-energy matrix has only one nonzero entry,

$$\mathbf{\Pi}(t_c, t_c') = \Pi(t_c, t_c') \begin{pmatrix} 1 & 0 \\ 0 & 0 \end{pmatrix}, \tag{A5}$$

where $\Pi(t_c, t_c')$ is given in (57). Putting (A3) and (A5) in (A4) gives

$$\partial_{t_c} D(t_c, t_c') = B(t_c, t_c'), \tag{A6}$$

$$\partial_{t_c} B(t_c, t_c') = -\delta(t_c, t_c') - \omega_0^2 D(t_c, t_c') - \oint \Pi(t_c, \tau_c) D(\tau_c, t_c')\, d\tau_c, \tag{A7}$$

$$\partial_{t_c} B^T(t_c, t_c') = C(t_c, t_c'), \tag{A8}$$

$$\partial_{t_c} C(t_c, t_c') = -\delta(t_c, t_c') - \omega_0^2 \tilde{B}(t_c, t_c') - \oint \Pi(t_c, \tau_c) \tilde{B}(\tau_c, t_c')\, d\tau_c. \tag{A9}$$

We use Langreth rules [75] and write Eqs. (50) and (A6)–(A9) together with their Hermitian conjugates in terms of greater, lesser, retarded, and advanced functions to get QKE,

$$+i\partial_t G^{\gtrless}(t, t') = \int [\Sigma^R(t, \tau) G^{\gtrless}(\tau, t') + \Sigma^{\gtrless}(t, \tau) G^A(\tau, t'')]\, d\tau, \tag{A10}$$

$$-i\partial_{t'} G^{\gtrless}(t, t') = \int [G^R(t, \tau) \Sigma^{\gtrless}(\tau, t') + G^{\gtrless}(t, \tau) \Sigma^A(\tau, t'')]\, d\tau, \tag{A11}$$

$$\Sigma^{\gtrless}(t, t') = ig^2 G^{\gtrless}(t, t') D^{\gtrless}(t, t'), \tag{A12}$$

$$\partial_t D^{\gtrless}(t, t') = B^{\gtrless}(t, t'), \tag{A13}$$

$$\partial_{t'} D^{\gtrless}(t, t') = \tilde{B}^{\gtrless}(t, t'), \tag{A14}$$

$$\partial_{t'} B^{\gtrless}(t, t') = \partial_t \tilde{B}^{\gtrless}(t, t') = F^{\gtrless}(t, t'), \tag{A15}$$

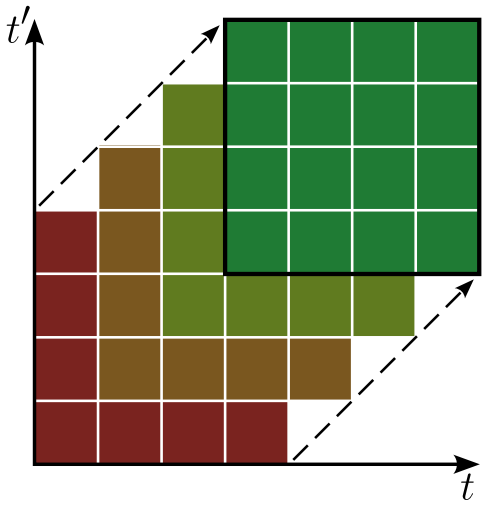

FIG. 9. Illustration of how QKE are solved in the two-dimensional time space.

$$\partial_t B^{\gtrless}(t, t') = -\omega_0^2 D^{\gtrless}(t, t') - \int [\Pi^R(t, \tau) D^{\gtrless}(\tau, t') + \Pi^{\gtrless}(t, \tau) D^A(\tau, t'')]\, d\tau, \tag{A16}$$

$$\partial_t F^{\gtrless}(t, t') = -\omega_0^2 \tilde{B}^{\gtrless}(t', t) - \int [\Pi^R(t, \tau) \tilde{B}^{\gtrless}(t', \tau) + \Pi^{\gtrless}(t, \tau) \tilde{B}^A(\tau, t'')]\, d\tau, \tag{A17}$$

$$\partial_{t'} F^{\gtrless}(t, t') = -\omega_0^2 B^{\gtrless}(t', t) - \int [B^R(t, \tau) \Pi^{\gtrless}(t', \tau) + B^{\gtrless}(t, \tau) \Pi^A(\tau, t'')]\, d\tau, \tag{A18}$$

$$\Pi^{\gtrless}(t, t') = -2ig^2 G^{\gtrless}(t, t') G^{\lessgtr}(t', t) + \mathfrak{D}^{\gtrless}(t, t'). \tag{A19}$$

The phonon self-energy contains the contribution from the bath given by (57). The retarded and advanced functions are defined according to Eqs. (24) and (25). Note that $\tilde{B}^A(t, t') \neq [B^A(t, t')]^T$ but

$$\tilde{B}^A(t, t') = \Theta(t' - t)\big[\tilde{B}^<(t, t') - \tilde{B}^>(t, t')\big] = \Theta(t' - t)\big[B^>(t', t) - B^<(t', t)\big] = B^R(t', t), \tag{A20}$$

therefore the causality of kinetic equations is respected.

In order to numerically solve QKE, we pay attention to the causal structure in (52) and use an implicit midpoint method on an $N \times N$ grid with step size dt (see Fig. 9). To access temperature T, we should be able to resolve frequencies comparable to T. Consequently, the grid size should satisfy the condition $N\, dt \gtrsim \pi T^{-1}$. Furthermore, the step size should be small enough to prevent instabilities of the solution at late stages of the evolution. The main numerical cost comes from increasing the grid size N. We tested two choices of $N = 3000$, $dt = 0.1$ and $N = 5000$, $dt = 0.05$ and the results were in agreement.

APPENDIX B: TOTAL ENERGY

The total energy is given by the expectation value of (3). The contribution of the free phonon term is given by

$$\langle H_{\rm Ph}(t)\rangle = \frac{i}{4}N\big(-\partial_t^2+\omega_0^2\big)D^K(t,t')|_{t'\to t}. \tag{B1}$$

To find the contribution of the interaction term we add the source term $-i\oint J(t)H_{\rm int}(t)\,dt$ to the action and take the functional derivative with respect to the source,

$$\overline{\langle H_{\rm int}(t)\rangle} = i\frac{\delta}{\delta J(t)}\left[\int \mathcal{D}[\psi,\bar\psi,\phi]\,\overline{e^{iS-i\oint J(t)H_{\rm int}(t)\,dt}}\right]. \tag{B2}$$

Evaluating the functional derivative results in

$$\overline{\langle H_{\rm int}(t)\rangle} = Ng^2\oint D(t,t_c')G(t,t_c')G(t_c',t)\,dt_c'. \tag{B3}$$

To simplify the expression for total energy, we note that (B3) can be written in terms of phonon self-energy given in (49) to get

$$\overline{\langle H_{\rm int}(t)\rangle} = \frac{i}{2}N\oint \Pi_{\rm YSYK}(t,t_c')D(t_c',t)\,dt_c', \tag{B4}$$

where $\Pi_{\rm YSYK}$ is the contribution of Yukawa-SYK interaction to phonon self-energy, excluding the coupling to the bath given by $\mathcal{D}(t,t')$. In the next step, we make use of SD equation for phonons (51) to write

$$\begin{aligned}\overline{\langle H_{\rm int}(t)\rangle} = &-\frac{i}{4}N(\partial_t^2+\omega_0^2)D^K(t,t')|_{t'\to t}\\ &-\frac{i}{2}N\oint \mathfrak{D}(t,t_c')D(t_c',t)\,dt_c'.\end{aligned} \tag{B5}$$

The total energy is found by adding (B1) to (B5), resulting in the cancellation of the term proportional to ω_0^2,

$$\begin{aligned}\frac{E(t)}{N} = &-\frac{i}{2}\partial_t^2 D^K(t,t')|_{t'\to t}\\ &-\frac{i}{4}\int[\mathfrak{D}^R(t,t')D^K(t',t)+\mathfrak{D}^K(t,t')D^A(t',t)]\,dt'.\end{aligned} \tag{B6}$$

The first term can be written as $\langle\pi^2(t)\rangle$ which was mentioned in Eq. (61) of the main text.

APPENDIX C: ENERGY TRANSFER RATE

The energy current operator is given by

$$\partial_t H_S = i[H_S+H_B+H_{SB},H_S] = i[H_{SB},H_S], \tag{C1}$$

where H_S is the Hamiltonian of an isolated system given by (3) and H_{SB} is defined in (12). After calculating the commutator we get

$$\partial_t H_S = -\sum_l X_l\dot\phi_l. \tag{C2}$$

The expectation value of $X_l\dot\phi_l$ reads as

$$\langle X_l(t)\dot\phi_l(t)\rangle = \oint \mathfrak{D}(t,t')\langle\phi_l(t')\dot\phi_l(t)\rangle\,dt', \tag{C3}$$

where $\mathfrak{D}(t,t')$ is the contour-ordered Green's function of the bath defined in (55). Therefore, the energy transfer rate is given by

$$\begin{aligned}\partial_t E(t) \equiv \langle\partial_t H_S\rangle &= -iN\oint \mathfrak{D}(t,t')\partial_t D(t',t)\,dt'\\ &= -\frac{iN}{2}\int_0^t[\mathfrak{D}^K(t',t)\partial_t D^A(t',t)\\ &\quad+\mathfrak{D}^R(t,t')\partial_t D^K(t',t)]dt',\end{aligned} \tag{C4}$$

which is the quoted result in Eq. (67) of the main text.

APPENDIX D: THE FERMI LIQUID ELECTRON-PHONON SYSTEM

Fermi liquid behavior can be obtained by adding a random hopping term H_t to the Yukawa-SYK Hamiltonian in Eq. (3)

$$H_t = -\frac{1}{\sqrt{N}}\sum_{ij,\sigma} t_{ij}\psi_{i\sigma}^\dagger\psi_{j\sigma}. \tag{D1}$$

The hopping amplitude $t_{ij} = t_{ij}' + it_{ij}''$ is a random Gaussian variable and satisfies

$$\overline{t_{ij}} = 0, \tag{D2}$$

$$\overline{t_{ij}'t_{nm}'} = \frac{t^2}{2}(\delta_{in}\delta_{jm}+\delta_{im}\delta_{jn}), \tag{D3}$$

$$\overline{t_{ij}''t_{nm}''} = \frac{t^2}{2}(\delta_{in}\delta_{jm}-\delta_{im}\delta_{jn}). \tag{D4}$$

The hopping term results in an extra contribution to the fermion self-energy in Eq. (48) given by

$$\Sigma_t(t_c,t_c') = t^2G(t_c,t_c'), \tag{D5}$$

where in the absence of the Yukawa interaction and at equilibrium yields the following fermion Green's function:

$$G^R(\omega) = \frac{2}{\omega+i\sqrt{4t^2-\omega^2}}. \tag{D6}$$

According to the scaling dimension of fermion operators $[\psi]=\Delta$ given by Eq. (6), H_t is a relevant operator near the Yukawa-SYK fixed point and we can treat the Yukawa interaction as a perturbation to randomly hopping fermions and free phonons. The Yukawa contribution to the imaginary parts of the fermion and phonon self-energies at equilibrium reads

$$\begin{aligned}\mathrm{Im}\,\Sigma_g^R(\omega) = &-g^2\int \mathrm{Im}\,G^R(\nu)\,\mathrm{Im}\,D^R(\omega-\nu)\\ &\times\left[\tanh\frac{\nu}{2T}-\coth\frac{\nu-\omega}{2T}\right]\frac{d\nu}{2\pi},\end{aligned} \tag{D7}$$

$$\begin{aligned}\mathrm{Im}\,\Pi_g^R(\omega) = &-2g^2\int \mathrm{Im}\,G^R(\nu)\,\mathrm{Im}\,G^R(\nu+\omega)\\ &\times\left[\tanh\frac{\nu+\omega}{2T}-\tanh\frac{\nu}{2T}\right]\frac{d\nu}{2\pi}.\end{aligned} \tag{D8}$$

We substitute G^R in Eq. (D8) from Eq. (D6). After putting the contribution from the coupling to the bath and the Yukawa interaction together we find

$$\mathrm{Im}\,\Pi^R(\omega) \approx -\gamma\sin\left(\frac{\pi a}{2}\right)\mathrm{sgn}\,(\omega)|\omega|^a - \frac{2g^2}{\pi t^2}\omega. \tag{D9}$$

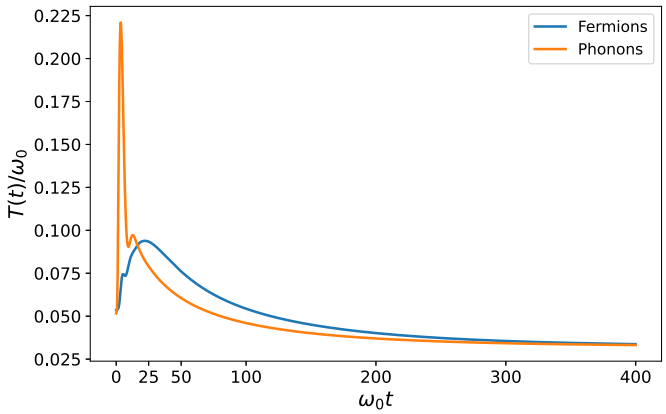

FIG. 10. Effective temperatures for a Fermi liquid Yukawa-SYK system coupled to an external Ohmic bath. The parameters are $t/\omega_0 = 1.0$, $g^2/\omega_0^3 = 0.7$, and $\gamma/\omega_0 = 0.2$.

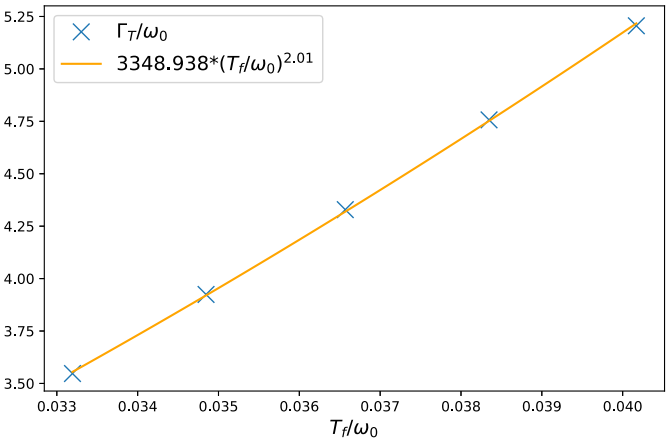

FIG. 11. Temperature relaxation rate for a Fermi liquid Yukawa-SYK system coupled to an external Ohmic bath. The parameters are $t/\omega_0 = 1.0$, $g^2/\omega_0^3 = 0.7$, and $\gamma/\omega_0 = 0.2$.

As expected for a fermionic system with a smooth DOS at the Fermi energy, the interaction of phonons with fermion charge fluctuations results in the Landau damping of phonons. Depending on the exponent of the bath a and temperature, phonons exhibit different relaxation behaviors. For Ohmic and sub-Ohmic baths ($a \leqslant 1$) the Yukawa interaction does not alter the dynamics of phonons at temperatures below the crossover scale $\omega^\star \sim (\gamma t^2/g^2)^{1/(1-a)}$ while for a super-Ohmic bath the Yukawa self-energy dominates the spectrum of phonons below $\omega^\star$. Typically, the system-bath coupling γ is a small parameter and the Yukawa vertex determines the relaxation of phonons down to very small temperatures. Note that in contrast to the SYK regime ($t \to 0$), phonons are not critical at $T \to 0$ and have a finite renormalized gap ω_r; therefore, for small energies we have $\mathrm{Im}\, D^R(\omega) \approx \frac{1}{\omega_r^4}\mathrm{Im}\, \Pi^R(\omega)$. Substituting Eq. (D9) into Eq. (D7) yields

$$\mathrm{Im}\, \Sigma_g^R(\omega) \approx -\frac{g^2}{2\pi\omega_r^4 t}\left[\gamma \sin\left(\frac{\pi a}{2}\right)|\omega|^{a-1} + \frac{2g^2}{\pi t^2}\right]|\omega|^2. \tag{D10}$$

Albeit the scaling of the fermion self-energy depends on the spectrum of the bath, we have $\Sigma(\omega)/\omega \xrightarrow{\omega\to 0} 0$ and therefore the scattering rate of fermions is consistent with the Fermi liquid picture.

By solving the kinetic equations for this system numerically, we can employ Eq. (58) to find the effective temperatures for fermions and phonons. As it can be seen in Fig. 10, phonons are colder than fermions during intermediate and late stages of the evolution as they are directly coupled to the bath, in contrast to the NFL phase discussed in the main text. Furthermore, we observe a late-time exponential relaxation of temperature $T - T_f \sim e^{-\Gamma_T t}$. However, the scaling of the relaxation rate Γ_T is different from the one for the critical system in Eq. (I). For an Ohmic bath ($a = 1$), numerics show $\Gamma_T \propto T^2$ (see Fig. 11) while for a super-Ohmic bath with $a = 1.2$ we get $\Gamma_T \propto T^{2.25}$. We can use the hydrodynamical approximation for the energy transfer rate in Eq. (68) together with a linear specific heat for the Fermi liquid to get

$$\Gamma_T \propto T^{1+a}, \tag{D11}$$

which is consistent with the results given above. The important observation here is that the relaxation of the FL is much slower than the SYK phase at small temperatures.

[1] D. A. Abanin, E. Altman, I. Bloch, and M. Serbyn, Colloquium: Many-body localization, thermalization, and entanglement, Rev. Mod. Phys. **91**, 021001 (2019).

[2] T. Mori, T. N. Ikeda, E. Kaminishi, and M. Ueda, Thermalization and prethermalization in isolated quantum systems: A theoretical overview, J. Phys. B: At. Mol. Opt. Phys. **51**, 112001 (2018).

[3] J. Marino, M. Eckstein, M. S. Foster, and A. M. Rey, Dynamical phase transitions in the collisionless pre-thermal states of isolated quantum systems: Theory and experiments, Rep. Prog. Phys. **85**, 116001 (2022).

[4] I. de Vega and D. Alonso, Dynamics of non-markovian open quantum systems, Rev. Mod. Phys. **89**, 015001 (2017).

[5] M. Rigol, V. Dunjko, V. Yurovsky, and M. Olshanii, Relaxation in a Completely Integrable Many-Body Quantum System: An *ab initio* Study of the Dynamics of the Highly Excited States of 1D Lattice Hard-Core Bosons, Phys. Rev. Lett. **98**, 050405 (2007).

[6] B. Pozsgay, M. Mestyán, M. A. Werner, M. Kormos, G. Zaránd, and G. Takács, Correlations after Quantum Quenches in the *xxz* Spin Chain: Failure of the Generalized Gibbs Ensemble, Phys. Rev. Lett. **113**, 117203 (2014).

[7] B. Wouters, J. De Nardis, M. Brockmann, D. Fioretto, M. Rigol, and J.-S. Caux, Quenching the Anisotropic Heisenberg Chain: Exact Solution and Generalized Gibbs Ensemble Predictions, Phys. Rev. Lett. **113**, 117202 (2014).

[8] L. Vidmar and M. Rigol, Generalized gibbs ensemble in integrable lattice models, J. Stat. Mech. (2016) 064007.

[9] J. Berges, Controlled nonperturbative dynamics of quantum fields out-of-equilibrium, Nucl. Phys. A **699**, 847 (2002).

[10] J. Berges, A. Rothkopf, and J. Schmidt, Nonthermal Fixed Points: Effective Weak Coupling for Strongly Correlated Systems Far From Equilibrium, Phys. Rev. Lett. **101**, 041603 (2008).

[11] A. Chiocchetta, A. Gambassi, S. Diehl, and J. Marino, Dynamical Crossovers in Prethermal Critical States, Phys. Rev. Lett. **118**, 135701 (2017).

[12] J. Berges, S. Borsányi, and C. Wetterich, Prethermalization, Phys. Rev. Lett. **93**, 142002 (2004).

[13] T. Langen, T. Gasenzer, and J. Schmiedmayer, Prethermalization and universal dynamics in near-integrable quantum systems, J. Stat. Mech. (2016) 064009.

[14] S. Sachdev and J. Ye, Gapless Spin-Fluid Ground State in a Random Quantum Heisenberg Magnet, Phys. Rev. Lett. **70**, 3339 (1993).

[15] A. Kitaev, A simple model of quantum holography (2015), http://online.kitp.ucsb.edu/online/entangled15/kitaev/.

[16] Y. Gu, A. Kitaev, S. Sachdev, and G. Tarnopolsky, Notes on the complex Sachdev-Ye-Kitaev model, J. High Energy Phys. 02 (2020) 157.

[17] D. Chowdhury, A. Georges, O. Parcollet, and S. Sachdev, Sachdev-Ye-Kitaev models and beyond: Window into non-fermi liquids, Rev. Mod. Phys. **94**, 035004 (2022).

[18] J. Maldacena and D. Stanford, Remarks on the Sachdev-Ye-Kitaev model, Phys. Rev. D **94**, 106002 (2016).

[19] J. Maldacena, S. H. Shenker, and D. Stanford, A bound on chaos, J. High Energy Phys. 08 (2016) 106.

[20] S. Sachdev, Bekenstein-Hawking Entropy and Strange Metals, Phys. Rev. X **5**, 041025 (2015).

[21] A. Jevicki, K. Suzuki, and J. Yoon, Bi-local holography in the SYK model, J. High Energy Phys. 07 (2016) 007.

[22] I. Esterlis and J. Schmalian, Cooper pairing of incoherent electrons: An electron-phonon version of the Sachdev-Ye-Kitaev model, Phys. Rev. B **100**, 115132 (2019).

[23] Y. Wang, Solvable Strong-Coupling Quantum-Dot Model with a Non-Fermi-Liquid Pairing Transition, Phys. Rev. Lett. **124**, 017002 (2020).

[24] Y. Wang and A. V. Chubukov, Quantum phase transition in the Yukawa-Syk model, Phys. Rev. Res. **2**, 033084 (2020).

[25] L. Classen and A. Chubukov, Superconductivity of incoherent electrons in the Yukawa Sachdev-Ye-Kitaev model, Phys. Rev. B **104**, 125120 (2021).

[26] A. Davis and Y. Wang, Quantum chaos and phase transition in the Yukawa–Sachdev-Ye-Kitaev model, Phys. Rev. B **107**, 205122 (2023).

[27] W. Wang, A. Davis, G. Pan, Y. Wang, and Z. Y. Meng, Phase diagram of the spin-$\frac{1}{2}$ yukawa–Sachdev-Ye-Kitaev model: Non-fermi liquid, insulator, and superconductor, Phys. Rev. B **103**, 195108 (2021).

[28] D. Hauck, M. J. Klug, I. Esterlis, and J. Schmalian, Eliashberg equations for an electron–phonon version of the Sachdev–Ye–Kitaev model: Pair breaking in non-fermi liquid superconductors, Ann. Phys. **417**, 168120 (2020).

[29] G.-A. Inkof, K. Schalm, and J. Schmalian, Quantum critical Eliashberg theory, the Sachdev-Ye-Kitaev superconductor and their holographic duals, npj Quant. Mater. **7**, 56 (2022).

[30] J. Bardeen, L. N. Cooper, and J. R. Schrieffer, Theory of superconductivity, Phys. Rev. **108**, 1175 (1957).

[31] G. Pan, W. Wang, A. Davis, Y. Wang, and Z. Y. Meng, Yukawa-syk model and self-tuned quantum criticality, Phys. Rev. Res. **3**, 013250 (2021).

[32] D. Chowdhury, Y. Werman, E. Berg, and T. Senthil, Translationally Invariant Non-Fermi-Liquid Metals with Critical Fermi Surfaces: Solvable Models, Phys. Rev. X **8**, 031024 (2018).

[33] J. Kim, E. Altman, and X. Cao, Dirac fast scramblers, Phys. Rev. B **103**, L081113 (2021).

[34] I. Esterlis, H. Guo, A. A. Patel, and S. Sachdev, Large-n theory of critical fermi surfaces, Phys. Rev. B **103**, 235129 (2021).

[35] H. Guo, A. A. Patel, I. Esterlis, and S. Sachdev, Large-n theory of critical Fermi surfaces. II. Conductivity, Phys. Rev. B **106**, 115151 (2022).

[36] M. Tikhanovskaya, S. Sachdev, and A. A. Patel, Maximal Quantum Chaos of the Critical Fermi Surface, Phys. Rev. Lett. **129**, 060601 (2022).

[37] I. Jang and P.-Y. Chang, Prethermalization and transient dynamics of the multi-channel kondo systems under generic quantum quenches: Insights form large-n Schwinger-Keldysh approach, arXiv:2303.02433 [cond-mat.str-el].

[38] L. V. Keldysh, Diagram technique for nonequilibrium processes, Sov. Phys. JETP **20**, 1018 (1965).

[39] L. Kadanoff and G. Baym, *Quantum Statistical Mechanics* (W.A. Benjamin Inc., New York, 1962).

[40] A. Kamenev, *Field Theory of Non-Equilibrium Systems* (Cambridge University Press, Cambridge, UK, 2011).

[41] A. Eberlein, V. Kasper, S. Sachdev, and J. Steinberg, Quantum quench of the Sachdev-Ye-Kitaev model, Phys. Rev. B **96**, 205123 (2017).

[42] R. Bhattacharya, D. P. Jatkar, and N. Sorokhaibam, Quantum quenches and thermalization in syk models, J. High Energy Phys. 07 (2019) 066.

[43] A. Haldar, P. Haldar, S. Bera, I. Mandal, and S. Banerjee, Quench, thermalization, and residual entropy across a non-fermi liquid to fermi liquid transition, Phys. Rev. Res. **2**, 013307 (2020).

[44] A. Larzul and M. Schiró, Quenches and (pre)thermalization in a mixed Sachdev-Ye-Kitaev model, Phys. Rev. B **105**, 045105 (2022).

[45] A. Almheiri, A. Milekhin, and B. Swingle, Universal constraints on energy flow and SYK thermalization, arXiv:1912.04912 (2019).

[46] P. Zhang, Evaporation dynamics of the Sachdev-Ye-Kitaev model, Phys. Rev. B **100**, 245104 (2019).

[47] Y. Cheipesh, A. I. Pavlov, V. Ohanesjan, K. Schalm, and N. V. Gnezdilov, Quantum tunneling dynamics in a complex-valued Sachdev-Ye-Kitaev model quench-coupled to a cool bath, Phys. Rev. B **104**, 115134 (2021).

[48] C. Kuhlenkamp and M. Knap, Periodically driven Sachdev-Ye-Kitaev Models, Phys. Rev. Lett. **124**, 106401 (2020).

[49] A. Caldeira and A. Leggett, Quantum tunnelling in a dissipative system, Ann. Phys. **149**, 374 (1983).

[50] M. Knap, M. Babadi, G. Refael, I. Martin, and E. Demler, Dynamical Cooper pairing in nonequilibrium electron-phonon systems, Phys. Rev. B **94**, 214504 (2016).

[51] M. Babadi, M. Knap, I. Martin, G. Refael, and E. Demler, Theory of parametrically amplified electron-phonon superconductivity, Phys. Rev. B **96**, 014512 (2017).

[52] Y.-Z. Chou, Y. Liao, and M. S. Foster, Twisting anderson pseudospins with light: Quench dynamics in terahertz-pumped BCS superconductors, Phys. Rev. B **95**, 104507 (2017).
[53] Y. Murakami, N. Tsuji, M. Eckstein, and P. Werner, Nonequilibrium steady states and transient dynamics of conventional superconductors under phonon driving, Phys. Rev. B **96**, 045125 (2017).
[54] H. P. Ojeda Collado, G. Usaj, J. Lorenzana, and C. A. Balseiro, Fate of dynamical phases of a BCS superconductor beyond the dissipationless regime, Phys. Rev. B **99**, 174509 (2019).
[55] Q. Yang, Z. Yang, and D. E. Liu, Intrinsic dissipative floquet superconductors beyond mean-field theory, Phys. Rev. B **104**, 014512 (2021).
[56] G. Mazza and M. Schirò, Dissipative dynamics of a fermionic superfluid with two-body losses, Phys. Rev. A **107**, L051301 (2023).
[57] F. Verstraete, M. M. Wolf, and J. Ignacio Cirac, Quantum computation and quantum-state engineering driven by dissipation, Nat. Phys. **5**, 633 (2009).
[58] E. G. Dalla Torre, E. Demler, T. Giamarchi, and E. Altman, Quantum critical states and phase transitions in the presence of non-equilibrium noise, Nat. Phys. **6**, 806 (2010).
[59] J. Eisert and T. Prosen, Noise-driven quantum criticality, arXiv:1012.5013 [quant-ph].
[60] S. P. Kelly, R. Nandkishore, and J. Marino, Exploring many-body localization in quantum systems coupled to an environment via Wegner-Wilson flows, Nucl. Phys. B **951**, 114886 (2020).
[61] S. Mukerjee, V. Oganesyan, and D. Huse, Statistical theory of transport by strongly interacting lattice fermions, Phys. Rev. B **73**, 035113 (2006).
[62] J. Lux, J. Müller, A. Mitra, and A. Rosch, Hydrodynamic long-time tails after a quantum quench, Phys. Rev. A **89**, 053608 (2014).
[63] A. Bohrdt, C. B. Mendl, M. Endres, and M. Knap, Scrambling and thermalization in a diffusive quantum many-body system, New J. Phys. **19**, 063001 (2017).
[64] I. Bouchoule, B. Doyon, and J. Dubail, The effect of atom losses on the distribution of rapidities in the one-dimensional Bose gas, SciPost Phys. **9**, 044 (2020).
[65] A. Bastianello, A. D. Luca, and R. Vasseur, Hydrodynamics of weak integrability breaking, J. Stat. Mech. (2021) 114003.
[66] J. Maldacena and A. Milekhin, SYK wormhole formation in real time, J. High Energy Phys. 04 (2021) 258.
[67] S. Banerjee and E. Altman, Solvable model for a dynamical quantum phase transition from fast to slow scrambling, Phys. Rev. B **95**, 134302 (2017).
[68] M. Kardar, *Statistical Physics of Particles* (Cambridge University Press, Cambridge, UK, 2007).
[69] S. F. Edwards and P. W. Anderson, Theory of spin glasses, J. Phys. F **5**, 965 (1975).
[70] K. Efetov, *Supersymmetry in Disorder and Chaos* (Cambridge University Press, Cambridge, UK, 1996).
[71] S. Sachdev, *Quantum Phase Transitions*, 2nd ed. (Cambridge University Press, Cambridge, UK, 2011).
[72] J. Kim, X. Cao, and E. Altman, Low-rank Sachdev-Ye-Kitaev models, Phys. Rev. B **101**, 125112 (2020).
[73] L. Grunwald, G. Passetti, and D. M. Kennes, Dynamical onset of light-induced unconventional superconductivity—A Yukawa-Sachdev-Ye-Kitaev study, arXiv:2307.09935 [cond-mat.supr-con].
[74] hpc.uni-mainz.de.
[75] D. C. Langreth, Linear and nonlinear response theory with applications, in *Linear and Nonlinear Electron Transport in Solids*, edited by J. T. Devreese and V. E. van Doren (Springer, Boston, MA, 1976), pp. 3–32.

Chapter 3

Non-equilibrium dynamics of spin glasses in CQED

In this chapter, we turn to the second main direction of the thesis, which concerns the dynamics of disorder-induced spin-glass phases, with particular relevance to recent experiments on spin glasses realized in confocal cavities. Through a bosonic extension of SYK model, we begin with a brief review of spin glasses and their theoretical description in equilibrium. We then outline how our approach addresses some of these challenges, with a particular emphasis on the non-equilibrium dynamics of such systems.

A model of bosons with random couplings

As a simple bosonic extension of the SYK Hamiltonian, we replace the Majorana operators by real bosonic variables and consider a random quadratic interaction

$$H = -\frac{1}{2}\sum_{i\neq j}^{N} J_{ij}\,\phi_i\phi_j, \tag{3.1}$$

where the symmetric random matrix J_{ij} is drawn from

$$\overline{J_{ij}} = 0, \qquad \overline{J_{ij}^2} = \frac{J^2}{N}. \tag{3.2}$$

This model has two immediate issues. First, it is dynamically trivial, since all terms in H commute. Second, for a generic disorder realization the spectrum is unbounded from below because J need not be positive definite. The first issue is remedied by adding a kinetic term

$$H_\pi = \frac{1}{2}\sum_{i=1}^{N} \pi_i^2, \tag{3.3}$$

while the second requires a stabilization mechanism that bounds the energy from below. A standard choice is the spherical constraint

$$\sum_i \phi_i^2 = N, \tag{3.4}$$

which prevents the fields from acquiring arbitrarily large amplitudes. [1] The resulting model is the quantum spherical 2-rotor model [91, 92, 93, 94]. Its physics is, however, qualitatively different from the SYK model.

To expose the difference with the fermionic case, we perform the disorder average and look for a replica-diagonal solution. In the large-N limit the problem reduces to saddle-point equations for the imaginary-time Green's function

$$G(\tau) = -\langle T\, \phi_i(\tau)\phi_i(0)\rangle, \tag{3.5}$$

which obeys the Dyson equation

$$G(i\omega_n) = -\frac{1}{\omega_n^2 + \lambda + \Sigma(i\omega_n)}, \qquad \omega_n = 2\pi n T, \tag{3.6}$$

with self-energy

$$\Sigma(i\omega_n) = J^2\, G(i\omega_n). \tag{3.7}$$

Here λ is the Lagrange multiplier enforcing Eq. (3.4). Analytic continuation to real frequencies gives the spectral density [93]

$$A(\omega) = -\mathrm{Im}\, G^R(\omega) = \frac{1}{2J^2}\,\mathrm{sgn}(\omega)\,\sqrt{4J^2 - \left(\omega^2 - \lambda\right)^2}, \tag{3.8}$$

which is supported where $|\omega^2 - \lambda| \le 2J$. The constraint fixes λ through

$$\int_{-\infty}^{+\infty} \frac{d\omega}{2\pi}\, A(\omega)\, \coth\!\left(\frac{\omega}{2T}\right) = 1. \tag{3.9}$$

As illustrated in Fig. 3.1, decreasing T lowers λ until, at $T = J$, the lower band edge reaches zero ($\lambda = 2J$) and the spectrum becomes gapless, signaling a phase transition. For $T < J$ the replica-diagonal saddle no longer exists: the equations admit no solution consistent with Eq. (3.9), indicating the breakdown of replica diagonality. In this low-temperature regime one must include inter-replica couplings and treat correlations using the Parisi scheme, which lies beyond our present scope. It suffices here to emphasize the central contrast with the fermionic SYK model. In the fermionic case, Fermi–Dirac statistics replace $\coth(\omega/2T)$ in Eq. (3.9) by $\tanh(\omega/2T)$, precluding condensation and leading to a thermodynamically stable state, whereas the bosonic model enters a glassy

[1] For fermions this instability does not arise because, unlike bosons, they cannot arbitrarily grow.

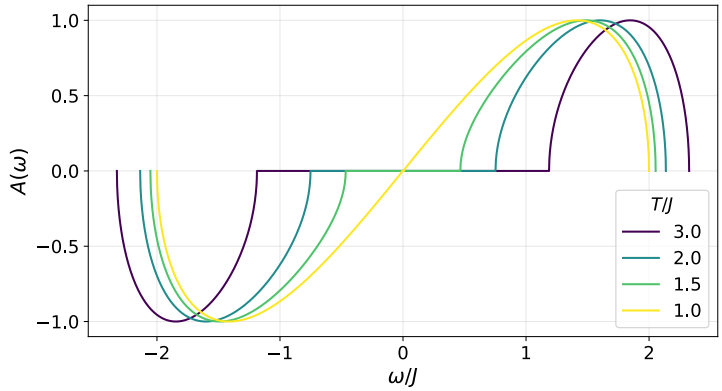

Figure 3.1: The spectral function of the quantum spherical 2-rotor model at different temperatures. A phase transition to the glass phase occurs at $T = J$, where the energy gap vanishes.

phase at low temperatures with RSB (cf. Chapter 1).

A hallmark of glassy phases is their extremely slow relaxation dynamics. This behavior arises from the fact that the free-energy landscape contains a macroscopic number of local minima, separated by large energy barriers. Upon cooling, the system becomes trapped in one of these minima, and thermal or quantum fluctuations require a long time to induce tunneling or hopping between minima. This leads to a pronounced slowing down of the relaxation process, which in turn gives rise to characteristic phenomena such as aging and memory effects, where the response of the system depends sensitively on its historyZ[42, 43].

The disordered bosonic model discussed above can be extended to systems of spins. A well-known case is the quantum Sherrington-Kirkpatrick (SK) model given by [95, 96, 93, 97]

$$H_{\mathrm{SK}} = h \sum_{i=1}^{N} \sigma_i^z + \sum_{i<j} J_{ij}\, \sigma_i^x \sigma_j^x, \tag{3.10}$$

where σ^α are Pauli operators satisfying $[\sigma_i^\alpha, \sigma_j^\beta] = 2i\delta_{ij}\epsilon_{\alpha\beta\gamma}\sigma_i^\gamma$ with $\alpha, \beta = x, y, z$, and random couplings J_{ij} is taken from a Gaussian distribution according to

$$\overline{J_{ij}} = 0, \quad \overline{J_{ij}^2} = \frac{J^2}{N}. \tag{3.11}$$

The SK model is a paramagnet for $h \gtrsim J$, while at $h \approx J$ it undergoes a phase transition to a spin glass phase with RSB [93, 97]. Since spin operators are bounded, we do not need to impose any extra constraints on them. As we see later, this model can be simulated in CQED experiments.

CQED realization of spin glasses

In experiments with ultracold gases in multimode confocal cavities, separate clusters of atoms are trapped at different positions inside the cavity while interacting with multiple cavity modes. The system is described by the Hamiltonian [54, 49, 50, 51]

$$H_{\mathrm{CQED}} = \sum_i \Delta_i S_i^z + \sum_\alpha \omega_\alpha a_\alpha^\dagger a_\alpha - g \sum_{i,\alpha} \Phi_\alpha(r_i)\left(a_\alpha^\dagger + a_\alpha\right) S_i^x, \tag{3.12}$$

where S_i^α denotes the total spin of cluster i with detuning Δ_i, a_α is the annihilation operator for cavity mode α with detuning ω_α, and g is the atom–cavity coupling strength, tunable via the intensity of an applied laser. The mode functions $\Phi_\alpha(r)$ specify the spatial profiles of the standing waves in the cavity. Photon leakage into the vacuum can be incorporated in the Lindblad formalism through jump operators $L_\alpha = \sqrt{\kappa_\alpha}\, a_\alpha$.

In the dispersive regime, $\omega_\alpha \gg \Delta_i, g$, and neglecting cavity losses, the cavity modes can be adiabatically eliminated, yielding the effective spin Hamiltonian[98, 99]

$$H_{\mathrm{eff}} = \sum_i \Delta_i S_i^z - \sum_{ij} J_{ij} S_i^x S_j^x, \tag{3.13}$$

with

$$J_{ij} = \sum_\alpha \frac{g^2}{\omega_\alpha} \Phi_\alpha(r_i)\, \Phi_\alpha(r_j), \tag{3.14}$$

the effective spin–spin couplings mediated by the cavity. The nature of the resulting many-body phase depends on the spatial structure of the mode functions Φ_α and the number of participating modes. If all Φ_α have uniform sign across the cavity, $J_{ij} > 0$ and the strong-coupling limit is a trivial ferromagnet. If Φ_α change sign between different cluster positions, J_{ij} becomes a sum of random terms. When the number of such random contributions remains small compared to the number of clusters, the system is not frustrated but realizes an associative memory phase [53], as in the Hopfield model [52]: upon cooling, the spins relax toward a configuration strongly overlapping with one of the Φ_α patterns [54], the choice of which is set by the initial state's overlap with Φ_α. When the number of cavity modes is sufficiently large compared to the number of clusters, the couplings J_{ij} can, by the central limit theorem, be treated as independent Gaussian random variables. In this limit, the effective Hamiltonian in Eq. (3.14) reduces to the SK model discussed above, with a spin-glass ground state.

Non-equilibrium dynamics of CQED spin glasses

We aim to describe the spin-glass dynamics of the setup discussed in the previous section, focusing on universal features that are insensitive to microscopic details. For the original

model in Eq. (3.12), analytical progress is challenging and has so far only been achieved using exact methods for small systems of clusters with single spins, after adiabatically eliminating the cavity modes.

To proceed, we consider the simplified model

$$H = \Delta \sum_{i=1}^{N} S_i^z + \omega_c \sum_{\alpha=1}^{M} a_\alpha^\dagger a_\alpha - \sum_{i,\alpha} g_{\alpha,i}\left(a_\alpha^\dagger + a_\alpha\right) S_i^x, \tag{3.15}$$

which closely resembles Eq. (3.12) but assumes uniform atomic and cavity detunings, consistent with experimental conditions. The couplings $g_{\alpha,i}$ are random Gaussian variables with statistics

$$\overline{g_{\alpha,i}} = 0, \qquad \overline{g_{\alpha,i} g_{\beta,j}} = \frac{g^2}{2S(M+N)}\, \delta_{ij}\, \delta_{\alpha\beta}, \tag{3.16}$$

where S is the spin length of each cluster. This model retains the essential features of H_{CQED}, including the emergence of an associative memory phase for $M \ll N$ and a spin-glass phase for $M \sim N$.

The ground state of this model can be analyzed for $S = 1/2$, for example by mapping spins to bosons and imposing a fixed spin-length constraint, as in Refs. [98, 99]. However, this approach is not suited for studying non-equilibrium dynamics, particularly for quenches from arbitrary initial spin states. Possible alternatives include semiclassical approximations [100] and controlled approximations based on non-equilibrium field theory, as developed in the two works shown below [101, 102]. The field-theoretical framework allows us to systematically incorporate several important effects, including the role of finite spin length S, which governs the strength of quantum fluctuations, as well as the explicit dynamics of the cavity modes as active degrees of freedom.

Far from equilibrium field theory for strongly coupled light and matter: Dynamics of frustrated multimode cavity QED

Hossein Hosseinabadi,[1,*] Darrick E. Chang,[2,3] and Jamir Marino[1]

[1]*Institut für Physik, Johannes Gutenberg-Universität Mainz, 55099 Mainz, Germany*

[2]*ICFO–Institut de Ciències Fotòniques, The Barcelona Institute of Science and Technology, 08860 Castelldefels, Spain*

[3]*ICREA–Institució Catalana de Recerca i Estudis Avançats, 08015 Barcelona, Spain*

(Received 26 December 2023; revised 6 June 2024; accepted 20 June 2024; published 26 December 2024)

Light-matter interfaces have now entered a new stage marked by the ability to engineer quantum correlated states under driven-dissipative conditions. To propel this new generation of experiments, we are confronted with the need to model nonunitary many-body dynamics in strongly coupled regimes by transcending traditional approaches in quantum optics. In this work, we contribute to this program by adapting a functional-integral technique, conventionally employed in high-energy physics, in order to obtain nonequilibrium dynamics for interacting light-matter systems. Our approach is grounded in constructing "two-particle irreducible" (2PI) effective actions, which provide a nonperturbative and conserving framework for describing quantum evolution at a polynomial cost in time. We apply our method to complement the analysis of spin-glass formation in the context of frustrated multimode cavity quantum electrodynamics, initiated in our accompanying work [Hosseinabadi *et al.*, Phys. Rev. Res. **xx**, xxxx (2024)]. Finally, we outline the capability of the technique to describe other near-term platforms in many-body quantum optics, and its potential to make predictions for this new class of experiments.

DOI: 10.1103/PhysRevResearch.6.043314

I. INTRODUCTION

The field of quantum simulation has recently undergone a transformation, evolving into a new realm of research where the worlds of condensed-matter physics and quantum optics merge. Today, an increasing array of platforms hosting many-body systems can accommodate both unitary and dissipative dynamics in a controlled fashion [1–6]. This circumstance paves the way for the exploration of phases of matter and strongly correlated behavior that have no counterparts in either thermodynamic equilibrium or isolated nonequilibrium conditions.

In contrast with conventional solid-state systems, driven-dissipative condensed matter (also known as many-body quantum optics) systems exhibit a host of innovative characteristics. In the former, dissipation poses the primary challenge to quantum coherence, while in the latter, dissipation is at times intentionally harnessed or even engineered to drive the system into entangled states [7–9].

Traditional solid-state physics focuses on understanding equilibrium phases of matter that result from the interplay of interactions and thermal fluctuations [10–13]. In the realm of driven-dissipative condensed matter, instead, emergent behavior can occur in dynamics or in the nonequilibrium steady state where the system settles. These novel responses usually arise from the intricate interplay of classical and quantum noise within the strongly coupled limit of a many-particle system. Finally, the nature of interactions fostering strong correlations takes on a fundamentally different character in the domain of quantum many-body optics. Here, short-range interactions originating from atoms or molecules coexist with long-range or even all-to-all interactions mediated by light, leading to fundamentally distinct cooperative mechanisms.

These distinctive features find natural occurrence in cavity quantum electrodynamics (cQED) experiments, which have occupied a central position in the field of driven-open quantum simulators for over a decade. In cavity QED, atoms and photons experience couplings as a consequence of their confinement within high-finesse optical cavities [14]. This confinement enables repeated light-matter scattering in nearly isolated conditions, achieving effectively strong interactions. Leveraging the flexibility, tunability, and engineering capabilities inherent in quantum simulators, these platforms have become ideal environments for realizing nonequilibrium phases of matter under driven-open conditions. Beyond fundamental research, applications extend to quantum information, where cavity QED currently holds the world record for spin squeezing [15,16], an entangled state which surpasses classical limits for metrology and sensing.

In the majority of these experiments, the dynamical behavior of the system can be reduced to a few degrees of freedom: typically, these are photon amplitudes and numbers in conjunction with the dynamics of a collective spin that encapsulates the motion of the entire assembly of atoms

*Contact author: hhossein@uni-mainz.de

[17–33]. This usually results from the all-to-all nature of photon-mediated interactions in the cavity, which allows for an effective mean-field description. Quantum fluctuations are subleading in the number of atoms when the dynamics of such macroscopic degrees of freedom are considered and the system's behavior can be effectively characterized through semiclassical descriptions [22].

This situation presents significant advantages when it comes to modeling cavity QED experiments. Simultaneously, it naturally prompts the exploration of conditions where the strong correlations inherent in these systems become dominant. In this context, we are witnessing the emergence of a novel category of experiments, where the true many-body nature of the platform emerges and it defies a description using only a few macroscopic degrees of freedom. These experiments encompass a variety of setups, such as Rydberg tweezer arrays integrated into optical cavities [34], atomic ensembles with adjustable loading capacities [35,36], and the fermionic variant of traditional cavity QED experiments [37].

All these experiments necessitate the integration of methods traditionally employed for addressing strongly correlated problems with the extra complication that detailed balance is broken and dynamics are nonunitary. Accessing the long-term evolution of open many-body systems subject to external (coherent or incoherent) drives as well as strong interactions, is one of the most challenging computational frontiers. Nevertheless, it has now become increasingly important in order to steer this new generation of cavity QED platforms.

Indeed, as numerous established platforms push the boundaries of the NISQ (noisy intermediate-scale quantum) era [38], a cavity QED platform endowed with strong correlations presents an intriguing opportunity. It would hold the potential for innovative strategies in quantum processing, leveraging the combined advantages offered by cooperative behavior [39], the interplay of long- and short-range interactions [34,40,41], the manipulation of controllable quantum fluctuations [42], including the potential to manipulate decoherence channels [43].

As of today, state of art methods to model these experiments would encompass a number of options. Refined versions of semiclassical techniques, such as discrete phase space representations of the Hilbert space, have been tailored for addressing the driven-dissipative dynamics of spin and bosonic systems [44–49]. Tensor network Ansätze, which retain the most informative correlations to describe dynamics, have been used to study phase transitions in driven open systems [50–57]. At the same time, cluster mean-field methods [58] or self-consistent Gaussian approximations [59] remain a straightforward, and, in some circumstances, competitive way, to qualitatively capture nonunitary dynamics.

In this paper, we introduce a method to tackle the dynamics of strongly interacting light-matter systems in the many-body limit [60,61]. It is an adaptation of the two-particle irreducible (2PI) effective action formalism which has been used in high-energy physics and cosmology [62–74], as well as in condensed-matter and atomic, molecular, and optical (AMO) physics [75–83]. The method involves deriving a quantum effective action for the system as a function of its two-point correlation functions. Such action gives exact equations of motion of two-point functions, and with some ingenuity also the dynamics of higher point correlation functions [84,85]. It is via a set of controlled nonperturbative approximations (large-N limit, dilute expansion, loop expansion) for the effective action [60,61,78,81] that the dynamics is numerically solved.

Equations of motion derived from 2PI effective actions, known as Dyson equations (DEs) [61], offer numerous advantages. They give rise to self-consistent dynamics of two-point functions free from secular effects [61,86]. Since approximations are directly performed at the level of the action, the resulting DE are *conserving*, in the sense they cannot spoil the conserved quantities of the original model. They also can seamlessly incorporate both coherent and dissipative dynamics, as functional-integral methods do not markedly differentiate between the two [87]. They do not suffer from limitations when degrees of freedom with unbounded Hilbert space, like photons or phonons, are included in dynamics. The dynamics governed by DE have polynomial time costs in system size and they can be run on a personal computer. The price to pay is formulating educated guesses on the physics of the problem, which are crucial for selecting the proper approximation scheme. Furthermore, these DE are known to semiquantitatively reproduce dynamics, and they are therefore excellent for elucidating the mechanisms at work in a given problem of interest, but less suited to fit with accuracy experimental curves, for instance. With these caveats, the method is highly flexible and applicable virtually to any driven-dissipative many particle system, made of fermions, bosons or spins, as we also expand in the conclusions of this paper.

In this work, we initiate our research program by applying this method to examine the dynamics of strongly correlated light-matter systems within multimode cavity QED. Our model is inspired by the experimental setup presented in Refs. [36,88–90] which involves several photonic modes connecting nodes (Fig. 1). Each of these nodes houses atomic ensembles with adjustable loading capacities. By manipulating the number of atoms in each node (ranging from a few to thousands in the experiment) by using optical tweezers, one can introduce tunable quantum fluctuations in the platform. These fluctuations enable the exploration of system dynamics, from strongly correlated to semiclassical regimes. Importantly, this flexibility is not unique to this platform [35,91] and represents a promising starting point for delving into many-body cavity QED beyond the domain of collective dynamic responses [18,19]. During the final stages of the current work, the experiment detailed in Ref. [92] verified the existence of a spin-glass (SG) phase within the quantum gas microscope platform of Refs. [36,88–90] for the first time through direct measurement of the configuration of spins in the system. In this paper, we complement the findings presented in our accompanying work on dynamical spin-glass formation [93] by providing a comprehensive derivation of nonequilibrium field theory for frustrated cavity QED and investigating the full spectrum of nonequilibrium phases and crossovers inherent to these systems. Our objective is to bridge the domains of AMO and the many-body community working at the interface of condensed matter and field theory.

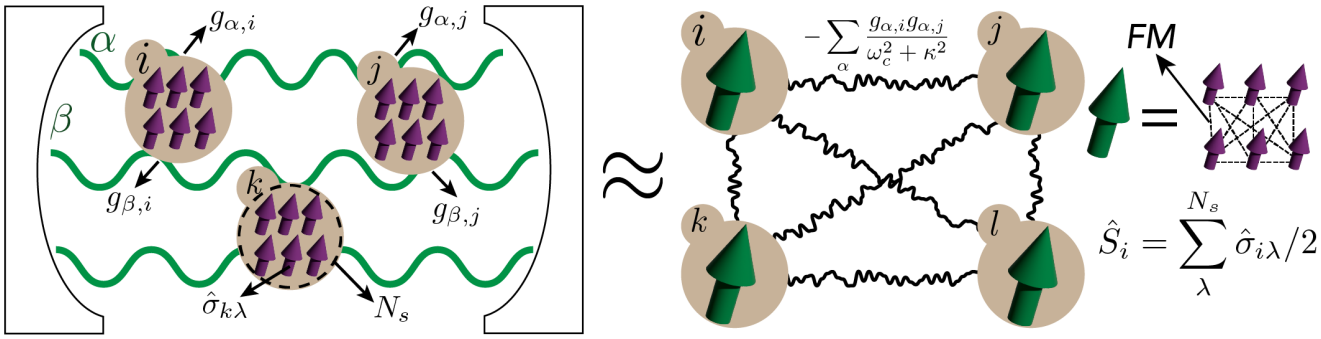

FIG. 1. Schematics of the model considered in this work: N clusters (tan circles) of N_s two-level atoms (spins) interact with M cavity modes (green lines) via static disordered couplings $g_{\alpha,i}$. Cavity modes mediate effective all-to-all interactions modulated among clusters. The effective interaction is modulated by static disorder and generates frustration and glassy dynamics. Each cluster can be taken as a large spin S with amplitude $N_s/2$. Cavity modes induce ferromagnetic (FM) interactions between spins within the same cluster.

II. OUTLINE OF THE PAPER

The goal of this work is to understand the far from equilibrium dynamics of SG phases in frustrated cavity QED with strong disorder, where fluctuations cannot be omitted and mean-field treatments are not applicable. We remark that our approach is distinct from those of Refs. [94,95] which by construction, are suitable only for the universal SG behavior at steady state, in two key aspects. First, the formalism developed here is applicable in far from equilibrium situations such as quench dynamics, while keeping track of the quantum nature of spins. Second, the platform of Refs. [36,88–90] naturally includes extra FM interactions which are unimportant in the steady state of the system [42], but as shown in this work, can qualitatively modify conventional SG dynamics away from equilibrium. We now briefly outline our key results which expand upon the results of our accompanying work [93].

A. Introduction to the model

We commence the paper by introducing the model in Sec. III. We briefly review previous works on the behavior of the model in different regimes of parameters at the steady state and motivate using our approach to treat its far from equilibrium dynamics.

B. Introduction to the method

We provide a brief introduction to effective action methods and nonequilibrium field theory in Sec. IV. This serves as a foundation for the detailed derivation of our formalism in the context of frustrated light-matter interactions in cavity QED, covered in Sec. V, where we develop a versatile approach to address real-time dynamics in a model for disordered cavity QED given in Fig. 1. To enhance accessibility, this section and its accompanying Appendixes are crafted to be reproducible from scratch by the interested reader.

C. Magnetization dynamics

In Sec. VI A, we show that the mean-field (MF) approximation, given by the leading-order contribution in our approach, predicts a paramagnetic (PM) to ferromagnetic (FM) phase transition of effective spin degrees of freedom in the universality class of infinite range Ising model, but it completely omits the effect of frustrated interactions generated by static disorder in the system. FM interactions are mediated by virtual photon exchange processes among spins within the same cluster, and in contrast with intercluster couplings, are not frustrated. In Sec. VI B we demonstrate that, upon the nonperturbative incorporation of disorder and fluctuations, our approach provides a dramatic improvement of MF results. As the focus of this work is the far from equilibrium dynamics of this system after interaction quenches, we first look at the dynamics of simple spin observables, such as global magnetization. We find that if the system is initiated in a symmetry-broken state with a finite total magnetization, the relaxation of magnetic order substantially depends on the coupling strength and the size of atomic ensembles N_s or equivalently, the amplitude of large spins $\hat{S}_i$ per each cluster. For weak couplings (Sec. VI B 1), global magnetization displays paramagnetic oscillations which are weakly damped due to the dephasing generated by static disorder. Upon increasing the coupling (Sec. VI B 2), spin relaxation changes from underdamped dynamics to overdamped dynamics without oscillations. In Sec. VI B 3 we address the effect of ensemble size N_s on magnetization dynamics. We show that in the overdamped regime and for small N_s, global magnetization $\langle \hat{S}^x \rangle$ relaxes quickly to zero while for large N_s, after an initial collapse to a finite value, it stays in a transient prethermal state with a slow spiral decay of the magnetization vector along the axis of temporary FM order. We benchmark 2PI with a semiclassical phase-space approximation [44,96] and demonstrate excellent agreement in the limit of large spins between the two, where the latter becomes exact. This indicates the viability of 2PI for approximating quantum dynamics by starting from the limit of large spins, and systematically incorporating quantum fluctuations as the spin size is lowered down to $S = 1/2$.

D. Dynamics of spin glass

To probe into the nature of the transition in the system as magnetization dynamics change from underdamped to overdamped, we consider more complex and richer spin observables in Sec. VI C. Particularly, and with the expectation

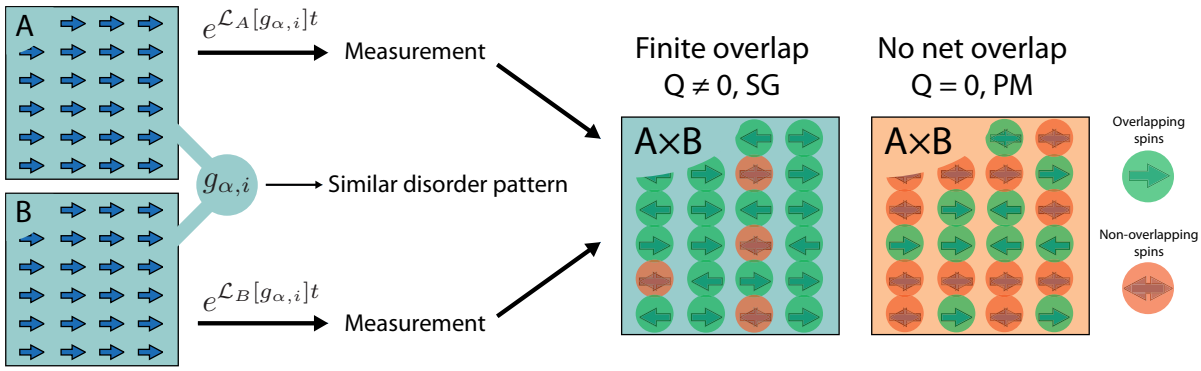

FIG. 2. Measuring SG order through the overlap of spin configurations (Q) between two similar, but independent, systems A and B which share the same pattern of disordered couplings $g_{\alpha,i}$. Starting from the same initial state for both systems and evolving both of them under similar Lindblad dynamics, we can still obtain different spin configuration for each of them by doing measurements and applying projections to the their states. If the systems are SG, the overlap remains finite at long times. For a PM, the relative orientations of spins in the two copies are random and only half of the spins share the same orientation as their counterparts.

of exploring SG order in the system, we consider the dynamics of two different order parameters for SG in Secs. VI C 2 and VI C 3. First, we consider the time evolution of the overlap of spin configurations between two identical systems (replicas) with a similar disorder profile but otherwise decoupled from each other. This overlap Q, which measures the statistical correlations between the two replicas only due to their shared disorder pattern, is a finite quantity in the SG phase and vanishes for a PM (Fig. 2), as has been demonstrated experimentally [92]. To obtain dynamics of the overlap, we extend the formalism of Keldysh field theory with technical similarity between our approach and the one introduced by Ref. [97] to study measurement-induced phase transitions. In the PM phase, the overlap parameter relaxes to zero after experiencing small temporary fluctuations, in contrast with the SG phase where the order parameter relaxes to a finite value. We show that weak cavity losses stabilize SG order by effectively cooling down the system. Stronger photon losses, on the other hand, suppress the SG phase. As a second measure of SG order, we consider the temporal correlations of spins over long times, conventionally known as the Edwards-Anderson (EA) [98,99] order parameter, corresponding to the overlap of two snapshots of the same system taken at long time intervals. We confirm that EA order parameter changes from zero in the PM phase, when the system loses its memory quickly, to a finite value in the SG phase, proving that the system is glassified. We proceed to show that spin fluctuations violate the fluctuation-dissipation theorem [86,100], a phenomenon conjectured to be closely related to replica symmetry breaking in SG systems [101].

E. Effect of resonant photons

In Sec. VI C 5, we consider the effect of photon frequency on the glass phase by looking at SG order parameter in a wide range of photon frequencies from fast photons to the resonance limit, where atomic and cavity detunings are close, and below. We see that the SG order is peaked close to the resonance, while it saturates in the adiabatic limit. At frequencies below the resonance, SG order is dramatically suppressed, resembling the suppression of various types of order by low-frequency lattice distortions (phonons) in solid-state physics. We also address briefly the spectrum of low-lying excitations in the SG phase, showing a continuum of sub-Ohmic modes at small energies.

The capability to include in the same set of dynamical equations variable ranges of coupling, tunable values of N_s and active photons, is one of the key merits of our approach. It allows us to solve for the dynamics of the full platform without the need to invoke large energy scale separations, effective descriptions suited only to atomic or photonic degrees of freedom, or to treat distinctly the quantum and semiclassical regimes. In this regard, the method has a degree of flexibility that appears promising to treat other strongly correlated driven-dissipative systems, as we discuss in the concluding Sec. VII.

III. THE MODEL

The experiment in Refs. [36,88–90] can be modeled by a system of N clusters, each one containing N_s two-level atoms encoded by the spin-1/2 operators $\sigma_{i\lambda}$, with cluster $1 \leqslant i \leqslant N$ and atom indices $1 \leqslant \lambda \leqslant N_s$, as shown in Fig. 1. The couplings between the atoms and the M photonic modes of the cavity are spatial-dependent and uncorrelated from each other, which justifies their modeling via random spin-boson couplings [94,95,102]. Starting from the same initial state for all spins, each cluster is equivalent to a single spin $S_i = \sum_\lambda \sigma_{i\lambda}/2$ with amplitude $S = N_s/2$. The parameter S can be tuned by loading few or several atoms in each cluster, and it dictates the strength of quantum fluctuations. For instance, at large S each cluster would be effectively described by a classical angular momentum, since its quantum noise would scale down as $1/S$ [18,103,104]. A minimal model for the system is given by the random Dicke model whose evolution is governed by $\partial_t \rho = -i[H, \rho] + \sum_{\alpha=1}^{M} \mathcal{D}[a_\alpha]\rho$, where

$$H = \frac{\Delta}{2}\sum_{i,\lambda}\sigma^z_{i\lambda} + \sum_\alpha \omega_\alpha a^\dagger_\alpha a_\alpha + \frac{1}{\sqrt{(M+N)N_s}}\sum_{i,\lambda,\alpha} g_{\alpha i}(a_\alpha + a^\dagger_\alpha)\sigma^x_{i\lambda}, \quad (1)$$

and

$$\mathcal{D}[a_\alpha]\rho = \kappa_\alpha(2a_\alpha \rho a_\alpha^\dagger - \{a_\alpha^\dagger a_\alpha, \rho\}). \tag{2}$$

We assume that cavity modes are nearly degenerate such that $\omega_\alpha = \omega_c$ and $\kappa_\alpha = \kappa$. The couplings $g_{\alpha i}$ are assumed to be random and chosen from a Gaussian distribution:

$$\overline{g_{\alpha i}} = 0, \quad \overline{g_{\alpha i} g_{\beta j}} = \delta_{\alpha\beta}\delta_{ij} g^2. \tag{3}$$

Couplings for spins in the same cluster are similar as we assume that the spatial size of each cluster is smaller than the wavelength of cavity modes. The scaling of the interaction term guarantees that the total energy is extensive in system size [105]. For $\omega_c \gg g, \Delta$ photons are the fastest degree of freedom in the problem; they quickly relax to stationary value and approximately, they mediate instantaneous interactions among spins. Assuming $\kappa = 0$, photons can be adiabatically eliminated [42,106–109] and the model in (1) is mapped to

$$H_{\text{eff}} = \sum_i H_i + H_{\text{int}}, \tag{4}$$

$$H_i \equiv \Delta S_i^z - \frac{4}{(N+M)N_s\omega_c}\left(\sum_\alpha g_{\alpha i}^2\right)\left(S_i^x\right)^2, \tag{5}$$

$$H_{\text{int}} \equiv -\frac{4}{(N+M)N_s\omega_c}\sum_{i\neq j}\sum_\alpha g_{\alpha i} g_{\alpha j} S_i^x S_j^x, \tag{6}$$

where $S_i^x = \sum_\lambda \sigma_{i\lambda}^x/2$ is the total spin operator for each cluster. For $N_s > 1$, each cluster in Eq. (5) is an infinite range quantum Ising model also known as the Lipkin-Meshkov-Glick [110] (LMG) model with Hamiltonian

$$H_{\text{LMG}} = \Delta S^z - \frac{J}{N_s}(S^x)^2. \tag{7}$$

H_{LMG} admits an exact solution using mean-field theory in the limit $N_s \to \infty$ and features a paramagnet (PM) to FM phase transition [23,111–115] at $\Delta = J$. The effective interactions between atoms within the same cluster in Eq. (5) are purely ferromagnetic and, to leading order, we can identify $J = 4g^2\eta/(1+\eta)\omega_c$ after disorder averaging, with $\eta = M/N$. Each cluster is further coupled to other clusters via Eq. (6), which is expected to generate frustration in the system. For $N_s = 1$, the ferromagnetic interaction vanishes since $(S^x)^2 = (\sigma^x)^2 = 1$ and this model becomes the quantum Hopfield model (QHM) [116]. The QHM has a PM ground state for sufficiently large Δ while for small Δ, the ground state crucially depends on the ratio η [117]. For small values $\eta < \eta_c \approx O(10^{-1})$, the system is in the memory retrieval phase [42,103,118,119], which is a Dicke model in disguise with multiple superradiant ground states. When the number of photon modes (M) surpasses a critical limit $\eta > \eta_c$ [117], frustrations dominate and turn the system into a quantum glass [94,95,104,120], arguably in the same universality class of the quantum Sherrington-Kirkpatrick [121,122] (SK) model. In this paper, we are interested in SG dynamics and will only consider the limit $\eta = 1$.

The many-body nature of the model (1) when photons participate in the dynamics prevents us from using exact diagonalization. Moreover, because of the frustrated couplings, mean-field (MF) methods or dynamics of cumulants expansions (CE) [22] are inapplicable. Instead, we attack this problem using methods of nonequilibrium quantum field theory (NEQFT). In the next section, we introduce the method using a simple example first, and then proceed to apply it to the model in Eq. (1). A treatment of the Dicke model without disordered couplings is also provided in Appendix G for comparison with the random Dicke model and pedagogical purposes.

IV. NONEQUILIBRIUM FIELD THEORY

A. Basics of two-particle irreducible formalism

Similar to classical mechanics, the dynamics of a quantum system can also be obtained from an action principle [62,123,124]. In particular, one can define a quantum effective action (EA) $\Gamma[\varphi, G]$ in terms of one-point $\varphi = \langle\phi\rangle$ and two-point $iG(t,t') = \langle\phi(t)\phi(t')\rangle_c$ correlation functions of the system, known as 2PI-EA, whose stationary solution with respect to correlation functions yields the equations of motion for those correlation functions [61]. The equations of motion include all quantum effects, and in principle, can be solved to obtain the exact-correlation functions of the system. However, this is only true if the full expression of 2PI-EA is known. For a system of real-valued bosonic fields, the general expression of Γ is given by

$$\Gamma[\varphi, G] = S_{\text{cl}}[\varphi] - \frac{i}{2}\text{Tr}\ln G + \frac{i}{2}\text{Tr}\left(G_0^{-1}G\right) + \Gamma_2[\varphi, G]. \tag{8}$$

The first term is the classical action, the rest of the terms capture fluctuations (both quantum and statistical [66]), and G_0 is the Green's function of the noninteracting system. The last term Γ_2 usually admits an expansion in terms of connected Feynman diagrams which cannot be disconnected by cutting at most two of their lines (hence the name two-particle irreducible). Often, it is only possible to do an approximation for Γ_2, by keeping only a finite number of diagrams or, similar to this work, an infinite subset of diagrams. This in turn yields an approximate solution for correlation functions and field expectation values. The main advantage of 2PI is that, despite the inevitable use of approximations, it is a conserving method [61,84]. This means that, the approximated dynamics respect all of the conservation laws of the original problem and therefore, is immune to the instabilities that many other methods of approximation for dynamics have. In addition to being a conserving method, in certain problems, including the one considered here, it is possible to obtain nonperturbative approximations for Γ_2, which produce qualitatively valid results for dynamics at long times [60,61,66,78,125,126].

B. Comparison with other approaches

There are various methods to explore many-body quantum dynamics theoretically and each one has its own advantages and shortcomings. Exact diagonalization (ED) gives accurate results but is often limited to very small system sizes, especially for open quantum systems where the size of the vector space grows even faster due to the necessity of working with mixed states. Methods based on matrix product states (MPSs) [127] are mostly limited to one spatial dimension and systems with local interactions and weak entanglement. Among the

most frequently used methods in the AMO community are cumulants expansion (CE) and truncated Wigner approximation (TWA) [96] together with its extension, discrete truncated Wigner approximation (DTWA) [44]. The main advantages of CE are simplicity and cheap computational cost. On the other hand, it is an uncontrolled approximation [128,129]. There is no *a priori* knowledge of its domain of applicability before solving the equations and checking the physical consistency of the results. Furthermore, to calculate correlation functions at different times in CE, one needs to resort to the quantum regression theorem [109,130], which complicates the calculations. TWA approximates quantum dynamics with classical statistical mechanics by sampling the initial probability distribution function from the system's initial wave function and, subsequently, evolving the system according to the classical equations of motion. The advantage of TWA is that it is a controlled approximation, since it can be expressed as the leading-order contribution in the expansion of dynamics in powers of $\hbar$, which turn out to be equivalent to classical statistical mechanics [61,96]. The drawback of TWA is its limitation to systems with weak quantum fluctuations and when quantum effects are not built up over time. For instance, TWA is unable to capture tunneling phenomena [96] even at the level of qualitative accuracy. While the calculation of nonlocal symmetric correlation functions is straightforward in TWA, to evaluate quantities such as response functions one needs to go to higher-order terms in $\hbar$ [96], considerably increasing the required effort to use the method. A detailed comparison of DTWA and 2PI for our system is provided in Sec. VI B 3 and Appendix F.

In comparison to CE and TWA, 2PI can be used to perform controlled approximations, provided that a control parameter exists in the system. In this case, the 2PI action admits an expansion in powers of the control parameter [61]. For instance, this parameter can be $\hbar$, similar to the example given before, or inverse of the components of a vector field or in our case, the inverse of the spin amplitude per cluster and the number of photon modes to the number of clusters. Moreover, symmetric and antisymmetric correlation functions are the quantities in terms of which the formalism is built and are the direct outcomes of calculations. 2PI also excels in capturing quantum effects, mainly because it involves a resummation of the perturbative expansion to infinite order. For instance, it has been used to study dynamics in strongly correlated systems of electrons [131–133] and phonons [134,135] with non-Fermi liquid (NFL) behavior and critical fluctuations. 2PI works well also when small quantum effects are accumulated over time, leading to drastic changes in the system at long times such as in tunneling phenomena [64,136]. Despite numerous advantages, 2PI has some limitations. First, the approximations that are usually made to retain only a subset of the diagrams in the effective action, such as $1/N$ expansions [60,61,63,78], give qualitatively valuable results about the universal trend of the dynamics, but are not tailored to have quantitative accuracy, i.e., they are not suitable for a point-wise comparison with experimental data. Sometimes, one needs to make educated guesses about which diagrams have to be kept to capture a certain aspect of the physics which is of interest. The exception to these is working in the weak coupling or the dilute limit, where collisions can be incorporated perturbatively [86,100]. Second, working with non-Gaussian initial states is difficult in 2PI as these require the inclusion of extra interaction vertices [61] that complicate the approximation. We emphasize that this restriction only holds for initial states. 2PI is not limited to Gaussian dynamics (such as second-order cumulants) and in fact, captures non-Gaussian correlations generated over time after initializing the systems in a Gaussian state.

V. TWO-PARTICLE IRREDUCIBLE FOR DISORDERED CAVITY QED

A. Keldysh action for spins

To treat Eq. (1) using field theory, we need a path integral representation for spin operators. Different spin representations include spin coherent-state path integral, the Holstein-Primakoff transformation and particularly, spinon representations in terms of Abrikosov fermions or Schwinger bosons [137,138]. In this work, we represent each spin-half operator in terms of three Majorana fermions (ψ^x, ψ^y, ψ^z) as [139–151] given by

$$\sigma^\alpha = -i\epsilon_{\alpha\beta\gamma}\psi^\beta\psi^\gamma, \quad \{\psi^\alpha, \psi^\beta\} = \delta_{\alpha\beta}, \tag{9}$$

where we have assumed summation over repeated indices. It is easy to check that (9) satisfies spin commutation relations $[\sigma^\alpha, \sigma^\beta] = 2i\epsilon_{\alpha\beta\gamma}\sigma^\gamma$. This representation was used by Refs. [150,151] to study the onset of superradiance in the steady state of the Dicke model with different types of external baths. We note that, although fermionic and bosonic spinons are formally equivalent (after projection into the physical sector of the Hilbert space), they can yield different results upon using further approximations. For instance, in 2PI we mostly start from "simple" initial states for which the values of correlation functions $G(t, t')$ are known only at a single initial time $t = t' = 0$. This corresponds to a Gaussian state for bosons and fermions (more precisely, the Gibbs state of a quadratic fermionic Hamiltonian [152]). In Appendix A, we show that a Gaussian state for Schwinger bosons is always a mixed state at least for one of the boson species and generates a relative error of $O((2S)^0)$ for the values of extensive quantities such as energy or the effective action. However, Gaussian states for fermionic spinons (complex or Majorana) can be pure states and do not introduce any errors in representing spin coherent states. As we show below, diagrammatic corrections beyond mean-field dynamics start at $O(1/2S)$ and are subleading to the error of using Gaussian states for Schwinger bosons. Hence, using fermionic spinons is in fact essential for the consistency of the approximation for all spin sizes and not only for $S \approx 1$, as long as we use Gaussian initial states.

The Keldysh action for "free" spins, corresponding to the first term in Eq. (1) and written in terms of Majorana fermions, has two parts

$$S_\sigma = S_{\rm B} + S_\Delta, \tag{10}$$

$$S_{\rm B} = \sum_i^N \sum_\lambda^{N_s} \sum_\alpha^{x,y,z} \oint \frac{i}{2}\psi^\alpha_{i\lambda}\partial_{t_c}\psi^\alpha_{i\lambda}dt_c, \tag{11}$$

$$S_\Delta = \sum_i^N \sum_\lambda^{N_s} \oint i\Delta\psi^x_{i\lambda}\psi^y_{i\lambda}dt_c, \tag{12}$$

where S_B is the contribution of the Berry phase of spins to the action [153]. The action in Eq. (10) can be compactly written as

$$S_\sigma = \frac{1}{2}\sum_{i}^{N}\sum_{\lambda}^{N_s}\oint \Psi_{i\lambda}^{T}\hat{G}_0^{-1}\Psi_{i\lambda}dt_c, \tag{13}$$

with $\Psi_{i\lambda}^{T} \equiv (\psi_{i\lambda}^{x}, \psi_{i\lambda}^{y}, \psi_{i\lambda}^{z})$. The inverse bare Green's function for fermions $\hat{G}_0^{-1}$ is defined as

$$\hat{G}_0^{-1} \equiv \begin{bmatrix} i\partial_{t_c} & i\Delta & 0 \\ -i\Delta & i\partial_{t_c} & 0 \\ 0 & 0 & i\partial_{t_c} \end{bmatrix}. \tag{14}$$

Finally, we define the fermion Green's function and its diagrammatic representation as

$$iG_{i\lambda,j\lambda'}^{\alpha,\beta}(t,t') \equiv \left\langle \psi_{i\lambda}^{\alpha}(t)\psi_{j\lambda'}^{\beta}(t')\right\rangle : \text{———————}. \tag{15}$$

Note that G is the dressed-fermion Green's function.

B. Keldysh action for photon sector

The dissipative Keldysh action for photons can be obtained directly from the Liouvillian by following the prescription given in Ref. [87]:

$$S_{\rm ph} = \int [\bar{a}_+(i\partial_t - \omega_c + i\kappa)a_+ - \bar{a}_-(i\partial_t - \omega_c - i\kappa)a_- - 2i\kappa\bar{a}_- a_+]dt. \tag{16}$$

Since the spin-photon coupling in Eq. (1) depends on the combination $(a + a^\dagger)$ of photon operators, dealing with interactions is simpler when we make the following transformation to real-valued photon fields (ϕ, π) given by

$$a_\pm = \sqrt{\frac{\omega_c}{2}}\left(\phi_\pm + i\frac{\pi_\pm}{\omega_c}\right). \tag{17}$$

Substitution in Eq. (16) gives

$$S_{\rm ph} = \frac{1}{2}\sum_{\alpha}^{M}\int \Phi_\alpha^T \hat{D}_0^{-1}\Phi_\alpha dt, \tag{18}$$

where $\Phi_\alpha^T \equiv (\phi_{\alpha+}, \pi_{\alpha+}, \phi_{\alpha-}, \pi_{\alpha-})$ and $\hat{D}_0^{-1}$ is a 4×4 matrix defined as

$$\hat{D}_0^{-1} = \begin{bmatrix} (\hat{D}_0^{-1})^{++} & (\hat{D}_0^{-1})^{+-} \\ (\hat{D}_0^{-1})^{-+} & (\hat{D}_0^{-1})^{--} \end{bmatrix}, \tag{19}$$

$$(\hat{D}_0^{-1})^{++} = \begin{bmatrix} -\omega_c^2 + i\kappa\omega_c & -\partial_t \\ \partial_t & -1 + i\frac{\kappa}{\omega_c} \end{bmatrix}, \tag{20}$$

$$(\hat{D}_0^{-1})^{+-} = \begin{bmatrix} -i\kappa\omega_c & -\kappa \\ \kappa & -i\frac{\kappa}{\omega_c} \end{bmatrix}, \tag{21}$$

$$(\hat{D}_0^{-1})^{-+} = \begin{bmatrix} -i\kappa\omega_c & \kappa \\ -\kappa & -i\frac{\kappa}{\omega_c} \end{bmatrix}, \tag{22}$$

$$(\hat{D}_0^{-1})^{--} = \begin{bmatrix} \omega_c^2 + i\kappa\omega_c & \partial_t \\ -\partial_t & 1 + i\frac{\kappa}{\omega_c} \end{bmatrix}. \tag{23}$$

Photon Green's functions are defined according to

$$iD_{\alpha,\beta}^{\rho,\rho'}(t,t') \equiv \left\langle \Phi_\alpha^\rho(t)\Phi_\beta^{\rho'}(t')\right\rangle_c, \tag{24}$$

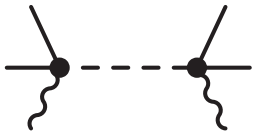

FIG. 3. Spin-photon interaction vertex after averaging over the disorder. The dashed line indicates the average $\overline{g_{\alpha,i}g_{\beta,j}}$.

where $\rho, \rho' = (\phi, \pi)$. We see that only the $D^{\phi\phi}$ component appears explicitly in the diagrams for the effective action and self-energies. Hence, only $D^{\phi\phi}$ requires a diagrammatic representation which is given by

$$iD_{\alpha,\beta}^{\phi\phi}(t,t') = \langle\phi_\alpha(t)\phi_\beta(t')\rangle_c : \sim\sim\sim\sim. \tag{25}$$

C. Spin-photon interaction

Using the conventions introduced above, the Keldysh action for the interaction term reads

$$S_{\rm int} = 2i\sqrt{\frac{2\omega_c}{(N+M)N_s}}\sum_{\alpha,i,\lambda}\oint dt_c g_{\alpha i}\phi_\alpha\psi_{i\lambda}^{y}\psi_{i\lambda}^{z}. \tag{26}$$

In principle, we can proceed by taking the average of the Keldysh action over the random couplings $g_{\alpha i}$. This yields an effective interaction defined by $e^{iS_{\rm eff}} = \overline{e^{iS_{\rm int}}}$, where

$$S_{\rm eff} \equiv -\frac{4ig^2\omega_c}{(N+M)N_s}\sum_{\alpha,i}\sum_{\lambda,\lambda'}\oint\oint dt_c dt_c' \phi_\alpha(t_c)\phi_\alpha(t_c')\psi_{i\lambda}^{y}(t_c) \times \psi_{i\lambda}^{z}(t_c)\psi_{i\lambda'}^{y}(t_c')\psi_{i\lambda'}^{z}(t_c'). \tag{27}$$

We have assumed that the initial state is not correlated with disorder profile (see comments in Secs. V D and V E for more details). The diagrammatic form of $S_{\rm eff}$ is given in Fig. 3. To have a systematic and controlled approximation in $1/N_s$ that captures the frustrated nature of the problem, we have to keep an infinite subset of 2PI diagrams shown in Fig. 4. A closed form for the corresponding summation can be found, as shown, for example, for the quantum $O(N)$ model in Refs. [60,61,63,83]. An easier approach is the auxiliary field method [60,61,63], based on the Hubbard-Stratonovich (HS) transformation [11,78,81,100]. HS transformation finds various applications in the study of collective effects in many-body systems such as plasmons [11], superconductivity [11,154], superfluidity [153] and quantum spin liquids [137]. The basic idea is to introduce a new field which we label as χ, that mediates the original interaction in $S_{\rm int}$. In our case, χ decouples the interaction between spins and cavity modes as diagrammatically illustrated in Fig. 5(a). The action of χ and its coupling to other degrees of freedom are given by (see Appendix B for a mathematical derivation)

$$S_{\rm int} \to S_\chi + S_{\chi\psi} + S_{g\chi\phi}, \tag{28}$$

where S_χ is the action of the HS defined as

$$S_\chi \equiv \frac{1}{2}\sum_{\alpha,\beta}^{M}\sum_{i,j}^{N}\sum_{\sigma,\sigma'}^{1,2}\oint\oint dt_c dt_c' \chi_{\alpha i}^{\sigma}(t_c) \left(\hat{W}_0^{-1}\right)_{\alpha i,\beta j}^{\sigma,\sigma'}(t_c,t_c')\,\chi_{\beta j}^{\sigma'}(t_c'). \tag{29}$$

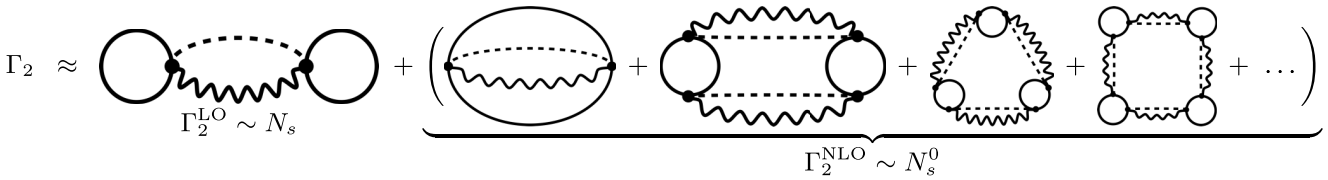

FIG. 4. Leading-order and next-to-leading-order diagrams in the $1/N_s$ expansion of 2PI action.

We name χ as the Ising field because it mediates the Ising-type interaction among spins as we see below. χ is a two-component real valued scalar field defined as

$$\vec{\chi}_{\alpha i} \equiv \left(\chi^1_{\alpha i}, \chi^2_{\alpha i}\right), \tag{30}$$

together with its inverse bare Green's function

$$\left(\hat{W}_0^{-1}\right)^{\sigma,\sigma'}_{\alpha i,\beta j}(t_c, t_c') \equiv \sqrt{N+M}\delta_{\alpha\beta}\delta_{ij}(\sigma^x)_{\sigma\sigma'}\delta(t_c, t_c'), \tag{31}$$

and its full Green's function

$$iW^{\sigma,\sigma'}_{\alpha i,\beta j}(t,t') \equiv \left\langle \chi^{\sigma}_{\alpha i}(t)\chi^{\sigma'}_{\beta j}(t')\right\rangle_c : \tag{32}$$

Note that the "free" part of the action for the Ising field S_χ is local in time and does not contain any time derivatives of χ. This makes the equations of motion for χ algebraic rather than differential. The latter is the generic case where the equations of motion for correlation functions form a system of coupled differential equations, and adiabatic elimination is equivalent to approximately ignoring the time derivatives of some of the dynamical variables, which are assumed to have a quick response compared with other timescales in the system. For the HS field, adiabatically eliminating χ is exact, which is equivalent to taking the Gaussian integral over χ in Eq. (29), and the result is given by $S_{\rm int}$ in Eq. (26). The next term in Eq. (28) is $S_{\chi\psi}$ which describes the coupling of fermions to the first component of χ:

$$S_{\chi\psi} \equiv -\frac{2i}{\sqrt{N_s}}\sum_{\alpha,i,\lambda}\oint dt_c \chi^1_{\alpha i}\psi^y_{i\lambda}\psi^z_{i\lambda}, \tag{33}$$

and $S_{g\chi\phi}$ describes the disordered interaction of photons with the second component of χ:

$$S_{g\chi\phi} \equiv \sqrt{2\omega_c}\sum_{\alpha,i}\oint dt_c \chi^2_{\alpha i} g_{\alpha i}\phi_\alpha. \tag{34}$$

The diagrammatic representations of the original vertex in Eq. (26) and the transformed ones [Eqs. (33) and (34)] are given in Fig. 5(a).

We show later that the two components of the Ising field correspond to different physical quantities. As will be shown in Sec. V H 1, χ^1 is related to the effective magnetic field experienced by each cluster and χ^2 is connected to magnetization. Similarly, the Green's functions of Ising fields are not just mathematical objects and have physical meanings. W can be expressed in terms of the original Green's functions as shown in Fig. 5(c). W^{22} is related to the spin-spin correlation function or equivalently, the four-point function of Majorana fermions,

$$\left\langle S^x_i(t)S^x_i(t')\right\rangle = -4\sum_{\lambda,\lambda'}^{N_s}\left\langle \psi^y_{i\lambda}(t)\psi^z_{i\lambda}(t)\psi^y_{i\lambda'}(t')\psi^z_{i\lambda'}(t')\right\rangle, \tag{35}$$

whose leading-order expansion is given by the same set of diagrams as W^{22} in Fig. 5(c), up to multiplication by an overall constant, as given by Eq. (78). Therefore, spin-spin correlation functions are natural byproducts of our formalism. Therefore, there is no need to solve the Bethe-Salpeter equations to obtain four-point functions of fermions, usually a cumbersome task particularly for out of equilibrium systems [78,85,155].

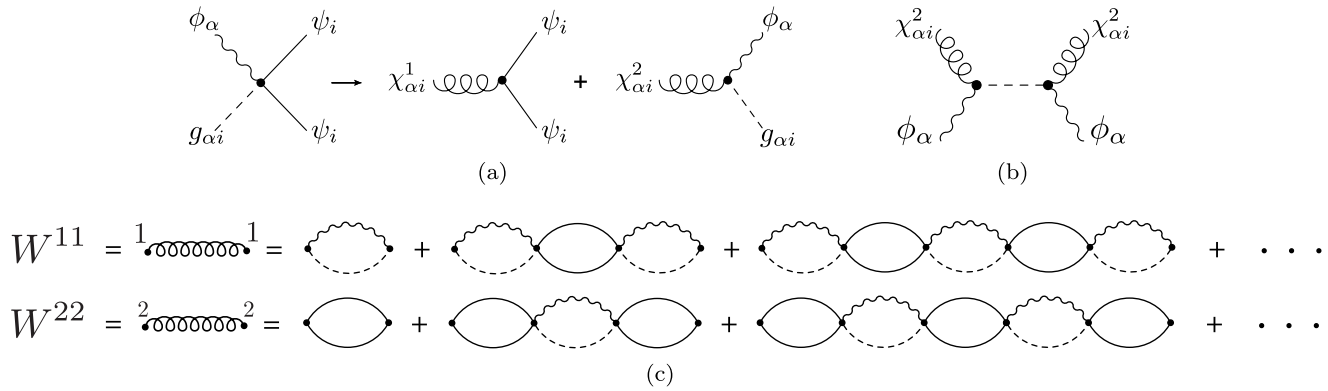

FIG. 5. (a) The original interaction vertex and the decoupled interactions after HS transformation. (b) The effective interaction between photons and the Ising field after disorder averaging. (c) Diagrammatic representation of the Ising (HS) field propagators. The appearing fermion and photon lines are assumed to be renormalized by interactions. W^{22} coincides with spin-spin correlation function, up to an overall multiplicative factor.

D. Disorder averaging

We can now take the average over the disordered couplings. In the Keldysh formalism, the average can be taken without resorting to the replica trick [100]. The only term in the action depending on g is $S_{g\chi\phi}$. The effective interaction after disorder averaging is given by $e^{iS_{\chi\phi}} = \overline{e^{iS_{g\chi\phi}}}$, where

$$S_{\chi\phi} = ig^2\omega_c \sum_{\alpha i} \oint \oint dt_c dt_c' \chi^2_{\alpha i}(t_c)\phi_\alpha(t_c)\chi^2_{\alpha i}(t_c')\phi_\alpha(t_c'), \quad (36)$$

is shown diagrammatically in Fig. 5(b). We have to make an important remark about the process of disorder averaging. In obtaining Eq. (36) we have assumed that the initial state of the system is not correlated with the disorder. This is valid for the initial states we consider in this paper. However, to study phenomena such as associative memory in multimode cavity QED [42,103,116,117,119,156], where a significant overlap of the initial spin configuration is required for memory retrieval, one has to assume that the initial state depends on $g_{\alpha i}$. In that case, disorder averaging will generate more terms than Eq. (36), which couple the initial state to the interaction vertex in Eq. (34).

E. Symmetry considerations

The symmetry structure of the model helps us to simplify the study of its dynamical response. Originally, the Hamiltonian in Eq. (1) is invariant only under a global Z_2 transformation that maps all spins and cavity modes simultaneously according to

$$\sigma^x_{i\lambda} \to -\sigma^x_{i\lambda}, \quad a_\alpha \to -a_\alpha. \quad (37)$$

According to the language of Refs. [87,157–159], in the absence of photon loss this is a quantum symmetry of the system with a conserved Z_2 charge. A quantum symmetry is a symmetry of the fields on each individual Keldysh contour, while a classical symmetry is the invariance of the Keldysh action under a simultaneous transformation of the fields on forward and backward contours [87]. With photon loss, the quantum symmetry is demoted to a classical symmetry without a conserved charge. However, starting from a symmetric initial state, a classical symmetry still guarantees that the symmetry will remain unbroken in the absence of symmetry-breaking perturbations.

The symmetry structure of the model is enriched after disorder averaging and using the fermion representation in Eq. (9). It can be easily verified that the disorder-averaged Keldysh action has the following sets of symmetries:

(1) A local Z_2 gauge symmetry under the transformation

$$\vec{\psi}_{i\lambda} \to -\vec{\psi}_{i\lambda}, \quad (38)$$

which holds for each spin separately. This symmetry is an artifact of representing spins in terms of quadratic fermion operators and is not physical. The initial state or external forces cannot break this symmetry. The important consequence of this symmetry is that

$$G^{\alpha,\beta}_{i\lambda,j\lambda'} \propto \delta_{ij}\delta_{\lambda\lambda'}. \quad (39)$$

(2) A Z_2 symmetry for each separate cluster i and Ising fields coupled to it:

$$\sigma^x_{i\lambda} \to -\sigma^x_{i\lambda} \ (\lambda = 1, \ldots, N_s), \quad (40)$$

$$\chi^\sigma_{\alpha i} \to -\chi^\sigma_{\alpha i} \ (\sigma = 1, 2;\ \alpha = 1, \ldots, M). \quad (41)$$

Equation (41) holds because the effective interaction in Eq. (36) is quadratic in χ. This symmetry is a classical symmetry with no conserved quantities.

(3) A Z_2 symmetry of each photon mode given by

$$\phi_\alpha \to -\phi_\alpha, \quad \pi_\alpha \to -\pi_\alpha. \quad (42)$$

This symmetry is also a result of $S_{\chi\phi}$ being quadratic in photon fields and is a weak symmetry. This symmetry implies that

$$D^{\rho,\rho'}_{\alpha,\beta} \propto \delta_{\alpha\beta}. \quad (43)$$

We see that the Z_2 symmetries of spin and photon sectors are decoupled. This means that, even if the initial state of spins breaks the symmetry, no photon coherence will be generated ($\overline{\langle a_\alpha(t)\rangle} = 0$). On the other hand, a finite value for $\sigma^x_{i\lambda}$ results in a finite value for $\chi^{1,2}_{\alpha i}$.

We again remark that the above arguments hold true only if the initial state of the system is not correlated with the disorder pattern, such that Eq. (36) is the only outcome of disorder averaging. Otherwise, a Z_2 broken initial state can in principle break the Z_2 symmetry of some of the photon modes. This happens for example, if the initial spin configuration has a strong overlap with a single disorder pattern corresponding to the photon mode α, such that

$$\lim_{N\to\infty} \frac{1}{NN_s} \left| \sum_i^N \sum_\lambda^{N_s} \langle \sigma^x_{i\lambda} \rangle_0 g_{\alpha i} \right| > 0, \quad (44)$$

or if a symmetry-breaking perturbation that favors a single pattern such as

$$\delta H = \epsilon \sum_{i,\lambda} g_{\alpha,i}\sigma^x_{i\lambda} \quad (45)$$

is applied to the system. In this case, one expects that for sufficiently small M/N, the pattern α to be activated and retrieved [103,117].

For the fully polarized initial states of spins considered in this problem and in the thermodynamic limit, we can safely take $\overline{\langle \phi_\alpha(t)\rangle} = 0$ throughout the evolution. Even starting from a state with $\langle\phi\rangle \neq 0$, its value will decay to zero as it cannot align itself with any of the disorder patterns.

F. Two-particle irreducible action

The 2PI action for the model given above is a functional of fermion, photon and Ising field correlation functions together with the expectation values of Ising fields and has the general form given by [61]

$$\begin{aligned}\Gamma[\tilde{\chi}, G, D, W] = {} & S_\chi[\tilde{\chi}] + \frac{i}{2}\mathrm{Tr}\ln G - \frac{i}{2}\mathrm{Tr}\left(G_0^{-1}G\right) \\ & - \frac{i}{2}\mathrm{Tr}\ln D + \frac{i}{2}\mathrm{Tr}\left(D_0^{-1}D\right) - \frac{i}{2}\mathrm{Tr}\ln W \\ & + \frac{i}{2}\mathrm{Tr}\left(W_0^{-1}W\right) + \Gamma_2[\tilde{\chi}, G, D, W]. \quad (46)\end{aligned}$$

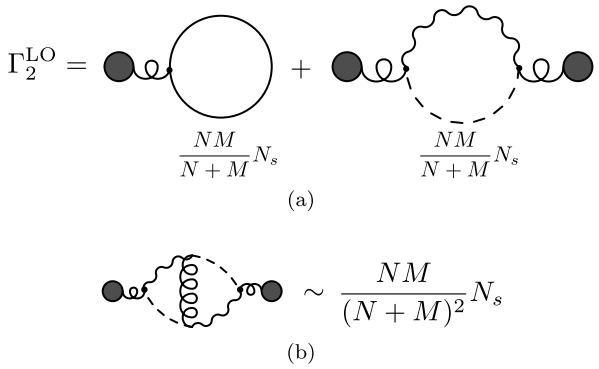

FIG. 6. (a) The leading-order contribution of interactions to 2PI action. The dashed line in the right diagram is not a Green's function and cannot be cut. (b) A diagram which linearly scales with N_s but is not extensive and neglected. Black circles connected to springs represent the expectation value of Ising field χ.

The expressions for S_χ, G_0, D_0, and W_0 were respectively given in Eqs. (29), (14), (19), and (31). $\tilde{\chi}$ is the expectation value of the Ising field

$$\tilde{\chi}^\sigma_{\alpha i}(t) \equiv \overline{\langle \chi^\sigma_{\alpha i}(t)\rangle}, \tag{47}$$

shown by a black circle connected to a spring in Fig. 6(a). The last term in Eq. (46) captures interactions and, as we mentioned in Sec. IV A, is given by the sum of 2PI diagrams. To systematically expand Γ_2, we need to specify how the expectation values and Green's functions of the Ising field scale with parameters of the system. According to Eq. (31), to the leading order in $(N+M)^{-1}$ we have

$$W^{12}_{i\alpha,j\beta} \sim \delta_{ij}\delta_{\alpha\beta} O\left(\frac{1}{\sqrt{N+M}}\right). \tag{48}$$

The diagonal elements W^{11} and W^{22} are zero at the bare level in Eq. (29). However, they become nonzero when the couplings of χ to ψ and ϕ are taken into account [Fig. 5(c)]. For W^{22} we have

$$W^{22}_{i\alpha,j\beta} \sim \delta_{ij} O\left(\frac{1}{N+M}\right). \tag{49}$$

As shown later, W^{11} has a subleading term due to interactions which contributes at leading order when it is summed over photon modes

$$W^{11}_{\alpha\beta} \sim \delta_{ij}\delta_{\alpha\beta} O\left(\frac{1}{N+M}\right) + \delta_{ij}(1-\delta_{\alpha\beta}) O\left(\frac{1}{(N+M)^2}\right). \tag{50}$$

Furthermore, $\tilde{\chi}$ will have the following scalings [Eqs. (73) and (72)]:

$$\tilde{\chi}^1 \sim O\left(\frac{\sqrt{N_s}}{N+M}\right), \quad \tilde{\chi}^2 \sim O\left(\sqrt{\frac{N_s}{N+M}}\right). \tag{51}$$

At last, the fermion-Ising vertex in Eq. (33) has

$$S_{\chi\psi} \sim \frac{1}{\sqrt{N_s}}. \tag{52}$$

We now have all of the necessary ingredients to perform a systematic expansion of Γ_2.

G. Diagrammatic evaluation of two-particle irreducible action

We are interested in the thermodynamic limit of the system in Eq. (1) where $N, M \to \infty$ while the ratio $\eta = M/N$ is kept fixed. Moreover, the number of spins per cluster N_s is assumed to be larger than one and will play the role of the control parameter for the expansion. Also, we assume that $N_s \ll N$, which is a valid assumption in the thermodynamic limit of the problem. The interaction part of the 2PI action, given by Γ_2 in Eq. (46), admits a diagrammatic expansion in terms of the connected vacuum bubbles of the theory which cannot be split into half by cutting one or two of their Green's function lines, also known as two-particle irreducible (2PI) graphs [61]. Below, we classify these diagrams for our system as leading-order (LO) terms

$$\Gamma_2^{\rm LO} \sim N_s, \tag{53}$$

and next-to-leading-order (NLO) terms

$$\Gamma_2^{\rm NLO} \sim N_s^0, \tag{54}$$

and higher-order terms which are ignored in this work. We also ignore terms which are subextensive.

The following discussion will also elucidate how the parameter controlling the strength of quantum fluctuations, N_s, enters naturally in the field theory description and in the DE derived from it. This is one of the key merits of the approach, at variance with more numerical oriented methods which have to deal with growing computational complexity as N_s is decreased.

1. Leading-order contributions

The LO terms have linear scaling with N_s and at the same time, scale extensively with system size. Two of these diagrams exist and both involve the expectation values of Ising fields, as shown in Fig. 6(a). Their mathematical expressions are given by

$$\Gamma_2^{\rm LO} = \frac{2}{\sqrt{N_s}} \sum_\alpha^M \sum_i^N \sum_\lambda^{N_s} \oint dt_c \tilde{\chi}^1_{\alpha i}(t_c) G^{y,z}_{i\lambda,i\lambda}(t_c,t_c) - g^2\omega_c \sum_\alpha^M \sum_i^N \oint\oint dt_c dt'_c \tilde{\chi}^2_{\alpha i}(t_c) D^{\phi\phi}_{\alpha,\alpha}(t_c,t'_c)\tilde{\chi}^2_{\alpha i}(t'_c). \tag{55}$$

Note that the disorder (dashed) line in Fig. 6(a) cannot be cut, as it is a part of the disorder averaged interaction vertex in Fig. 5(b). Accordingly, the right diagram in Fig. 6(a) is not two-particle reducible. It can be shown, by solving the resulting equations of motion derived from Eq. (55), that the LO terms describe a dynamical mean-field interaction of spin expectation values $\overline{\langle\sigma^x\rangle}$ mediated by photons through their response function (see Sec. VI A). Therefore, the LO contribution describes the LMG coupling in Eq. (5) with the inclusion of retardation effects due to photon dynamics.

We note that there are other terms that scale linearly with N_s, such as the one given in Fig. 6(b), but all of them scale nonextensively with system size and can be neglected in the thermodynamic limit.

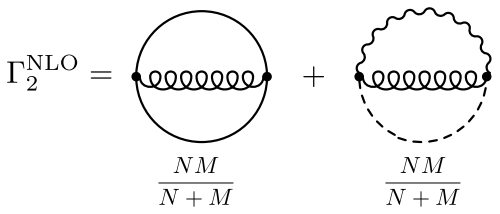

FIG. 7. Next-to-leading-order contributions to 2PI action.

2. Next-to-leading-order contributions

The NLO diagrams do not scale with N_s but still scale linearly with the number of clusters N. There are two NLO diagrams shown in Fig. 7 and their formulas are given by

$$\Gamma_2^{\rm NLO} = -\frac{2}{N_s}\sum_{\alpha,\beta}^{M}\sum_{i}^{N}\sum_{\lambda}^{N_s}\oint\oint dt_c dt_c' W^{11}_{\alpha i,\beta i}(t_c,t_c') \times\left[G^{y,z}_{i\lambda}(t_c,t_c')G^{z,y}_{i\lambda}(t_c,t_c') - G^{y,y}_{i\lambda}(t_c,t_c')G^{z,z}_{i\lambda}(t_c,t_c')\right] - ig^2\omega_c\sum_{\alpha}^{M}\sum_{i}^{N}\oint\oint dt_c dt_c' W^{22}_{\alpha i,\alpha i}(t_c,t_c')D^{\phi\phi}_{\alpha\alpha}(t_c,t_c'). \tag{56}$$

The rest of the terms in Γ_2 are either next-to-next-to-leading-order (NNLO) in $1/N_s$ or scale subextensively with system size (Fig. 8). In this work we neglect these terms and take

$$\Gamma_2 \approx \Gamma_2^{\rm LO} + \Gamma_2^{\rm NLO}. \tag{57}$$

It is worth showing which diagrams we are keeping in terms of the original action prior to HS transformation (Fig. 4). As mentioned before, the LO part describes a retarded self-interaction of the spin expectation value expressed in terms of fermion Green's function [according to Eq. (9)]:

$$\overline{\langle\sigma^x\rangle} = 2G^{z,y}_{-+}(t,t), \tag{58}$$

given by closed loops in the first term of Fig. 4, within the same cluster and mediated by photons. In the regime of fast photons and at steady state, this reduces to the ferromagnetic interaction in Eq. (6). For NLO terms, the two diagrams in Fig. 7 are equivalent to the sum of an infinite number of diagrams in the original representation of the theory, shown in the brackets of Fig. 4. This can be verified by plugging the diagrammatic expression of W given in Fig. 5(c) into the diagrams of Fig. 7, and subsequently substitute the lines for bare W with simple dots, as the latter is just a constant. This

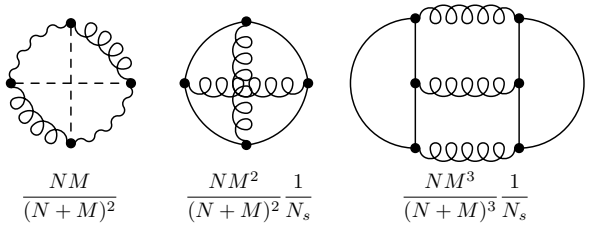

FIG. 8. Some of the neglected diagrams in this work which appear after NLO terms. The left diagram is subextensive in system size and the rest are NNLO in $1/N_s$.

infinite series is a byproduct of disordered couplings. For the Dicke model without disorder (see Appendix G), only the first NLO diagram would contribute since in the absence of disorder, dashed lines would disappear. This makes the rest of NLO diagrams two-particle-*reducible* and hence, forbidden in the expansion of Γ_2.

H. Equations of motion

Green's functions and field expectation values are obtained from the stationary solution of QEA which is found from

$$\frac{\delta\Gamma}{\delta\tilde{\chi}^{\sigma}_{\alpha i}(t)} = 0, \quad \frac{\delta\Gamma}{\delta W^{\sigma\sigma'}_{\alpha i,\beta j}(t_c,t_c')} = 0, \tag{59}$$

$$\frac{\delta\Gamma}{\delta D^{\rho\rho'}_{\alpha,\beta}(t_c,t_c')} = 0, \quad \frac{\delta\Gamma}{\delta G^{\alpha\beta}_{i\lambda,j\lambda'}(t_c,t_c')} = 0. \tag{60}$$

After taking functional derivatives of Eq. (46), we see that the equations of motion for Green's functions can always be cast compactly as

$$\hat{G}^{-1} = \hat{G}_0^{-1} - \hat{\Sigma}, \tag{61}$$

$$\hat{D}^{-1} = \hat{D}_0^{-1} - \hat{\Pi}, \tag{62}$$

$$\hat{W}^{-1} = \hat{W}_0^{-1} - \hat{\Omega}, \tag{63}$$

known as Dyson equations [61,86,100]. The matrices $\hat{\Sigma}$, $\hat{\Pi}$, and $\hat{\Omega}$ are fermion, photon, and Ising field self-energies, respectively. They are given in terms of the functional derivatives of Γ_2 as

$$\Sigma^{\alpha,\beta}_{i\lambda,j\lambda'}(t_c,t_c') \equiv -2i\frac{\delta\Gamma_2}{\delta G^{\beta,\alpha}_{j\lambda',i\lambda}(t_c',t_c)}, \tag{64}$$

$$\Pi^{\rho,\rho'}_{\alpha,\beta}(t_c,t_c') \equiv +2i\frac{\delta\Gamma_2}{\delta D^{\rho',\rho}_{\beta,\alpha}(t_c',t_c)}, \tag{65}$$

$$\Omega^{\sigma,\sigma'}_{\alpha i,\beta j}(t_c,t_c') \equiv +2i\frac{\delta\Gamma_2}{\delta W^{\sigma',\sigma}_{\beta j,\alpha i}(t_c',t_c)}. \tag{66}$$

Due to their large size, the expanded forms of Eqs. (61)–(63), required for numerically solving them, are given in Appendix C. We only mention the important details here. The fermion and photon Green's functions will be diagonal in the spin-site and photon-mode bases, respectively. Due to permutation symmetry [18,19,160] we also have

$$G^{\alpha,\beta}_{i\lambda,j\lambda'}(t_c,t_c') = \delta_{ij}\delta_{\lambda\lambda'}G^{\alpha,\beta}(t_c,t_c'), \tag{67}$$

$$D^{\rho,\rho'}_{\alpha,\beta}(t_c,t_c') = \delta_{\alpha\beta}D^{\rho,\rho'}(t_c,t_c'). \tag{68}$$

The same is true for their self-energies. The Ising field's Green's function and its self-energy will acquire off-diagonal elements only in the photon indices. Due to the emergent permutation symmetry after disorder averaging, all diagonal elements of W and Ω are the same. This holds also for the off-diagonal elements of W and Ω:

$$W^{\sigma,\sigma'}_{\alpha i,\alpha j}(t_c,t_c') = \delta_{ij}V^{\sigma,\sigma'}(t_c,t_c'), \tag{69}$$

$$W^{\sigma,\sigma'}_{\alpha i,\beta j}(t_c,t_c') = \delta_{ij}U^{\sigma,\sigma'}(t_c,t_c'), \quad \alpha\neq\beta. \tag{70}$$

A similar argument applies to $\tilde{\chi}$, and it has the same value for all sites and photon modes:

$$\tilde{\chi}^{\sigma}_{\alpha i}(t) = \tilde{\chi}^{\sigma}(t). \tag{71}$$

We proceed similarly to the previous section. We find the equations of motion at LO first and then consider the NLO corrections.

1. Equations of motion at leading order

For $\tilde{\chi}$, one always finds that it has the same value on forward and backward Keldysh contours, as it should be since these are classical variables. From Eqs. (55) and (59) we have

$$\frac{\delta\Gamma^{\rm LO}}{\delta\tilde{\chi}^1} = 0 \to \tilde{\chi}^2(t) = -2\sqrt{\frac{N_s}{N+M}}G^{y,z}_{-+}(t,t), \tag{72}$$

$$\frac{\delta\Gamma^{\rm LO}}{\delta\tilde{\chi}^2} = 0 \to \tilde{\chi}^1(t) = \frac{2g^2\omega_c}{\sqrt{N+M}}\int_0^t dt' D^{\phi\phi}_R(t,t')\tilde{\chi}^2(t'), \tag{73}$$

where $D^{\phi\phi}_R$ is the photon response function defined as (for details see Appendix C)

$$D^{\phi\phi}_R(t,t') \equiv -i\Theta(t-t')\overline{\langle[\hat{\phi}(t),\hat{\phi}(t')]\rangle}, \tag{74}$$

which describes the response of the photons to an external linear perturbation. Note that the time variables used in Eq. (74) are normal variables and are not defined on the time contour. Substituting (72) into (73) gives

$$\tilde{\chi}^1(t) = -\frac{4g^2\omega_c\sqrt{N_s}}{N+M}\int_0^t dt' D^{\phi\phi}_R(t,t')G^{y,z}_{-+}(t',t'), \tag{75}$$

in agreement with the scaling relations for $\tilde{\chi}$ given in Eq. (51).

For Σ we have at leading order

$$\Sigma^{\alpha,\beta}_{\rm LO}(t_c,t'_c) = \quad = -\frac{2iM}{\sqrt{N_s}}\epsilon_{x\alpha\beta}\delta(t_c,t'_c)\tilde{\chi}^1(t_c). \tag{76}$$

The temporally local elements of fermion self-energy describe the effective magnetic-field spins experience due to interactions. Accordingly, Eq. (76) describes a time-dependent magnetic field B_x in the $\hat{x}$ direction experienced by each spin. This sheds light on the physical meaning of the first component of the HS field: it is the magnetic field experienced by each spin and its Green's functions give the fluctuations of this field. This could be inferred also from Eq. (33) which describes the coupling of $\sigma^x = -2i\psi^z\psi^y$ to χ_1. Similarly, Eqs. (72) and (58) relate χ^2 to $\langle\sigma^x\rangle$ as

$$\overline{\langle S^x_i(t)\rangle} = -\sqrt{(N+M)N_s}\tilde{\chi}^2(t)/2. \tag{77}$$

Furthermore, it can be shown that W^{22} is related to the two-point correlation function of the large spins $S^x_i = \sum_\lambda \sigma^x_{i\lambda}/2$ through

$$\overline{\langle S^x_i(t_c)S^x_i(t'_c)\rangle_c} = i(N+M)N_sV^{22}(t_c,t'_c)/4. \tag{78}$$

Equation (78) can be rigorously proven by introducing source terms in the Keldysh action which are coupled to σ^x, and then taking functional derivatives with respect to the sources twice (cf. Appendix B). By substituting $\tilde{\chi}^1$ from Eq. (75) into Eq. (76), the effective magnetic field B_x is found to be

$$B_x(t) = -\frac{4g^2\omega_cM}{N+M}\int_0^t dt' D^{\phi\phi}_R(t,t')G^{y,z}_K(t',t'). \tag{79}$$

Interpreting Eq. (79) is straightforward now; spins perturb photons whose displacement is given by ϕ which acts as an effective field applied to spins through the Dicke coupling in Eq. (1), creating a self-interaction for spins.

Last, we investigate the photon sector at LO by calculating the photon self-energy Π. Since all terms in Γ_2 only depend on the $\phi\phi$ component of D, the only nonzero element of photon self-energy is $\Pi^{\phi\phi}$ given by

$$\Pi^{\phi\phi}_{\rm LO}(t_c,t'_c) = \quad = -2iNg^2\omega_c\tilde{\chi}^2(t_c)\tilde{\chi}^2(t'_c). \tag{80}$$

Written in terms of normal time variables, it is easy to show that $\Pi^{\rm LO}$ does not alter the spectrum or equivalently [11,100], the response function of photons. Hence, its only effect is to increase the photon population. At this order, spins pump photons, but without generating any finite values for $\langle\phi\rangle$. As couplings to different clusters have different signs, their MF contributions cancel out each other in the thermodynamic limit and photon pumping is realized only at the level of fluctuations. Furthermore, no changes of $D^{\phi\phi}_R$ at this order of approximation means that the kernel of the effective interaction between spins is given by its noninteracting form, i.e., it is the response function of a damped (for $\kappa \neq 0$) harmonic oscillator. We note that the self-energy of the Ising field vanishes at this order.

We summarize the physics of the problem in the LO approximation. There is an effective Ising-like interaction of spins within the same cluster with a retarded kernel given by the response of cavity photons in the noninteracting limit. Photons are coherently pumped by spins, but their energy levels and loss rates remain unaffected. At this order of approximation, the model behaves very similar to the MF solution of the Dicke model. The effective retarded spin-spin interaction is generated also for the Dicke model, if we formally solve the equation of motion for the photon mode in terms of σ^x and then, substitute them back in the equations of motion for spins.

2. Equations of motion at next-to-leading order

As is evident from Eq. (56), $\Gamma^{\rm NLO}_2$ does not depend on $\tilde{\chi}$. Therefore, Eqs. (72) and (73) describe $\tilde{\chi}$ to NLO. Accordingly, the general picture of an effective MF interaction between spins remain unaltered. Although the interaction kernel given by $D^{\phi\phi}_R$ will be renormalized by fluctuations at NLO.

The self-energies at NLO are found from the functional derivatives of $\Gamma^{\rm NLO}_2$ and are given by

$$\Sigma^{\alpha,\beta}_{\rm NLO}(t_c,t'_c) = \quad = \frac{4iM}{N_s}\big(V^{11}(t_c,t'_c) + (M-1)U^{11}(t_c,t'_c)\big) \times \sum_{\gamma,\delta}\epsilon_{x\alpha\gamma}\epsilon_{x\beta\delta}G^{\gamma,\delta}(t_c,t'_c), \tag{81}$$

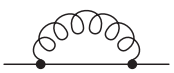

$$\Pi^{\phi\phi}_{\mathrm{NLO}}(t_c,t'_c) = \quad = 2Ng^2\omega_c V^{22}(t_c,t'_c). \tag{82}$$

Ising self-energies are nonvanishing at this order are

$$(\Omega_{\mathrm{NLO}})^{11}_{\alpha\beta}(t_c,t'_c) = \quad = 4ig^2\omega_c \times \left(G^{yy}(t_c,t'_c)G^{zz}(t_c,t'_c) - G^{yz}(t_c,t'_c)G^{zy}(t_c,t'_c)\right), \tag{83}$$

$$(\Omega_{\mathrm{NLO}})^{22}_{\alpha\beta}(t_c,t'_c) = \quad = 2g^2\omega_c\delta_{\alpha\beta}D^{\phi\phi}(t_c,t'_c). \tag{84}$$

We see that the off-diagonal element of W given by U is multiplied by an extra factor of $O(M)$ in Eq. (81), and it has to be kept though it is subleading compared with the diagonal element V. The resulting equations of motion are a system of 36 coupled integro-differential equations for different components of Green's functions and $\tilde{\chi}$. The complete expressions for these equations are given in Appendix C in terms of the symmetric (Keldysh) and antisymmetric (retarded and advanced) correlation functions.

3. Evaluation of glass order parameter

The formalism developed so far is sufficient to calculate some of the correlation functions of our system which are usually the quantities of interest for quantum dynamics. However, for systems with static disorder, we can define new types of expectation values depending on the order of calculating operator expectation values and disorder averaging [99]. As will be explained in Sec. VI C 2, the spin overlap quantity

$$Q(t) \equiv \frac{1}{N_s^2}\overline{\langle S^x_{i,A}(t)S^x_{i,B}(t)\rangle_c} \tag{85}$$

between two similar copies (A and B) of the system, which measures the statistical correlations between A and B generated by the disorder, is of particular importance in our analysis (cf. Fig. 2). $Q(t)$ cannot be evaluated directly in terms of the "normal" correlation functions, simply because of the noncommutativity of taking expectation values and disorder averaging in Eq. (85). However, it can still be calculated thanks to the versatility of the Keldysh approach in dealing with quenched disorder [11,100]. The correlation between the value of an observable $\hat{O}$ in two systems before disorder averaging can be written as

$$\langle\hat{\mathcal{O}}_A(t)\hat{\mathcal{O}}_B(t)\rangle = \int \mathcal{D}[\phi_A]\mathcal{D}[\phi_B]\mathcal{O}_A(t)\mathcal{O}_B(t)e^{iS[\phi_A,g_{\alpha i}]+iS[\phi_B,g_{\alpha i}]}. \tag{86}$$

Note that up to this point fields belonging to different copies, ϕ_A and ϕ_B, do not interact with each other. We can now straightforwardly find

$$Q(t) = \int \mathcal{D}[\phi_A]\mathcal{D}[\phi_B]\mathcal{O}_A(t)\mathcal{O}_B(t)\overline{e^{iS[\phi_A,g_{\alpha i}]+iS[\phi_B,g_{\alpha i}]}}. \tag{87}$$

Since the actions of both copies depend on the same realization of $g_{\alpha i}$, averaging over disorder couples fields of different replicas, and generates an effective interaction between them. However, the effective interaction only affects inter-replica quantities of the form given in Eq. (86). Before applying Eq. (87) to our problem, we make some remarks about our finding. Clearly, there is a strong resemblance between our result and the replica trick [11,99,161,162] as they both involve more than one copy of the system. However, there are also crucial differences between the two. In the replica trick the number of replicas is taken to zero via analytical continuation while here we are strictly working with two copies of the system. Depending on the particular system and other parameters such as temperature, RSB may or may not occur while the system is nevertheless a glass [99,122]. However, as we explain later (cf. Sec. VI C 2), if one-point functions are vanishing while Q is finite, the system has glassy behavior. Despite these differences, we call Eq. (87) the "replicated model" for convenience. We note that a similar replica approach has been used by Ref. [97] to study measurement-induced phase transitions due to continuous-time measurements.

We apply Eq. (87) to the HS transformed interaction part of the action in Eq. (28). $S_{g\chi\phi}$ is the only term depending on $g_{\alpha i}$ and has to be averaged in Eq. (87). The result of disorder averaging are three terms, two of them couple fields from the same copies and correspond to the effective vertex $S_{\chi\phi}$ in Eq. (36). The third term gives an interaction between fields of different copies and reads

$$S^{AB}_{\chi\phi} = 2ig^2\omega_c\sum_{\alpha i}\iint dt_c dt'_c\chi^2_{\alpha i,A}(t_c)\phi_{\alpha,A}(t_c)\chi^2_{\alpha i,B}(t'_c)\phi_{\alpha,B}(t'_c). \tag{88}$$

Using this "replicated Keldysh field theory," we can obtain $Q(t)$ in terms of the diagonal ($t = t'$) elements of inter-replica correlation functions. To distinguish inter-replica correlators from the normal ones, we represent the former with a tilde mark below them such as $\underset{\sim}{D}^{\rho,\rho'}_{\alpha,\beta}(t_c,t'_c)$. For example, for Q we have

$$Q(t) = i\frac{N+M}{8N_s}\underset{\sim}{V}^{22}(t,t). \tag{89}$$

For the replicated theory, there will be four more independent equations of motion that have to be solved in addition to those of the previous section. Crucially, these extra equations do not alter the dynamics of replica-diagonal quantities, as expected, since replicas are just abstractions and are not "aware" of each other. Nonreplica diagonal quantities, on the other hand, depend both on replica diagonal and nonreplica diagonal correlation functions. Furthermore, all of the nonreplica diagonal response functions turn out to vanish, as perturbing one replica cannot leave any effects on the other one. We leave the details of the calculations and the extra equations of motion to Appendix D.

VI. RESULTS

In this section, we report our findings in the following order. First, we discuss in Sec. VI A the results of approximating the effective action only to LO. In Sec. VI B, we demonstrate that the NLO corrections significantly change the dynamics

for all values of N_s, motivating the necessity of keeping NLO effects. In Sec. VI C, we discuss the formation of SG phase in the system by studying various physical characteristics of SG in our system. We also address the effect of spin size N_s and photon frequency on the glassy behavior of the system.

We study the quench dynamics starting from a polarized spin state specified by the angles (θ_0, φ_0) such that

$$\langle \vec{\sigma} \rangle_0 = (\sin\theta_0 \cos\varphi_0,\ \sin\theta_0 \sin\varphi_0,\ \cos\theta_0), \tag{90}$$

and the vacuum state for photons $|0\rangle$ satisfying $\hat{a}|0\rangle = 0$. We turn on the spin-photon coupling g at $t = 0$ and let the system evolve.

A. Results at leading order

The equations of motion for the diagonal elements of fermion Green's functions become decoupled from the nondiagonal elements at LO. This allows us to write the dynamics of magnetization $\vec{m} = \langle \vec{\sigma} \rangle$ in a transparent form as (Appendix E 1)

$$\frac{d}{dt} m_x(t) = -\Delta m_y(t), \tag{91}$$

$$\frac{d}{dt} m_y(t) = \Delta m_x(t) - J\omega_c^2 \int_0^t m_z(t) D_R^{\phi\phi}(t,t') m_x(t') dt', \tag{92}$$

$$\frac{d}{dt} m_z(t) = J\omega_c^2 \int_0^t m_y(t) D_R^{\phi\phi}(t,t') m_x(t') dt', \tag{93}$$

where J is the coupling of LMG model defined in Eq. (4). The photon response function $D_R^{\phi\phi}$ is given by its bare value at LO which is (the minus of) the response function of a damped harmonic oscillator

$$D_R^{\phi\phi}(t-t') = -\frac{\Theta(t-t')}{\omega_c^2} e^{-\kappa(t-t')} \sin\omega_c(t-t'). \tag{94}$$

Equations (91)–(93) describe the motion of classical angular-momentum variables with a conserved vector length $|\vec{m}| = 1$. Adiabatic elimination of photons [163] amounts to approximate the integral in Eq. (93) as

$$\begin{aligned} &\approx m_y(t) m_z(t) \int_0^t D_R^{\phi\phi}(t-t') dt' \approx m_y(t) m_z(t) \int_0^\infty D_R^{\phi\phi}(t') dt' \\ &\approx -\frac{1}{\omega_c(\omega_c^2 + \kappa^2)} m_y(t) m_z(t). \end{aligned} \tag{95}$$

Substituting (95) into Eqs. (92) and (93) results in the MF equations of motion for LMG model with a coupling modified by photon loss according to $J \to J\omega_c^2/(\omega_c^2 + \kappa^2)$. From a physical point of view, the above derivation shows that, at LO, our approximation maps each cluster to a classical LMG system *without coupling to other clusters*. Therefore, the LO approximation describes the FM-to-PM transition of an infinite-range Ising model with retarded interactions. The critical coupling of this system is determined according to the condition $\Delta = J$ [111] to be

$$g_c = \frac{1}{2}\sqrt{\frac{\Delta(\omega_c^2 + \kappa^2)}{\omega_c} \frac{N+M}{M}}. \tag{96}$$

Although only valid in the adiabatic regime of the MF solution, we use g_c throughout this paper and scale the coupling g according to it when comparing our results for different values of Δ, ω_c, or κ. Clearly, dynamics at LO do not have any features unexplored in the past, and we only report the results of our simulations as a consistency check of our approach. In Fig. 9 we have shown the dynamics of spins initiated close to an equilibrium state of Eqs. (91)–(93) inside the FM phase. We see that for fast photons (top panel of Fig. 9), the system remains close to the minimum with oscillations which are smoothed by photon loss. For slow photons when adiabatic elimination does not work (bottom panel of Fig. 9), the fluctuations induced by photon dynamics relieve FM correlations and can create rare tunneling events. With photon loss, the destructive effect of slow photons on FM order is reduced due to the effective damping that slows down the spins towards the bottom of the nearby energy minimum.

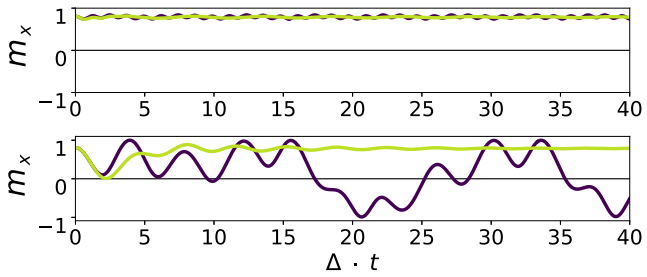

FIG. 9. Dynamics at the leading-order of approximation describing the motion of classical spins coupled via a retarded interaction, for $g/g_c = 1.27$ and $(\theta_0, \varphi_0) = (0.7\pi, 0)$. (top panel) Dynamics of spins in the adiabatic limit $\omega_c/\Delta = 5.0$ and for $\kappa = 0$ (dark purple curve) and $\kappa/\Delta = 0.5$ (light green curve). (bottom panel) The same as the top panel only for slow photons $\omega_c = \Delta$, showing tunneling events when photon loss is weak.

Having explored spin dynamics at LO, we now discuss the evolution of the photon sector. As we said before, the response of photons given by the retarded function $D_R^{\phi\phi}$ is unaltered by interactions at LO. However, the symmetric correlation function of photons and photon population are affected by the coupling to spins. Spins pump cavity modes due to the presence of the transverse field Δ, and as shown in Fig. 10, create large oscillations (if $\kappa = 0$) or a superradiant burst (if $\kappa \neq 0$) in the population of photons $n(t)$. We do not discuss dynamics of the PM phase in LO approximation here due to

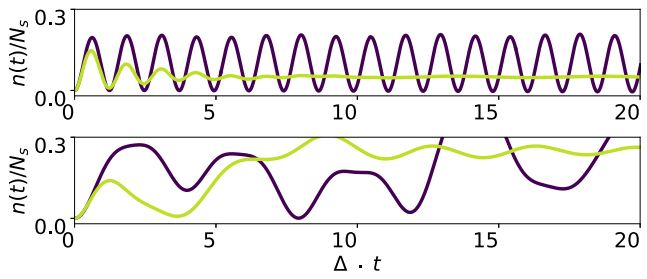

FIG. 10. Evolution of photon population per each mode normalized by cluster size N_s, for $g/g_c = 1.27$ and $(\theta_0, \varphi_0) = (0.7\pi, 0)$. (top panel) The adiabatic limit $\omega_c/\Delta = 5.0$ and for $\kappa = 0$ (dark purple curve) and $\kappa/\Delta = 0.5$ (light green curve). (bottom panel) The same as the top panel only for slow photons $\omega_c = \Delta$.

their trivial nature, and will show them in comparison with NLO results later.

The insufficiency of the LO approximation is clear by above observations. At this order of approximation, the size of each cluster N_s only appears as an overall scaling factor in photon number $n(t) \propto N_s$, and spin dynamics do not depend on N_s. The latter is not physically valid, as we expect fluctuations to affect spin dynamics noticeably when the spin per each cluster $\hat{S}_i = \sum_\lambda \hat{\sigma}_{i\lambda}/2$ becomes smaller as N_s is decreased. The other important shortcoming of LO approximation is visible in the dynamics of photon population in the adiabatic limit without loss, where the amplitude of the oscillations in $n(t)$ does not change and remains constant (Fig. 10). In reality, photons experience dissipation even in a perfect cavity because they can be reabsorbed by spins over longer timescales and the system is expected to equilibrate eventually. It is clear from the discussion above that LO approximation fails to capture this effect. As we see next, NLO corrections take into account fluctuations and the reabsorption of photons, in addition to nontrivial regimes of dynamics such as glassy behavior.

B. Results at next-to-leading order for large spins

Below we report on the dynamics at NLO for quenches to PM and FM phases of the system in the limit of many spins per cluster ($N_s = 10^5$). We note that we label these phases according to the behavior of the system at the MF level. The dynamics may change significantly when going beyond MF theory, making these labels inaccurate a posteriori.

1. Dynamics in the paramagnetic phase

We initialize the system in the ground state of photons and the spin state with $(\theta_0, \varphi_0) = (0.7\pi, 0)$ in Eq. (90). We choose a coupling below g_c given in Eq. (96) and consider both cases of perfect and lossy cavities.

The results for fast photons ($\omega_c/\Delta = 5$) are shown in Fig. 11, in comparison with LO results. We see that the evolution of m_x is considerably altered by taking fluctuations into account. Spin dynamics is now damped even in the absence of photon loss. This is expected because dissipation is a natural byproduct of interactions in a many-body system. We also see that photon loss has a minor impact on spin dynamics as it is weaker than the fluctuation-induced dissipation. As shown in the middle panel of Fig. 11, σ^z shows a surprising behavior at NLO by not relaxing to its minimum value, in contrast with the LO result which at least, when $\kappa \neq 0$, approaches -1. However, there is a clear explanation for this phenomenon. The value of g^2 gives the variance of the disordered coupling in the system. This means that, while most of the individual couplings for each realization of the disorder are smaller than g, some of them are still large enough to weaken the PM configuration of the ground state without causing a phase transition in the system. The fact that this behavior is purely due to random interactions is supported by our observation that the NLO approximation for nondisordered Dicke model results in the decay of spins into a state with $\sigma^z = -1$ in the PM phase. We also have shown the evolution of the spin vector

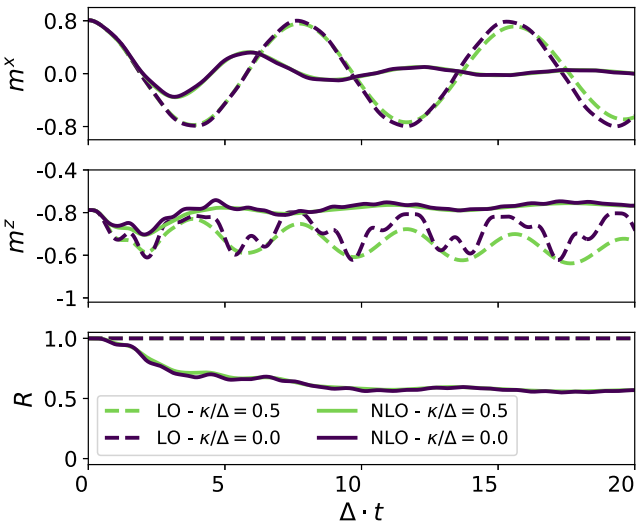

FIG. 11. Comparison of spin dynamics at LO and NLO approximations for a large spin size ($N_s = 10^5$), following a PM quench ($g/g_c = 0.71$) and in the limit of fast photons $\omega_c/\Delta = 5$ with ($\kappa/\Delta = 0.5$) and without photon loss. Top, middle, and bottom rows show the evolution of m_x, m_z, and the expectation value of spin size, respectively. Spins dephase to a single point due to random static couplings in the system.

size defined by

$$R(t) \equiv \sqrt{(m_x)^2 + (m_y)^2 + (m_z)^2} \tag{97}$$

in Fig. 11. While R is a constant of motion of Eqs. (91)–(93), it changes when fluctuations are considered. The final state of the system is a PM with a smaller spin size. Note that $R(t \to \infty)$ is independent of the initial state and is always smaller than one even at the lowest temperatures, only due to the frustrated nature of the system. In the following discussion, $R(t)$ will be a useful proxy for assessing the impact of correlations in dynamics. It is the radius of the Bloch sphere, given at $t = 0$ by the spin coherent state in Eq. (90), and a constant of motion for all-to-all interacting spin systems with homogeneous couplings and collective dissipation [18,114,164]. It stays constant over time because in this class of systems, the MF approximation is exact in the thermodynamic limit and therefore no higher-order cumulants are formed, which would make $R(t)$ shrink, signaling the onset of a strongly correlated regime.

Spin dynamics at NLO approximation for the case of resonant photons $\omega_c = \Delta$ are illustrated in Fig. 12. As expected, dynamics become more irregular both at LO and NLO and photon loss has a more dramatic effect on the dynamics.

2. Dynamics in the ferromagnetic phase

We quench the coupling to $g = 1.27 g_c$ where a FM state is realized at LO, as shown previously,. The initial spin vector is again taken to be $(\theta_0, \varphi_0) = (0.7\pi, 0)$, such that spins are close to the ground state of the classical model in Eqs. (91)–(93) at the chosen coupling strength. Similar to the PM case, we take a large spin size ($N_s = 10^5$) where the effect of NLO corrections is supposed to be small. It will become clear that

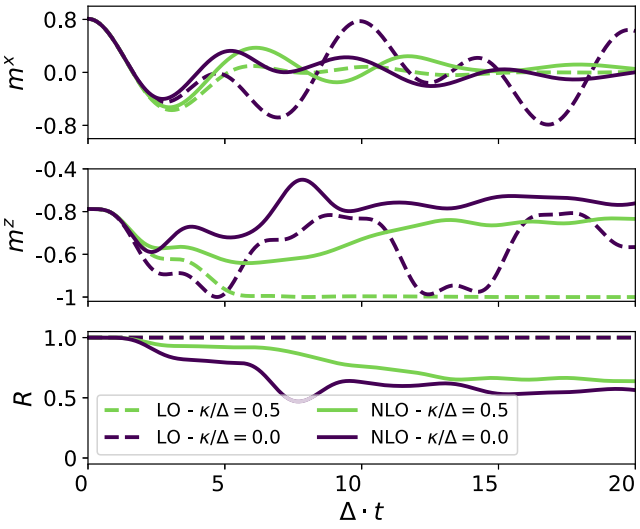

FIG. 12. Comparison of spin dynamics at LO and NLO approximations for a large spin size ($N_s = 10^5$), following a PM quench ($g/g_c = 0.71$) and in the limit of resonant photons $\omega_c = \Delta$ with ($\kappa/\Delta = 0.5$) and without photon loss. Top, middle, and bottom rows show the evolution of m_x, m_z, and the expectation value of spin size, respectively. Spins dephase to a single point due to random static couplings in the system.

this is an incorrect assumption and NLO contributions are significant.

The results of the numerics for the adiabatic limit $\omega_c/\Delta = 5$ are depicted in Fig. 13 at LO and NLO approximations. At LO, m_x and m_z show small oscillations around the equilibrium of the MF dynamics and the spin vector is confined to the surface of the Bloch sphere ($R = 1$). Fluctuations captured at NLO drastically alter the dynamics. All components of spin decay and the spin vector shrinks toward the center of the Bloch sphere. The spin decay features an interesting profile. For an initial period, the relaxation is quick and spins experience a collapse to a smaller but finite value. Following this, the relaxation becomes very slow and the spin vector spirals around the axis of FM order of the LO solution (Fig. 14). This situation is similar to the phenomenon of prethermalization in the quench dynamics of many-body quantum systems [23,66,78,165–172], although here the system can be open. The prethermal behavior is also seen in the time evolution of photon number $n(t)$ shown in Fig. 15(a). During the prethermal plateau of spins, $n(t)$ has a nearly stationary value with a slow growth [visible in the overall slope of the light curve in Fig. 15(b) towards the true equilibrium state. Photon losses only qualitatively affect spin dynamics, by weakly accelerating the process of relaxation.

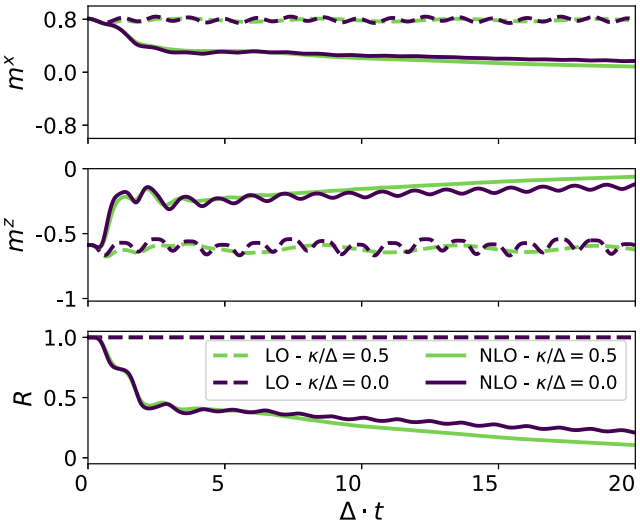

FIG. 13. Comparison of spin dynamics at LO and NLO approximations for a large spin size ($N_s = 10^5$), following a FM quench ($g/g_c = 1.27$) and in the limit of fast photons $\omega_c/\Delta = 5$ with ($\kappa/\Delta = 0.5$) and without photon loss. (top panel) Following a quick collapse, the decay of FM order parameter strongly slows down and a prethermal plateau forms. The middle and bottom panels show the evolution of m_z and the radius of the Bloch sphere, respectively.

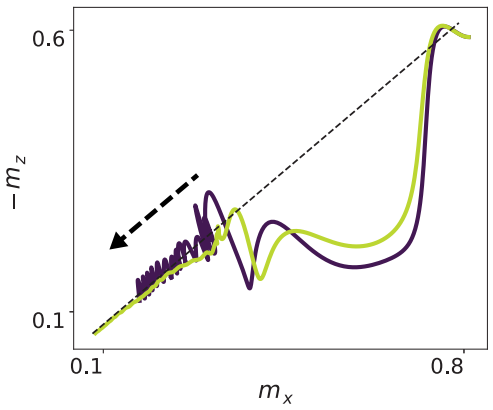

FIG. 14. Evolution of spin vectors projected to the xz plane for large cluster size $N_s = 10^5$ and for $\kappa/\Delta = 0$ (dark purple curve) and $\kappa/\Delta = 0.5$ (light green curve). Spins feature a spiral relaxation around the axis of FM ordering (dashed line) and towards the origin (parallel to the arrow).

As we emphasized before, labeling the system as a FM for $g > g_c$ is only valid at the MF level. It is clear from the

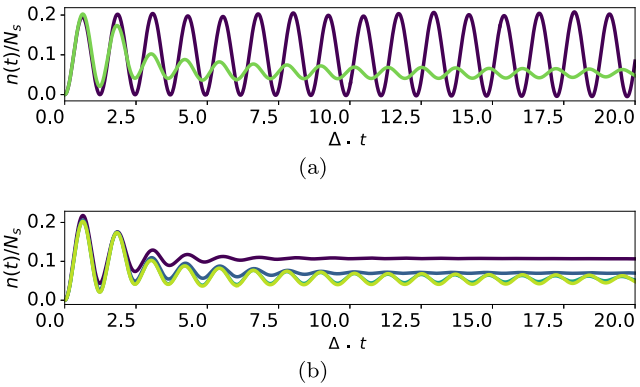

FIG. 15. (a) Photon population for a quench into the ordered phase with $g/g_c = 1.27$, $\omega_c/\Delta = 5$, and $\kappa = 0$ at LO (dark purple curve) and NLO (light green curve). (b) Photon number per mode for $g/g_c = 1.27$ and for $N = 1000, 200, 20, 5$ (light to dark curves). Relaxation of late-time oscillations is faster for smaller N_s.

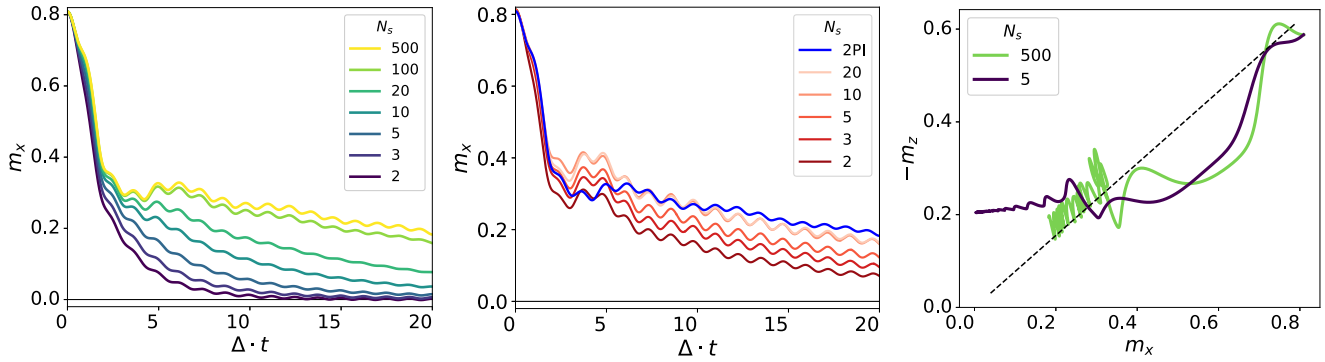

(a) (b) (c)

FIG. 16. Spin dynamics for different numbers of spin sizes $S = N_s/2$, for $g/g_c = 1.13$, and $\omega_c/\Delta = 5$ without losses. (a) 2PI results show faster relaxation for smaller spins sizes due to enhanced fluctuations. The prethermal magnetization plateau disappears when N_s is decreased due to stronger fluctuations and for $N_s = 2,\ 3$ the system is PM, as demonstrated in Fig. 21 (b) Dynamics obtained from DTWA. Relaxation is less sensitive to spin size. The blue curve is 2PI result for $N_S = 500$, showing good agreement with DTWA for large N_s. (c) Comparison of spin vectors projected to the xz plane for small and large cluster sizes, in adiabatic $\omega_c/\Delta = 5$ and for $\kappa/\Delta = 0$. The FM spiral of large spin ensembles crosses over to a quicker, smooth relaxation for smaller values of N_s.

previous section that the system is not truly a FM as the magnetization decays with time. In the upcoming sections, we provide evidence that the system is, in fact, a spin glass (SG) in this regime. However, it is not possible to uniquely determine a SG by only looking at single spin observables. The only indirect evidence for SG that we have so far is the slow relaxation of magnetization. We again remark that our results are expected to be correct for $\eta \gtrsim 1$ where the model in Eq. (1) is expected to host a SG [94,118].

3. *Dependence of the spin dynamics on cluster size and the semiclassical limit*

The number of spins per cluster N_s not only is a control parameter for the expansion of the effective action but also determines the strength of fluctuations in the system. This assumption stems from the conventional understanding that larger spins often exhibit a more classical behavior compared with small spins [23,93]. As was said before, the size of the spin for each cluster is determined by the number of spins inside each cluster N_s via $S = N_s/2$. Our solution of the problem also supports that fluctuations are stronger for smaller values of spins per cluster. This can be seen, for example, in Eq. (81) where the fermion self-energy scales as N_s^{-1}.

The dynamics of spins at NLO are shown in Fig. 16(a) for different cluster sizes. The main effect of lowering N_s is a faster relaxation of spins. As N_s is decreased, quantum fluctuations become stronger and the transient magnetization lasts shorter. In the other limit $S \gg 1$, dynamics become classical [93]. This can be verified by comparing 2PI results with semiclassical approximations such as DTWA. As shown in Fig. 16(b), in the limit of large spins, DTWA approaches a limiting value, and agrees well with 2PI even quantitatively. Since DTWA becomes exact for large spins [47], this agreement shows the validity of our diagrammatic expansion in the large spin limit [61]. DTWA results display limited sensitivity to spin size, and only predict a qualitative modification of the magnetization plateau. This is due to the fact that as a semiclassical method, DTWA misses quantum tunneling effects which are important for small values of N_s. Both 2PI and DTWA predict a prethermal magnetization plateau at large N_s. Further comparison of 2PI and DTWA is provided in Appendix F. For sufficiently small N_s, the prethermal state is completely bypassed and the system experiences a quick relaxation towards equilibrium [Fig. 16(c)]. Similarly, photon number relaxes faster for smaller N_s, while for larger cluster sizes it has weakly damped oscillations [Fig. 15(b)].

C. Dynamics of spin glass

The results of NLO approximation given in previous sections indicate that the strong-coupling limit of the model in Eq. (1) is not a FM and corrections due to frustration and fluctuations drastically change the MF phase diagram. From the $N_s = 1$ limit of the problem [94,95,118], we know that the system hosts a SG at sufficiently low temperatures and strong couplings. The main questions are the following:

(i) What are the physical signatures of SG in and out of equilibrium?

(ii) Can our formalism capture the far from equilibrium dynamics of SG?

In the upcoming sections, we discuss two direct measures of SG phase. First, we consider the disorder average of the square of local magnetization of each spin ensemble which gives a proxy of the presence of frozen spin configurations. The second one is related to the ability of the system to retain its memory of the far past and is connected to the phenomenon of aging, encoded in two-point correlation functions of the system for large time separations. We demonstrate that 2PI can access both of these measures and is able to track their evolution in real time.

1. *Characteristics of spin glass*

According to Landau's theory of phase transitions (PT), different phases of matter can be classified according to their symmetries [153,173,174]. A phase transition corresponds to a change in the symmetry group of a physical system. For example, the PM-to-FM transition of an Ising FM corresponds

to the spontaneous breaking of the Z_2 symmetry of the Hamiltonian. The occurrence of the PT is signaled by the continuous growth of a parameter which vanishes on one side of the transition. Such parameter is termed as the order parameter and the way it grows with the control parameter of the transition provides us with important information about the nature of the PT [11,153,174]. While the PM-to-SG phase transition fits into the symmetry-breaking paradigm, the proper definition of an order parameter for SG has been a subject of debate for decades, with various candidates [98,99,162]. In the following, we consider two of these proposed order parameters to study the formation of SG in our system.

2. Statistical correlations between similar samples

One way to detect SG order is to compare several systems, also known as replicas [99,162], which share the same pattern of the couplings $g_{\alpha,i}$ in Eq. (1). In the SG phase, we expect to find a finite and stationary correlation between the configuration of spins in different replicas. In the simplest case, consider two replicas, which we label as A and B, whose state is given by the density matrix

$$\rho(t) = \rho_A(\{g_{\alpha,i}\}, t) \otimes \rho_B(\{g_{\alpha,i}\}, t). \tag{98}$$

$\rho(t)$ remains a separable state since replicas do not physically interact with each other. We initialize both systems in the same state and let them evolve with time. Since both replicas share the same disorder profile and initial states, they will have the same state given by the same density matrix $\rho_A(t) = \rho_B(t)$. However, to compare the profile of magnetization in the two systems and to obtain correlations between them, we have to measure spins in the local basis of S_i^x operators in both replicas. The outcomes of the measurements are not necessarily the same between the two systems. Nevertheless, we can expect a finite overlap between the measured spin configurations of the replicas in the SG phase for each disorder pattern and also after averaging the outcome over the disorder. The simplest overlap is given by

$$Q(t) = \frac{1}{N_s^2} \overline{\langle S_{i,A}^x(t) S_{i,B}^x(t) \rangle_c}, \tag{99}$$

where we have included a normalization factor. As long as the systems are not in the FM phase, a finite value for Q at long times implies SG order. An extra textbook condition for the viability of Q is that the $\mathbb{Z}_2$ symmetry should be broken explicitly either by a small term in the Hamiltonian or by the initial state [11,13,174]. We take the latter route below by starting from spin states with finite $\langle S^x \rangle$. The decay of magnetization shown in Sec. VI B 2 guarantees that the system is not FM at long times and, hence, a finite Q means the system is SG. We explained how to extract Q using the 2PI formalism in Sec. V H 3. In the following we show the dynamics of Q as the light-matter coupling g and the photon loss κ are varied.

We initialize the system in a state with $m_i^x = 1$ and quench g from zero to a sufficiently large value. We monitor the dynamics of Q for different values of photon loss from $\kappa = 0$ (closed system) to $\kappa = 0.5\Delta$. As can be seen in Fig. 17(a), after some fluctuations caused by the quench, Q approaches zero at long times when the system is not coupled to the bath. An explanation for this behavior is that the initial energy E_i of

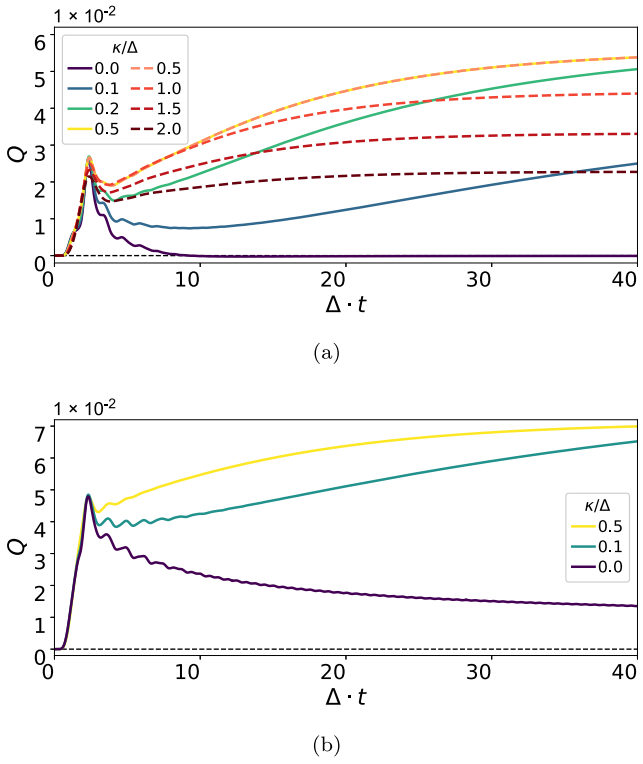

FIG. 17. Dynamics of the overlap parameter Q for different values of system-bath coupling κ. (a) For $\theta_0 = 0.5\pi$, the energy density after the quench is large and the final temperature is too high to realize a SG, unless the system is allowed to cool down via photon loss. However, for $\kappa \gtrsim \Delta$ (dashed lines), photon loss weakens SG order. (b) For $\theta_0 = 0.7\pi$, energy density is smaller and the system enters a weak SG state without coupling to the bath, but it saturates to a smaller value of Q, and, hence, glass order is weaker in this case. The other parameters are $g/g_c = 1.13$, $\omega_c/\Delta = 5.0$, $N_s = 5$, and $\eta = 1$.

the system with respect to the postquench Hamiltonian is large enough to put the system in a high-temperature equilibrium PM state if the system is closed. For finite photon loss, Q starts to grow after $t \gtrsim \kappa^{-1}$, the timescale of cooling by photon loss. For $\kappa \lesssim \Delta$, the sole effect of photon loss is cooling, which enhances the growth of Q. For $\kappa \gtrsim \Delta$, dissipation becomes detrimental to SG, as shown by dashed lines in Fig. 17(a). This behavior can be explained by resorting to the stochastic interpretation of Lindblad dynamics [109,175]. For weak losses $\kappa \lesssim \Delta$, cavity loss induces dephasing of spins in the x direction given by the jump operator S^x. Dephasing can be modeled exactly by considering a non-Hermitian Hamiltonian in conjunction with repeated weak projections into the eigenstates of S^x to conserve the norm of the state [109,175]. These repeated projections compete with the transverse field Δ and stabilize the ordering of spins in the x direction. For $\kappa \gtrsim \Delta$, cavity loss induces atomic decay and stimulation with different amplitudes [104,163] which in turn, suppress spin ordering in the x direction.

The explanation given above for the role of photon loss in the dynamics is supported by the behavior of quenches with smaller E_i. We note that E_i can be calculated easily for the

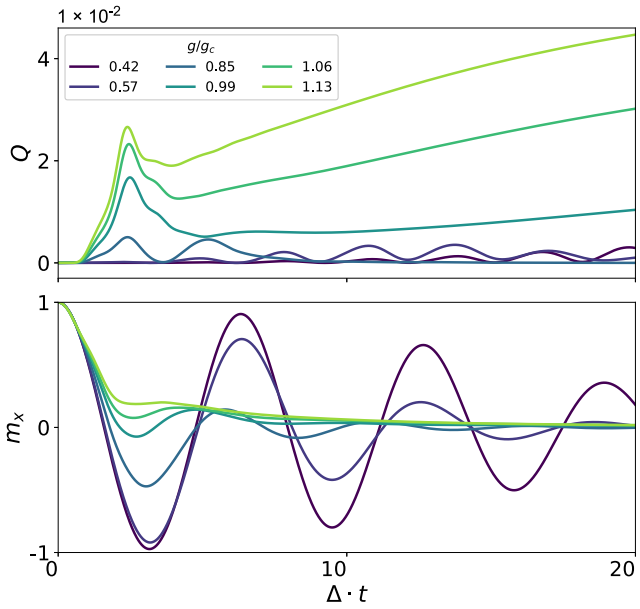

FIG. 18. Dynamics of SG order parameter (top panel) and total magnetization (bottom panel) for different values of coupling strength. g_c is the critical coupling in the MF theory. This plot shows that the observed value of g_c is smaller than the one obtained from the LO approximation. The other parameters are $\kappa/\Delta = 0.5$, $\omega_c/\Delta = 5.0$, $N_s = 5$, and $\eta = 1$.

initial states considered in this work:

$$E_i = \tfrac{1}{2} N N_s \Delta \cos\theta_0, \tag{100}$$

since we have $g = 0$ in the prequench Hamiltonian. By initializing spins closer to $\theta_0 = \pi$, we can reduce the energy density and attain a lower temperature final state for isolated quenches. For instance, for $\theta_0 = 0.7\pi$ the system enters the SG phase even without losses [Fig. 17(b)], although Q is smaller for $\kappa = 0$ compared with $\kappa > 0$ due to the absence of cooling.

Finally, we consider the emergence of SG order as the coupling g is increased. Taking $N_s = 5$ and starting from $\theta_0 = 0.5\pi$ while connecting the system to an external bath by switching on the photon loss, we look at Q for quenches to different values of g as shown in the top panel of Fig. 18. For weak couplings, $Q(t)$ oscillates and decays to zero. When g becomes large enough, Q grows to a finite value at long times. We see in the bottom panel of Fig. 18 that spin dynamics changes from underdamped to overdamped at the same coupling where Q becomes finite. In Fig. 18 the coupling g is scaled with g_c which was the critical coupling of the MF limit in Eq. (96). A finite value of Q for $g/g_c < 1$ indicates that NLO contributions shift the boundary of PM and SG phases towards SG.

3. *Temporal correlations and aging phenomena*

As discussed before, the diagnosis of SG phase requires the evidence of a frozen spin configuration, which breaks the symmetry of the Hamiltonian and, at the same time, has no global magnetization. In the previous section we discussed (the square of) the instantaneous magnetization for each site and showed that it is finite in the glass phase while magnetization relaxes to zero. The latter feature distinguished SG from FM. Another way to confirm a frozen spin state in the system is to look at the temporal correlation between the magnetization of each site at large time separations. For example, we take a cluster and its total spin operator S^x at two different times t and t'. If spins are frozen, they do not fluctuate strongly in time and the overlap of magnetization for the same site at two different times is large. In fact, it remains finite even if $|t - t'| \to \infty$. For classical degrees of freedom one has

$$q_{\rm EA} \equiv \lim_{|t-t'|\to\infty} \overline{\langle S^x(t) S^x(t')\rangle} > 0, \tag{101}$$

which is the Edwards-Anderson (EA) order parameter [98,99]. It is clear that the above condition can also imply FM order in the system. To exclude FM, the disorder averaged magnetization $\overline{\langle S^x\rangle}$ should also vanish. For the case of quantum operators in our problem, the correlator in Eq. (101) can be generalized to

$$C(\tau, \tau - t) \equiv \frac{1}{N_s^2} \overline{\langle \{ S_i^x(\tau), S_i^x(\tau - t)\}\rangle_c}. \tag{102}$$

In the following, we consider the behavior of C for the same quenches discussed in the previous section. It will be shown that C changes its behavior at the same points where Q in Eq. (85) becomes finite. Therefore, both C and Q are consistent measures of SG order in the system.

We again look at the effect of photon loss on quenches from hot (with $\theta_0 = 0.5\pi$) and cold (with $\theta_0 = 0.7\pi$) initial states of the system, according to Eq. (100). We consider $C(\tau, \tau - t)$ for different values of the "waiting time" τ after the quench as a function of t. In Fig. 19(a), we have shown C for $\theta_0 = \pi/2$ and for zero and finite κ. We see that C behaves differently depending on whether the system is isolated or not. When the system is closed [dashed lines in Fig. 19(a)], it ends up in a high-temperature PM state with correlations that relax quickly to equilibrium and show weak dependence on the waiting time after the quench τ. The correlations also decay quickly with t, meaning that local magnetization loses the memory of its past quickly in the PM phase. When the system is allowed to cool by emitting photons to the outside of the cavity, a SG phase emerges (solid lines in Fig. 19(a). C becomes strongly dependent on the waiting time τ and there is a crossover in the behavior of C for $t \ll \tau$ and $t \approx \tau$. The latter behavior is termed aging [176,177] and is another feature of quenches into SG phases. In aging, the decay of $C(\tau, \tau - t)$ with t becomes slower for "older" systems with larger τ. In this picture, there is a plateau in C for $t \ll \tau$ [Fig. 19(a)] whose height gives the EA order parameter. The plateau is more visible in figures shown in upcoming sections.

Aging is closely related to the lack of thermalization in spin glasses [101,176,178,179]. The system is unable to reach equilibrium because of its highly rugged energy landscape in which adjacent energy configurations, connected by local spin flips, are separated by large energy barriers. As a result, ergodicity is broken and the system will not thermalize [178]. The relation between aging and thermalization can be made more explicit by using the fluctuation dissipation theorem (FDT) and fluctuation dissipation ratio (FDR) defined below. At thermal equilibrium, the symmetric correlation function

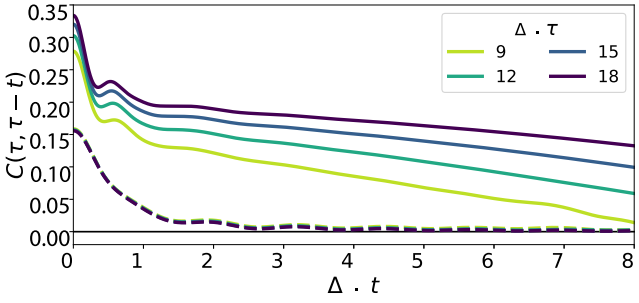

(a)

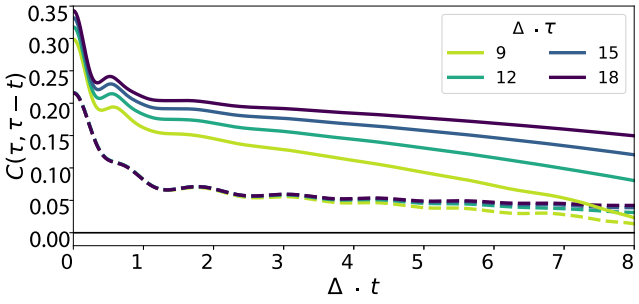

(b)

FIG. 19. (a) Symmetric correlation function C at different waiting times for quenches from an initial state with high energy density $\theta_0 = \pi/2$. For $\kappa = 0$ (dashed lines), the system heats up to PM state and C quickly decays to zero for $t \to \infty$ (lines are almost on top of each other). For $\kappa/\Delta = 0.5$ (solid lines) the system cools down to SG where C remains finite for $t \to \infty$. (b) C for an initial state with low energy density $\theta_0 = 0.7\pi$. Regardless of κ the system ends up in the glass phase, however, SG order is stronger for $\kappa/\Delta = 0.5$ (solid lines) where the system is cooled, compared with $\kappa = 0$ (dashed lines). For both figures $\omega_c/\Delta = 5.0$, $g/g_c = 1.27$, $\eta = 1$, and $N_s = 5$.

$C(t, t')$ and the response function $R(t, t')$ of an observable $\mathcal{O}$ are connected to each other via FDT [11,86,100]:

$$R(t - t') = -i \int \frac{d\omega}{2\pi} e^{-i\omega(t-t')} \tanh\left(\frac{\omega}{2T}\right) \tilde{C}(\omega), \tag{103}$$

where $\tilde{C}(\omega) = \int dt \exp(i\omega t) C(t)$ is the Fourier transform of C and T is the temperature. At long times or in the classical limit $\omega \ll T$, we can approximate $\tanh(\omega/2T) \approx \omega/2T$ to get for $t > t'$

$$R(t, t') \approx -\frac{1}{2T} \partial_{t'} C(t, t'). \tag{104}$$

By integration we get

$$C(t, t') - C(t, t) = 2T \chi(t, t'), \tag{105}$$

where χ is the integrated response defined as

$$\chi(t, t') \equiv \int_{t'}^{t} R(t, t'') dt''. \tag{106}$$

Equation (105) can be generalized to out of equilibrium regimes as [178,180–182]

$$C(\tau, \tau - t) - C(\tau, \tau) = 2T_{\text{eff}}(\tau, t) \chi(\tau, \tau - t), \tag{107}$$

where T_{eff} is the time-dependent effective temperature. T_{eff} can be read from the slope of the plot of χ versus C. If a system is coupled to an external bath with temperature T the fluctuation dissipation ratio $X(\tau, t)$ is defined as

$$X(\tau, t) \equiv \frac{T}{T_{\text{eff}}(\tau, t)}. \tag{108}$$

Therefore, X measures the deviation of the system from true equilibrium at temperature T [177–179]. For generic systems that thermalize efficiently, $T_{\text{eff}} \to T$ and $X \to 1$. For glassy systems, on the other hand, X can show a multistage behavior, where the plot of χ versus C changes its slope. Furthermore, FDR may never reach the limit $X \to 1$, and the system will not thermalize at all.

In Fig. 20(a) we have shown χ in terms of C for the PM phase of our model. We see that the plots have an almost constant slope [small deviations are mostly due to the error of numerical integration in Eq. (106)] and, therefore, the PM phase has a unique temperature. For quenches inside the SG phase [Fig. 20(b)], χ acquires a distinct profile. The long-time effective temperature [related to the slope of the dashed line in Fig. 20(b)] and the short-time effective temperature are different [101,179,183]. This is a direct consequence of aging in the system. q_{EA} can be read from the value of C at which the change of slope happens [101,184]. For larger τ, the vertical section of the curve lasts longer which also corresponds to a wider plateau of $C(\tau, \tau - t)$. The effective temperature of SG in Fig. 20(b) is larger than that of the PM in Fig. 20(a) by about a factor of five, and hence $X \approx 0.2$. We remark that there is a close connection between the violation of FDT and replica symmetry breaking (RSB) in spin glasses [101], which suggest that the model under consideration hosts RSB, in agreement with the recent cavity QED experiment of Ref. [92].

While photon loss was necessary to realize SG for the high-energy initial state with $\theta_0 = \pi/2$, if we reduce the initial energy density by starting from a lower energy state with $\theta_0 = 0.7\pi$, the system becomes SG regardless of coupling it to the bath [Fig. 19(b). However, the height of the plateau for $\kappa = 0$ is smaller, as the quench inside the SG phase is shallower in this case. This is in complete agreement with the behavior of Q given in Figs. 17(a) and 17(b).

4. *Effect of spin size on spin-glass formation*

In Sec. VI B 3, it was shown that smaller spins are more susceptible to quantum fluctuations by considering the evolution of total magnetization of the system. Here, we briefly address the imprint of quantum fluctuations on SG dynamics as viewed through the lens of the overlap parameter Q. Our analysis will be more qualitative here, compared with the comprehensive approach of our other work [93] where the quantum to classical crossover of SG was studied by looking at aging dynamics.

We take an initial state with $\theta_0 = 0.7\pi$ and $\kappa = 0$. For systems with different spin sizes, we monitor the overlap Q which is shown in Fig. 21. For $N_s \leqslant 3$, the overlap vanishes at $t \to \infty$, indicating a PM state phase due to excessive heat generated by the quench, while Q remains finite for larger N_s. This is consistent with mean-field theory calculations of

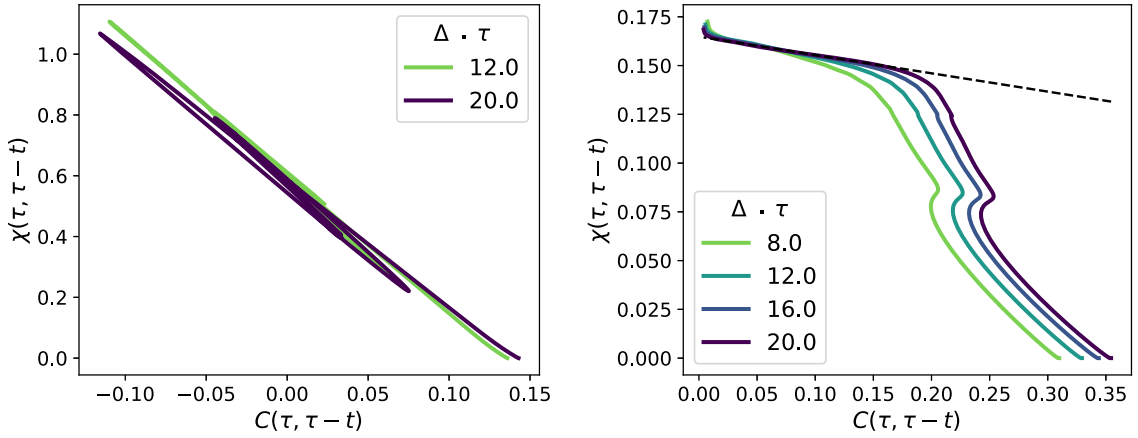

FIG. 20. Integrated response χ versus C for different waiting times τ. (a) In PM phase, the slope is constant and is proportional to the inverse of temperature. (b) In SG state, dynamics have multiple timescales and the slope changes with t. The parameters are $\Delta/\omega_c = 0.2$, $\kappa/\Delta = 0.5$, $g/g_c = 1.27$, and $N_s = 5$.

Ref. [161] which predict a lower PM-to-SG transition temperature for smaller spins. Figure 21 also shows that Q is more sensitive to spin size for small S. In the opposite limit of large N_s, corresponding to a classical SG, Q is bounded from above by its upper limit at $N_S \to \infty$. The mean-field like oscillations of Q at $N_S \gg 1$ further support the classical behavior of this limit. Hence, the profile of Q is qualitatively consistent with the findings of Ref. [93] on the crossover between quantum and classical SG.

5. *Spin glass away from the adiabatic limit*

At last, we consider the effect of changing photon frequency ω_c on the glass phase. 2PI formalism allows us to treat the problem in all ranges of frequencies and not just in the regime of fast photons where photons can be adiabatically eliminated [163,185,186]. We follow the same tradition as previous sections and scale g with g_c in Eq. (96). However, as will be explained later, this scaling does not alter the general picture given below.

As explained before, initializing the system in a symmetric spin state helps it to reach the steady state earlier. This reduces the required numerical resources to access the SG phase in steady state (for a discussion of the numerical costs see Appendix E). We look at $C(\tau, \tau - t)$ for sufficiently large values of τ and a fixed t. This gives us an estimate of the EA order parameter $q_{\rm EA}$ as a measure of glassiness in the system. $q_{\rm EA}$ is shown in Fig. 22 for simulations with different photon frequencies. $q_{\rm EA}$ displays a peak below $\omega_c = \Delta$, vanishes quickly as $\omega_c \to 0$ and saturates in the adiabatic limit $\omega_c \gg \Delta$. The quick decay of SG order for small photon frequencies is an expected feature. For instance, phonons tend to relieve magnetic or density orderings in solid-state platforms because they have smaller energy gaps and are thermally excited easily. The observed peak in $q_{\rm EA}$ can be explained as a resonance effect by looking at the coherent part of the frequency-dependent interaction between spins following

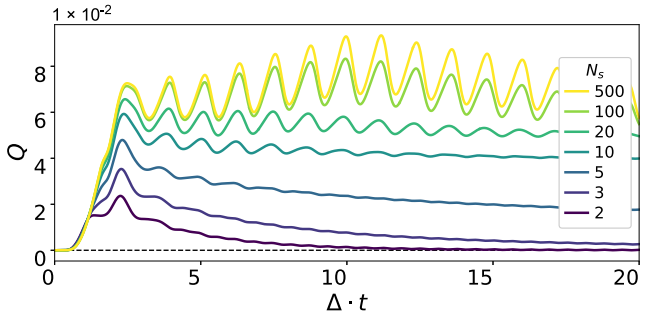

FIG. 21. Spin overlap Q after interaction quenches to $g = 1.13g_c$ starting from $\theta_0 = 0.7\pi$ without photon loss and for different spin sizes. Overlap decreases for smaller N_s and due to heating, vanishes for $N_s = 2$, 3 for which the critical temperature is smaller. Other parameters are $\Delta/\omega_c = 0.2$.

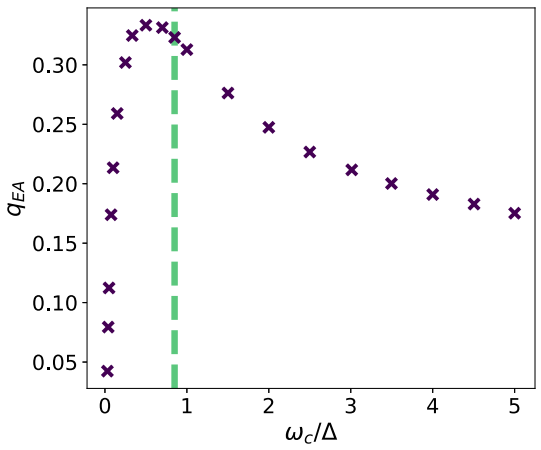

FIG. 22. Dependence of SG order parameter at a fixed waiting time after the quench $\Delta \times \tau = 12.0$ on photon frequency ω_c. SG is strongest close to a resonance frequency near Δ. Dashed line indicates the analytical estimate of the resonance frequency $\omega^\star$. The other parameters are $g/g_c = 1.27$, $\kappa/\Delta = 0.5$, $N_s = 20$, and $\eta = 1$.

integrating out photons, which has the form

$$H_{\rm int} = \sum_{i,j}^{N} \sum_{\lambda,\lambda'}^{N_s} \int \frac{d\omega}{2\pi} \sigma^x_{i\lambda}(-\omega) V^{ij}_{\rm eff}(\omega) \sigma^x_{j\lambda'}(\omega), \tag{109}$$

with

$$V^{ij}_{\rm eff}(\omega) \sim \sum_{\alpha}^{M} g_{\alpha,i} g_{\alpha,j} \omega_c {\rm Re}[D^R(\omega)]. \tag{110}$$

D^R is the bare retarded Green's function of photons given by

$$D^R(\omega) = \frac{1}{(\omega + i\kappa)^2 - \omega_c^2}. \tag{111}$$

Equation (109) is obtained by integrating out photons in the original action, resulting in the following spin-spin interaction in the Keldysh action

$$S_{\sigma\sigma} = -\sum_{\alpha}^{M} \sum_{i,j}^{N} \sum_{\lambda,\lambda'}^{N_s} g_{\alpha,i} g_{\alpha,j} \omega_c \int \frac{d\omega}{2\pi} \begin{pmatrix} \sigma^x_c(-\omega) & \sigma^x_q(-\omega) \end{pmatrix}_{i\lambda} \times \begin{pmatrix} 0 & D^A(\omega) \\ D^R(\omega) & D^K(\omega) \end{pmatrix} \begin{pmatrix} \sigma^x_c(\omega) \\ \sigma^x_q(\omega) \end{pmatrix}_{j\lambda'}. \tag{112}$$

We decompose the kernel matrix into its real and imaginary parts. The former is Hermitian and can be attributed to an effective Hamiltonian given by Eq. (109), while the imaginary part describes dissipation [87]. The (c, q) indices in Eq. (112) are defined in Appendix C in terms of contour indices. To evaluate the strength of the interaction we can put $g_{\alpha,i} g_{\beta,j} \sim g^2$ to get

$$V_{\rm eff}(\omega) \sim g^2 \omega_c \frac{\omega^2 - \omega_c^2 - \kappa^2}{\left(\omega^2 - \omega_c^2 - \kappa^2\right)^2 + 4\kappa^2\omega^2}. \tag{113}$$

In the adiabatic limit the relevant energy scales in the problem are small compared with photonic energy scales ($\omega \ll \omega_c, \kappa$) and we get

$$V_{\rm eff}(\omega \to 0) \sim -g^2\omega_c/\left(\omega_c^2 + \kappa^2\right) \sim -\left(\frac{g}{g_c}\right)^2 \Delta. \tag{114}$$

If we scale g with g_c such that $g^2 = r g_c^2$, where r is a dimensionless number, the effective interaction becomes insensitive to ω_c. Therefore, changing ω_c should not affect the SG order in the system. This is consistent with Fig. 22 where $q_{\rm EA}$ approaches a constant value at large frequencies. For smaller values of ω_c and κ, however, the dependence of effective interaction in Eq. (113) on ω becomes important. One possible approximation is to use the "on-shell approximation" and substitute $\omega \approx \Delta$. Using this approximation and expanding the effective spin-spin interaction to nonzero leading order in Δ, recovers the atom-only description of Ref. [163] which also captures the dissipative part of the Lindblad dynamics. Nevertheless, this approach fails to describe the dependence of spin order on ω_c, and, in particular, the resonance behavior in Fig. 22. However, if we use the on-shell approximation and simply substitute $|\omega| = \Delta$ in $V_{\rm eff}(\omega)$ and do not expand it in Δ, we find that $V_{\rm eff}$ has two peaks close to $\omega^\star$ given by

$$\omega^\star \equiv \sqrt{\Delta^2 - \kappa^2}, \tag{115}$$

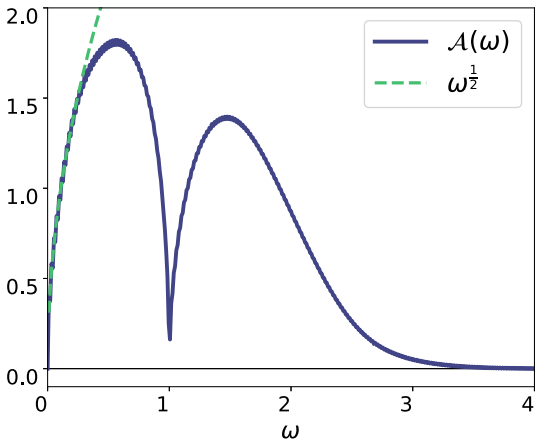

FIG. 23. Atom spectral density in the glass phase for a long waiting time after the quench $\Delta \cdot \tau = 60.0$ as a function of frequency. Atoms form a continuum of sub-Ohmic modes at small energies. The minimum is due to vacuum Rabi splitting. The other parameters are $g/g_c = 1.27$, $\kappa = 0$, $\theta_0 = \pi$, $N_s = 5$, and $\eta = 1$.

with attractive ($V_{\rm eff} > 0$) and repulsive ($V_{\rm eff} < 0$) sides for $\omega_c > \omega^\star$ and $\omega_c < \omega^\star$, respectively. $\omega^\star$ is marked in Fig. 22 and is in good agreement with the numerics.

Nevertheless, there is a feature that cannot be straightforwardly explained by the on-shell approximation used above. $V_{\rm eff}(\Delta)$ vanishes at $\omega_c = \omega^\star$, but the SG order does not show any signs of the suppression of interactions. A possible explanation for this discrepancy is that due to strong interactions, the spin spectral density defined in terms of the imaginary part of the response function [Eq. (78)]

$$\mathcal{A}(\omega) = -\frac{(N+M)N_s}{4} {\rm Im}[V^{22}(\omega)], \tag{116}$$

is modified compared with the noninteracting limit and the atomic peak at $\omega = \Delta$ is highly broadened. It is believed that quantum SGs are critical with a gapless spectrum of excitations [94,95,183,187]. For SK and disordered SU(N) Heisenberg models, Refs. [187] and [183] obtained an Ohmic spectrum with $\sim\omega$. For a closed Dicke SG at zero temperature, Ref. [94] predicted a similar Ohmic profile, while for Dicke SG connected to a Markovian bath Ref. [95] obtained a sub-Ohmic $\sim\omega^{\frac{1}{2}}$ dependence for $\omega \lesssim \kappa$. We have plotted the atomic spectral density for a low temperature quench *without photon losses* within our approach in Fig. 23. We see that $\mathcal{A}(\omega)$ displays a gapless spectrum at low frequencies, but with a sub-Ohmic dispersion $\sim\omega^{\frac{1}{2}}$, even though the system is not coupled to a Markovian bath. One explanation, although unlikely due to the similar symmetry of this model to the SK model, is that the system is in a different universality class with different exponents. Another possibility is that the final state long after the quench is at finite temperature with many emitted photons existing in the cavity, which act as an effective bath for spins. The exponent can be read experimentally using rf spectroscopy to compare with theoretical predictions.

VII. CONCLUSIONS

In this work we have provided a diagrammatic derivation of nonperturbative DE suited to describe spin-glass formation far from equilibrium in the cavity QED platform of Refs. [36,88–90]. Very recently, the same group has reported the observation of SG order [92] and associated replica symmetry breaking, which is a notoriously hard experimental task. We predict that SG order in this system can be obstructed by transient, competing ferromagnetism when the atomic ensembles trapped in the cavity are largely occupied. We show that SG order is enhanced by strong quantum fluctuations (few atoms per ensemble) and when photons are active and resonant with the atomic transitions. The set of DE derived here have the flexibility to explore simultaneously a broad set of parameters' regimes (weak or strong coupling, variable ranges of N_s, adiabatic elimination and active photons) without resorting to descriptions valid only in a corner of parameter space.

Our work sets also the stage for studying the crossover from strongly correlated regimes to semiclassical dynamics in other cavity QED platforms with tunable loading capabilities [35]. The dynamics of these systems are at reach of state-of-art 2PI-DE since interactions, although inhomogeneous, are all-to-all and this allows for more controlled diagrammatic expansions and numerical integration. At the same time, many of the new-generation cavity QED experiments combine short and all-to-all interactions, introducing a notion of dimensionality and lattice spacing that would make the numerical solution of the 2PI-DE more challenging.

We are currently making progress in this direction by exploring various experimental platforms:

Rydberg arrays integrated in optical cavities. The experiment in Ref. [34] marked the first combination of strong, short-range Rydberg interactions with conventional photon-mediated long-range coupling. Analyzing these systems beyond mean-field theory opens up possibilities for exploring exotic phases of matter. These include spin liquids that are protected from dissipation [34] or limit cycles [188] that persist in the presence of strong classical and quantum noise. This line of research should also provide novel opportunities to explore topological order and lattice gauge theories in the context of atom-light interfaces [34].

Cavity QED with programable spin-exchange interactions. Reference [35] reports the realization of programmable nonlocal interactions in an array of atomic ensembles within an optical cavity. This experiment introduces a U(1) variant [91] to the work discussed here because it focuses on spin-exchange interactions rather than ferromagnetic (Z_2-invariant) interactions. The ability to program the distance-dependent interactions with a sophisticated combination of Raman sidebands and magnetic-field gradients enables the engineering of dimensionality, topology, and metric as needed. This opens the door to studying quantum optimization problems on tree-like [189] or fully connected geometries in cavity QED, bridging the gap between quantum information and many-body quantum optics.

Natural and synthetic correlated emission. In recent years, there has been a surge of interest in the study of dissipative spin problems that describe correlated emission in atomic ensembles. The key idea is that emission into free space involves multiple scattering and interference effects, making the phenomenon more complex than in traditional textbook quantum optics [190–194]. This mechanism is typically encoded in a Lindblad equation that is nonlocal in space, or equivalently nondiagonal in jump operators. While solutions for a few atomic excitations are accessible [193], the many-body regime of correlated emission remains largely unexplored. This would be of significance for Rydberg experiments realizing atomic mirrors via this mechanism [96,195] and for applications in the cavity QED experiment of Refs. [35,196], where correlated emission could be artificially engineered [43,197,198]. This would enable the synthesis of many-body entangled states using dissipation, by leveraging the full potent of programmable cavity QED in the domain of nonunitary dynamics.

On the interdisciplinary front, 2PI-DE for dissipative spin dynamics could also serve to guide dissipative quantum state preparation in hybrid AMO-spintronics platforms which rely on correlated emission to entangle NV centers [199].

This list of subjects is by no means exhaustive. For instance, 2PI-DE may be one of the few methods with sufficient versatility to treat the intrinsically strongly correlated dynamics of fermionic cavity QED experiments [37,200,201]. We hope that this set of potential applications will motivate readers from different communities to embark on the fascinating challenge to study the next generation of many-body quantum optics experiments using dynamical field theory methods.

ACKNOWLEDGMENTS

We are thankful to A. N. Mikheev for carefully proof reading the paper, and to D. Gribben for early contributions to this project. H.H. and J.M. acknowledge financial support by the Deutsche Forschungsgemeinschaft (DFG, German Research Foundation): through Project-ID 429529648, TRR 306 QuCoLiMa ("Quantum Cooperativity of Light and Matter") and through TRR 288 - 422213477 (project B09). This project has been supported by the QuantERA II Programme that has received funding from the European Union's Horizon 2020 research and innovation programme under Grant Agreement No 101017733 ("QuSiED") and by the DFG (Project No. 499037529). D.C. acknowledges support from the European Union, under European Research Council Grant Agreement No. 101002107 (NEWSPIN); the Government of Spain under the Severo Ochoa Grant CEX2019-000910-S [MCIN/AEI/10.13039/501100011033]); QuantERA II project QuSiED, cofunded by the European Union Horizon 2020 research and innovation programme (Grant No. 101017733) and the Government of Spain (European Union NextGenerationEU/PRTR PCI2022-132945 funded by MCIN/AEI/10.13039/501100011033); Generalitat de Catalunya (CERCA program and AGAUR Project No. 2021 SGR 01442); Fundació Cellex, and Fundació Mir-Puig.

APPENDIX A: SCHWINGER BOSONS AND ABRIKOSOV FERMIONS

In this Appendix, we compare the Schwinger boson and the Abrikosov fermion representations of spins for treating dynamics and demonstrate that the latter is substantially more

accurate for 2PI, if we limit ourselves to Gaussian initial states. We remark that the Majorana fermion representation can be written in terms of complex fermions and therefore, provides similar advantages and, additionally, requires less numerical resources due to working with a smaller number of Green's functions.

Consider the Schwinger boson representation [138,153]

$$S^z = \tfrac{1}{2}(a^\dagger a - b^\dagger b), \tag{A1}$$

$$S^+ = a^\dagger b, \tag{A2}$$

together with the constraint

$$a^\dagger a + b^\dagger b = 2S. \tag{A3}$$

We take the spin state $|M_z = S\rangle$ such that $S^z|S\rangle = S|S\rangle$. This corresponds to the following bosonic state:

$$|\psi\rangle = |n_a = 2S\rangle \otimes |n_b = 0\rangle. \tag{A4}$$

However, $|n_a = 2S\rangle$ is not a Gaussian state, as can be checked easily. We can approximate it by a mixed Gaussian state

$$\rho_{G_b} \equiv \lim_{\epsilon\to\infty} \frac{e^{-H_{G_b}(\epsilon)}}{\mathrm{Tr}(e^{-H_{G_b}(\epsilon)})}, \tag{A5}$$

where

$$H_{G_b}(\epsilon) \equiv \ln\left(1 + \frac{1}{2S}\right) a^\dagger a + \epsilon b^\dagger b. \tag{A6}$$

$H_{G_b}(\epsilon)$ has been chosen such that

$$\mathrm{Tr}(\rho_G a^\dagger a) = 2S, \tag{A7}$$

$$\mathrm{Tr}(\rho_G b^\dagger b) = 0, \tag{A8}$$

in order to satisfy Eqs. (A1) and (A3) at the level of expectation values. However, the squares of Eqs. (A1) and (A3) are not satisfied,

$$\frac{1}{4}\langle (a^\dagger a - b^\dagger b)^2\rangle_G = \frac{S}{2}(1+4S) \neq S^2, \tag{A9}$$

$$\langle (a^\dagger a + b^\dagger b)^2\rangle_G = 2S(1+4S) \neq 4S^2. \tag{A10}$$

We note that the errors are larger than the quantities themselves. If we could use coherent states for bosons, the errors would be $O(S)$ and therefore, subleading at least for large S. But this is not permissible, as coherent states break the local U(1) gauge symmetry of the Schwinger bosons given by $(a_i, b_i) \to (a_i e^{i\psi_i}, b_i e^{i\psi_i})$.

Alternatively, we can express a spin of size S using Abrikosov fermions [137]

$$S^z = \frac{1}{2}\sum_{n=1}^{2S} (f_n^\dagger f_n - c_n^\dagger c_n), \tag{A11}$$

$$S^+ = \sum_{n=1}^{2S} f_n^\dagger c_n, \tag{A12}$$

where f_n and c_n are fermion annihilation operators that satisfy the usual anticommutation relations. Physical states should satisfy the following constraint:

$$f_n^\dagger f_n + c_n^\dagger c_n = 1, \tag{A13}$$

which implies

$$\sum_n (f_n^\dagger f_n + c_n^\dagger c_n) = 2S. \tag{A14}$$

For the spin state $|M_z = S\rangle$ we can use the following Gaussian fermionic state:

$$\rho_{G_f} \equiv \lim_{\epsilon\to\infty} \frac{e^{-H_{G_f}(\epsilon)}}{\mathrm{Tr}(e^{-H_{G_f}(\epsilon)})}, \tag{A15}$$

where

$$H_{G_f}(\epsilon) \equiv \epsilon \sum_n (c_n^\dagger c_n - f_n^\dagger f_n). \tag{A16}$$

The advantage of fermionic spinons is that ρ_{G_f} is in fact, a pure state for $\epsilon \to \infty$. In this case, it is easy to see that ρ_{G_f} satisfies Eqs. (A13) and (A14) exactly and not only at the level of expectation values. Note that while we assumed a fully polarized spin state in the $+\hat{z}$ direction above, the argument is general and holds for any other spin coherent states after a proper unitary transformation. Therefore, fermionic Gaussian states can exactly represent any spin coherent state without introducing errors.

APPENDIX B: HUBBARD-STRATONOVICH TRANSFORMATION

We use the following identity;

$$1 = \int \mathcal{D}[\chi^1, \chi^2] e^{iS_\chi}, \tag{B1}$$

where S_χ is defined in Eq. (29). This identity follows from the fact that the integral is Gaussian. Then, we shift the integration variable according to

$$\vec{\chi}_{\alpha i} \to \vec{\chi}_{\alpha i} + \hat{W}_0 \otimes \vec{A}_{\alpha i}. \tag{B2}$$

The notation $\otimes$ is matrix multiplication over all indices (time and species). $\hat{W}_0$ was given by Eq. (31) and $\vec{A}_{\alpha i}$ is defined as

$$\vec{A}_{\alpha i}(t_c) \equiv \begin{pmatrix} -\frac{2i}{\sqrt{N_s}} \sum_\lambda \psi^y_{i\lambda}(t_c)\psi^z_{i\lambda}(t_c) \\ \sqrt{2\omega_c} g_{\alpha i}\phi_\alpha(t_c) \end{pmatrix}. \tag{B3}$$

Applying the shift yields

$$1 = \int \mathcal{D}[\chi^1, \chi^2] e^{iS_\chi + iS_{\chi\psi} + iS_{g\chi\phi} - iS_{\mathrm{int}}}, \tag{B4}$$

where $S_{\chi\psi}$, $S_{g\chi\phi}$, and S_{int} are respectively given by Eqs. (33), (34), and (26). Since S_{int} does not depend on χ we can move it to the left-hand side (LHS) to get

$$e^{iS_{\mathrm{int}}} = \int \mathcal{D}[\chi^1, \chi^2] e^{iS_\chi + iS_{\chi\psi} + iS_{g\chi\phi}}. \tag{B5}$$

Therefore, we can substitute the right-hand side (RHS) of the above expression in the original action.

To prove the connection between the spin-correlation function and the Green's function of HS field in Eq. (78), we add source terms to the Keldysh action:

$$S \to S + \sum_i \oint J_i S_i^x dt. \tag{B6}$$

The spin-correlation function can be found from

$$\left\langle S_i^x(t)S_i^x(t')\right\rangle = -\frac{\delta^2 Z[J]}{\delta J_i(t)\delta J_i(t')}, \tag{B7}$$

where Z is the generating functional

$$Z[J] \equiv \int \mathcal{D}[\psi,\phi,\pi,\chi]e^{iS-i\sum_j \int J_j S_j^x dt}. \tag{B8}$$

The source term can be absorbed into $S_{\chi\psi}$ as

$$S_{\chi\psi} \to -\frac{2i}{\sqrt{N_s}}\sum_{\alpha,i,\lambda}\oint dt_c\left(\chi^1_{\alpha i}-\frac{\sqrt{N_s}}{2M}J_i\right)\psi^y_{i\lambda}\psi^z_{i\lambda}. \tag{B9}$$

We shift χ^1 according to

$$\chi^1_{\alpha i} \to \chi^1_{\alpha i}+\frac{\sqrt{N_s}}{2M}J_i, \tag{B10}$$

which generates a coupling between J and χ^2:

$$S_{\chi J} = \frac{(N+M)}{2M}Ns\sum_{\alpha}^{M}\sum_{i}^{N}\oint dt\,\chi^2_{\alpha i}(t)J_i(t). \tag{B11}$$

Now we take functional derivatives with respect to the source and get

$$\left\langle S_i^x(t)S_i^x(t')\right\rangle = \frac{N+M}{4M^2}N_s\sum_{\alpha,\beta}^{M}\left\langle\chi^2_{\alpha i}(t)\chi^2_{\beta i}(t')\right\rangle. \tag{B12}$$

Using permutation symmetry we have $\langle\chi^2_{\alpha i}(t)\chi^2_{\beta i}(t')\rangle = iU^{22}(t,t') = iV^{22}(t,t')$ which yields

$$\left\langle S_i^x(t)S_i^x(t')\right\rangle = i\frac{(N+M)N_s}{4}V^{22}(t,t'). \tag{B13}$$

APPENDIX C: DYSON EQUATIONS

For any practical calculation, we need to write equations in terms of normal time variables. DE are more transparent if we write fields in the classical or quantum basis defined as [100]

$$\phi_c(t) \equiv \frac{1}{\sqrt{2}}[\phi_+(t)+\phi_-(t)], \tag{C1}$$

$$\phi_q(t) \equiv \frac{1}{\sqrt{2}}[\phi_+(t)-\phi_-(t)], \tag{C2}$$

where t is a normal time variable. The retarded, advanced and Keldysh (RAK) Green's functions are defined as [86,100]

$$G^R(t,t') \equiv -i\langle\phi_c(t)\phi_q(t')\rangle, \tag{C3}$$

$$G^A(t,t') \equiv -i\langle\phi_q(t)\phi_c(t')\rangle, \tag{C4}$$

$$G^K(t,t') \equiv -i\langle\phi_c(t)\phi_c(t')\rangle. \tag{C5}$$

Accordingly, we define the six-component fermion field

$$\Psi^T_{i\lambda}(t) \equiv \left(\psi^x_c(t),\psi^y_c(t),\psi^z_c(t),\psi^x_q(t),\psi^y_q(t),\psi^z_q(t)\right), \tag{C6}$$

where we have omitted the $i\lambda$ index on the RHS for simplicity. Then, the action for free fermions S_σ in Eq. (10) reads

$$S_\sigma = \frac{1}{2}\sum_{i}^{N}\sum_{\lambda}^{N_s}\int_0^t \Psi^T_{i\lambda}\hat{G}_0^{-1}\Psi_{i\lambda}dt, \tag{C7}$$

with

$$\hat{G}_0^{-1} \equiv \begin{bmatrix} 0 & \left(\hat{G}_0^A\right)^{-1} \\ \left(\hat{G}_0^R\right)^{-1} & 0 \end{bmatrix}, \tag{C8}$$

$$\left(\hat{G}_0^R\right)^{-1} = \left[\left(\hat{G}_0^A\right)^{-1}\right]^\dagger \equiv \begin{bmatrix} i\partial_t & i\Delta & 0 \\ -i\Delta & i\partial_t & 0 \\ 0 & 0 & i\partial_t \end{bmatrix}. \tag{C9}$$

For self-energies we define

$$\hat{\Sigma}^R \equiv \tfrac{1}{2}(\hat{\Sigma}^{++}-\hat{\Sigma}^{+-}-\hat{\Sigma}^{--}+\hat{\Sigma}^{-+}), \tag{C10}$$

$$\hat{\Sigma}^A \equiv \tfrac{1}{2}(\hat{\Sigma}^{++}+\hat{\Sigma}^{+-}-\hat{\Sigma}^{--}-\hat{\Sigma}^{-+}), \tag{C11}$$

$$\hat{\Sigma}^K \equiv \tfrac{1}{2}(\hat{\Sigma}^{++}+\hat{\Sigma}^{+-}+\hat{\Sigma}^{--}+\hat{\Sigma}^{-+}). \tag{C12}$$

DEs have a simple structure in terms of RAK functions:

$$\begin{bmatrix} 0 & \left(\hat{G}_0^A\right)^{-1}-\hat{\Sigma}^A \\ \left(\hat{G}_0^R\right)^{-1}-\hat{\Sigma}^R & -\hat{\Sigma}^K \end{bmatrix}\begin{bmatrix} \hat{G}^K & \hat{G}^R \\ \hat{G}^A & 0 \end{bmatrix} = \mathbb{1}, \tag{C13}$$

$$\left(\hat{G}_0^R\right)^{-1}\hat{G}^R = \mathbb{1}+\hat{\Sigma}^R\hat{G}^R, \tag{C14}$$

$$\left(\hat{G}_0^R\right)^{-1}\hat{G}^K = \hat{\Sigma}^R\hat{G}^K+\hat{\Sigma}^K\hat{G}^A. \tag{C15}$$

The fermion self-energy matrix at NLO reads

$$\hat{\Sigma}^{ss'}_{\rm NLO} = \begin{bmatrix} 0 & 0 & 0 \\ 0 & \tilde{\Sigma}^{ss'}_{yy} & \tilde{\Sigma}^{ss'}_{yz} \\ 0 & \tilde{\Sigma}^{ss'}_{zy} & \tilde{\Sigma}^{ss'}_{zz} \end{bmatrix} (s,s'=\pm). \tag{C16}$$

Following Eq. (81), the expanded forms of the components of Σ are given by

$$\tilde{\Sigma}^{ss'}_{yy}(t,t') = +\frac{4i}{N_s}\left[MV^{11}_{ss'}(t,t')+M(M-1)U^{11}_{ss'}(t,t')\right]G^{ss'}_{zz}(t,t'), \tag{C17}$$

$$\tilde{\Sigma}^{ss'}_{zz}(t,t') = +\frac{4i}{N_s}\left[MV^{11}_{ss'}(t,t')+M(M-1)U^{11}_{ss'}(t,t')\right]G^{ss'}_{yy}(t,t'), \tag{C18}$$

$$\tilde{\Sigma}^{ss'}_{yz}(t,t') = -\frac{4i}{N_s}\left[MV^{11}_{ss'}(t,t')+M(M-1)U^{11}_{ss'}(t,t')\right]G^{ss'}_{zy}(t,t'), \tag{C19}$$

$$\tilde{\Sigma}^{ss'}_{zy}(t,t') = -\frac{4i}{N_s}\left[MV^{11}_{ss'}(t,t')+M(M-1)U^{11}_{ss'}(t,t')\right]G^{ss'}_{yz}(t,t'). \tag{C20}$$

We do not write RAK self-energies in terms of RAK Green's functions because it is numerically less costly to find them from Eqs. (C10)–(C12). We define $B_x(t)$ as

$$B_x(t) \equiv \frac{2M}{\sqrt{N_s}} \tilde{\chi}^1(t), \tag{C21}$$

which captures the fermion self-energy at LO [Eq. (76)]. Then, the expanded DEs for retarded fermion Green's functions are given by

$$i\partial_t G^R_{xx}(t,t') + i\Delta G^R_{yx}(t,t') = \delta(t-t'), \tag{C22}$$

$$i\partial_t G^R_{xy}(t,t') + i\Delta G^R_{yy}(t,t') = 0, \tag{C23}$$

$$i\partial_t G^R_{xz}(t,t') + i\Delta G^R_{yz}(t,t') = 0, \tag{C24}$$

$$i\partial_t G^R_{yx}(t,t') - i\Delta G^R_{xx}(t,t') - iB_x(t)G^R_{zx}(t,t') = \int_0^t \left[\tilde{\Sigma}^R_{yy}(t,t'')G^R_{yx}(t'',t') + \tilde{\Sigma}^R_{yz}(t,t'')G^R_{zx}(t'',t')\right]dt'', \tag{C25}$$

$$i\partial_t G^R_{yy}(t,t') - i\Delta G^R_{xy}(t,t') - iB_x(t)G^R_{zy}(t,t') = \delta(t-t') + \int_0^t \left[\tilde{\Sigma}^R_{yy}(t,t'')G^R_{yy}(t'',t') + \tilde{\Sigma}^R_{yz}(t,t'')G^R_{zy}(t'',t')\right]dt'', \tag{C26}$$

$$i\partial_t G^R_{yz}(t,t') - i\Delta G^R_{xz}(t,t') - iB_x(t)G^R_{zz}(t,t') = \int_0^t \left[\tilde{\Sigma}^R_{yy}(t,t'')G^R_{yz}(t'',t') + \tilde{\Sigma}^R_{yz}(t,t'')G^R_{zz}(t'',t')\right]dt'', \tag{C27}$$

$$i\partial_t G^R_{zx}(t,t') + iB_x(t)G^R_{yx}(t,t') = \int_0^t \left[\tilde{\Sigma}^R_{zy}(t,t'')G^R_{yx}(t'',t') + \tilde{\Sigma}^R_{zz}(t,t'')G^R_{zx}(t'',t')\right]dt'', \tag{C28}$$

$$i\partial_t G^R_{zy}(t,t') + iB_x(t)G^R_{yy}(t,t') = \int_0^t \left[\tilde{\Sigma}^R_{zy}(t,t'')G^R_{yy}(t'',t') + \tilde{\Sigma}^R_{zz}(t,t'')G^R_{zy}(t'',t')\right]dt'', \tag{C29}$$

$$i\partial_t G^R_{zz}(t,t') + iB_x(t)G^R_{yz}(t,t') = \delta(t-t') + \int_0^t \left[\tilde{\Sigma}^R_{zy}(t,t'')G^R_{yz}(t'',t') + \tilde{\Sigma}^R_{zz}(t,t'')G^R_{zz}(t'',t')\right]dt''. \tag{C30}$$

For Keldysh components we have

$$i\partial_t G^K_{xx}(t,t') + i\Delta G^K_{yx}(t,t') = 0, \tag{C31}$$

$$i\partial_t G^K_{xy}(t,t') + i\Delta G^K_{yy}(t,t') = 0, \tag{C32}$$

$$i\partial_t G^K_{xz}(t,t') + i\Delta G^K_{yz}(t,t') = 0, \tag{C33}$$

$$\begin{aligned} i\partial_t G^K_{yx}(t,t') - i\Delta G^K_{xx}(t,t') - iB_x(t)G^K_{zx}(t,t') = \int_0^t \Big[&\tilde{\Sigma}^R_{yy}(t,t'')G^K_{yx}(t'',t') + \tilde{\Sigma}^R_{yz}(t,t'')G^K_{zx}(t'',t') \\ &+ \tilde{\Sigma}^K_{yy}(t,t'')G^A_{yx}(t'',t') + \tilde{\Sigma}^K_{yz}(t,t'')G^A_{zx}(t'',t')\Big]dt'', \end{aligned} \tag{C34}$$

$$\begin{aligned} i\partial_t G^K_{yy}(t,t') - i\Delta G^K_{xy}(t,t') - iB_x(t)G^K_{zy}(t,t') = \int_0^t \Big[&\tilde{\Sigma}^R_{yy}(t,t'')G^K_{yy}(t'',t') + \tilde{\Sigma}^R_{yz}(t,t'')G^K_{zy}(t'',t') \\ &+ \tilde{\Sigma}^K_{yy}(t,t'')G^A_{yy}(t'',t') + \tilde{\Sigma}^K_{yz}(t,t'')G^A_{zy}(t'',t')\Big]dt'', \end{aligned} \tag{C35}$$

$$\begin{aligned} i\partial_t G^K_{yz}(t,t') - i\Delta G^K_{xz}(t,t') - iB_x(t)G^K_{zz}(t,t') = \int_0^t \Big[&\tilde{\Sigma}^R_{yy}(t,t'')G^K_{yz}(t'',t') + \tilde{\Sigma}^R_{yz}(t,t'')G^K_{zz}(t'',t') \\ &+ \tilde{\Sigma}^K_{yy}(t,t'')G^A_{yz}(t'',t') + \tilde{\Sigma}^K_{yz}(t,t'')G^A_{zz}(t'',t')\Big]dt'', \end{aligned} \tag{C36}$$

$$\begin{aligned} i\partial_t G^K_{zx}(t,t') + iB_x(t)G^K_{yx}(t,t') = \int_0^t \Big[&\tilde{\Sigma}^R_{zy}(t,t'')G^K_{yx}(t'',t') + \tilde{\Sigma}^R_{zz}(t,t'')G^K_{zx}(t'',t') \\ &+ \tilde{\Sigma}^K_{zy}(t,t'')G^A_{yx}(t'',t') + \tilde{\Sigma}^K_{zz}(t,t'')G^A_{zx}(t'',t')\Big]dt'', \end{aligned} \tag{C37}$$

$$\begin{aligned} i\partial_t G^K_{zy}(t,t') + iB_x(t)G^K_{yy}(t,t') = \int_0^t \Big[&\tilde{\Sigma}^R_{zy}(t,t'')G^K_{yy}(t'',t') + \tilde{\Sigma}^R_{zz}(t,t'')G^K_{zy}(t'',t') \\ &+ \tilde{\Sigma}^K_{zy}(t,t'')G^A_{yy}(t'',t') + \tilde{\Sigma}^K_{zz}(t,t'')G^A_{zy}(t'',t')\Big]dt'', \end{aligned} \tag{C38}$$

$$i\partial_t G^K_{zz}(t,t') + iB_x(t)G^K_{yz}(t,t') = \int_0^t \Big[\tilde{\Sigma}^R_{zy}(t,t'')G^K_{yz}(t'',t') + \tilde{\Sigma}^R_{zz}(t,t'')G^K_{zz}(t'',t') + \tilde{\Sigma}^K_{zy}(t,t'')G^A_{yz}(t'',t') + \tilde{\Sigma}^K_{zz}(t,t'')G^A_{zz}(t'',t')\Big]dt''. \tag{C39}$$

Advanced functions can be obtained from $\hat{G}^A = [\hat{G}^R]^\dagger$ and do not require separate computation.

Photons fields in (c, q) basis are cast into a multicomponent field defined by

$$\Phi^T_\alpha(t) \equiv (\phi_{\alpha,c}, \pi_{\alpha,c}, \phi_{\alpha,q}, \pi_{\alpha,q}), \tag{C40}$$

with the free action (Eq. (18)

$$S_{\rm ph} = \frac{1}{2}\sum_\alpha^M \int_0^t \Phi^T_\alpha \hat{D}_0^{-1}\Phi_\alpha dt, \tag{C41}$$

where

$$\hat{D}_0^{-1} \equiv \begin{bmatrix} 0 & (\hat{D}_0^{-1})^A \\ (\hat{D}_0^{-1})^R & (\hat{D}_0^{-1})^K \end{bmatrix}, \tag{C42}$$

$$(\hat{D}_0^{-1})^R = [(\hat{D}_0^{-1})^A]^\dagger \equiv \begin{bmatrix} -\omega_c^2 & -\kappa - \partial_t \\ \kappa + \partial_t & -1 \end{bmatrix}, \tag{C43}$$

$$(\hat{D}_0^{-1})^K \equiv \begin{bmatrix} 2i\kappa\omega_c & 0 \\ 0 & 2i\kappa/\omega_c \end{bmatrix}. \tag{C44}$$

Note that $(\hat{D}_0^{-1})^K$ is not the inverse of the bare Keldysh function, for details see Ref. [100]. Similar to fermions, DE has the general structure

$$\begin{bmatrix} 0 & (\hat{D}_0^A)^{-1} - \hat{\Pi}^A \\ (\hat{D}_0^R)^{-1} - \hat{\Pi}^R & (\hat{D}_0^K)^{-1} - \hat{\Pi}^K \end{bmatrix} \begin{bmatrix} \hat{D}^K & \hat{D}^R \\ \hat{D}^A & 0 \end{bmatrix} = \mathbb{1}, \tag{C45}$$

$$(\hat{D}_0^R)^{-1}\hat{D}^R = \mathbb{1} + \hat{\Pi}^R\hat{D}^R, \tag{C46}$$

$$(\hat{D}_0^R)^{-1}\hat{D}^K + (\hat{D}_0^K)^{-1}\hat{D}^A = \hat{\Pi}^R\hat{D}^K + \hat{\Pi}^K\hat{D}^A. \tag{C47}$$

The photon self-energy matrix $\hat{\Pi}$ only has one nonzero entry in (ϕ, π) basis

$$\hat{\Pi}^{R/A/K} = \begin{bmatrix} \Pi^{R/A/K} & 0 \\ 0 & 0 \end{bmatrix}, \tag{C48}$$

where Π was given in Eq. (82). The expanded DE for retarded photon functions are given by

$$-(\partial_t + \kappa)D^R_{\pi\phi}(t,t') - \omega_c^2 D^R_{\phi\phi}(t,t') = \delta(t-t') + \int_0^t \Pi^R(t,t'')D^R_{\phi\phi}(t'',t')dt'', \tag{C49}$$

$$-(\partial_t + \kappa)D^R_{\pi\pi}(t,t') - \omega_c^2 D^R_{\phi\pi}(t,t') = \int_0^t \Pi^R(t,t'')D^R_{\phi\pi}(t'',t')dt'', \tag{C50}$$

$$+(\partial_t + \kappa)D^R_{\phi\phi}(t,t') - D^R_{\pi\phi}(t,t') = 0, \tag{C51}$$

$$+(\partial_t + \kappa)D^R_{\phi\pi}(t,t') - D^R_{\pi\pi}(t,t') = \delta(t-t'), \tag{C52}$$

and for Keldysh functions:

$$-(\partial_t + \kappa)D^K_{\pi\phi}(t,t') - \omega_c^2 D^K_{\phi\phi}(t,t') + 2i\kappa\omega_c D^A_{\phi\phi}(t,t') = \int_0^t \big[\Pi^R(t,t'')D^K_{\phi\phi}(t'',t') + \Pi^K(t,t'')D^A_{\phi\phi}(t'',t')\big]dt'', \tag{C53}$$

$$-(\partial_t + \kappa)D^K_{\pi\pi}(t,t') - \omega_c^2 D^K_{\phi\pi}(t,t') + 2i\kappa\omega_c D^A_{\phi\pi}(t,t') = \int_0^t \big[\Pi^R(t,t'')D^K_{\phi\pi}(t'',t') + \Pi^K(t,t'')D^A_{\phi\pi}(t'',t')\big]dt'', \tag{C54}$$

$$+(\partial_t + \kappa)D^K_{\phi\phi}(t,t') - D^K_{\pi\phi}(t,t') + \frac{2i\kappa}{\omega_c}D^A_{\pi\phi}(t,t') = 0, \tag{C55}$$

$$+(\partial_t + \kappa)D^K_{\phi\pi}(t,t') - D^K_{\pi\pi}(t,t') + \frac{2i\kappa}{\omega_c}D^A_{\pi\pi}(t,t') = 0. \tag{C56}$$

As mentioned in the main text, the off-diagonal ($\alpha \neq \beta$) elements of Ising field Green's functions have to be retained and DE for Ising field Green's functions couple diagonal (V) and off-diagonal (U) elements of W. The compact form of the DEs for W is

$$\begin{bmatrix} 0 & (\hat{W}_0^A)^{-1} - \hat{\Omega}^A \\ (\hat{W}_0^R)^{-1} - \hat{\Omega}^R & -\hat{\Omega}^K \end{bmatrix} \begin{bmatrix} \hat{W}^K & \hat{W}^R \\ \hat{W}^A & 0 \end{bmatrix} = \mathbb{1}. \tag{C57}$$

The self-energy matrices are diagonal in the two-dimensional space of the Ising field components

$$\hat{\Omega}^{R/A/K} = \begin{bmatrix} \Omega_{11}^{R/A/K} & 0 \\ 0 & \Omega_{22}^{R/A/K} \end{bmatrix}, \tag{C58}$$

where Ω_{11} and Ω_{22} were given in Eqs. (83) and (84). It is convenient to decompose W into its free and renormalized parts

$$W \equiv W_0 + \tilde{W}, \tag{C59}$$

yielding

$$\tilde{W}^R = W_0^R \Omega^R W_0^R + W_0^R \Omega^R \tilde{W}^R. \tag{C60}$$

$$\tilde{W}^K = W_0^R \Omega^K W_0^A + W_0^R \Omega^R \tilde{W}^K + W_0^R \Omega^K \tilde{W}^A. \tag{C61}$$

The expanded form of Eq. (C60) in the retarded sector is given by (note that $U_0 = V_0^{11} = V_0^{22} = 0$)

$$\tilde{V}_{11}^R(t,t') = \frac{1}{N+M}\Omega_{22}^R(t,t') + \frac{1}{\sqrt{N+M}}\int_0^t \Omega_{22}^R(t,t'')\tilde{V}_R^{21}(t'',t')dt'', \tag{C62}$$

$$\tilde{U}_{11}^R(t,t') = \frac{1}{\sqrt{N+M}}\int_0^t \Omega_{22}^R(t,t'')\tilde{U}_{21}^R(t'',t')dt'', \tag{C63}$$

$$\tilde{V}_{12}^R(t,t') = \tilde{U}_{12}^R(t,t') = \frac{1}{\sqrt{N+M}}\int_0^t \Omega_{22}^R(t,t'')\tilde{V}_{22}^R(t'',t')dt'', \tag{C64}$$

$$\tilde{V}_{21}^R(t,t') = \tilde{U}_{21}^R(t,t') = \frac{1}{\sqrt{N+M}}\int_0^t \Omega_{11}^R(t,t'')\big[\tilde{V}_{11}^R(t'',t') + (M-1)\tilde{U}_{11}^R(t'',t')\big]dt'', \tag{C65}$$

$$\tilde{V}_{22}^R(t,t') = \tilde{U}_{22}^R(t,t') = \frac{1}{N+M}\Omega_{11}^R(t,t') + \frac{1}{\sqrt{N+M}}\int_0^t \Omega_{11}^R(t,t'')\big[\tilde{V}_{12}^R(t'',t') + (M-1)\tilde{U}_{12}^R(t'',t')\big]dt'', \tag{C66}$$

and for Eq. (C61) we have

$$\tilde{V}_{11}^K(t,t') = \frac{1}{N+M}\Omega_{22}^K(t,t') + \frac{1}{\sqrt{N+M}}\int_0^t \big[\Omega_{22}^R(t,t'')\tilde{V}_{21}^R(t'',t') + \Omega_{22}^K(t,t'')\tilde{V}_{21}^A(t'',t')\big]dt'', \tag{C67}$$

$$\tilde{U}_{11}^K(t,t') = \frac{1}{\sqrt{N+M}}\int_0^t \big[\Omega_{22}^R(t,t'')\tilde{U}_{21}^K(t'',t') + \Omega_{22}^K(t,t'')\tilde{U}_{21}^A(t'',t')\big]dt'', \tag{C68}$$

$$\tilde{V}_{12}^K(t,t') = \tilde{U}_{12}^K(t,t') = \frac{1}{\sqrt{N+M}}\int_0^t \big[\Omega_{22}^R(t,t'')\tilde{V}_{22}^K(t'',t') + \Omega_{22}^K(t,t'')\tilde{V}_{22}^A(t'',t')\big]dt'', \tag{C69}$$

$$\begin{aligned}\tilde{V}_{21}^K(t,t') = \tilde{U}_{21}^K(t,t') = {} & \frac{1}{\sqrt{N+M}}\int_0^t \Omega_{11}^R(t,t'')\big[\tilde{V}_{11}^K(t'',t') + (M-1)\tilde{U}_{11}^K(t'',t')\big]dt'' \\ & + \int_0^t \Omega_{11}^K(t,t'')\big[\tilde{V}_{11}^A(t'',t') + (M-1)\tilde{U}_{11}^A(t'',t')\big]dt'',\end{aligned} \tag{C70}$$

$$\begin{aligned}\tilde{V}_{22}^K(t,t') = \tilde{U}_{22}^K(t,t') = {} & \frac{1}{N+M}\Omega_{11}^K(t,t') + \frac{1}{\sqrt{N+M}}\int_0^t \Omega_{11}^R(t,t'')\big[\tilde{V}_{12}^K(t'',t') + (M-1)\tilde{U}_{12}^K(t'',t')\big]dt'' \\ & + \int_0^t \Omega_{11}^K(t,t'')\big[\tilde{V}_{12}^A(t'',t') + (M-1)\tilde{U}_{12}^A(t'',t')\big]dt''.\end{aligned} \tag{C71}$$

DE have a causal structure [81,131,134] with solutions that propagate in time such that the values of Green's functions at each time step only depend on their values at previous times, allowing us to efficiently solve them using conventional numerical methods for differential equations.

APPENDIX D: EVALUATION OF THE OVERLAP PARAMETER

After the procedure discussed in Sec. V H 3, fields of different replicas will be coupled to each other. Seemingly, this increases the complexity of the problem because one usually

has to consider larger Green's function matrices. However, the inter-replica couplings do not affect the dynamics of replica diagonal correlators. Therefore, the dynamics generated by DE given above are still valid. To evaluate replica off-diagonal Green's functions, we have to derive extra dynamical equations that take replica diagonal Green's functions as inputs. Further simplifications occur by noting that replica off-diagonal fermion Green's functions vanish due to the local Z_2 gauge symmetry of the fermionic representation for spins $\psi \to -\psi$. The only nonzero replica off-diagonal self-energies are

$$\underset{\sim}{\Pi}_{\rm LO}(t_c, t_c') = -2iNg^2\omega_c \tilde{\chi}^2(t_c)\tilde{\chi}^2(t_c'), \tag{D1}$$

$$\underset{\sim}{\Pi}_{\rm NLO}(t_c, t_c') = 2Ng^2\omega_c \underset{\sim}{V}^{22}(t_c, t_c'), \tag{D2}$$

$$\underset{\sim}{\Omega}^{22}(t_c, t_c') = 2g^2\omega_c \underset{\sim}{D}^{\phi\phi}(t_c, t_c'). \tag{D3}$$

We also note that off-diagonal Green's functions only have Keldysh (symmetric) components. This is natural because replicas are only mathematical entities without real physical interactions with each other. DE governing $\underset{\sim}{D}$ are given by

$$-(\partial_t + \kappa)\underset{\sim}{D}^K_{\phi\phi}(t, t') + \underset{\sim}{D}^K_{\pi\phi}(t, t') = 0, \tag{D4}$$

$$-(\partial_t + \kappa)\underset{\sim}{D}^K_{\phi\pi}(t, t') + \underset{\sim}{D}^K_{\pi\pi}(t, t') = 0, \tag{D5}$$

$$\begin{aligned} &-(\partial_t + \kappa)\underset{\sim}{D}^K_{\pi\phi}(t, t') - \omega_c^2 \underset{\sim}{D}^K_{\phi\phi}(t, t') \\ &= \int_0^t \left[\Pi^R(t, t'')\underset{\sim}{D}^K_{\phi\phi}(t'', t') + \underset{\sim}{\Pi}^K(t, t'')D^A_{\phi\phi}(t'', t')\right]dt''. \end{aligned} \tag{D6}$$

$$\begin{aligned} &-(\partial_t + \kappa)\underset{\sim}{D}^K_{\pi\pi}(t, t') - \omega_c^2 \underset{\sim}{D}^K_{\phi\pi}(t, t') \\ &= \int_0^t \left[\Pi^R(t, t'')\underset{\sim}{D}^K_{\phi\pi}(t'', t') + \underset{\sim}{\Pi}^K(t, t'')D^A_{\phi\pi}(t'', t')\right]dt''. \end{aligned} \tag{D7}$$

For Ising field correlators we have

$$\begin{aligned} \underset{\sim}{U}^K_{11}(t, t') = \frac{1}{\sqrt{M+N}} \int_0^t &\left[\Omega^R_{22}(t, t'')\underset{\sim}{V}^K_{21}(t'', t')\right. \\ &\left. + \underset{\sim}{\Omega}^K_{22}(t, t'')V^A_{21}(t'', t')\right]dt'', \end{aligned} \tag{D8}$$

$$\underset{\sim}{V}^K_{11}(t, t') = \frac{1}{M+N}\underset{\sim}{\Omega}^K_{22}(t, t') + \underset{\sim}{U}^K_{11}(t, t'), \tag{D9}$$

$$\begin{aligned} \underset{\sim}{V}^K_{12}(t, t') = \underset{\sim}{U}^K_{12}(t, t') = \frac{1}{\sqrt{N+M}} \int_0^t &\left[\Omega^R_{22}(t, t'')\underset{\sim}{V}^K_{22}(t'', t')\right. \\ &\left. + \underset{\sim}{\Omega}^K_{22}(t, t'')V^A_{22}(t'', t')\right]dt'', \end{aligned} \tag{D10}$$

$$\begin{aligned} \underset{\sim}{V}^K_{21}(t, t') &= \underset{\sim}{U}^K_{21}(t, t') \\ &= \frac{1}{\sqrt{N+M}} \int_0^t \Omega^R_{11}(t, t'') \\ &\quad \times \left[\underset{\sim}{V}^K_{11}(t'', t') + (M-1)\underset{\sim}{U}^K_{11}(t'', t')\right]dt'', \end{aligned} \tag{D11}$$

$$\underset{\sim}{V}^K_{22}(t, t') = \frac{M}{\sqrt{N+M}} \int_0^t \Omega^R_{11}(t, t'')\underset{\sim}{V}^K_{12}(t'', t')dt''. \tag{D12}$$

These equations can be numerically solved using the same approach explained in Appendix E.

APPENDIX E: NUMERICAL SOLUTION OF DYSON EQUATIONS

Solving Dyson equations (DEs) is only possible using numerical integration. To solve DEs numerically, we discretize both time variables of the correlation functions according to

$$G(t, t') \to G(i, j) \tag{E1}$$

and solve the problem on a two-dimensional time grid with time spacing Δt. Assuming that correlation functions are known for $i, j \leqslant l$, which is an $l \times l$ square in the time grid, we evaluate the time derivates for fermion and photon Green's functions using Dyson equations in Eqs. (C22)–(C39) and (C49)–(C56). The memory integrals only depend on the values of correlation functions at $i, j \leqslant l$ and can be evaluated using various numerical integration methods to be chosen depending on the desired accuracy. The equations for HS correlation functions in Eqs. (C62)–(C71) involve no time derivatives and HS correlation functions are directly found from their equations at each step. Using the values for the time derivatives allows us to predict the values of Green's functions for $i, j \leqslant l + 1$ using Euler's method. However, the predicted value is usually not accurate enough and leads to numerical instabilities for long time evolutions. To remedy this issue, one can use more accurate approaches such as Runge-Kutta or predictor-corrector methods. For this work, we used a two-step predictor-corrector method. The reader is referred to an Appendix in Ref. [81] for a detailed discussion of the two-step predictor-corrector method for DEs.

The main numerical costs are due to memory integrals on the RHS of DEs. At each step of the integration, the numerical cost of evaluating memory integrals scales with l^2, where l is the (discretized) evolution time since the initial state. The quadratic scaling with l stems from the fact that at each step, memory integrals should be evaluated for l points on the edge of the square given by $i, j \leqslant l$ and for each point, the cost of numerical integration scales with l. We can reduce the numerical costs by using the analytical properties of Green's functions by only evaluating Green's functions on one side of the diagonal ($i \geqslant j$) explicitly and finding their values for $i < j$ using a combination of complex conjugation or transposition. Nevertheless, the numerical costs increase with the evolution time. To reduce the cost further, one may truncate memory integrals and keep the memory of the system up to a certain point in the past. However, this truncation is not permissible for our glassy system since the integrands have significant contributions at long times due to strong memory effects in the SG phase, and omitting memory effects prevents us to capture glassy dynamics. In this case, the overall cost of evolving the system for l steps using serial computation scales as l^3. Using parallel computation, we could achieve a slower increase of the runtime with l given by

$$t_{\rm runtime} \sim l^\beta, \tag{E2}$$

where $2 < \beta < 3$. For this work, each simulation took about three minutes for time evolutions up to $\Delta \times t = 20$. Longer simulations like those in Figs. 17(a) and 17(b) took about 30 minutes to complete. To obtain the spectral density at $\Delta \times \tau = 60$ in Fig. 23, the simulation took about two hours. The computation time and resources would be less if the

inter-replica overlap parameter did not need to be evaluated. All of the simulations were done on a personal computer.

1. Equations of motion at leading order

At LO fermion self-energies will only have local terms captured by B_x and the RHS of Eqs. (C31)–(C39) vanishes. We want to find the time derivatives of spin expectation values $m^\alpha = \langle \sigma^\alpha \rangle$. Using Eq. (9) we have

$$\frac{d}{dt} m^\alpha(t) = -i\,\epsilon_{\alpha\beta\gamma} \frac{d}{dt} \langle \psi^\beta(t) \psi^\gamma(t) \rangle = \frac{1}{2} \epsilon_{\alpha\beta\gamma} \frac{d}{dt} G^K_{\beta\gamma}(t,t). \tag{E3}$$

We use the chain rule to write

$$\frac{d}{dt} G^K_{\beta\gamma}(t,t) = (\partial_t + \partial_{t'}) G^K_{\beta\gamma}(t,t')|_{t'=t}. \tag{E4}$$

In DEs we have time derivatives of Green's functions only with respect to t. However, $\partial_{t'} G$ can be obtained easily by noting that

$$G^K_{\alpha\beta}(t,t') = -G^K_{\beta\alpha}(t',t), \tag{E5}$$

$$\rightarrow \partial_{t'} G^K_{\alpha\beta}(t,t')|_{t=t'} = -\partial_t G^K_{\beta\alpha}(t',t)|_{t'=t}. \tag{E6}$$

For example, to find $d\langle \sigma^z \rangle / dt$ we use Eq. (C32)

$$\partial_t G^K_{xy}(t,t')|_{t'=t} = -\Delta G^K_{yy}(t,t), \tag{E7}$$

and Eq. (C34)

$$\begin{aligned} \partial_{t'} G^K_{xy}(t,t')|_{t'=t} &= -\partial_t G^K_{yx}(t',t)|_{t'=t} \\ &= -\Delta G^K_{xx}(t,t) - B_x(t) G^K_{zx}(t,t), \end{aligned} \tag{E8}$$

to get

$$\frac{d}{dt} G^K_{xy}(t,t) = -B_x(t) G^K_{zx}(t,t), \tag{E9}$$

where we have used $G^K_{\alpha\alpha}(t,t) = 0$. Using $G^K_{zx}(t,t) = m_y(t)$ we get

$$\frac{d}{dt} m_z(t) = -B_x(t) m_y(t). \tag{E10}$$

Using B_x from Eq. (79) we get

$$\frac{d}{dt} m_z(t) = J\omega_c^2 \int_0^t k^y(t) D_R^{\phi\phi}(t,t') m_x(t') dt', \tag{E11}$$

which is the LO equation of motion for m_z given in Eq. (93). Equations (91) and (92) can be obtained similarly using DE at LO for other components of G^K.

APPENDIX F: COMPARISON BETWEEN TWO-PARTICLE IRREDUCIBLE AND DISCRETE TRUNCATED WIGNER APPROXIMATION

In this Appendix, we further compare the results of 2PI and DTWA for aging dynamics. We consider finite cavity loss $\kappa \neq 0$ which is implemented by solving a stochastic Langevin equation for cavity modes. Aging dynamics, given by the behavior of the correlation function in Eq. (102), is shown in Fig. 24. The 2PI results, which have been given in another work by us [93], are shown here over a longer timescale for a better comparison. 2PI predicts that C approaches a limiting

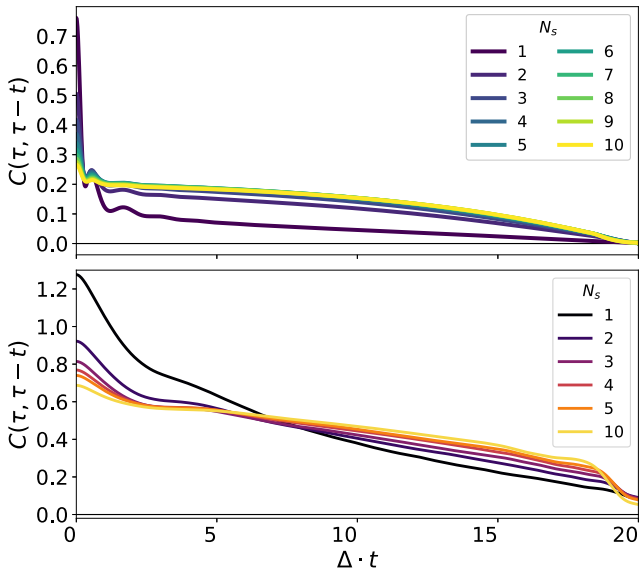

FIG. 24. Comparison of aging dynamics obtained from 2PI (top panel) and DTWA (bottom panel) for different cluster sizes. Parameters are $g/g_c = 1.27$, $\Delta/\omega_c = 0.2$, and $\kappa/\Delta = 0.5$.

value as N_s is increased. This limit corresponds to a classical SG with larger correlations at long times. For small N_s correlation are strongly suppressed by quantum fluctuations although the SG phase still survives. DTWA shows a qualitatively similar behavior for large N_s, where C approaches the same limit for $N_s \gtrsim 10$, with a relatively flat profile for a wide range of t. However, the agreement for large N_s is qualitative for aging dynamics, in contrast with the quantitative agreement of the two methods for magnetization dynamics presented in Sec. VI B 3. Similar to the magnetization dynamics, DTWA predicts less sensitivity to spin size down to $N_s = 1$, although it still predicts weaker SG. This has to be compared with 2PI, where C drastically changes for small spins, and particularly for $N_s = 1$. Furthermore, 2PI predicts a different correlation profile at between short ($t \lesssim \Delta^{-1}$) and long ($t \gtrsim \Delta^{-1}$) time separations, with a crossover of behavior at $t \sim \Delta^{-1}$. This sharp crossover was attributed to the small size of the local Hilbert space for small spins in Ref. [93], where quantum effects are more important. DTWA shows a crossover as well, but the timescale does not match Δ^{-1} which is the natural timescale for quantum fluctuations due to the transverse field Δ to affect local dynamics. Furthermore, the crossover is weaker and more smooth.

APPENDIX G: TWO-PARTICLE IRREDUCIBLE FOR THE SINGLE-MODE DICKE MODEL WITHOUT DISORDER

For the sake of completeness, we give a concise derivation of far from equilibrium dynamics for the singe-mode Dicke model [18] below, using a systematic expansion of the 2PI effective action in powers of the system size N.

For the Dicke model defined by

$$H = \frac{\Delta}{2} \sum_i^N \sigma_i^z + \omega_c a^\dagger a + \frac{g}{\sqrt{N}} \sum_i (a + a^\dagger) \sigma_i^x, \tag{G1}$$

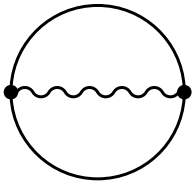

FIG. 25. The NLO contribution to 2PI action for the Dicke model.

the Keldysh actions for spins and photons are the same as Eqs. (10) and (18) together with their RAK representations in Eqs. (C7) and (C41). The main difference is the spin-photon coupling part of the action

$$S_{\rm int} = 2ig\sqrt{\frac{2\omega_c}{N}}\sum_i^N \oint dt_c \phi \psi_i^y \psi_i^z. \tag{G2}$$

In this case, the expectation value of the photon field $\varphi \equiv \langle\phi\rangle$ can be finite. It is straightforward to show that at NLO, the 2PI action reads:

$$\Gamma[\varphi,\pi,D,G] = S_{\rm cl}[\varphi,\pi] + \frac{i}{2}{\rm Tr}\ln D^{-1} + \frac{i}{2}{\rm Tr}\big(D_0^{-1}D\big) - \frac{i}{2}{\rm Tr}\ln G^{-1} - \frac{i}{2}{\rm Tr}\big(\tilde{G}_0^{-1}G\big) + \Gamma_2[D,G]. \tag{G3}$$

$S_{\rm cl}$ is obtained by substituting φ and π in $S_{\rm ph}$ in Eq. (18). $\tilde{G}_0$ contains the contribution of φ to spin dynamics

$$\tilde{G}_0^{-1} \equiv \begin{bmatrix} 0 & \big(\tilde{G}_0^A\big)^{-1} \\ \big(\tilde{G}_0^R\big)^{-1} & 0 \end{bmatrix}, \tag{G4}$$

$$\big(\tilde{G}_0^R\big)^{-1} \equiv \begin{bmatrix} i\partial_t & i\Delta & 0 \\ -i\Delta & i\partial_t & 2ig\sqrt{2\omega_c/N}\varphi \\ 0 & -2ig\sqrt{2\omega_c/N}\varphi & i\partial_t \end{bmatrix}, \tag{G5}$$

$$\big(\tilde{G}_0^A\big)^{-1} = \big[\big(\tilde{G}_0^R\big)^{-1}\big]^\dagger. \tag{G6}$$

The last term Γ_2 is given at NLO [$O(N^0)$] by the diagram in Fig. 25 and reads

$$\Gamma_2^{\rm NLO} = \frac{4\omega_c g^2}{N}\sum_j \oint\oint dt_c dt_c' D^{\phi\phi}(t_c,t_c')\big[G_{jj}^{yy}(t_c,t_c')G_{jj}^{zz}(t_c,t_c') - G_{jj}^{yz}(t_c,t_c')G_{jj}^{zy}(t_c,t_c')\big]. \tag{G7}$$

The DEs for fermions are similar to those for the disordered model, provided that we substitute

$$B_x(t) = -2g\sqrt{\frac{2\omega_c}{N}}\varphi(t) \tag{G8}$$

and use the following fermion self-energies in the basis of contour branches

$$\Sigma_{yz}^{ss'}(t,t') = -\frac{8i\omega_c g^2}{N}D_{\phi\phi}^{ss'}(t,t')G_{zy}^{ss'}(t,t'), \tag{G9}$$

$$\Sigma_{zy}^{ss'}(t,t') = -\frac{8i\omega_c g^2}{N}D_{\phi\phi}^{ss'}(t,t')G_{yz}^{ss'}(t,t'), \tag{G10}$$

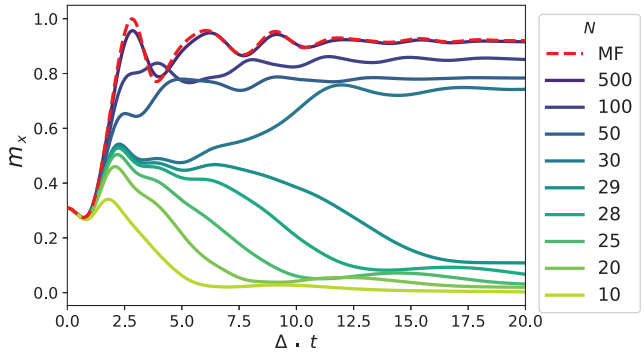

FIG. 26. Spin dynamics for a quench into the SR phase of the Dicke model with photon loss, starting from $\theta_0 = 0.9\pi$. For $N < N^\star$ where $N^\star = 30$, the symmetry is restored by fluctuations. $N^\star$ depends on the degree of symmetry breaking in the initial state. The other parameters are $g/g_c = 1.6$, $\Delta/\omega_c = 0.4$, and $\kappa/\omega_c = 0.2$.

$$\Sigma_{yy}^{ss'}(t,t') = +\frac{8i\omega_c g^2}{N}D_{\phi\phi}^{ss'}(t,t')G_{zz}^{ss'}(t,t'), \tag{G11}$$

$$\Sigma_{zz}^{ss'}(t,t') = +\frac{8i\omega_c g^2}{N}D_{\phi\phi}^{ss'}(t,t')G_{yy}^{ss'}(t,t'). \tag{G12}$$

The equations of motion (EOM) for classical fields are given by

$$(\partial_t + \kappa)\varphi = \pi, \tag{G13}$$

$$(\partial_t + \kappa)\pi + \omega_0^2\varphi + g\sqrt{2N\omega_0}G_{zy}^K(t,t) = 0. \tag{G14}$$

The DEs for photons are identical to those for the disordered system with the photon self-energy

$$\Pi^{ss'}(t,t') = -8i\omega_c g^2\big(G_{yz}^{ss'}(t,t')G_{zy}^{ss'}(t,t') - G_{yy}^{ss'}(t,t')G_{zz}^{ss'}(t,t')\big), \tag{G15}$$

given in the basis of contour branches.

Dynamics at LO are equivalent to the mean-field treatment of the Dicke model with the critical coupling

$$g_c = \frac{1}{2}\sqrt{\frac{\Delta\big(\omega_c^2+\kappa^2\big)}{\omega_c}}. \tag{G16}$$

At NLO the inclusion of fluctuations modifies the dynamics for smaller system sizes. For instance, after quenching the coupling into the SR regime $g > g_c$, the system may not end up in a symmetry broken state with $\langle a\rangle \neq 0$, even if the initial state is not symmetric (Fig. 26). For smaller values of N, one should choose a larger $m_x()$, otherwise the symmetry will be restored. The symmetry restoration is due to the fact that for smaller values of N fluctuation are stronger, resulting in the enhancement of the tunneling between the different minima in the energy of the system. This does not mean that the system is not in a SR state for small N. The photon population still saturates at a finite value $\approx N$.

[1] A. Browaeys and T. Lahaye, Many-body physics with individually controlled Rydberg atoms, Nat. Phys. **16**, 132 (2020).

[2] D. E. Chang, V. Vuletić, and M. D. Lukin, Quantum nonlinear optics—photon by photon, Nat. Photon. **8**, 685 (2014).

[3] T. Byrnes, N. Y. Kim, and Y. Yamamoto, Exciton–polariton condensates, Nat. Phys. **10**, 803 (2014).

[4] C. Monroe, W. C. Campbell, L.-M. Duan, Z.-X. Gong, A. V. Gorshkov, P. W. Hess, R. Islam, K. Kim, N. M. Linke, G. Pagano *et al.*, Programmable quantum simulations of spin systems with trapped ions, Rev. Mod. Phys. **93**, 025001 (2021).

[5] A. Blais, A. L. Grimsmo, S. M. Girvin, and A. Wallraff, Circuit quantum electrodynamics, Rev. Mod. Phys. **93**, 025005 (2021).

[6] E. Altman, K. R. Brown, G. Carleo, L. D. Carr, E. Demler, C. Chin, B. DeMarco, S. E. Economou, M. A. Eriksson, K.-M. C. Fu, M. Greiner, K. R. Hazzard, R. G. Hulet, A. J. Kollár, B. L. Lev, M. D. Lukin, R. Ma, X. Mi, S. Misra, C. Monroe, *et al.*, Quantum simulators: Architectures and opportunities, PRX Quantum **2**, 017003 (2021).

[7] F. Verstraete, M. M. Wolf, and J. Ignacio Cirac, Quantum computation and quantum-state engineering driven by dissipation, Nat. Phys. **5**, 633 (2009).

[8] P. M. Harrington, E. J. Mueller, and K. W. Murch, Engineered dissipation for quantum information science, Nat. Rev. Phy **4**, 660 (2022).

[9] S. Diehl, A. Micheli, A. Kantian, B. Kraus, H. Büchler, and P. Zoller, Quantum states and phases in driven open quantum systems with cold atoms, Nat. Phys. **4**, 878 (2008).

[10] S. Sachdev, *Quantum Phases of Matter* (Cambridge University Press, Cambridge, 2023).

[11] A. Altland and B. D. Simons, *Condensed Matter Field Theory* (Cambridge University Press, Cambridge, 2010).

[12] G. D. Mahan, *Many-Particle Physics* (Springer Science & Business Media, New York, 2000).

[13] P. M. Chaikin, T. C. Lubensky, and T. A. Witten, *Principles of Condensed Matter Physics* (Cambridge University Press Cambridge, 1995), Vol. 10.

[14] H. Walther, B. T. Varcoe, B.-G. Englert, and T. Becker, Cavity quantum electrodynamics, Rep. Prog. Phys. **69**, 1325 (2006).

[15] O. Hosten, N. J. Engelsen, R. Krishnakumar, and M. A. Kasevich, Measurement noise 100 times lower than the quantum-projection limit using entangled atoms, Nature (London) **529**, 505 (2016).

[16] O. Hosten, R. Krishnakumar, N. J. Engelsen, and M. A. Kasevich, Quantum phase magnification, Science **352**, 1552 (2016).

[17] S. P. Kelly, J. K. Thompson, A. M. Rey, and J. Marino, Resonant light enhances phase coherence in a cavity QED simulator of fermionic superfluidity, Phys. Rev. Res. **4**, L042032 (2022).

[18] P. Kirton, M. M. Roses, J. Keeling, and E. G. Dalla Torre, Introduction to the Dicke model: From equilibrium to nonequilibrium, and vice versa, Adv. Quantum Technol. **2**, 1800043 (2019).

[19] J. Keeling, M. J. Bhaseen, and B. D. Simons, Collective dynamics of Bose-Einstein condensates in optical cavities, Phys. Rev. Lett. **105**, 043001 (2010).

[20] R. J. Valencia-Tortora, S. P. Kelly, T. Donner, G. Morigi, R. Fazio, and J. Marino, Crafting the dynamical structure of synchronization by harnessing bosonic multilevel cavity QED, Phys. Rev. Res. **5**, 023112 (2023).

[21] O. Chelpanova, A. Lerose, S. Zhang, I. Carusotto, Y. Tserkovnyak, and J. Marino, Intertwining of lasing and superradiance under spintronic pumping, Phys. Rev. B **108**, 104302 (2023).

[22] P. Kirton and J. Keeling, Suppressing and restoring the Dicke superradiance transition by dephasing and decay, Phys. Rev. Lett. **118**, 123602 (2017).

[23] J. Marino, M. Eckstein, M. S. Foster, and A. M. Rey, Dynamical phase transitions in the collisionless pre-thermal states of isolated quantum systems: Theory and experiments, Rep. Prog. Phys. **85**, 116001 (2022).

[24] J. A. Muniz, D. Barberena, R. J. Lewis-Swan, D. J. Young, J. R. Cline, A. M. Rey, and J. K. Thompson, Exploring dynamical phase transitions with cold atoms in an optical cavity, Nature (London) **580**, 602 (2020).

[25] R. Lewis-Swan, Unifying scrambling, thermalization and entanglement through measurement of fidelity out-of-time-order correlators in the Dicke model, Nat. Commun. **10**, 1581 (2019).

[26] M. A. Norcia, R. J. Lewis-Swan, J. R. Cline, B. Zhu, A. M. Rey, and J. K. Thompson, Cavity-mediated collective spin-exchange interactions in a strontium superradiant laser, Science **361**, 259 (2018).

[27] N. Dogra, M. Landini, K. Kroeger, L. Hruby, T. Donner, and T. Esslinger, Dissipation-induced structural instability and chiral dynamics in a quantum gas, Science **366**, 1496 (2019).

[28] F. Ferri, R. Rosa-Medina, F. Finger, N. Dogra, M. Soriente, O. Zilberberg, T. Donner, and T. Esslinger, Emerging dissipative phases in a superradiant quantum gas with tunable decay, Phys. Rev. X **11**, 041046 (2021).

[29] D. Dreon, A. Baumgärtner, X. Li, S. Hertlein, T. Esslinger, and T. Donner, Self-oscillating pump in a topological dissipative atom–cavity system, Nature (London) **608**, 494 (2022).

[30] K. Baumann, C. Guerlin, F. Brennecke, and T. Esslinger, Dicke quantum phase transition with a superfluid gas in an optical cavity, Nature (London) **464**, 1301 (2010).

[31] P. Kongkhambut, J. Skulte, L. Mathey, J. G. Cosme, A. Hemmerich, and H. Keßler, Observation of a continuous time crystal, Science **377**, 670 (2022).

[32] H. Keßler, P. Kongkhambut, C. Georges, L. Mathey, J. G. Cosme, and A. Hemmerich, Observation of a dissipative time crystal, Phys. Rev. Lett. **127**, 043602 (2021).

[33] J. Klinder, H. Keßler, M. Wolke, L. Mathey, and A. Hemmerich, Dynamical phase transition in the open Dicke model, Proc. Natl. Acad. Sci. USA **112**, 3290 (2015).

[34] H. Kong, J. Taylor, Y. Dong, and K. Choi, Melting a Rydberg ice to a topological spin liquid with cavity vacuum fluctuation, arXiv:2109.03741.

[35] A. Periwal, E. S. Cooper, P. Kunkel, J. F. Wienand, E. J. Davis, and M. Schleier-Smith, Programmable interactions and emergent geometry in an array of atom clouds, Nature (London) **600**, 630 (2021).

[36] R. M. Kroeze, B. P. Marsh, K.-Y. Lin, J. Keeling, and B. L. Lev, High cooperativity using a confocal-cavity–QED microscope, PRX Quantum **4**, 020326 (2023).

[37] N. Sauerwein, F. Orsi, P. Uhrich, S. Bandyopadhyay, F. Mattiotti, T. Cantat-Moltrecht, G. Pupillo, P. Hauke, and J.-P. Brantut, Engineering random spin models with atoms in a high-finesse cavity, Nat. Phys. **19**, 1128 (2023).

[38] K. Bharti, A. Cervera-Lierta, T. H. Kyaw, T. Haug, S. Alperin-Lea, A. Anand, M. Degroote, H. Heimonen, J. S. Kottmann, T. Menke *et al.*, Noisy intermediate-scale quantum algorithms, Rev. Mod. Phys. **94**, 015004 (2022).

[39] A. S. Sørensen and K. Mølmer, Entangling atoms in bad cavities, Phys. Rev. A **66**, 022314 (2002).

[40] A. Rudelis, A cavity-coupled Rydberg atom array platform for quantum computing, Ph.D. thesis, Massachusetts Institute of Technology, 2023.

[41] Y.-T. Chen, M. Szurek, B. Hu, J. de Hond, B. Braverman, and V. Vuletic, High finesse bow-tie cavity for strong atom-photon coupling in Rydberg arrays, Opt. Express **30**, 37426 (2022).

[42] B. P. Marsh, Y. Guo, R. M. Kroeze, S. Gopalakrishnan, S. Ganguli, J. Keeling, and B. L. Lev, Enhancing associative memory recall and storage capacity using confocal cavity QED, Phys. Rev. X **11**, 021048 (2021).

[43] K. Seetharam, A. Lerose, R. Fazio, and J. Marino, Correlation engineering via nonlocal dissipation, Phys. Rev. Res. **4**, 013089 (2022).

[44] J. Schachenmayer, A. Pikovski, and A. M. Rey, Many-body quantum spin dynamics with Monte Carlo trajectories on a discrete phase space, Phys. Rev. X **5**, 011022 (2015).

[45] C. D. Mink, D. Petrosyan, and M. Fleischhauer, Hybrid discrete-continuous truncated Wigner approximation for driven, dissipative spin systems, Phys. Rev. Res. **4**, 043136 (2022).

[46] J. Huber, A. M. Rey, and P. Rabl, Realistic simulations of spin squeezing and cooperative coupling effects in large ensembles of interacting two-level systems, Phys. Rev. A **105**, 013716 (2022).

[47] J. Huber, P. Kirton, and P. Rabl, Phase-space methods for simulating the dissipative many-body dynamics of collective spin systems, SciPost Phys. **10**, 045 (2021).

[48] W. Verstraelen, D. Huybrechts, T. Roscilde, and M. Wouters, Quantum and classical correlations in open quantum spin lattices via truncated-cumulant trajectories, PRX Quantum **4**, 030304 (2023).

[49] S. P. Kelly, A. M. Rey, and J. Marino, Effect of active photons on dynamical frustration in cavity QED, Phys. Rev. Lett. **126**, 133603 (2021).

[50] C. Mc Keever and M. H. Szymańska, Stable iPEPO tensor-network algorithm for dynamics of two-dimensional open quantum lattice models, Phys. Rev. X **11**, 021035 (2021).

[51] J. Cui, J. I. Cirac, and M. C. Bañuls, Variational matrix product operators for the steady state of dissipative quantum systems, Phys. Rev. Lett. **114**, 220601 (2015).

[52] A. A. Gangat, I. T. Te, and Y.-J. Kao, Steady states of infinite-size dissipative quantum chains via imaginary time evolution, Phys. Rev. Lett. **119**, 010501 (2017).

[53] D. Kilda, A. Biella, M. Schirò, R. Fazio, and J. Keeling, On the stability of the infinite projected entangled pair operator ansatz for driven-dissipative 2D lattices, SciPost Phys. Core **4**, 005 (2021).

[54] A. Kshetrimayum, H. Weimer, and R. Orús, A simple tensor network algorithm for two-dimensional steady states, Nat. Commun. **8**, 1291 (2017).

[55] E. Mascarenhas, H. Flayac, and V. Savona, Matrix-product-operator approach to the nonequilibrium steady state of driven-dissipative quantum arrays, Phys. Rev. A **92**, 022116 (2015).

[56] H. Weimer, A. Kshetrimayum, and R. Orús, Simulation methods for open quantum many-body systems, Rev. Mod. Phys. **93**, 015008 (2021).

[57] S. P. Kelly, R. Nandkishore, and J. Marino, Exploring many-body localization in quantum systems coupled to an environment via Wegner-Wilson flows, Nucl. Phys. B **951**, 114886 (2020).

[58] J. Jin, A. Biella, O. Viyuela, L. Mazza, J. Keeling, R. Fazio, and D. Rossini, Cluster mean-field approach to the steady-state phase diagram of dissipative spin systems, Phys. Rev. X **6**, 031011 (2016).

[59] B. Zhu, J. Marino, N. Y. Yao, M. D. Lukin, and E. A. Demler, Dicke time crystals in driven-dissipative quantum many-body systems, New J. Phys. **21**, 073028 (2019).

[60] J. Berges, Controlled nonperturbative dynamics of quantum fields out of equilibrium, Nucl. Phys. A **699**, 847 (2002).

[61] J. Berges, Introduction to nonequilibrium quantum field theory, in *AIP Conference Proceedings* (American Institute of Physics, 2004), Vol. 739, pp. 3–62.

[62] J. M. Cornwall, R. Jackiw, and E. Tomboulis, Effective action for composite operators, Phys. Rev. D **10**, 2428 (1974).

[63] G. Aarts, D. Ahrensmeier, R. Baier, J. Berges, and J. Serreau, Far-from-equilibrium dynamics with broken symmetries from the $1/N$ expansion of the 2PI effective action, Phys. Rev. D **66**, 045008 (2002).

[64] F. Cooper, J. F. Dawson, and B. Mihaila, Quantum dynamics of phase transitions in broken symmetry $\lambda\varphi^4$ field theory, Phys. Rev. D **67**, 056003 (2003).

[65] A. Arrizabalaga, J. Smit, and A. Tranberg, Tachyonic preheating using 2PI-1/N dynamics and the classical approximation, J. High Energy Phys. 10 (2004) 017.

[66] J. Berges, S. Borsányi, and C. Wetterich, Prethermalization, Phys. Rev. Lett. **93**, 142002 (2004).

[67] J. Berges, D. Gelfand, and J. Pruschke, Quantum theory of fermion production after inflation, Phys. Rev. Lett. **107**, 061301 (2011).

[68] J. Berges and S. Roth, Topological defect formation from 2PI effective action techniques, Nucl. Phys. B **847**, 197 (2011).

[69] T. Gasenzer, L. McLerran, J. M. Pawlowski, and D. Sexty, Gauge turbulence, topological defect dynamics, and condensation in Higgs models, Nucl. Phys. A **930**, 163 (2014).

[70] B. Nowak, J. Schole, and T. Gasenzer, Universal dynamics on the way to thermalization, New J. Phys. **16**, 093052 (2014).

[71] A. Piñeiro Orioli, K. Boguslavski, and J. Berges, Universal self-similar dynamics of relativistic and nonrelativistic field theories near nonthermal fixed points, Phys. Rev. D **92**, 025041 (2015).

[72] J. Berges, K. Boguslavski, A. Chatrchyan, and J. Jaeckel, Attractive versus repulsive interactions in the Bose-Einstein condensation dynamics of relativistic field theories, Phys. Rev. D **96**, 076020 (2017).

[73] J. Berges and B. Wallisch, Nonthermal fixed points in quantum field theory beyond the weak-coupling limit, Phys. Rev. D **95**, 036016 (2017).

[74] R. Walz, K. Boguslavski, and J. Berges, Large-n kinetic theory for highly occupied systems, Phys. Rev. D **97**, 116011 (2018).

[75] A. M. Rey, B. L. Hu, E. Calzetta, A. Roura, and C. W. Clark, Nonequilibrium dynamics of optical-lattice-loaded Bose-Einstein-condensate atoms: Beyond the Hartree-Fock-Bogoliubov approximation, Phys. Rev. A **69**, 033610 (2004).

[76] K. Balzer and M. Bonitz, Nonequilibrium properties of strongly correlated artificial atoms—a Green's functions approach, J. Phys. A: Math. Theor. **42**, 214020 (2009).

[77] M. Kronenwett and T. Gasenzer, Far-from-equilibrium dynamics of an ultracold fermi gas, Appl. Phys. B: Lasers Opt. **102**, 469 (2011).

[78] M. Babadi, E. Demler, and M. Knap, Far-from-equilibrium field theory of many-body quantum spin systems: Prethermalization and relaxation of spin spiral states in three dimensions, Phys. Rev. X **5**, 041005 (2015).

[79] S. Bock, A. Liluashvili, and T. Gasenzer, Buildup of the Kondo effect from real-time effective action for the Anderson impurity model, Phys. Rev. B **94**, 045108 (2016).

[80] S. Erne, R. Bücker, T. Gasenzer, J. Berges, and J. Schmiedmayer, Universal dynamics in an isolated one-dimensional Bose gas far from equilibrium, Nature (London) **563**, 225 (2018).

[81] A. Schuckert, A. Piñeiro Orioli, and J. Berges, Nonequilibrium quantum spin dynamics from two-particle irreducible functional integral techniques in the Schwinger boson representation, Phys. Rev. B **98**, 224304 (2018).

[82] A. G. Burchards, J. Feldmeier, A. Schuckert, and M. Knap, Coupled hydrodynamics in dipole-conserving quantum systems, Phys. Rev. B **105**, 205127 (2022).

[83] J. Lang, M. Buchhold, and S. Diehl, Field theory for the dynamics of the open $o(n)$ model, Phys. Rev. B **109**, 064310 (2024).

[84] M. Babadi, *Non-Equilibrium Dynamics of Artificial Quantum Matter* (Harvard University, 2013).

[85] M. E. Carrington, W.-J. Fu, P. Mikula, and D. Pickering, Four-point vertices from the 2PI and 4PI effective actions, Phys. Rev. D **89**, 025013 (2014).

[86] J. Rammer, *Quantum Field Theory of Non-Equilibrium States* (Cambridge University Press, Cambridge, 2007).

[87] L. M. Sieberer, M. Buchhold, and S. Diehl, Keldysh field theory for driven open quantum systems, Rep. Prog. Phys. **79**, 096001 (2016).

[88] V. D. Vaidya, Y. Guo, R. M. Kroeze, K. E. Ballantine, A. J. Kollár, J. Keeling, and B. L. Lev, Tunable-range, photon-mediated atomic interactions in multimode cavity QED, Phys. Rev. X **8**, 011002 (2018).

[89] A. J. Kollár, A. T. Papageorge, K. Baumann, M. A. Armen, and B. L. Lev, An adjustable-length cavity and Bose–Einstein condensate apparatus for multimode cavity QED, New J. Phys. **17**, 043012 (2015).

[90] Y. Guo, R. M. Kroeze, V. D. Vaidya, J. Keeling, and B. L. Lev, Sign-changing photon-mediated atom interactions in multimode cavity quantum electrodynamics, Phys. Rev. Lett. **122**, 193601 (2019).

[91] G. Bentsen, I.-D. Potirniche, V. B. Bulchandani, T. Scaffidi, X. Cao, X.-L. Qi, M. Schleier-Smith, and E. Altman, Integrable and chaotic dynamics of spins coupled to an optical cavity, Phys. Rev. X **9**, 041011 (2019).

[92] R. M. Kroeze, B. P. Marsh, D. A. Schuller, H. S. Hunt, S. Gopalakrishnan, J. Keeling, and B. L. Lev, Replica symmetry breaking in a quantum-optical vector spin glass, arXiv:2311.04216.

[93] H. Hosseinabadi, D. E. Chang, and J. Marino, preceding paper, Quantum-to-classical crossover in the spin glass dynamics of cavity QED simulators, Phys. Rev. Res. **6**, 043313 (2024).

[94] P. Strack and S. Sachdev, Dicke quantum spin glass of atoms and photons, Phys. Rev. Lett. **107**, 277202 (2011).

[95] M. Buchhold, P. Strack, S. Sachdev, and S. Diehl, Dicke-model quantum spin and photon glass in optical cavities: Nonequilibrium theory and experimental signatures, Phys. Rev. A **87**, 063622 (2013).

[96] K. Srakaew, P. Weckesser, S. Hollerith, D. Wei, D. Adler, I. Bloch, and J. Zeiher, A subwavelength atomic array switched by a single Rydberg atom, Nat. Phys. **19**, 714 (2023).

[97] M. Buchhold, Y. Minoguchi, A. Altland, and S. Diehl, Effective theory for the measurement-induced phase transition of Dirac fermions, Phys. Rev. X **11**, 041004 (2021).

[98] S. F. Edwards and P. W. Anderson, Theory of spin glasses, J. Phys. F: Met. Phys. **5**, 965 (1975).

[99] K. Binder and A. P. Young, Spin glasses: Experimental facts, theoretical concepts, and open questions, Rev. Mod. Phys. **58**, 801 (1986).

[100] A. Kamenev, *Field Theory of Non-Equilibrium Systems* (Cambridge University Press, Cambridge, 2011).

[101] E. Marinari, G. Parisi, F. Ricci-Tersenghi, and J. J. Ruiz-Lorenzo, Violation of the fluctuation-dissipation theorem in finite-dimensional spin glasses, J. Phys. A: Math. Gen. **31**, 2611 (1998).

[102] A. Wierzchucka, F. Piazza, and P. W. Claeys, Integrability, multifractality, and two-photon dynamics in disordered Tavis-Cummings models, Phys. Rev. A **109**, 033716 (2024).

[103] E. Fiorelli, M. Marcuzzi, P. Rotondo, F. Carollo, and I. Lesanovsky, Signatures of associative memory behavior in a multimode Dicke model, Phys. Rev. Lett. **125**, 070604 (2020).

[104] B. P. Marsh, R. M. Kroeze, S. Ganguli, S. Gopalakrishnan, J. Keeling, and B. L. Lev, Entanglement and replica symmetry breaking in a driven-dissipative quantum spin glass, Phys. Rev. X **14**, 011026 (2024).

[105] M. Kac, G. Uhlenbeck, and P. Hemmer, On the van der Waals theory of the vapor-liquid equilibrium. I. Discussion of a one-dimensional model, J. Math. Phys. **4**, 216 (1963).

[106] G. S. Agarwal, R. R. Puri, and R. P. Singh, Atomic Schrödinger cat states, Phys. Rev. A **56**, 2249 (1997).

[107] J. K. Asbóth, P. Domokos, H. Ritsch, and A. Vukics, Self-organization of atoms in a cavity field: Threshold, bistability, and scaling laws, Phys. Rev. A **72**, 053417 (2005).

[108] S. Gopalakrishnan, B. L. Lev, and P. M. Goldbart, Atom-light crystallization of Bose-Einstein condensates in multimode cavities: Nonequilibrium classical and quantum phase transitions, emergent lattices, supersolidity, and frustration, Phys. Rev. A **82**, 043612 (2010).

[109] H.-P. Breuer and F. Petruccione, *The Theory of Open Quantum Systems* (Oxford University Press, 2002).

[110] H. Lipkin, N. Meshkov, and A. Glick, Validity of many-body approximation methods for a solvable model: (I). Exact solutions and perturbation theory, Nucl. Phys. **62**, 188 (1965).

[111] B. Sciolla and G. Biroli, Dynamical transitions and quantum quenches in mean-field models, J. Stat. Mech. (2011) P11003.

[112] B. Žunkovič, M. Heyl, M. Knap, and A. Silva, Dynamical quantum phase transitions in spin chains with long-range interactions: Merging different concepts of nonequilibrium criticality, Phys. Rev. Lett. **120**, 130601 (2018).

[113] A. Lerose, B. Žunkovič, J. Marino, A. Gambassi, and A. Silva, Impact of nonequilibrium fluctuations on prethermal dynamical phase transitions in long-range interacting spin chains, Phys. Rev. B **99**, 045128 (2019).

[114] N. Defenu, T. Donner, T. Macrì, G. Pagano, S. Ruffo, and A. Trombettoni, Long-range interacting quantum systems, Rev. Mod. Phys. **95**, 035002 (2023).

[115] W. Berdanier, J. Marino, and E. Altman, Universal dynamics of stochastically driven quantum impurities, Phys. Rev. Lett. **123**, 230604 (2019).

[116] J. J. Hopfield, Neural networks and physical systems with emergent collective computational abilities, Proc. Natl. Acad. Sci. USA **79**, 2554 (1982).

[117] D. J. Amit, H. Gutfreund, and H. Sompolinsky, Storing infinite numbers of patterns in a spin-glass model of neural networks, Phys. Rev. Lett. **55**, 1530 (1985).

[118] S. Gopalakrishnan, B. L. Lev, and P. M. Goldbart, Frustration and glassiness in spin models with cavity-mediated interactions, Phys. Rev. Lett. **107**, 277201 (2011).

[119] P. Rotondo, M. Cosentino Lagomarsino, and G. Viola, Dicke simulators with emergent collective quantum computational abilities, Phys. Rev. Lett. **114**, 143601 (2015).

[120] P. Rotondo, E. Tesio, and S. Caracciolo, Replica symmetry breaking in cold atoms and spin glasses, Phys. Rev. B **91**, 014415 (2015).

[121] D. Sherrington and S. Kirkpatrick, Solvable model of a spin-glass, Phys. Rev. Lett. **35**, 1792 (1975).

[122] P. Ray, B. K. Chakrabarti, and A. Chakrabarti, Sherrington-Kirkpatrick model in a transverse field: Absence of replica symmetry breaking due to quantum fluctuations, Phys. Rev. B **39**, 11828 (1989).

[123] W. Heisenberg and H. Euler, Consequences of Dirac's theory of positrons, Eur. Phys. J. A **98**, 714 (1936).

[124] R. Jackiw and A. Kerman, Time-dependent variational principle and the effective action, Phys. Lett. A **71**, 158 (1979).

[125] J. Berges and J. Serreau, Parametric resonance in quantum field theory, Phys. Rev. Lett. **91**, 111601 (2003).

[126] J. Berges and D. Sexty, Bose-Einstein condensation in relativistic field theories far from equilibrium, Phys. Rev. Lett. **108**, 161601 (2012).

[127] F. Verstraete, J. J. García-Ripoll, and J. I. Cirac, Matrix product density operators: Simulation of finite-temperature and dissipative systems, Phys. Rev. Lett. **93**, 207204 (2004).

[128] M. Sánchez-Barquilla, R. E. F. Silva, and J. Feist, Cumulant expansion for the treatment of light–matter interactions in arbitrary material structures, J. Chem. Phys. **152**, 034108 (2020).

[129] R. Paškauskas and M. Kastner, Equilibration in long-range quantum spin systems from a BBGKY perspective, J. Stat. Mech. (2012) P02005.

[130] C. Gardiner and P. Zoller, *Quantum Noise: A Handbook of Markovian and Non-Markovian Quantum Stochastic Methods with Applications to Quantum Optics* (Springer Science & Business Media, New York, 2004).

[131] A. Eberlein, V. Kasper, S. Sachdev, and J. Steinberg, Quantum quench of the Sachdev-ye-Kitaev model, Phys. Rev. B **96**, 205123 (2017).

[132] A. Haldar, P. Haldar, S. Bera, I. Mandal, and S. Banerjee, Quench, thermalization, and residual entropy across a non-fermi liquid to Fermi liquid transition, Phys. Rev. Res. **2**, 013307 (2020).

[133] C. Kuhlenkamp and M. Knap, Periodically driven Sachdev-Ye-Kitaev models, Phys. Rev. Lett. **124**, 106401 (2020).

[134] H. Hosseinabadi, S. P. Kelly, J. Schmalian, and J. Marino, Thermalization of non-Fermi-liquid electron-phonon systems: Hydrodynamic relaxation of the Yukawa-Sachdev-Ye-Kitaev model, Phys. Rev. B **108**, 104319 (2023).

[135] L. Grunwald, G. Passetti, and D. M. Kennes, Dynamical onset of light-induced unconventional superconductivity–a Yukawa-Sachdev-Ye-Kitaev study, Commun. Phys. **7**, 79 (2024).

[136] L. Batini, A. Chatrchyan, and J. Berges, Real-time dynamics of false vacuum decay, Phys. Rev. D **109**, 023502 (2024).

[137] E. Fradkin, *Field Theories of Condensed Matter Physics*, 2nd ed. (Cambridge University Press, Cambridge, 2013).

[138] A. Auerbach, *Interacting Electrons and Quantum Magnetism* (Springer Science & Business Media, New York, 1998).

[139] W. Mao, P. Coleman, C. Hooley, and D. Langreth, Spin dynamics from Majorana fermions, Phys. Rev. Lett. **91**, 207203 (2003).

[140] A. Shnirman and Y. Makhlin, Spin-spin correlators in the Majorana representation, Phys. Rev. Lett. **91**, 207204 (2003).

[141] J. Martin, Generalized classical dynamics, and the 'classical analogue' of a Fermi oscillator, Proc. R. Soc. London, Ser. A **251**, 536 (1959).

[142] H. J. Spencer and S. Doniach, Low-temperature anomaly of electron-spin resonance in dilute alloys, Phys. Rev. Lett. **18**, 994 (1967).

[143] H. J. Spencer, Theory of *s-d* scattering in dilute magnetic alloys with spin-$\frac{1}{2}$ impurities, Phys. Rev. **171**, 515 (1968).

[144] F. Berezin and M. Marinov, Particle spin dynamics as the Grassmann variant of classical mechanics, Ann. Phys. (NY) **104**, 336 (1977).

[145] B. S. Shastry and D. Sen, Majorana fermion representation for an antiferromagnetic spin-chain, Phys. Rev. B **55**, 2988 (1997).

[146] R. R. Biswas, L. Fu, C. R. Laumann, and S. Sachdev, SU(2)-invariant spin liquids on the triangular lattice with spinful Majorana excitations, Phys. Rev. B **83**, 245131 (2011).

[147] P. Schad, B. N. Narozhny, G. Schön, and A. Shnirman, Nonequilibrium spin noise and noise of susceptibility, Phys. Rev. B **90**, 205419 (2014).

[148] P. Schad, Y. Makhlin, B. Narozhny, G. Schön, and A. Shnirman, Majorana representation for dissipative spin systems, Ann. Phys. (NY) **361**, 401 (2015).

[149] P. Schad, A. Shnirman, and Y. Makhlin, Using Majorana spin-$\frac{1}{2}$ representation for the spin-boson model, Phys. Rev. B **93**, 174420 (2016).

[150] E. G. Dalla Torre, Y. Shchadilova, E. Y. Wilner, M. D. Lukin, and E. Demler, Dicke phase transition without total spin conservation, Phys. Rev. A **94**, 061802(R) (2016).

[151] Y. Shchadilova, M. M. Roses, E. G. Dalla Torre, M. D. Lukin, and E. Demler, Fermionic formalism for driven-dissipative multilevel systems, Phys. Rev. A **101**, 013817 (2020).

[152] J. Surace and L. Tagliacozzo, Fermionic Gaussian states: An introduction to numerical approaches, SciPost Phys. Lect. Notes54 (2022).

[153] S. Sachdev, *Quantum Phase Transitions*, 2nd ed. (Cambridge University Press, Cambridge, 2011).

[154] M. V. Feigel'man, A. I. Larkin, and M. A. Skvortsov, Keldysh action for disordered superconductors, Phys. Rev. B **61**, 12361 (2000).

[155] A. Arrizabalaga *et al.*, Quantum field dynamics and the 2PI effective action, Ph.D. thesis, University of Amsterdam, 2004.
[156] F. Carollo and I. Lesanovsky, Exactness of mean-field equations for open Dicke models with an application to pattern retrieval dynamics, Phys. Rev. Lett. **126**, 230601 (2021).
[157] V. V. Albert and L. Jiang, Symmetries and conserved quantities in Lindblad master equations, Phys. Rev. A **89**, 022118 (2014).
[158] B. Buča and T. Prosen, A note on symmetry reductions of the lindblad equation: Transport in constrained open spin chains, New J. Phys. **14**, 073007 (2012).
[159] S. Lieu, R. Belyansky, J. T. Young, R. Lundgren, V. V. Albert, and A. V. Gorshkov, Symmetry breaking and error correction in open quantum systems, Phys. Rev. Lett. **125**, 240405 (2020).
[160] N. Shammah, S. Ahmed, N. Lambert, S. De Liberato, and F. Nori, Open quantum systems with local and collective incoherent processes: Efficient numerical simulations using permutational invariance, Phys. Rev. A **98**, 063815 (2018).
[161] A. J. Bray and M. A. Moore, Replica theory of quantum spin glasses, J. Phys. C: Solid State Phys. **13**, L655 (1980).
[162] M. Mézard, G. Parisi, and M. A. Virasoro, *Spin Glass Theory and Beyond: An Introduction to the Replica Method and Its Applications* (World Scientific Publishing Company, Singapore, 1987), Vol. 9.
[163] S. B. Jäger, T. Schmit, G. Morigi, M. J. Holland, and R. Betzholz, Lindblad master equations for quantum systems coupled to dissipative bosonic modes, Phys. Rev. Lett. **129**, 063601 (2022).
[164] G. Piccitto, M. Wauters, F. Nori, and N. Shammah, Symmetries and conserved quantities of boundary time crystals in generalized spin models, Phys. Rev. B **104**, 014307 (2021).
[165] J. Marino and A. Silva, Relaxation, prethermalization, and diffusion in a noisy quantum Ising chain, Phys. Rev. B **86**, 060408(R) (2012).
[166] J. Marino and A. Silva, Nonequilibrium dynamics of a noisy quantum Ising chain: Statistics of work and prethermalization after a sudden quench of the transverse field, Phys. Rev. B **89**, 024303 (2014).
[167] S. Lorenzo, T. Apollaro, G. Palma, R. Nandkishore, A. Silva, and J. Marino, Remnants of anderson localization in prethermalization induced by white noise, Phys. Rev. B **98**, 054302 (2018).
[168] J. F. Rodriguez-Nieva, A. Piñeiro Orioli, and J. Marino, Far-from-equilibrium universality in the two-dimensional Heisenberg model, Proc. Natl. Acad. Sci. USA **119**, e2122599119 (2022).
[169] M. Marcuzzi, J. Marino, A. Gambassi, and A. Silva, Prethermalization from a low-density Holstein-Primakoff expansion, Phys. Rev. B **94**, 214304 (2016).
[170] M. Marcuzzi, J. Marino, A. Gambassi, and A. Silva, Prethermalization in a nonintegrable quantum spin chain after a quench, Phys. Rev. Lett. **111**, 197203 (2013).
[171] B. Bertini, F. H. L. Essler, S. Groha, and N. J. Robinson, Prethermalization and thermalization in models with weak integrability breaking, Phys. Rev. Lett. **115**, 180601 (2015).
[172] S. Schütz and G. Morigi, Prethermalization of atoms due to photon-mediated long-range interactions, Phys. Rev. Lett. **113**, 203002 (2014).
[173] L. D. Landau and E. M. Lifshitz, *Statistical Physics* (Elsevier, Amsterdam, 2013), Vol. 5.
[174] M. Kardar, *Statistical Physics of Fields* (Cambridge University Press, Cambridge, 2007).
[175] A. J. Daley, Quantum trajectories and open many-body quantum systems, Adv. Phys. **63**, 77 (2014).
[176] J.-P. Bouchaud, Weak ergodicity breaking and aging in disordered systems, J. Phys. I **2**, 1705 (1992).
[177] P. Calabrese and A. Gambassi, Ageing properties of critical systems, J. Phys. A: Math. Gen. **38**, R133 (2005).
[178] L. F. Cugliandolo and J. Kurchan, On the out-of-equilibrium relaxation of the Sherrington-Kirkpatrick model, J. Phys. A: Math. Gen. **27**, 5749 (1994).
[179] L. F. Cugliandolo and G. Lozano, Real-time nonequilibrium dynamics of quantum glassy systems, Phys. Rev. B **59**, 915 (1999).
[180] L. F. Cugliandolo and J. Kurchan, Analytical solution of the off-equilibrium dynamics of a long-range spin-glass model, Phys. Rev. Lett. **71**, 173 (1993).
[181] L. F. Cugliandolo, J. Kurchan, and L. Peliti, Energy flow, partial equilibration, and effective temperatures in systems with slow dynamics, Phys. Rev. E **55**, 3898 (1997).
[182] L. Foini, L. F. Cugliandolo, and A. Gambassi, Fluctuation-dissipation relations and critical quenches in the transverse field Ising chain, Phys. Rev. B **84**, 212404 (2011).
[183] A. Georges, O. Parcollet, and S. Sachdev, Mean field theory of a quantum Heisenberg spin glass, Phys. Rev. Lett. **85**, 840 (2000).
[184] G. Biroli and O. Parcollet, Out-of-equilibrium dynamics of a quantum Heisenberg spin glass, Phys. Rev. B **65**, 094414 (2002).
[185] F. Damanet, A. J. Daley, and J. Keeling, Atom-only descriptions of the driven-dissipative Dicke model, Phys. Rev. A **99**, 033845 (2019).
[186] R. Palacino and J. Keeling, Atom-only theories for U(1) symmetric cavity-QED models, Phys. Rev. Res. **3**, L032016 (2021).
[187] A. Andreanov and M. Müller, Long-range quantum Ising spin glasses at $t = 0$: Gapless collective excitations and universality, Phys. Rev. Lett. **109**, 177201 (2012).
[188] J. Gelhausen, M. Buchhold, A. Rosch, and P. Strack, Quantum-optical magnets with competing short- and long-range interactions: Rydberg-dressed spin lattice in an optical cavity, SciPost Phys. **1**, 004 (2016).
[189] G. Bentsen, T. Hashizume, A. S. Buyskikh, E. J. Davis, A. J. Daley, S. S. Gubser, and M. Schleier-Smith, Treelike interactions and fast scrambling with cold atoms, Phys. Rev. Lett. **123**, 130601 (2019).
[190] A. Asenjo-Garcia, M. Moreno-Cardoner, A. Albrecht, H. J. Kimble, and D. E. Chang, Exponential improvement in photon storage fidelities using subradiance and "selective radiance" in atomic arrays, Phys. Rev. X **7**, 031024 (2017).
[191] S. J. Masson, I. Ferrier-Barbut, L. A. Orozco, A. Browaeys, and A. Asenjo-Garcia, Many-body signatures of collective decay in atomic chains, Phys. Rev. Lett. **125**, 263601 (2020).
[192] L. Henriet, J. S. Douglas, D. E. Chang, and A. Albrecht, Critical open-system dynamics in a one-dimensional optical-lattice clock, Phys. Rev. A **99**, 023802 (2019).
[193] A. Albrecht, L. Henriet, A. Asenjo-Garcia, P. B. Dieterle, O. Painter, and D. E. Chang, Subradiant states of quantum bits coupled to a one-dimensional waveguide, New J. Phys. **21**, 025003 (2019).

[194] A. Asenjo-Garcia, H. Kimble, and D. E. Chang, Optical waveguiding by atomic entanglement in multilevel atom arrays, Proc. Natl. Acad. Sci. USA **116**, 25503 (2019).

[195] J. Rui, D. Wei, A. Rubio-Abadal, S. Hollerith, J. Zeiher, D. M. Stamper-Kurn, C. Gross, and I. Bloch, A subradiant optical mirror formed by a single structured atomic layer, Nature (London) **583**, 369 (2020).

[196] E. J. Davis, G. Bentsen, L. Homeier, T. Li, and M. H. Schleier-Smith, Photon-mediated spin-exchange dynamics of spin-1 atoms, Phys. Rev. Lett. **122**, 010405 (2019).

[197] K. Seetharam, A. Lerose, R. Fazio, and J. Marino, Dynamical scaling of correlations generated by short- and long-range dissipation, Phys. Rev. B **105**, 184305 (2022).

[198] J. Marino, Universality class of Ising critical states with long-range losses, Phys. Rev. Lett. **129**, 050603 (2022).

[199] X. Li, J. Marino, D. E. Chang, and B. Flebus, A solid-state platform for cooperative quantum phenomena, arXiv:2309.08991.

[200] P. Uhrich, S. Bandyopadhyay, N. Sauerwein, J. Sonner, J.-P. Brantut, and P. Hauke, A cavity quantum electrodynamics implementation of the Sachdev–Ye–Kitaev model, arXiv:2303.11343.

[201] K. Roux, H. Konishi, V. Helson, and J.-P. Brantut, Strongly correlated fermions strongly coupled to light, Nat. Commun. **11**, 2974 (2020).

Quantum-to-classical crossover in the spin glass dynamics of cavity QED simulators

Hossein Hosseinabadi [1,*] Darrick E. Chang [2,3] and Jamir Marino [1]
[1]*Institut für Physik, Johannes Gutenberg-Universität Mainz, 55099 Mainz, Germany*
[2]*ICFO–Institut de Ciències Fotòniques, The Barcelona Institute of Science and Technology, 08860 Castelldefels, Spain*
[3]*ICREA–Institució Catalana de Recerca i Estudis Avançats, 08015 Barcelona, Spain*

(Received 26 December 2023; revised 6 June 2024; accepted 26 November 2024; published 26 December 2024)

By solving the quench dynamics of a frustrated many-body spin-boson problem, we investigate the role of spin size on the dynamical formation of spin-glass order. In particular, we observe that quantum and classical spin glasses exhibit markedly different evolution. The former displays a quick relaxation of magnetization together with an exponential dependence of the spin-glass order parameter on spin size, while the latter has long-lasting prethermal magnetization and a spin-glass order parameter independent of spin size. The quantum-to-classical crossover is sharp and occurs for relatively small spins, highlighting the fragility of the quantum regime. Furthermore, we show that spin-glass order is resonantly enhanced when the frequency of the bosonic mediators of the interactions approaches the value of the transverse field. Our predictions are directly applicable to the nonequilibrium dynamics of all spin-glass systems with SU(2) spins, such as the quantum Sherrington-Kirkpatrick model, and they can be examined in recently developed multimode cavity QED experiments.

DOI: 10.1103/PhysRevResearch.6.043313

I. INTRODUCTION

Spin glasses (SGs) are frozen states of spins due to competing interactions generated by strong static disorder in their host materials [1,2]. Disorder prohibits the formation of long-range ferromagnetic (FM) or antiferromagnetic (AFM) orders and at the same time, hinders the melting of the frozen state by fluctuations and the formation of a paramagnetic (PM) state. SGs occupy a distinctive position in the field of disordered systems for their significance in our understanding of ergodicity breaking and for their broad range of applications from neural networks to optimization problems encompassing dynamics of complex biological systems and quantum information [3]. While disordered magnetic materials have historically been the main context for investigating SG, state-of-the-art quantum simulators possess the capacity to fabricate strongly correlated systems under controlled settings [4,5]. This presents a unique opportunity to understand the interplay of disorder, fluctuations and interactions in the emergence of complex phases of matter, free from the complications and microscopic details of real-world samples.

A particularly interesting objective is to discern the boundary separating quantum and classical SG. Numerous quantum many-body systems admit effective classical descriptions [6,7] even though their constituents have quantum behavior. This quantum-to-classical (QC) crossover is usually a result of the competition between decoherence, enhanced by the system-environment coupling or the temperature [8,9], and quantum fluctuations, which are stronger at lower dimensions and higher densities [10,11]. In spin systems, the size of spins (S) is another control parameter for the strength of quantum fluctuations [7,12–14]. From an experimental point of view, adjusting S is often a formidable task, primarily because it is intrinsic to the material being investigated. The cavity QED experiment reported in Refs. [15–18] provides an instance of a platform capable of quantum-simulating an SG (see in particular the note at the end of this work), with a high degree of control over parameters of the system, including the size of spins. The experiment consists of an ensemble of ultracold atomic clusters trapped by optical tweezers, coupled to each other via long-range frustrated interactions mediated by cavity photons [Fig. 1(a)]. This platform has been shown to be a simulator of associative memory and SG phases [19–28]. However, accessing the broad spectrum of dynamical responses in SG systems, and in particular this platform, would require to solve a frustrated dissipative quantum many-body system with retarded (photon-mediated) interactions. In general, there have been limited attempts thus far to solve for the time evolution of text-book models of SG and similar disordered systems [29–36].

II. OUTLINE OF RESULTS

In this work we make a significant stride in addressing far-from-equilibrium dynamics in quantum SGs and, in particular, those realized by frustrated light-matter interactions in cavity QED by providing a nonperturbative solution of their

*Contact author: hhossein@uni-mainz.de

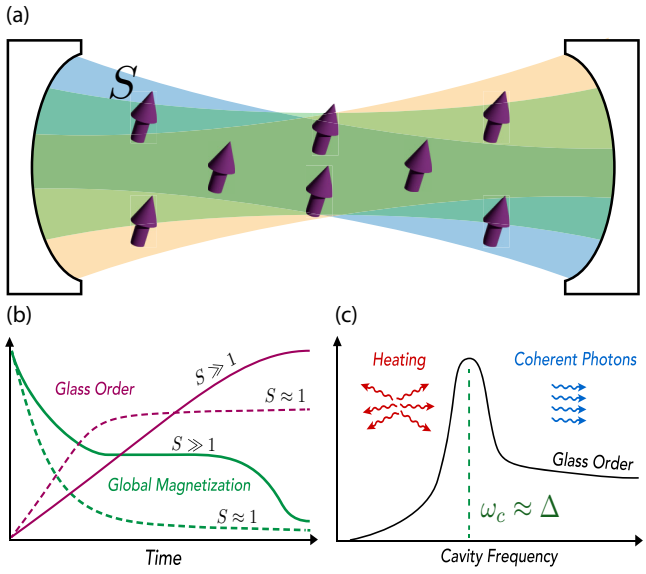

FIG. 1. (a) Schematics of the system considered in this work. Clusters of two-level atoms can be modeled as spins of size S. Coupling to a multiple cavity modes of different spatial profile results in frustrated long-range interactions among large spins, which can stabilize a spin-glass phase. (b) Generic behavior of the system after an interaction quench. SG order parameter grows much faster for small spins compared with large spins, but to a smaller value, due to stronger quantum fluctuations. (c) Resonantly enhanced SG order, as the frequency of interaction mediators (cavity photons) approaches the atomic splitting Δ.

long-time dynamics. We show that while SG order prevails for all spin sizes, it displays qualitatively different dynamical responses for different values of S [Fig. 1(b)]. For small S, which we label as quantum SG, we observe weak aging where the memory of the initial state is drastically blurred by quantum fluctuations, alongside with a quick growth of the SG order parameter to a finite but small value. For large S, the system displays stronger signatures of aging akin to classical spin glasses, with a slow growth of the SG order parameter. The QC crossover is quite sharp and the system fully classicalizes at spin sizes only few times larger than $\hbar$, the fundamental unit of angular momentum, with an exponential dependence of SG order parameter on S, demonstrating the fragility of quantum SG against decoherence. S can be controlled in cavity QED experiments by adjusting the atomic load of each cluster trapped by optical tweezers and, in principle, can be tuned down to the quantum limit $S = 1/2$ by activating Rydberg blockade within each cluster [27]. Moreover, we show that tuning the photon gap to resonance with the atomic splitting enhances SG order [Fig. 1(c)]. We note that this is a nontrivial result due to the trade-off between atom-atom interactions and incoherent generation of photons, both of which are enhanced close to the resonance [37–39]. While the former stabilizes SG, the latter leads to heating, which generally has a detrimental effect on ordered phases of matter. We show that below the resonance, heating dominates and SG order quickly approaches zero.

III. MODEL

Inspired by cavity QED experiments [15–18,28], we consider a system of N clusters, each one containing N_s two-level atoms, placed inside a multimode cavity with M nearly degenerate modes. Atoms are encoded by the Pauli operators $\sigma_{i\lambda}$, with cluster $1 \leqslant i \leqslant N$ and atom indices $1 \leqslant \lambda \leqslant N_s$. Taking $\hbar \equiv 1$ in this work, the evolution of the system is given by a quantum master equation $\partial_t \rho = -i[H, \rho] + \sum_{\alpha=1}^{M} \mathcal{D}[a_\alpha]\rho$ for a dissipative spin-boson model [22,23], where

$$H = \frac{\Delta}{2} \sum_{i,\lambda} \sigma^z_{i\lambda} + \omega_c \sum_{\alpha} a^\dagger_\alpha a_\alpha + \sum_{i,\lambda,\alpha} g_{\alpha i}(a_\alpha + a^\dagger_\alpha)\sigma^x_{i\lambda}, \quad (1)$$

and $\mathcal{D}[a_\alpha]\rho = \kappa(2a_\alpha \rho a^\dagger_\alpha - \{a^\dagger_\alpha a_\alpha, \rho\})$. The couplings between the atoms and the photon modes of the cavity are spatially dependent and uncorrelated from each other, which justifies their modeling via random couplings [22,23,36]. Accordingly, $g_{\alpha i}$ are assumed to be random and chosen from a Gaussian distribution with $\overline{g_{\alpha i}} = 0$ and $\overline{g_{\alpha i} g_{\beta j}} = \delta_{\alpha\beta}\delta_{ij} g^2/(N+M)N_s$. Couplings for spins in the same cluster are similar as we assume that the spatial size of each cluster is smaller than the wavelength of cavity modes. Starting from the same initial state for all spins, each cluster is equivalent to a single spin $2\hat{S}_i \equiv \sum_\lambda \hat{\sigma}_{i\lambda}$ with amplitude $S = N_s/2$. The parameter S can be tuned by loading few or many atoms in each cluster, and it dictates the strength of quantum fluctuations. For instance, at large S each cluster would be effectively described by a classical angular momentum, since its quantum noise would scale down as $1/S$ [25,27,40]. Integrating out photons leads to frustrated spin interactions [41–43], and Eq. (1) is mapped to the Hopfield model (HM) [19]. The HM has a PM ground state for sufficiently small g. For g larger than a critical value g_c, a phase transition occurs and the ground state crucially depends on the ratio $\eta \equiv M/N$ [20]. For $\eta < \eta_c \approx O(10^{-1})$, the system is in the memory retrieval phase [21,25,26], which is a FM in disguise [1] with multiple superradiant ground states. For $\eta > \eta_c$ [20], frustration dominates and turns the system into a spin glass [22,23,27,44] described by the Sherrington-Kirkpatrick model [45,46]. For a correct description of quench dynamics or in the limit of dynamically active photons $\omega_c \approx \Delta$, photons have to be retained as dynamical degrees of freedom and cannot be integrated out [41–43]. For this, we resort to nonequilibrium quantum field theory (NEQFT), covered comprehensively in an accompanying article [47].

IV. DYNAMICS OF SPIN-GLASS FORMATION

Throughout this work we take $N = M$, ensuring the existence of SG phase for sufficiently strong couplings [20,22]. The initial state is the vacuum state for photons and a uniform product state for spins specified by the vector $(\sin\theta_0, \cos\theta_0)$ in the xz plane. We let the system evolve after suddenly switching on the coupling at $t = 0$. For sufficiently weak couplings, the system is a PM and spins precess around the z axis and dephase due to disorder, similar to an underdamped oscillator. As the coupling is increased, the system undergoes a phase transition into an SG. The simplest manifestation of the transition is the overdamped relaxation of global magne-

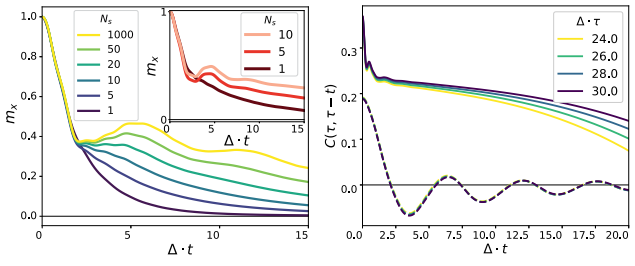

(a) (b)

FIG. 2. (a) Dependence of average magnetization m_x on spin size (N_s) for quenches into SG phase with $g/\Delta \approx 2.0$. Inset shows results of semiclassical (DTWA) calculations. (b) Spin correlation function at different waiting times after the quench for $N_s = 5$. For quenches to PM phase ($g/\Delta \approx 0.18$), correlations decay quickly with t and show weak sensitivity to the waiting time τ (dashed lines). For quenches to SG phase ($g/\Delta \approx 0.4$), correlations remain finite at long time separations and the system retains the memory of its past (solid lines). The other parameters are $\omega_c/\Delta = 5.0$ and $\kappa/\Delta = 0.5$.

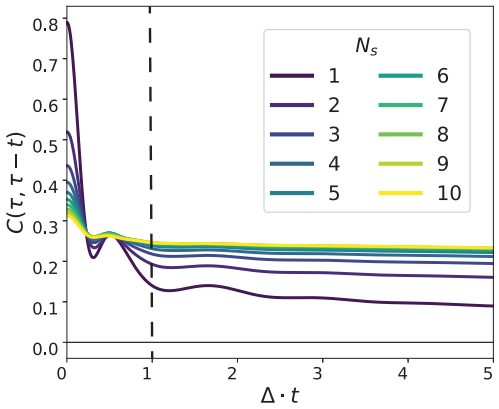

FIG. 3. Dependence of temporal correlations on spin size in SG phase. Short time correlations are stronger for small spins, due to the smaller size of local Hilbert space (cf. main text). Small spins are susceptible to quantum fluctuations and their correlations are sharply suppressed for $\Delta t \gtrsim 1$ (marked by dashed line), leading to a quantum SG with weak aging. Large spins are robust against quantum fluctuations and realize a classical SG with stronger aging. The waiting time is $\Delta\tau = 30$ together with $g/\Delta \approx 0.4$, $\omega_c/\Delta = 5.0$, and $\kappa/\Delta = 0.5$.

tization to zero: $m_x \equiv \overline{\langle \sigma_i^x \rangle}$ is shown in Fig. 2(a), displaying a crucial dependence on spin size. At early times, spin dynamics are insensitive to S, and m_x quickly collapses to a finite value. After this point, trajectories for different spin sizes start to depart, and relaxation becomes slow for larger spins. This behavior can be attributed to the inefficiency of quantum fluctuations to erase the memory of the initial state for larger spins where a few applications of the transverse field (ΔS^z) only changes the amplitude of m_x, in contrast with small spins which can be entirely flipped over similar timescales. The long-lasting, transient magnetic order for large N_s is reminiscent of prethermalization, where a system approaches true equilibrium over long times due to disorder or an extensive number of nearly conserved local quantities [48–51]. In the inset of Fig. 2(a) we have shown the results of a semiclassical treatment of the problem based on discrete truncated Wigner approximation (DTWA) [38,52], displaying qualitative agreement with NEQFT for large spins. However, DTWA predicts a slower relaxation for small S, possibly because as a semiclassical approach it ignores quantum fluctuations [53], which facilitate tunneling between local minima in the energy landscape of the SG.

The standard measure of SG order is the Edwards-Anderson [23,54] order parameter given by the $t \to \infty$ limit of the symmetric correlation function

$$C(\tau, \tau - t) \equiv \frac{1}{N_s^2} \overline{\langle \{ S_i^x(\tau), S_i^x(\tau - t) \} \rangle}. \tag{2}$$

The system is a SG, if alongside with $m_x = 0$, the quantity $q_{\mathrm{EA}}(\tau) \equiv \lim_{t\to\infty} C(\tau, \tau - t)$ is finite, which indicates a finite overlap between spin configurations at long time separations, a direct consequence of a frozen spin state. We quench the system from a PM state with $\theta_0 = \pi$ such that $m_x(0) = 0$. As shown in Fig. 2(b), C exhibits qualitatively different behaviors in PM and SG phases. In the former, the long-time correlations are weak and the system reaches equilibrium quickly, as indicated by the lack of sensitivity to the waiting time τ after the quench. On the other hand, correlations decay very weakly with t and show strong dependence on the waiting time for quenches into SG. Figure 2(b) hints at the onset of aging, which is a salient feature of glassy systems and an indirect signature of the breakdown of fluctuation-dissipation relations, or in other words of ergodicity [1,2]. In aging, the system strongly retains the memory of its past for infinitely long times after the quench. The inability to lose the memory of the initial state is a result of slow dynamics due to a rugged energy landscape generated by the disorder [55].

V. EFFECT OF SPIN SIZE ON SPIN-GLASS DYNAMICS

As previously discussed, the spin size $S = N_s/2$ is a crucial parameter which allows us to study the interplay of frustration and quantum fluctuations. We have already discussed the role of S on the dynamics of global magnetization as a proxy of glassy behavior. In this section, we directly address quantum effects in the evolution of SG order parameter and subsequently, characterize quantum and classical SGs based on their dynamical signatures in a unified framework. The correlation function C is shown in Fig. 3 for different spin sizes, with a different dependence at small and long time separations (t). Short time ($t \lesssim \Delta^{-1}$) correlations are stronger for small spins, while they quickly flatten as S grows. This behavior is easily explained by considering a generic local spin state $|\psi\rangle = \sum_M c_M |M, S\rangle$ with $S^x|M, S\rangle = M|M, S\rangle$. For $t \lesssim \Delta^{-1}$ we can approximate $C(t, t') \approx C(t, t)$ which yields $C(t, t) = \sum_M (M/S)^2 |c_M|^2$. In the SG phase, local magnetization is finite and $|c_M|^2$ has an asymmetrical distribution peaked around a finite value of M, leading to $C(t, t) \leqslant 1$ where equality is approached only in the extreme case of a fully polarized state, or when S is small. Particularly, for $S = 1/2$ we always have $C(t, t) = 1$, simply because the local Hilbert space is small. The slight deviation from the exact value for $S = 1/2$ in Fig. 3

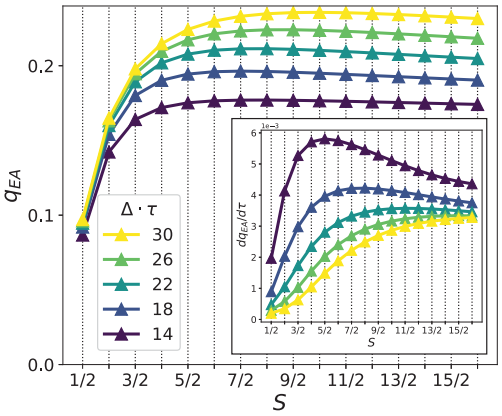

FIG. 4. Effect of spin size on SG order. $q_{\rm EA}$ is suppressed by quantum fluctuations for small spins. It shows a sharp QC crossover at $S \approx 2$ (in units of $\hbar$) where it becomes weakly sensitive to S and relaxes slowly to its final value. Inset shows rate of change of SG order parameter. Compared with classical SG, quantum SG relaxes more quickly at initial times. At later times, dynamics become slow for all spin sizes, but they are faster for large spins because $q_{\rm EA}$ should still grow to reach the steady state. The results are for $g/\Delta \approx 0.4$, $\omega_c/\Delta = 5.0$, and $\kappa/\Delta = 0.5$.

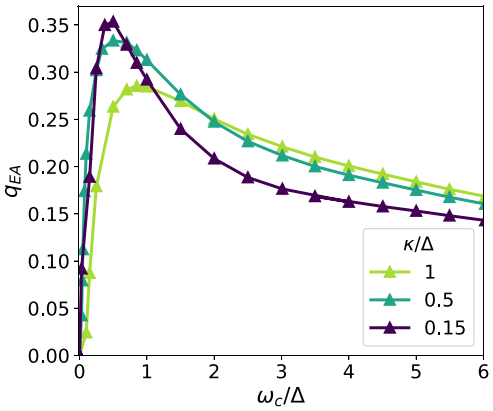

FIG. 5. Resonantly enhanced SG order. In the limit $\omega_c \gg \Delta$ photons are coherently driven and SG order is independent of ω_c. Near the resonance $\omega_c \approx \Delta$, SG order is amplified. For $\omega_c \lesssim \Delta$, photons are incoherently generated which leads to heating and weak SG. The resonance width scales with photon loss rate κ. The coupling is adjusted as ω_c is varied according to $g \approx 0.9[\Delta(\omega_c^2 + \kappa^2)/\omega_c]^{1/2}$. The waiting time and the spin size respectively are $\Delta\tau = 12.0$ and $S = 10$.

signals the validity of our approximation to capture quantum corrections to the dynamics. Long time correlations follow the opposite behavior; large spins are robust against quantum fluctuation and their correlation is weakly affected for $t \gtrsim \Delta^{-1}$. For $S \approx 1$, correlations decay sharply at $t \approx \Delta^{-1}$ which is the timescale of a single spin flip by the magnetic field (marked by the dashed line in Fig. 3). Moreover, we see that long time correlations are drastically weaker for small S compared with large S. Accordingly, the separation of short and long timescales for $S \approx 1$ and the lack of it for $S \gg 1$ motivate us to respectively label these as quantum and classical SG. This distinction is further supported by the dependence of SG order parameter $q_{\rm EA}$ on S at different waiting times after the quench (Fig. 4). $q_{\rm EA}$ grows quickly with S as the quantum noise is suppressed, and almost saturates for $S \gtrsim 2$, suggesting the system is already a classical SG (corresponding to $S \to \infty$). The growth of $q_{\rm EA}$ versus S empirically admits an exponential fit of the form $q_{\rm EA} = q_c - r_q\, e^{-AS}$, where q_c is the classical value and r_q is the amplitude of quantum corrections which are exponentially suppressed in S. The quantities q_c, r_q, and A depend on other parameters including the waiting time τ. The exponential behavior holds up to larger values of S as τ is increased (Fig. 4), because the order parameter growth is initially slower at larger S and becomes faster later (inset of Fig. 4). The quick approach of $q_{\rm EA}$ to its steady state value for quantum SG in contrast with its slow growth for classical SG is another dynamical signature of the two regimes. A classical SG is glassier with a larger order parameter, stronger frustration and hence, slower dynamics.

VI. ROLE OF PHOTONS

We now shortly discuss the effect of photons on the SG phase, as we change their frequency ω_c. In the adiabatic limit ($\omega_c \gg \Delta$), the critical coupling depends on ω_c through $g_c \sim [(\omega_c^2 + \kappa^2)/\omega_c]^{1/2}$ [22]. Accordingly, we scale g with ω_c similarly to g_c. In this way, when we compare physics at different values of ω_c, the distance from the critical point remains fixed which enables us to isolate the effect of dynamically active photons (retardation effects). The dependence of SG order parameter on ω_c is shown in Fig. 5. For $\omega_c/\Delta \gg 1$, $q_{\rm EA}$ approaches a constant value, consistent with the adopted scaling of g. As ω_c is reduced, SG order gets enhanced until it reaches a maximum around $\omega_c \approx \Delta$ with a width that increases with photon loss κ. Reducing ω_c further causes $q_{\rm EA}$ to vanish quickly over a small energy window. The peak in $q_{\rm EA}$ is the outcome of an intricate competition between two elements. First, the strength of photon-mediated interactions, which is resonantly enhanced as $\omega_c \to \Delta$. Second, the generation of incoherent photons by atoms which is limited by energy conservation, and is amplified when the energy scales of atomic and cavity excitations are close. Incoherent photons lead to heating, which subsequently weakens the SG order. The energy for heating is provided by the laser drive responsible for the emergence of the Dicke coupling in Eq. (1), after adiabatically eliminating virtual transitions to high-energy intermediate states [26,27,56]. We see that the resonant enhancement dominates dissipation at $\omega_c \approx \Delta$, while as we reduce ω_c below the resonance, heating takes over and melts the SG. Energy conservation for incoherent photon generation has to be satisfied over a narrower energy window as cavity losses decrease, leading to a sharper resonance peak in Fig. 5. The location of the resonance peak does not exactly match $\omega_c = \Delta$ due to the renormalization and broadening of atomic and cavity energy levels by interactions. A similar resonance mechanism has been proposed recently [39] to enhance superconductivity out of equilibrium, without controlling for heating. Our findings suggest the enhancement is robust with respect to heating effects.

VII. METHOD

To derive the results of this work, we used the Keldysh field theory [57,58] extended to open quantum systems [59]. Using a fermionic representation for spins [60,61] and employing a conserving approximation based on a quantum effective action (QEA) [50,62–71] for the system, we dynamically monitored the onset of SG in the thermodynamic limit. We expanded QEA in powers of $1/N_s$, corresponding to successive atom-photon scattering processes [47].

VIII. PERSPECTIVES

The distinction between quantum and classical SG dynamics addressed in this work holds beyond cavity QED platforms and encompass SG systems whose constituent degrees of freedom are the generators of the SU(2) group [1]. These include the canonical cases of infinite range quantum Ising and Heisenberg SG models, as well as the quantum p-spin model [1,2]. Furthermore, the dynamics of Eq. (1) directly maps to the Sherrington-Kirkpatrick model at large photon frequencies [22]. On the other hand, the physics of frustrated systems with finite range interactions is more intricate and the interplay of quantum fluctuations, dimensionality and symmetries can change the behavior of QC crossover. For instance, in short range and low-dimensional systems of small spins, quantum fluctuations may destabilize SG order towards a quantum spin liquid phase [72–74]. This would represent a natural follow-up direction of our work.

Furthermore, the QC crossover explored here should also manifest in the aging dynamics of quenches close to the FM or AFM critical points of quantum spin systems, without disorder [75–78]. Finally, our findings concerning the resonant enhancement of SG order appear promising for systems in which a collective mode generates an effective interaction. The interaction can then be activated or amplified via an external drive to realize novel phases of matter without equilibrium counterparts such as those facilitated by driven excitons in doped moiré systems [79] or driven phonons in photo-enhanced superconductors [37,39,80]. Our work suggests that the resonance condition should also be able to stabilize these emergent nonequilibrium phases [39,81].

ACKNOWLEDGMENTS

We thank F. Balducci, J. Keeling, and R. J. Valencia-Tortora for useful discussions, and D. Gribben for early contributions to this line of research. H.H. and J.M. acknowledge financial support by the Deutsche Forschungsgemeinschaft (DFG, German Research Foundation) through Project-ID 429529648, TRR 306 QuCoLiMa ("Quantum Cooperativity of Light and Matter"), and through TRR 288 - 422213477 (project B09). This project has been supported by the QuantERA II Programme that has received funding from the European Union's Horizon 2020 research and innovation programme under Grant Agreement No 101017733 ("QuSiED") and by the DFG (Project No. 499037529). D.E.C. acknowledges support from the European Union, under European Research Council Grant Agreement No. 101002107 (NEWSPIN); the Government of Spain under the Severo Ochoa Grant CEX2019-000910-S [MCIN/AEI/10.13039/501100011033]); QuantERA II project QuSiED, cofunded by the European Union Horizon 2020 research and innovation programme (No. 101017733) and the Government of Spain (European Union NextGenerationEU/PRTR PCI2022-132945 funded by MCIN/AEI/10.13039/501100011033); Generalitat de Catalunya (CERCA program and AGAUR Project No. 2021 SGR 01442); Fundació Cellex, and Fundació Mir-Puig.

[1] K. Binder and A. P. Young, Spin glasses: Experimental facts, theoretical concepts, and open questions, Rev. Mod. Phys. **58**, 801 (1986).

[2] M. Mézard, G. Parisi, and M. A. Virasoro, *Spin Glass Theory and Beyond: An Introduction to the Replica Method and Its Applications* (World Scientific Publishing Company, 1987), Vol. 9.

[3] D. L. Stein and C. M. Newman, *Spin Glasses and Complexity* (Princeton University Press, 2013), Vol. 4.

[4] E. Altman, K. R. Brown, G. Carleo, L. D. Carr, E. Demler, C. Chin, B. DeMarco, S. E. Economou, M. A. Eriksson, K.-M. C. Fu, M. Greiner, K. R. Hazzard, R. G. Hulet, A. J. Kollár, B. L. Lev, M. D. Lukin, R. Ma, X. Mi, S. Misra, C. Monroe *et al.*, Quantum simulators: Architectures and opportunities, PRX Quantum **2**, 017003 (2021).

[5] C. Gross and I. Bloch, Quantum simulations with ultracold atoms in optical lattices, Science **357**, 995 (2017).

[6] D. S. Golubev and A. D. Zaikin, Quantum decoherence in disordered mesoscopic systems, Phys. Rev. Lett. **81**, 1074 (1998).

[7] A. Altland and B. D. Simons, *Condensed Matter Field Theory* (Cambridge University Press, 2010).

[8] M. Arndt, A. Buchleitner, R. N. Mantegna, and H. Walther, Experimental study of quantum and classical limits in microwave ionization of rubidium Rydberg atoms, Phys. Rev. Lett. **67**, 2435 (1991).

[9] W. H. Zurek, Decoherence, einselection, and the quantum origins of the classical, Rev. Mod. Phys. **75**, 715 (2003).

[10] A. J. Leggett, *Quantum Liquids: Bose Condensation and Cooper Pairing in Condensed-Matter Systems* (Oxford University Press, 2006).

[11] Y.-S. Ra, M. C. Tichy, H.-T. Lim, O. Kwon, F. Mintert, A. Buchleitner, and Y.-H. Kim, Nonmonotonic quantum-to-classical transition in multiparticle interference, Proc. Natl. Acad. Sci. USA **110**, 1227 (2013).

[12] A. Chubukov and D. Golosov, Quantum theory of an antiferromagnet on a triangular lattice in a magnetic field, J. Phys.: Condens. Matter **3**, 69 (1991).

[13] T. Coletta, T. A. Tóth, K. Penc, and F. Mila, Semiclassical theory of the magnetization process of the triangular lattice Heisenberg model, Phys. Rev. B **94**, 075136 (2016).

[14] D. Yamamoto, T. Sakurai, R. Okuto, S. Okubo, H. Ohta, H. Tanaka, and Y. Uwatoko, Continuous control of classical-quantum crossover by external high pressure in the

coupled chain compound $CsCuCl_3$, Nat. Commun. **12**, 4263 (2021).
[15] V. D. Vaidya, Y. Guo, R. M. Kroeze, K. E. Ballantine, A. J. Kollár, J. Keeling, and B. L. Lev, Tunable-range, photon-mediated atomic interactions in multimode cavity QED, Phys. Rev. X **8**, 011002 (2018).
[16] R. M. Kroeze, B. P. Marsh, K.-Y. Lin, J. Keeling, and B. L. Lev, High cooperativity using a confocal-cavity–QED microscope, PRX Quantum **4**, 020326 (2023).
[17] A. J. Kollár, A. T. Papageorge, K. Baumann, M. A. Armen, and B. L. Lev, An adjustable-length cavity and Bose–Einstein condensate apparatus for multimode cavity QED, New J. Phys. **17**, 043012 (2015).
[18] Y. Guo, R. M. Kroeze, V. D. Vaidya, J. Keeling, and B. L. Lev, Sign-changing photon-mediated atom interactions in multimode cavity quantum electrodynamics, Phys. Rev. Lett. **122**, 193601 (2019).
[19] J. J. Hopfield, Neural networks and physical systems with emergent collective computational abilities, Proc. Natl. Acad. Sci. USA **79**, 2554 (1982).
[20] D. J. Amit, H. Gutfreund, and H. Sompolinsky, Storing infinite numbers of patterns in a spin-glass model of neural networks, Phys. Rev. Lett. **55**, 1530 (1985).
[21] S. Gopalakrishnan, B. L. Lev, and P. M. Goldbart, Frustration and glassiness in spin models with cavity-mediated interactions, Phys. Rev. Lett. **107**, 277201 (2011).
[22] P. Strack and S. Sachdev, Dicke quantum spin glass of atoms and photons, Phys. Rev. Lett. **107**, 277202 (2011).
[23] M. Buchhold, P. Strack, S. Sachdev, and S. Diehl, Dicke-model quantum spin and photon glass in optical cavities: Nonequilibrium theory and experimental signatures, Phys. Rev. A **87**, 063622 (2013).
[24] P. Rotondo, M. C. Lagomarsino, and G. Viola, Dicke simulators with emergent collective quantum computational abilities, Phys. Rev. Lett. **114**, 143601 (2015).
[25] E. Fiorelli, M. Marcuzzi, P. Rotondo, F. Carollo, and I. Lesanovsky, Signatures of associative memory behavior in a multimode Dicke model, Phys. Rev. Lett. **125**, 070604 (2020).
[26] B. P. Marsh, Y. Guo, R. M. Kroeze, S. Gopalakrishnan, S. Ganguli, J. Keeling, and B. L. Lev, Enhancing associative memory recall and storage capacity using confocal cavity QED, Phys. Rev. X **11**, 021048 (2021).
[27] B. P. Marsh, R. M. Kroeze, S. Ganguli, S. Gopalakrishnan, J. Keeling, and B. L. Lev, Entanglement and replica symmetry breaking in a driven-dissipative quantum spin glass, Phys. Rev. X **14**, 011026 (2024).
[28] R. M. Kroeze, B. P. Marsh, D. A. Schuller, H. S. Hunt, S. Gopalakrishnan, J. Keeling, and B. L. Lev, Replica symmetry breaking in a quantum-optical vector spin glass, arXiv:2311.04216.
[29] L. F. Cugliandolo and G. Lozano, Real-time nonequilibrium dynamics of quantum glassy systems, Phys. Rev. B **59**, 915 (1999).
[30] M. P. Kennett, C. Chamon, and J. Ye, Aging dynamics of quantum spin glasses of rotors, Phys. Rev. B **64**, 224408 (2001).
[31] G. Biroli and O. Parcollet, Out-of-equilibrium dynamics of a quantum Heisenberg spin glass, Phys. Rev. B **65**, 094414 (2002).
[32] L. Rademaker and D. A. Abanin, Slow nonthermalizing dynamics in a quantum spin glass, Phys. Rev. Lett. **125**, 260405 (2020).
[33] S. J. Thomson, P. Urbani, and M. Schiró, Quantum quenches in isolated quantum glasses out of equilibrium, Phys. Rev. Lett. **125**, 120602 (2020).
[34] S. Pappalardi, A. Polkovnikov, and A. Silva, Quantum echo dynamics in the Sherrington-Kirkpatrick model, SciPost Phys. **9**, 021 (2020).
[35] S. Bera, K. Y. V. Lokesh, and S. Banerjee, Quantum-to-classical crossover in many-body chaos and scrambling from relaxation in a glass, Phys. Rev. Lett. **128**, 115302 (2022).
[36] A. Wierzchucka, F. Piazza, and P. W. Claeys, Integrability, multifractality, and two-photon dynamics in disordered Tavis-Cummings models, Phys. Rev. A **109**, 033716 (2024).
[37] M. Babadi, M. Knap, I. Martin, G. Refael, and E. Demler, Theory of parametrically amplified electron-phonon superconductivity, Phys. Rev. B **96**, 014512 (2017).
[38] S. P. Kelly, A. M. Rey, and J. Marino, Effect of active photons on dynamical frustration in cavity QED, Phys. Rev. Lett. **126**, 133603 (2021).
[39] C. J. Eckhardt, S. Chattopadhyay, D. M. Kennes, E. A. Demler, M. A. Sentef, and M. H. Michael, Theory of resonantly enhanced photo-induced superconductivity, Nat. Commun. **15**, 2300 (2024).
[40] P. Kirton, M. M. Roses, J. Keeling, and E. G. Dalla Torre, Introduction to the Dicke model: From equilibrium to nonequilibrium, and vice versa, Adv. Quantum Technol. **2**, 1800043 (2019).
[41] F. Damanet, A. J. Daley, and J. Keeling, Atom-only descriptions of the driven-dissipative Dicke model, Phys. Rev. A **99**, 033845 (2019).
[42] R. Palacino and J. Keeling, Atom-only theories for U(1) symmetric cavity-QED models, Phys. Rev. Res. **3**, L032016 (2021).
[43] S. B. Jäger, T. Schmit, G. Morigi, M. J. Holland, and R. Betzholz, Lindblad master equations for quantum systems coupled to dissipative bosonic modes, Phys. Rev. Lett. **129**, 063601 (2022).
[44] P. Rotondo, E. Tesio, and S. Caracciolo, Replica symmetry breaking in cold atoms and spin glasses, Phys. Rev. B **91**, 014415 (2015).
[45] D. Sherrington and S. Kirkpatrick, Solvable model of a spin-glass, Phys. Rev. Lett. **35**, 1792 (1975).
[46] P. Ray, B. K. Chakrabarti, and A. Chakrabarti, Sherrington-Kirkpatrick model in a transverse field: Absence of replica symmetry breaking due to quantum fluctuations, Phys. Rev. B **39**, 11828 (1989).
[47] H. Hosseinabadi, D. E. Chang, and J. Marino, following paper, Far from equilibrium field theory for strongly coupled light and matter: Dynamics of frustrated multimode cavity QED, Phys. Rev. Res. **6**, 043314 (2024).
[48] J. Berges, S. Borsányi, and C. Wetterich, Prethermalization, Phys. Rev. Lett. **93**, 142002 (2004).
[49] B. Bertini, F. H. L. Essler, S. Groha, and N. J. Robinson, Prethermalization and thermalization in models with weak integrability breaking, Phys. Rev. Lett. **115**, 180601 (2015).
[50] M. Babadi, E. Demler, and M. Knap, Far-from-equilibrium field theory of many-body quantum spin systems: Prethermalization and relaxation of spin spiral states in three dimensions, Phys. Rev. X **5**, 041005 (2015).

[51] J. Marino, M. Eckstein, M. S. Foster, and A. M. Rey, Dynamical phase transitions in the collisionless pre-thermal states of isolated quantum systems: theory and experiments, Rep. Prog. Phys. **85**, 116001 (2022).
[52] J. Schachenmayer, A. Pikovski, and A. M. Rey, Many-body quantum spin dynamics with Monte Carlo trajectories on a discrete phase space, Phys. Rev. X **5**, 011022 (2015).
[53] A. Polkovnikov, Phase space representation of quantum dynamics, Ann. Phys. (NY) **325**, 1790 (2010).
[54] S. F. Edwards and P. W. Anderson, Theory of spin glasses, J. Phys. F: Met. Phys. **5**, 965 (1975).
[55] L. F. Cugliandolo and J. Kurchan, On the out-of-equilibrium relaxation of the Sherrington-Kirkpatrick model, J. Phys. A: Math. Gen. **27**, 5749 (1994).
[56] F. Mivehvar, F. Piazza, T. Donner, and H. Ritsch, Cavity QED with quantum gases: New paradigms in many-body physics, Adv. Phys. **70**, 1 (2021).
[57] A. Kamenev, *Field Theory of Non-Equilibrium Systems* (Cambridge University Press, 2011).
[58] J. Rammer, *Quantum Field Theory of Non-Equilibrium States* (Cambridge University Press, 2007).
[59] L. M. Sieberer, M. Buchhold, and S. Diehl, Keldysh field theory for driven open quantum systems, Rep. Prog. Phys. **79**, 096001 (2016).
[60] A. Shnirman and Y. Makhlin, Spin-spin correlators in the Majorana representation, Phys. Rev. Lett. **91**, 207204 (2003).
[61] W. Mao, P. Coleman, C. Hooley, and D. Langreth, Spin dynamics from Majorana fermions, Phys. Rev. Lett. **91**, 207203 (2003).
[62] J. M. Cornwall, R. Jackiw, and E. Tomboulis, Effective action for composite operators, Phys. Rev. D **10**, 2428 (1974).
[63] J. Berges, Controlled nonperturbative dynamics of quantum fields out of equilibrium, Nucl. Phys. A **699**, 847 (2002).
[64] J. Berges, Introduction to nonequilibrium quantum field theory, AIP Conf. Proc. **739**, 3 (2004).
[65] E. A. Calzetta and B.-L. B. Hu, *Nonequilibrium Quantum Field Theory* (Cambridge University Press, 2009).
[66] A. Eberlein, V. Kasper, S. Sachdev, and J. Steinberg, Quantum quench of the Sachdev-Ye-Kitaev model, Phys. Rev. B **96**, 205123 (2017).
[67] A. Haldar, P. Haldar, S. Bera, I. Mandal, and S. Banerjee, Quench, thermalization, and residual entropy across a non-Fermi liquid to Fermi liquid transition, Phys. Rev. Res. **2**, 013307 (2020).
[68] H. Hosseinabadi, S. P. Kelly, J. Schmalian, and J. Marino, Thermalization of non-fermi-liquid electron-phonon systems: Hydrodynamic relaxation of the Yukawa-Sachdev-Ye-Kitaev model, Phys. Rev. B **108**, 104319 (2023).
[69] J. Lang, M. Buchhold, and S. Diehl, Field theory for the dynamics of the open $O(N)$ model, Phys. Rev. B **109**, 064310 (2024).
[70] T. Bode, M. Kajan, F. Meirinhos, and J. Kroha, Non-Markovian dynamics of open quantum systems via auxiliary particles with exact operator constraint, Phys. Rev. Res. **6**, 013220 (2024).
[71] M. Gopalakrishna, Y. Pavlyukh, and C. Verdozzi, Time resolved optical response of the Dicke's model via the nonequilibrium Green's function approach, arXiv:2312.13874.
[72] L. Balents, Spin liquids in frustrated magnets, Nature (London) **464**, 199 (2010).
[73] L. Savary and L. Balents, Quantum spin liquids: A review, Rep. Prog. Phys. **80**, 016502 (2017).
[74] Y. Zhou, K. Kanoda, and T.-K. Ng, Quantum spin liquid states, Rev. Mod. Phys. **89**, 025003 (2017).
[75] P. Calabrese and A. Gambassi, Ageing properties of critical systems, J. Phys. A: Math. Gen. **38**, R133 (2005).
[76] P. Gagel, P. P. Orth, and J. Schmalian, Universal postquench prethermalization at a quantum critical point, Phys. Rev. Lett. **113**, 220401 (2014).
[77] P. Gagel, P. P. Orth, and J. Schmalian, Universal postquench coarsening and aging at a quantum critical point, Phys. Rev. B **92**, 115121 (2015).
[78] A. Chiocchetta, A. Gambassi, S. Diehl, and J. Marino, Dynamical crossovers in prethermal critical states, Phys. Rev. Lett. **118**, 135701 (2017).
[79] H. Yang and Y.-H. Zhang, Exciton and light induced ferromagnetism from doping a moiré Mott insulator, Phys. Rev. B **110**, L041115 (2024).
[80] M. Knap, M. Babadi, G. Refael, I. Martin, and E. Demler, Dynamical cooper pairing in nonequilibrium electron-phonon systems, Phys. Rev. B **94**, 214504 (2016).
[81] S. P. Kelly, J. K. Thompson, A. M. Rey, and J. Marino, Resonant light enhances phase coherence in a cavity QED simulator of fermionic superfluidity, Phys. Rev. Res. **4**, L042032 (2022).

Chapter 4

Conclusion and Outlook

In this thesis, we investigated the non-equilibrium dynamics of two strongly disordered quantum many-body models, the Yukawa-SYK and random Dicke model, coupled to external environments. Using the Keldysh formalism of field theory, we derived a closed set of dynamical equations whose numerical solutions provided the time evolution of both field expectation values and two-point correlation functions. By analyzing the statistical and spectral components of these correlation functions and their mutual relations, we traced the evolution of excitation spectra and populations, and identified the conditions under which the systems reach stationary states following quenches, as well as whether these states are thermal or not.

For the Yukawa–SYK model, we found that intrinsic relaxation of physical observables occurs on very short timescales, while the overall thermalization process is governed by the efficiency of energy exchange with the external bath. This efficiency, in turn, is strongly influenced by the model's critical properties. In contrast, the random Dicke model exhibited markedly different behavior. In the strong-coupling regime, relaxation was slow for both expectation values and correlation functions, where the latter showed clear aging, a hallmark of glassy dynamics. We further explored how different parameters impact the spin glass phase, highlighting the role of spin size in controlling quantum fluctuations, the influence of cavity losses, and the dynamics in the slow-cavity regime, where photons actively participate beyond merely mediating effective spin–spin interactions.

The work presented in this thesis can be extended in several directions. One possibility is to study dynamics in finite-dimensional extensions of the SYK and Yukawa–SYK models [83] using the same field-theoretic approach, but applied to different lattice geometries. Such geometries can produce distinct fermionic dispersions and, consequently, different non-equilibrium relaxation profiles. Another natural direction is to investigate spin glasses in finite dimensions, beyond the all-to-all interaction limit. This is a theoretically challenging problem, since most available analytical results rely on mean-field theory. Phenomenological approaches based on the Ginzburg–Landau description of replica correlation functions [94, 103] exist. However, spin glasses with short-range interactions

typically have a very large upper critical dimension. For instance, renormalization group analysis for Ising spins [94] yields $d_{\mathrm{uc}} = 8$, with the model flowing to strong coupling and lacking perturbatively accessible fixed points. In such cases, one could explore large-S expansions, similar to the method employed in this work, as a viable route for analytical progress.

Quantum simulators, such as CQED platforms and Rydberg systems, are now capable of studying systems with engineered disorder. For spin glasses, experiments have already realized the glass phase [49, 51]. There are also proposals for simulating the SYK model using CQED [69, 70]. Extending these proposals to the Yukawa–SYK model appears feasible, with the role of phonons played by a subset of cavity modes. Along this line, one could also probe the emergence of the strange metal phase in CQED systems. Another promising route is to use the platform introduced in Ref. [71] to engineer frustrated exchange interactions, enabling the simulation of quantum XY spin glasses. An additional interesting direction is the simulation of metallic glasses in optical cavities, as proposed in Ref. [104]. Such systems are predicted to exhibit distinct universal properties compared to insulating glassy systems [103, 105].

Quantum simulators of spin glasses may also open new opportunities for computation theory. Determining the optimal spin configuration for a given disorder realization becomes a challenging task as the system size increases. The conventional approach of classical annealing, physically equivalent to cooling the system towards its optimal state, has only limited success in solving such global optimization problems. In quantum spin glasses, one can perform quantum annealing, which exploits quantum fluctuations and tunneling between multiple energy minima, and is expected to yield faster optimization in certain cases [106], representing a concrete instance of quantum advantage. An advantage of quantum simulators of spin glasses lies in their computational universality: many hard combinatorial optimization problems can be mapped onto finding the ground state of a suitably engineered spin-glass Hamiltonian [107].

Bibliography

[1] Anatoli Polkovnikov, Krishnendu Sengupta, Alessandro Silva, and Mukund Vengalattore. Colloquium: Nonequilibrium dynamics of closed interacting quantum systems. *Rev. Mod. Phys.*, 83:863–883, Aug 2011.

[2] Jamir Marino, Martin Eckstein, Matthew S Foster, and Ana Maria Rey. Dynamical phase transitions in the collisionless pre-thermal states of isolated quantum systems: theory and experiments. *Reports on Progress in Physics*, 85(11):116001, 2022.

[3] Julian Schwinger. Brownian motion of a quantum oscillator. *Journal of Mathematical Physics*, 2(3):407–432, 1961.

[4] Leonid Veniaminovich Keldysh. Diagram technique for nonequilibrium processes. *Zh. Eksp. Teor. Fiz*, 47(4):151–165, 1964.

[5] Leo P Kadanoff. *Quantum statistical mechanics*. CRC Press, 2018.

[6] Eytan Barouch and Barry M McCoy. Statistical mechanics of the x y model. ii. spin-correlation functions. *Physical Review A*, 3(2):786, 1971.

[7] Josh M Deutsch. Quantum statistical mechanics in a closed system. *Physical review a*, 43(4):2046, 1991.

[8] Mark Srednicki. Chaos and quantum thermalization. *Physical review e*, 50(2):888, 1994.

[9] Guifré Vidal. Efficient classical simulation of slightly entangled quantum computations. *Physical review letters*, 91(14):147902, 2003.

[10] Guifré Vidal. Efficient simulation of one-dimensional quantum many-body systems. *Physical review letters*, 93(4):040502, 2004.

[11] Román Orús. Tensor networks for complex quantum systems. *Nature Reviews Physics*, 1(9):538–550, 2019.

[12] Mari Carmen Bañuls. Tensor network algorithms: A route map. *Annual Review of Condensed Matter Physics*, 14(1):173–191, 2023.

[13] Andreas M Läuchli and Corinna Kollath. Spreading of correlations and entanglement after a quench in the one-dimensionalbose–hubbard model. *Journal of Statistical Mechanics: Theory and Experiment*, 2008(05):P05018, 2008.

[14] C Kollath, U Schollwöck, and W Zwerger. Spin-charge separation in cold fermi gases: A real time analysis. *Physical review letters*, 95(17):176401, 2005.

[15] Salvatore R Manmana, Stefan Wessel, Reinhard M Noack, and Alejandro Muramatsu. Strongly correlated fermions after a quantum quench. *Physical review letters*, 98(21):210405, 2007.

[16] Steven R White and Adrian E Feiguin. Real-time evolution using the density matrix renormalization group. *Physical review letters*, 93(7):076401, 2004.

[17] S. Hofferberth, I. Lesanovsky, B. Fischer, T. Schumm, and J. Schmiedmayer. Non-equilibrium coherence dynamics in one-dimensional bose gases. *Nature*, 449(7160):324–327, 2007.

[18] Yean-an Liao, Ann Sophie C Rittner, Tobias Paprotta, Wenhui Li, Guthrie B Partridge, Randall G Hulet, Stefan K Baur, and Erich J Mueller. Spin-imbalance in a one-dimensional fermi gas. *Nature*, 467(7315):567–569, 2010.

[19] M. Gring, M. Kuhnert, T. Langen, T. Kitagawa, B. Rauer, M. Schreitl, I. Mazets, D. Adu Smith, E. Demler, and J. Schmiedmayer. Relaxation and prethermalization in an isolated quantum system. *Science*, 337(6100):1318–1322, 2012.

[20] Tim Langen, Remi Geiger, and Jörg Schmiedmayer. Ultracold atoms out of equilibrium. *Annu. Rev. Condens. Matter Phys.*, 6(1):201–217, 2015.

[21] K. Kim, M. S. Chang, S. Korenblit, R. Islam, E. E. Edwards, J. K. Freericks, G. D. Lin, L. M. Duan, and C. Monroe. Quantum simulation of frustrated ising spins with trapped ions. *Nature*, 465(7298):590–593, 2010.

[22] C. Monroe, W. C. Campbell, L.-M. Duan, Z.-X. Gong, A. V. Gorshkov, P. W. Hess, R. Islam, K. Kim, N. M. Linke, G. Pagano, P. Richerme, C. Senko, and N. Y. Yao. Programmable quantum simulations of spin systems with trapped ions. *Rev. Mod. Phys.*, 93:025001, Apr 2021.

[23] Morten Kjaergaard, Mollie E Schwartz, Jochen Braumüller, Philip Krantz, Joel I-J Wang, Simon Gustavsson, and William D Oliver. Superconducting qubits: Current state of play. *Annual Review of Condensed Matter Physics*, 11(1):369–395, 2020.

[24] Alexandre Blais, Arne L Grimsmo, Steven M Girvin, and Andreas Wallraff. Circuit quantum electrodynamics. *Reviews of Modern Physics*, 93(2):025005, 2021.

[25] Herbert Walther, Benjamin TH Varcoe, Berthold-Georg Englert, and Thomas Becker. Cavity quantum electrodynamics. *Reports on Progress in Physics*, 69(5):1325, 2006.

[26] Farokh Mivehvar, Francesco Piazza, Tobias Donner, and Helmut Ritsch. Cavity qed with quantum gases: New paradigms in many-body physics. *Advances in Physics*, 70(1):1–153, 2021.

[27] Immanuel Bloch, Jean Dalibard, and Wilhelm Zwerger. Many-body physics with ultracold gases. *Reviews of modern physics*, 80(3):885–964, 2008.

[28] Christian Gross and Immanuel Bloch. Quantum simulations with ultracold atoms in optical lattices. *Science*, 357(6355):995–1001, 2017.

[29] Kristian Baumann, Christine Guerlin, Ferdinand Brennecke, and Tilman Esslinger. Dicke quantum phase transition with a superfluid gas in an optical cavity. *nature*, 464(7293):1301–1306, 2010.

[30] Helmut Ritsch, Peter Domokos, Ferdinand Brennecke, and Tilman Esslinger. Cold atoms in cavity-generated dynamical optical potentials. *Reviews of Modern Physics*, 85(2):553–601, 2013.

[31] Francesco Ferri, Rodrigo Rosa-Medina, Fabian Finger, Nishant Dogra, Matteo Soriente, Oded Zilberberg, Tobias Donner, and Tilman Esslinger. Emerging dissipative phases in a superradiant quantum gas with tunable decay. *Physical Review X*, 11(4):041046, 2021.

[32] Philip W Anderson. Absence of diffusion in certain random lattices. *Physical review*, 109(5):1492, 1958.

[33] Elihu Abrahams, Philip W Anderson, Donald C Licciardello, and Tiruppattur V Ramakrishnan. Scaling theory of localization: Absence of quantum diffusion in two dimensions. *Physical Review Letters*, 42(10):673, 1979.

[34] Patrick A Lee and Tiruppattur V Ramakrishnan. Disordered electronic systems. *Reviews of modern physics*, 57(2):287, 1985.

[35] Ferdinand Evers and Alexander D Mirlin. Anderson transitions. *Reviews of Modern Physics*, 80(4):1355–1417, 2008.

[36] Sajeev John. Strong localization of photons in certain disordered dielectric superlattices. *Physical review letters*, 58(23):2486, 1987.

[37] Giacomo Roati, Chiara D'Errico, Leonardo Fallani, Marco Fattori, Chiara Fort, Matteo Zaccanti, Giovanni Modugno, Michele Modugno, and Massimo Inguscio. Anderson localization of a non-interacting bose–einstein condensate. *Nature*, 453(7197):895–898, 2008.

[38] Rahul Nandkishore and David A Huse. Many-body localization and thermalization in quantum statistical mechanics. *Annu. Rev. Condens. Matter Phys.*, 6(1):15–38, 2015.

[39] Dmitry A Abanin, Ehud Altman, Immanuel Bloch, and Maksym Serbyn. Colloquium: Many-body localization, thermalization, and entanglement. *Reviews of Modern Physics*, 91(2):021001, 2019.

[40] Michael Schreiber, Sean S Hodgman, Pranjal Bordia, Henrik P Lüschen, Mark H Fischer, Ronen Vosk, Ehud Altman, Ulrich Schneider, and Immanuel Bloch. Observation of many-body localization of interacting fermions in a quasirandom optical lattice. *Science*, 349(6250):842–845, 2015.

[41] Jacob Smith, Aaron Lee, Philip Richerme, Brian Neyenhuis, Paul W Hess, Philipp Hauke, Markus Heyl, David A Huse, and Christopher Monroe. Many-body localization in a quantum simulator with programmable random disorder. *Nature Physics*, 12(10):907–911, 2016.

[42] Kurt Binder and A Peter Young. Spin glasses: Experimental facts, theoretical concepts, and open questions. *Reviews of Modern physics*, 58(4):801, 1986.

[43] Konrad H Fischer and John A Hertz. *Spin glasses*. Number 1. Cambridge university press, 1993.

[44] Samuel Frederick Edwards and Phil W Anderson. Theory of spin glasses. *Journal of Physics F: Metal Physics*, 5(5):965, 1975.

[45] Giorgio Parisi. Infinite number of order parameters for spin-glasses. *Physical Review Letters*, 43(23):1754, 1979.

[46] Giorgio Parisi. The order parameter for spin glasses: a function on the interval 0-1. *Journal of Physics A: Mathematical and General*, 13(3):1101, 1980.

[47] Giorgio Parisi. A sequence of approximated solutions to the sk model for spin glasses. *Journal of Physics A: Mathematical and General*, 13(4):L115, 1980.

[48] Giorgio Parisi. Order parameter for spin-glasses. *Physical Review Letters*, 50(24):1946, 1983.

[49] Ronen M Kroeze, Brendan P Marsh, David Atri Schuller, Henry S Hunt, Sarang Gopalakrishnan, Jonathan Keeling, and Benjamin L Lev. Replica symmetry breaking in a quantum-optical vector spin glass. *arXiv preprint arXiv:2311.04216*, 2023.

[50] Brendan P Marsh, Ronen M Kroeze, Surya Ganguli, Sarang Gopalakrishnan, Jonathan Keeling, and Benjamin L Lev. Entanglement and replica symmetry breaking in a driven-dissipative quantum spin glass. *Physical Review X*, 14(1):011026, 2024.

[51] Brendan P Marsh, David Atri Schuller, Yunpeng Ji, Henry S Hunt, Giulia Z Socolof, Deven P Bowman, Jonathan Keeling, and Benjamin L Lev. A multimode cavity qed ising spin glass. *arXiv preprint arXiv:2505.22658*, 2025.

[52] John J Hopfield and David W Tank. Computing with neural circuits: A model. *Science*, 233(4764):625–633, 1986.

[53] Sarang Gopalakrishnan, Benjamin L Lev, and Paul M Goldbart. Frustration and glassiness in spin models with cavity-mediated interactions. *Physical review letters*, 107(27):277201, 2011.

[54] Brendan P Marsh, Yudan Guo, Ronen M Kroeze, Sarang Gopalakrishnan, Surya Ganguli, Jonathan Keeling, and Benjamin L Lev. Enhancing associative memory recall and storage capacity using confocal cavity qed. *Physical Review X*, 11(2):021048, 2021.

[55] Subir Sachdev and Jinwu Ye. Gapless spin-fluid ground state in a random quantum heisenberg magnet. *Physical review letters*, 70(21):3339, 1993.

[56] Lucile Savary and Leon Balents. Quantum spin liquids: a review. *Reports on Progress in Physics*, 80(1):016502, 2016.

[57] Alexei Kitaev. A simple model of quantum holography., Talks at KITP, April 7, 2015 and May 27, 2015.

[58] Juan Maldacena and Douglas Stanford. Remarks on the sachdev-ye-kitaev model. *Physical Review D*, 94(10):106002, 2016.

[59] Juan Maldacena, Stephen H Shenker, and Douglas Stanford. A bound on chaos. *Journal of High Energy Physics*, 2016(8):1–17, 2016.

[60] Sean A Hartnoll, Andrew Lucas, and Subir Sachdev. *Holographic quantum matter*. 2018.

[61] Shao-Kai Jian, Chunxiao Liu, Xiao Chen, Brian Swingle, and Pengfei Zhang. Measurement-induced phase transition in the monitored sachdev-ye-kitaev model. *Physical review letters*, 127(14):140601, 2021.

[62] Richard A Davison, Wenbo Fu, Antoine Georges, Yingfei Gu, Kristan Jensen, and Subir Sachdev. Thermoelectric transport in disordered metals without quasiparticles: The sachdev-ye-kitaev models and holography. *Physical Review B*, 95(15):155131, 2017.

[63] Yingfei Gu, Alexei Kitaev, Subir Sachdev, and Grigory Tarnopolsky. Notes on the complex sachdev-ye-kitaev model. *Journal of High Energy Physics*, 2020(2):1–74, 2020.

[64] Debanjan Chowdhury, Antoine Georges, Olivier Parcollet, and Subir Sachdev. Sachdev-ye-kitaev models and beyond: Window into non-fermi liquids. *Reviews of Modern Physics*, 94(3):035004, 2022.

[65] Aavishkar A Patel, Haoyu Guo, Ilya Esterlis, and Subir Sachdev. Universal theory of strange metals from spatially random interactions. *Science*, 381(6659):790–793, 2023.

[66] Chenyuan Li, Davide Valentinis, Aavishkar A Patel, Haoyu Guo, Jörg Schmalian, Subir Sachdev, and Ilya Esterlis. Strange metal and superconductor in the two-dimensional yukawa-sachdev-ye-kitaev model. *Physical Review Letters*, 133(18):186502, 2024.

[67] Jan Zaanen. Planckian dissipation, minimal viscosity and the transport in cuprate strange metals. *SciPost Physics*, 6(5):061, 2019.

[68] Philip W Phillips, Nigel E Hussey, and Peter Abbamonte. Stranger than metals. *Science*, 377(6602):eabh4273, 2022.

[69] Philipp Uhrich, Soumik Bandyopadhyay, Nick Sauerwein, Julian Sonner, Jean-Philippe Brantut, and Philipp Hauke. A cavity quantum electrodynamics implementation of the sachdev–ye–kitaev model. *arXiv preprint arXiv:2303.11343*, 2023.

[70] Rahel Baumgartner, Pietro Pelliconi, Soumik Bandyopadhyay, Francesca Orsi, Nick Sauerwein, Philipp Hauke, Jean-Philippe Brantut, and Julian Sonner. Quantum simulation of the sachdev-ye-kitaev model using time-dependent disorder in optical cavities. *arXiv preprint arXiv:2411.17802*, 2024.

[71] Avikar Periwal, Eric S Cooper, Philipp Kunkel, Julian F Wienand, Emily J Davis, and Monika Schleier-Smith. Programmable interactions and emergent geometry in an array of atom clouds. *Nature*, 600(7890):630–635, 2021.

[72] Jürgen Berges. Introduction to nonequilibrium quantum field theory. In *AIP Conference Proceedings*, volume 739, pages 3–62. American Institute of Physics, 2004.

[73] Alex Kamenev. *Field theory of non-equilibrium systems*. Cambridge University Press, 2023.

[74] L M Sieberer, M Buchhold, and S Diehl. Keldysh field theory for driven open quantum systems. *Reports on Progress in Physics*, 79(9):096001, August 2016.

[75] Aleksandr N Mikheev, Hossein Hosseinabadi, and Jamir Marino. Prethermalization of light and matter in cavity-coupled rydberg arrays. *arXiv preprint arXiv:2504.06267*, 2025.

[76] Heinz-Peter Breuer and Francesco Petruccione. *The theory of open quantum systems*. OUP Oxford, 2002.

[77] Martino Stefanini, Aleksandra A Ziolkowska, Dmitry Budker, Ulrich Poschinger, Ferdinand Schmidt-Kaler, Antoine Browaeys, Atac Imamoglu, Darrick Chang, and Jamir Marino. Is lindblad for me? *arXiv preprint arXiv:2506.22436*, 2025.

[78] Konstantin Efetov. *Supersymmetry in disorder and chaos*. Cambridge university press, 1999.

[79] Guy Gur-Ari, Raghu Mahajan, and Abolhassan Vaezi. Does the syk model have a spin glass phase? *Journal of High Energy Physics*, 2018(11):1–20, 2018.

[80] CL Baldwin and B Swingle. Quenched vs annealed: Glassiness from sk to syk. *Physical Review X*, 10(3):031026, 2020.

[81] Hossein Hosseinabadi, Shane P. Kelly, Jörg Schmalian, and Jamir Marino. Thermalization of non-fermi-liquid electron-phonon systems: Hydrodynamic relaxation of the yukawa-sachdev-ye-kitaev model. *Phys. Rev. B*, 108:104319, Sep 2023.

[82] Joseph Polchinski and Vladimir Rosenhaus. The Spectrum in the Sachdev-Ye-Kitaev Model. *JHEP*, 04:001, 2016.

[83] Ilya Esterlis, Haoyu Guo, Aavishkar A. Patel, and Subir Sachdev. Large N theory of critical Fermi surfaces. *Phys. Rev. B*, 103(23):235129, 2021.

[84] Ar Abanov and Andrey V Chubukov. Quantum-critical theory of the spin-fermion model and its application to cuprates: Normal state analysis. *Advances in Physics*, 52(3):119–218, 2003.

[85] Ilya Esterlis and Jörg Schmalian. Cooper pairing of incoherent electrons: an electron-phonon version of the Sachdev-Ye-Kitaev model. *Phys. Rev. B*, 100(11):115132, 2019.

[86] Laura Classen and Andrey Chubukov. Superconductivity of incoherent electrons in the Yukawa Sachdev-Ye-Kitaev model. *Phys. Rev. B*, 104(12):125120, 2021.

[87] Gian-Andrea Inkof, Koenraad Schalm, and Jörg Schmalian. Quantum critical eliashberg theory, the sachdev-ye-kitaev superconductor and their holographic duals. *npj Quantum Materials*, 7(1), June 2022.

[88] Andreas Eberlein, Valentin Kasper, Subir Sachdev, and Julia Steinberg. Quantum quench of the Sachdev-Ye-Kitaev Model. *Phys. Rev. B*, 96(20):205123, 2017.

[89] Ritabrata Bhattacharya, Dileep P. Jatkar, and Nilakash Sorokhaibam. Quantum Quenches and Thermalization in SYK models. *JHEP*, 07:066, 2019.

[90] Y. Cheipesh, A. I. Pavlov, V. Ohanesjan, K. Schalm, and N. V. Gnezdilov. Quantum tunneling dynamics in a complex-valued Sachdev-Ye-Kitaev model quench-coupled to a cool bath. *Phys. Rev. B*, 104(11):115134, 2021.

[91] B. Derrida. Random-energy model: Limit of a family of disordered models. *Phys. Rev. Lett.*, 45:79–82, Jul 1980.

[92] D.J. Gross and M. Mezard. The simplest spin glass. *Nuclear Physics B*, 240(4):431–452, 1984.

[93] J. Ye, S. Sachdev, and N. Read. Solvable spin glass of quantum rotors. *Phys. Rev. Lett.*, 70:4011–4014, Jun 1993.

[94] N. Read, Subir Sachdev, and J. Ye. Landau theory of quantum spin glasses of rotors and ising spins. *Phys. Rev. B*, 52:384–410, Jul 1995.

[95] David Sherrington and Scott Kirkpatrick. Solvable model of a spin-glass. *Phys. Rev. Lett.*, 35:1792–1796, Dec 1975.

[96] Jonathan Miller and David A. Huse. Zero-temperature critical behavior of the infinite-range quantum ising spin glass. *Phys. Rev. Lett.*, 70:3147–3150, May 1993.

[97] A. Andreanov and M. Müller. Long-range quantum ising spin glasses at t=0: Gapless collective excitations and universality. *Phys. Rev. Lett.*, 109:177201, Oct 2012.

[98] Philipp Strack and Subir Sachdev. Dicke quantum spin glass of atoms and photons. *Phys. Rev. Lett.*, 107:277202, Dec 2011.

[99] Michael Buchhold, Philipp Strack, Subir Sachdev, and Sebastian Diehl. Dicke-model quantum spin and photon glass in optical cavities: Nonequilibrium theory and experimental signatures. *Physical Review A*, 87(6), June 2013.

[100] Shane P. Kelly, Ana Maria Rey, and Jamir Marino. Effect of active photons on dynamical frustration in cavity qed. *Physical Review Letters*, 126(13), April 2021.

[101] Hossein Hosseinabadi, Darrick E. Chang, and Jamir Marino. Far from equilibrium field theory for strongly coupled light and matter: Dynamics of frustrated multi-mode cavity QED. *Phys. Rev. Res.*, 6(4):043314, 2024.

[102] Hossein Hosseinabadi, Darrick E. Chang, and Jamir Marino. Quantum-to-classical crossover in the spin glass dynamics of cavity QED simulators. *Phys. Rev. Res.*, 6(4):043313, 2024.

[103] Subir Sachdev, N. Read, and R. Oppermann. Quantum field theory of metallic spin glasses. *Phys. Rev. B*, 52:10286–10294, Oct 1995.

[104] Markus Müller, Philipp Strack, and Subir Sachdev. Quantum charge glasses of itinerant fermions with cavity-mediated long-range interactions. *Phys. Rev. A*, 86:023604, Aug 2012.

[105] Anirvan M. Sengupta and Antoine Georges. Non-fermi-liquid behavior near a t=0 spin-glass transition. *Phys. Rev. B*, 52:10295–10302, Oct 1995.

[106] Giuseppe E. Santoro, Roman Martoňák, Erio Tosatti, and Roberto Car. Theory of quantum annealing of an ising spin glass. *Science*, 295(5564):2427–2430, 2002.

[107] Andrew Lucas. Ising formulations of many np problems. *Frontiers in Physics*, 2, 2014.

Curriculum Vitae

Personal Data

Name:	Hossein Hosseinabadi
Contact:	hhossein@uni-mainz.de
Address:	Room 03-422, Staudingerweg 7, 55128 Mainz
Nationality:	Iran

Research Interests

Quantum Many-Body Systems, Non-Equilibrium Dynamics, Disordered Systems, Open Quantum Systems.

Education

Oct 2021 - Jan 2026	Ph.D. in Physics, Johannes Gutenberg University, Mainz, Germany. Dissertation: "Non-equilibrium Dynamics of Disordered Quantum Many-Body Systems". Advisor: Prof. Jamir Marino. Final Grade: summa cum laude.
Oct 2017 - Oct 2019	M.Sc. in Physics, Sharif University of Technology, Tehran, Iran. Dissertation: "Spin-orbit interaction and topological vortices in unconventional superconductors". Advisor: Prof. Mehdi Kargarian. Thesis Grade: Excellent.
Oct 2013 - Oct 2017	B.Sc. in Physics, Sharif University of Technology, Tehran, Iran.
Oct 2009 - Oct 2013	High School Diploma, Shahid Beheshti High School, Tehran, Iran.

Awards and Honors

2019	Ranked First in the Iranian National Exam for PhD Studies in Physics.
2018	Distinguished Undergraduate Student in Physics.
2017	Gold Medal in the National Physics Olympiad for University Students.
2017	Ranked First in the Iranian National Exam for Master Studies in Physics.
2012	Silver Medal in the National Physics Olympiad for High School Students.